UNIVERSITAT POLITÈCNICA
DE CATALUNYA
BARCELONATECH

PhD program in Construction Engineering

# Risk-based highway bridge inspection intervals

**Doctoral thesis by:**

Giorgio Anitori

**Thesis advisor:**

Prof. Joan Ramon Casas

Department of Civil and Environmental Engineering

Barcelona, January 2021

# General Information

## PhD candidate


| | |
|---|---|
| Name | Giorgio Anitori |
| Academic profile | Civil Engineer |
| Institution | Universitat Politècnica de Catalunya (UPC) |
| E-mail | giorgio.anitori@upc.edu |


## Thesis advisor


| | |
|---|---|
| Name | Joan Ramon Casas Rius |
| Academic profile | Prof, Dr., Civil Engineer |
| Institution | Universitat Politècnica de Catalunya (UPC) |
| E-mail | joan.ramon.casas@upc.edu |

## Abstract

Infrastructure maintenance programs establish schedules for routine inspections of highway bridges with little consideration of their current conditions. The time interval between two inspections is traditionally set based on experience and on engineering judgment. For example, in the US considerable expenditures are incurred to meet the required biennial routine inspection of all bridges many of which may be in good condition. It is therefore of great interest for the engineering community to develop an approach to control inspection schedules of individual bridges and minimize their associated costs using rational criteria that account for the lower risk of postponing the inspection of bridges that are subject to reduced deterioration mechanisms and low traffic loadings. The implementation of such a risk-based approach would go a long way in helping optimize the limited resources available for maintaining the vast highway infrastructure system.

The object of this Ph.D. dissertation is to develop a rational approach for determining a risk-based optimum time interval between bridge inspections. The proposed theoretical approach subsequently serves for proposing a simple procedure that is implementable in routine practice by bridge engineers using easily available bridge-specific data.

To illustrate the proposed procedure using actual bridge data, the work uses highway data from the state of New York (NYS) in the United States of America (USA) in the form of Weigh-in-Motion (WIM) truck traffic data and bridge records provided through the National Bridge Inventory (NBI) database. These data are used to develop a theoretical framework able to define the capacity of bridges probabilistically and the risk of bridge failure if a bridge's inspection is deferred for a limited period of time.

Typically, a bridge structure's load carrying capacity is estimated by means of a linear elastic analysis to determine the effects of applied nominal legal or design loads on the most critical members even though member strength is evaluated based on ultimate limit state. Such an approach is known to provide a fair level of precision and conservative results. While the approach takes into consideration the level of deterioration of the most critical bridge members based on field inspection reports, it ignores the actual intensity and frequency of heavy truckloads, the actual bridge system behavior, or the forecast of bridge deterioration between inspection intervals. In this study, actual bridge truck data obtained from WIM systems are used to estimate the maximum loads on the bridge that may be quite different from the nominal legal or design loads set in bridge codes and specifications. Also, the effect of system behavior is considered by implementing structural analysis models that take into account the non-linear behavior of the material constituents and the evolution of the load distribution when bridge members undergo post-yielding deformations. This enables the study to reach a greater level of accuracy than standard calculation procedures and to consider the improved performance of bridges with structurally redundant configurations. Furthermore, strength deterioration over time is included in the model by studying load rating historical data extracted from the NBI database.

Probabilistic models of system behavior and loading are applied to obtain a probabilistic assessment of the risk of deferring the inspection interval of a bridge of interest. The optimum bridge inspection interval is obtained by minimizing the risk of bridge failure obtained by combining the probability of failure and the cost of failure. The latter is calculated by estimating the costs of potential failure-related casualties, bridge reconstruction, traffic disruption, environmental impact and bridge inspection cost.

The calculations performed in this dissertation based on data collected in the state of New York are limited to simple span composite steel-concrete superstructures that constitute a large proportion of short to medium span bridges in North America. However, the same concepts can be extended to other types of superstructures and other regions of the world as appropriate data become available.

The conclusions of this study include the demonstration of the inadequacy of utilizing a standard two-year inspection interval for all bridges. To overcome this problem a simplified procedure is proposed for an easy practical engineers' application.

**Keywords**: Bridge Inspection, Structural Redundancy, Highway Bridges, Live load, Structural Reliability, Probabilistic Risk Assessment, Deterioration Models.

Los programas de mantenimiento de infraestructuras establecen planes periódicos de inspección básica en los cuales el posible estado de los puentes en el momento de la inspección tiene relativamente poca importancia. El intervalo temporal entre dos inspecciones se fija sobre la base de la práctica habitual y sobre experiencia pasada. Por ejemplo, en los Estados Unidos de América una gran parte del presupuesto de gasto destinado al mantenimiento de la red de infraestructuras se deriva al plan de inspecciones bienales de puentes aunque en muchos casos muestran buenas condiciones estructurales. Por esta razón, es de suma importancia para la comunidad el desarrollo de protocolos para controlar el plan de inspección de puentes y minimizar los costes asociados a través de criterios racionales, para poder destinar los recursos asignados a inspección allí donde más falta hacen. Dichos criterios tienen que ser capaces de reconocer aquellos puentes que presentan mayor riesgo debido a la exposición a procesos de deterioro y a sobrecarga de tráfico intenso y minimizar los costes de inspección asociados. La implementación de estrategias basadas en criterios de riesgo permite optimizar el presupuesto total disponible para el mantenimiento de las redes de carreteras

El objeto de esta tesis doctoral es el desarrollo de un procedimiento racional basado en el cálculo del riesgo para determinar el intervalo óptimo entre dos inspecciones básicas. El enfoque teórico propuesto se emplea posteriormente para la aplicación en la práctica de dichos criterios utilizando datos de partida fáciles de obtener para el usuario final que esté interesado en aplicar el método para un puente en concreto.

La metodología propuesta en este trabajo se materializa a través de los datos disponibles de la red de carreteras del estado de Nueva York (NYS) en Estados Unidos de América (USA), desde mediciones de tráfico del tipo Weigh-in-Motion (WIM) hasta informaciones en el marco de la base de datos del National Bridge Inventory (NBI). Esos datos se utilizan para desarrollar una base metodológica capaz de calcular la capacidad portante de superestructuras desde el punto de vista probabilista y cuantificar el incremento de riesgo que supone incrementar el intervalo de la inspección básica, actualmente fijado en dos años

En la práctica actual, el cálculo de la capacidad portante de puentes sujetos a sobrecarga de tráfico (en estado límite de servicio y último) se lleva a cabo a partir de modelos típicamente elástico-lineales en los que se evalúan los esfuerzos para el elemento más crítico y sucesivamente se considera el cálculo no lineal para la verificación de dicho elemento. Este enfoque está aceptado y ha demostrado su validez y fiabilidad en numerosas aplicaciones. Sin embargo, a pesar de que estos modelos pueden tener en cuenta el deterioro detectado en las campañas de inspección, normalmente no consideran sobrecargas de tráfico realistas, el comportamiento estructural del conjunto del puentes y no sólo de sus elementos por separado, o la evolución posible del deterioro entre intervalos de inspección. En este estudio, se emplean datos de tráfico real obtenidos de sistemas WIM para estimar la sobrecarga de tráfico máxima esperada que puede ser bastante diferente de la que típicamente sugieren los códigos de diseño y evaluación estructural de puentes. De la misma manera, la respuesta conjunta de la estructura se tiene en cuenta en este trabajo utilizando modelos capaces de simular el comportamiento no-lineal de los materiales y la evolución de la redistribución de los esfuerzos cuando la estructura se encuentra en rangos de deformaciones próximos a rotura. Esto permite

mejorar el cálculo de la capacidad estructural y detectar aquellos puentes cuya configuración tipológica y topológica resulta en un comportamiento redundante que no es posible tener en cuenta en los modelos de cálculo tradicionales. Además, se incluye en el modelo el deterioro de los materiales tras estudiar datos históricos sobre la pérdida de capacidad portante de una gran cantidad de puentes seleccionados del NBI.

Para el cálculo de los intervalos de inspección se emplea el concepto de riesgo, que a su vez se basa en modelos de cálculo probabilistas. El intervalo de inspección óptimo se obtiene minimizando el riesgo de fallo obtenido combinando la probabilidad de fallo con el coste asociado. El coste del fallo se obtiene estimando los costes potenciales relativos como víctimas, heridos, reconstrucción del puente, interrupción del tráfico vehicular, impacto ambiental y coste de inspección.

Los cálculos llevados a cabo en esta tesis están basados en datos de la región del estado de Nueva York y limitados a puentes simplemente apoyados con superestructura mixta acero-hormigón que constituye una importante tipología en el ámbito norteamericano. Sin embargo los mismos conceptos pueden ser aplicados a otras regiones del mundo a medida que la información necesaria se encuentre disponible.

El estudio demuestra la ineficiencia de utilizar un intervalo de inspección de dos años para todos los puentes y propone una metodología simplificada para calcular el intervalo de inspección recomendado para ser implementada en la práctica ingenieril de una forma sencilla.

**Palabras clave**: Inspección de puentes, Redundancia estructural, Sobrecarga de tráfico, Fiabilidad estructural, Riesgo, Deterioro.

## Resum

Els programes de manteniment de infraestructures estableixen plans periòdics d'inspecció bàsica en els quals l'estat actual dels ponts té relativament poca importància a l´hora de definir l´interval de temps. L'interval temporal entre dues inspeccions es basa normalment en la practica habitual i en la experiència passada. Per exemple, als Estats Units d'Amèrica una gran part del pressupost de despesa destinat al manteniment de la xarxa d'infraestructures es deriva al pla d'inspeccions biennal de ponts tot i que, aquests, en molts casos mostren bones condicions estructurals. Per això la comunitat enginyeril està interessada en el desenvolupament de protocols que controlin el pla d'inspecció de ponts i que minimitzin els costos associats a traves de criteris racionals. Aquets criteris han de ser capaços de reconèixer els ponts que presenten un risc alt degut a la elevada exposició a processos de deteriorament i a sobrecarrega de tràfic intens i minimitzar els costos d'inspecció associats. L'implementació d'estratègies basades en el càlcul del risc permet optimitzar el pressupost total disponible per al manteniment de les xarxes de carreteres.

L'objecte d'aquesta tesi doctoral es el desenvolupament d'un procediment racional basat en el càlcul del risc per a estimar l'interval òptim entre dues inspeccions bàsiques. L'estratègia teòrica proposada es fa servir posteriorment per a la aplicació practica d'aquests criteris utilitzant dades inicials fàcils d'obtenir per l'usuari final que estigui interessat en aplicar el mètode per a un pont en concret.

La metodologia proposada en aquest treball utilitza dades de la xarxa de carreteres del estat de Nova York (NYS) als Estats Units d'Amèrica (USA), a partir de mesures de tràfic del tipus Weigh-in-Motion (WIM) i de informacions provinents de la base de dades del National Bridge Inventory (NBI). Aquestes dades es fan servir per a desenvolupar una eina metodològica capaç de calcular la capacitat estructural de superestructures des del punt de vista probabilista i quantificar l'increment de risc al que la societat està sotmesa en cas de decidir incrementar l'interval d'inspecció per damunt dels 2 anys.

El càlcul de la capacitat resistent de ponts subjectes a sobrecarrega de tràfic (en estat límit de servei i últim), típicament es du a terme a partir de models globals elàstic-lineals on s'avaluen els esforços per l'element més crític i a continuació es considera el càlcul no lineal per a aquest element de manera aïllada. Aquesta estratègia està acceptada i ha demostrat la seva validesa i efectivitat en nombroses aplicacions. . Malgrat aquests models poden tenir en compte el deteriorament detectats per les campanyes d'inspecció, normalment no consideren sobrecarregues de tràfic realistes, el comportament estructural conjunt dels diferents elements del pont o la evolució del deteriorament entre intervals d'inspecció. En aquest estudi, es fan servir dades de tràfic real obtingudes de sistemes WIM per a estimar la sobrecarrega de tràfic màxima esperada que pot ser força diferent de la que típicament suggereixen els codis de disseny i avaluació estructural de ponts. A més, l'efecte de resposta global del pont es té en compte en aquest treball utilitzant models capaços de simular el comportament no-lineal dels materials i l'evolució de la redistribució dels esforços quan l'estructura es troba en rangs de deformacions propers a l´esgotament de la estructura. Això permet millorar el càlcul de la capacitat estructural i detectar els ponts amb una configuració que resulta ser

redundant i que no es manifesta en models de càlcul tradicionals. A més, en el model teòric, s'inclou el deteriorament dels materials arran d'estudiar la pèrdua de capacitat d'una gran quantitat de ponts seleccionats del NBI al llarg del seu període de servei.

Per al càlcul dels intervals d'inspecció es fa servir el concepte de risc, que a la vegada es basa en models de càlcul probabilistes. L'interval d'inspecció òptim s'obté minimitzant el risc de fallada obtingut combinant la probabilitat de fallada amb el cost associat. El cost de fallada s'obté estimant els costos potencials relatius com víctimes, ferits, reconstrucció del pont, interrupció del tràfic vehicular, impacte ambiental i cost d'inspecció.

Els càlculs duts a terme en aquesta tesi estan basats en dades de la regió del estat de Nova York i limitats a ponts simplement recolzats amb superestructura mixta acer-formigó que constitueix una important tipologia en el àmbit nord americà. No obstant, els mateixos conceptes poden ser aplicats a altres regions del mon a mesura que la informació necessària estigui a disposició.

L'estudi demostra la ineficiència d'utilitzar un interval d'inspecció de dos anys per a tots els ponts i proposa una metodologia simplificada per calcular l'interval d'inspecció recomanat per ser implementat en la practica ingenieril d'una manera senzilla.

**Paraules clau**: Inspecció de ponts, Redundància estructural de ponts, Ponts d'autopista, Sobrecarrega de tràfic, Fiabilitat estructural, Càlcul probabilista del risc, Models de deteriorament.

## Chapters

# Contents

## List of Figures

## List of Tables

# 1 Introduction

## 1.1 Background

A visual inspection forms the first step of a bridge's condition assessment process on the basis of which more accurate evaluations, such as non-destructive or coupon testing, may be undertaken if warranted and preliminary decisions on maintenance are made. Bridge owners adopt different policies for managing infrastructure lifelines depending on many factors with an overall goal of minimizing monetary outlays while maintaining an adequate safety level for the infrastructure. The main objective of the first visual inspection stage is to identify damaged bridges and prioritize maintenance budget allocations to those in worst condition.

Although different owners have different rules for ranking bridges, field experience of the inspectors and the judgment of the engineering team are still key factors in influencing decisions on what additional in-depth bridge condition evaluations, numerical analysis processes and maintenance strategies should be undertaken. Automated bridge management with the help of permanent monitoring devices is being employed for few specific bridges, but a completely automated bridge management system does not seem feasible at this point in time because of the high cost of applying health monitoring devices at large scale. Despite rapid advancement in the field, such as the implementation of National Bridge Element (NBE) inspection and the adoption of AASHTOWare, additional research effort is needed to further reduce the subjectivity in some aspects of the current bridge assessment process.

The routine visual inspection process, which is carried out for all bridges, has peculiarities depending on regulations as well as owner needs and requirements. Routine inspections are normally performed every two years and usually involve a general evaluation of the structure using limited sets of tools. Inspection reports document the appraisal of the inspectors, describe the level of deterioration, and include photos of deteriorated components. The simple visual inspection may be followed up with in-depth inspections for bridges flagged as critical.

In the US, the current National Bridge Inspection Standards (NBIS, 2004) mandate that bridges undergo routine inspections on a two-year schedule. Given a total of more than 600,000 bridge in the US and that a typical inspection of a short to medium span bridge costs about, $ 6,000, the bridge inspection mandate alone is costing the US over than two billion dollars per year. The amount spent on bridge inspection alone forms a significant proportion of US Federal government outlays on all projects to improve roadway safety and mobility, repair aging bridges and highways, and promote the efficient movement of freight. In fact, fiscal year 2019, FHWA (Federal Highway Administration) has requested $ 46.0 billion for streamlining highway infrastructure project delivery (FHWA, 2019a).

Bridge condition ratings extracted from the NBI database show that the typical 2-year interval used for routine inspections may be too conservative for newly constructed bridges or bridges where the environmental conditions are favorable leading to low structural deterioration over time. The variation of

bridge condition can be evaluated by analyzing the trends of condition ratings over short periods of time. Figures 1-1, 1-2 and 1-3 give histograms showing how long it takes for condition ratings obtained from NBI of decks, superstructures and substructures respectively to change from their current status. The data represent the condition of roughly 17,000 bridges of the New York State (NYS) infrastructure network. For the part labelled "0", the figures give four bins (2 years, 3, years, 4 years and 5 years) these bins give the percentage of bridges that had remained in the same condition rating they currently have for the different previous four year time intervals. The bin labelled "1" shows the percent of bridges where the condition rating value experienced an improvement by one condition rating level within a given time interval (e.g. due to repair). Likewise, the percent of bridges that have shown a decrease by one condition rating classification (in the last years) are shown in the group of bins labelled "-1". The group of bins labelled "-2" gives the same information for the bridges that underwent a two-level reduction in condition rating. For example, Figure 1-2 shows that 69% of the bridge superstructures remain in the same condition for at least 2 years, 64% have remained in the same condition in the last 3 years, 58% have remained in the same condition for the last 4 years and 54% have remained in the same condition for the last 5 years. The histograms in Figures 1-2 and 1-3 give roughly similar percentages. Overall, the figures show that that more than 50% of NYS bridges have maintained their current condition ratings for the last 5 years.

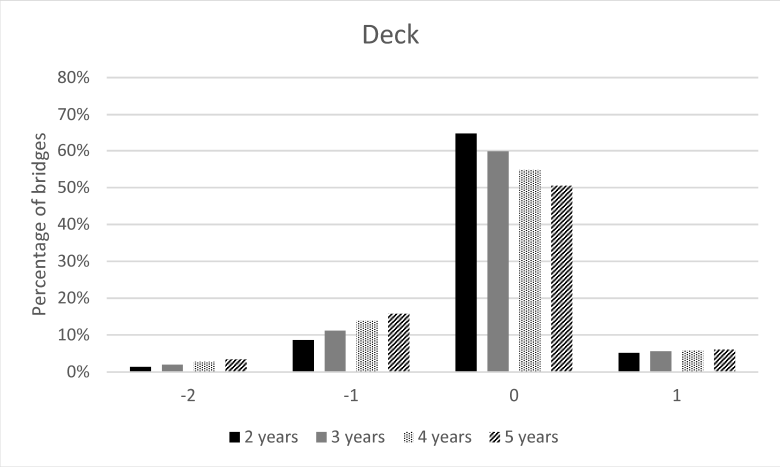


**Figure 1-1. Deck condition rating variation for 2, 3, 4 and 5-year intervals.**

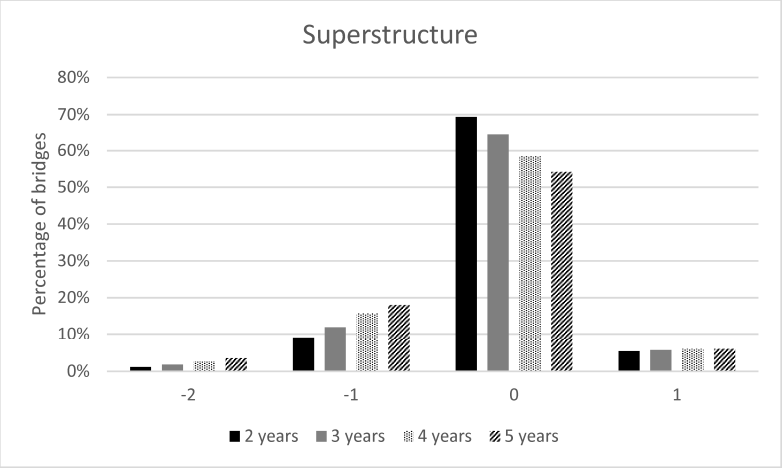


**Figure 1-2. Superstructure condition rating variation for 2, 3, 4 and 5-year intervals.**

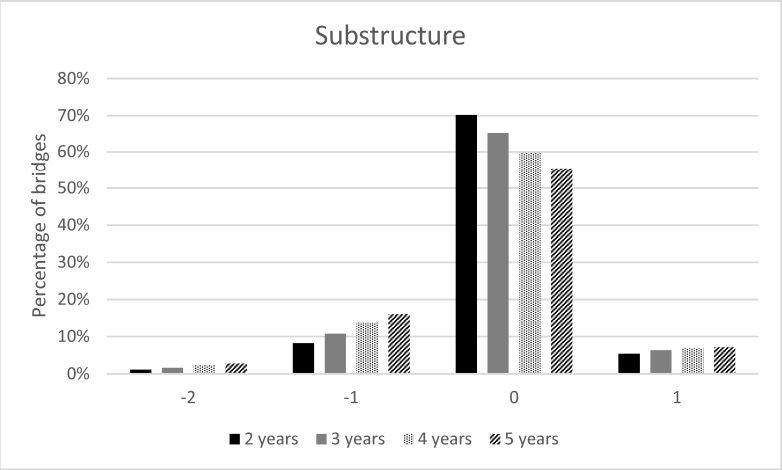


**Figure 1-3. Substructure condition rating variation for 2, 3, 4 and 5-year intervals.**

After determining the condition of bridge components, each bridge's load carrying capacity is determined to provide its load rating. Current procedures for evaluating a bridge structure's load carrying capacity use linear elastic analyses to determine the effects of applied nominal legal or design loads on the most critical member even though member strength assessment is based on ultimate limit state. Such an approach is known to provide conservative results which are very suitable for designing and constructing new bridges but often underestimates the ability of existing bridges to carry current loads. This is because, after applying code-specified live load factors, factored nominal legal loads and design loads may not accurately reflect the maximum loads applied on the bridge and the analysis procedure does not accurately reflect the non-linear behavior of the bridge's material constituents and the interaction between the members that often lead to a higher system capacity than that of the individual members.

In order to improve current asset management procedures, the Moving Ahead for Progress in the 21st Century Act (MAP-21) amended 23 U.S.C. 119 to require State Departments of Transportation (DOTs) to develop risk-based Transportation Asset Management Plans (TAMPs). On October 24, 2016, the FHWA adopted a final TAMP rule that elaborates on the MAP-21 requirements. This asset management requirement is applicable to all transportation assets including highway bridges. It is however noted that the recently adopted risk-based method for bridge condition and safety evaluation procedures are mostly based on a subjective assessment of the risk rather than rigorous risk assessment principles.

The above information explains the great interest expressed by the engineering community to develop rational criteria for controlling the schedule of bridge inspections that will help optimize the bridge inspection process and improve infrastructure management practices in order to direct the limited available resources toward upgrading those bridges in most need of rehabilitation or replacement. Simplified risk-informed procedures have been recently proposed to help achieve that goal. In particular, there is a keen interest in delaying the inspection of bridges that have low risk of failure. While the use of simplified risk-informed procedures is desired for efficient implementation in routine bridge engineering practice, the validity of any proposed simplified procedures must be verified by comparing their outcomes to those obtained from more rigorous risk analysis methods.

## 1.2 Research Objectives

The main goal of this Ph.D. dissertation is to develop a risk-based approach to determine optimum bridge inspection schedules that take into consideration the probability of bridge failure and the direct and indirect consequences of failure. Evaluating the probability of bridge failure involves the reliability analysis of bridge structural systems taking into consideration a statistical evaluation of bridge loads and the expected deterioration of bridge members over time between inspections and the capability of the bridge system to withstand damage through structural redundancy. Specifically, the objectives of the study can be described as follows:

- Analyze Weigh-in-Motion (WIM) truck traffic data to calibrate probabilistic live load models that will reflect current loading of bridges for application during the reliability analysis of highway bridge structural systems.
- Use NBI data on load rating to establish a probabilistic model of bridge member deterioration between inspection intervals.
- Calculate system reliability of typical bridge configurations using efficient simulation methods. These calculations should account for the non-linear behavior of structural members and the interaction of the members to reflect the intrinsic redundancy in bridge structures.

- Canvass the literature to collect models that quantify the direct and indirect consequences of bridge failures and their impact on the users and the environment.
- Develop a rigorous risk-based procedure for determining an optimum bridge inspection schedule that accounts for the probability of bridge failure, the consequences of failure and the cost of inspection using bridge specific structural data and other information provided by the NBI.

## 1.3 Methodology

The concept of risk is used in many fields of engineering to recognize that not all engineered products have the same importance, which is defined by the purpose they serve and the likelihood of their failure. Specifically, for the proper assessment of a highway bridge, it is important to not only evaluate its reliability but also to determine its importance within the infrastructure network. The application of risk-informed methods in structural engineering has been advancing in the design of buildings where the design process accounts for the importance of the structure by setting buildings into classes related to the demand on the structure. For example, both Eurocode 8 (CEN, 2004) and ASCE 7-16 (2017) for the seismic design of buildings and other structures define importance classes depending on the purpose of the structure or its expected type of occupancy and the chances that a local failure would lead to a system's failure. This somewhat rough classification ensures that the different activities the structure is expected to accommodate are identified and prioritized by society. Likewise, Eurocode 0 (CEN, 2002) defines, for general structures, three classes of consequences (CC1, CC2 and CC3) and associates a target reliability index to each of them. Once again, the different classes are linked to different degrees of loss of human life or economic, social and environmental consequences. In fact, it is convenient to evaluate the importance of a structure by evaluating the consequences of its interrupted service and its resilience. Once this point is set, it is easier to establish a classification of structure importance even for structures that serve the same purpose.

A general definition of risk is often presented in terms of the probability of failure times the consequences of failure (Equation 1-1). The consequences are often set in monetary terms in order to simplify the risk assessment process and easily combine different types of consequences. A simplified formulation of risk can be presented as (Ang & Tang, 2004):

$$\text{Risk} = p_f \times \mathrm{C} \tag{1-1}$$

where $p_f$ if the probability of failure and C is the consequence of failure (or loss) which can be expressed in monetary terms to assess the costs of failure, which may include direct costs, such as the cost of the structure

and loss of life, as well as indirect costs, such as user costs, economic losses, and environmental, societal, and political impacts.

A risk-based approach for bridge inspection purposes should account for the variation of risk with time. In fact, both the probability of failure through demand and capacity and the consequences of failure vary over time. Demand in the bridge evaluation process is due to truck traffic loads and capacity represents the ability of the structure to resist the applied loads. Specifically, the probability of failure depends on the evolution of live load over time due to changes in heavy traffic volume and the increase in the expected maximum load for longer return periods. Likewise, structural resistance changes due to deterioration or repair. Additionally, the uncertainties in the models used in evaluating the probability of failure would increase over time because forecasting future loads and structural material properties and the associated behavior of the structure become more difficult as projection time increases. Some of these time-dependent uncertainties could be controlled through various means. For example, a bridge mounted with a health monitoring system is less risky than a bridge inspected periodically because the variation of the structural parameters of the monitored bridge are constantly known while in the second case the parameters can only be estimated with some accuracy only at inspection while their estimation between inspections carry higher levels of uncertainty. Similarly, the costs of failure may increase over time due to inflation and changes in the value of money as well as economy-driven variations in traffic and in the importance of the bridge to the users and the community it serves. Also, bridge repair and rehabilitation costs may depend on the levels of damage accumulated over time and the frequency and type of maintenance actions it undergoes. In summary, cost projections are subject to uncertainties due to political, economic and environmental factors.

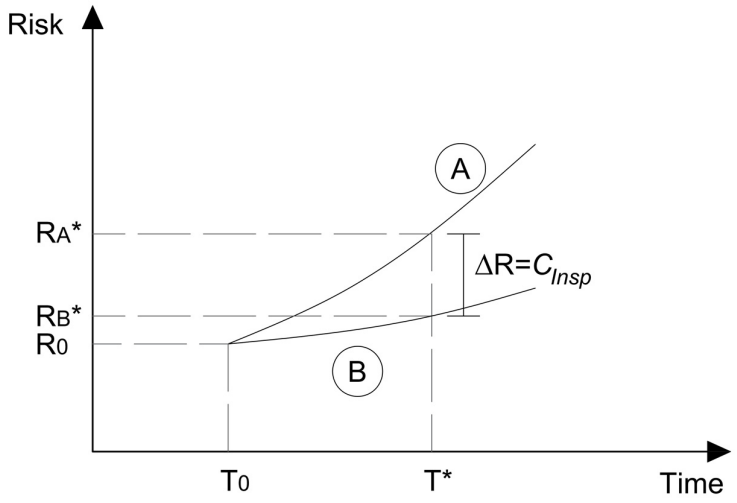


**Figure 1-4. Risk over time for an inspected bridge and for a non-inspected bridge.**

These concepts are used in this work to define a model for evaluating risk over time, as shown qualitatively in Figure 1-4 where $T_0$ represents the time when the last previous inspection was performed. The risk $R_0$ at time $T_0$ can be calculated based on the assessed level of deterioration and the accuracy of the method used for the condition assessment (e.g. visual inspection or more advanced methods). Curve A represents the evolution of risk over time assuming that no additional intermediate information about risk is available. That is, risk can only be estimated by projecting information available at time $T_0$ and therefore its assessment includes high levels of uncertainty obtained by the statistical analysis of a large population of bridges. On the other hand, a theoretical curve B can be defined assuming that accurate assessment of risk over time may be available for example through continuous bridge condition and load monitoring as well as more accurate assessment of economic activities and other changes in the community served by the specific bridge under study. This increased knowledge about the state of a specific bridge would generally lead to a smaller increase of the risk in curve B over time than that described by curve A, primarily due to the reduction in the uncertainties associated with determining the parameters and random variables that are used to estimate the risk. The difference between curves A and B represents the risk tolerance of society and bridge owners who may be willing to accept the higher risk represented by curve A associated with delaying the inspection and the condition assessment process and reducing the associated cost outlays. On the other hand, when the difference between the two curves reaches an intolerable level, it may be more efficient to obtain an improved assessment of the bridge by undertaking an inspection and incurring the associated cost of condition assessment and improved assessment of risk. Thus, the difference between curves A and B at any given time represents the increased risk due to not performing the inspection. When the cost of inspection, $C_{\text{Insp}}$ at time $T^*$ is lower than the relative difference, $\Delta R$, between the estimated risks in curves A and B, it becomes more efficient to incur the expense of performing an inspection and obtaining a better assessment of the safety and probability failure of the bridge as well as improving the assessment of the consequences of failure. In other words, $T^*$ represents the time where the increased risk associated with delaying bridge inspection is no longer justifiable due to the fact that the lower cost of inspection will bring about a higher confidence in the safety of the bridge and "higher peace of mind" so to speak. If the bridge inspection does not lead to significant improvements in the risk of failure, then appropriate actions for rehabilitating or replacing the bridge should be considered.

This Ph.D. dissertation will develop methods to help bridge engineers perform such risk assessment procedure using easy to collect bridge data. The risk assessment will assist bridge owners in making decisions based on rational criteria that take into consideration all relevant structural, economic and societal factors.

## 1.4 Dissertation Outline

To achieve the above stated objectives, this dissertation is divided into eight chapters as follows:

- Chapter 1 gave a brief background and stated the justification for this proposed research. The chapter also stated the objectives of the study and gave a brief summary of the proposed research approach.
- In Chapter 2, the state of the art related to the main topics of interest to this Thesis is reviewed. A brief introduction of the inspection procedures carried out in Europe and US is presented. Next, typical methods for including system behavior in structural calculations and the consideration of structural redundancy are described based on information in the existing literature. Finally, the main concepts of risk-based structural assessment approaches are reviewed.
- Chapter 3 deals with the US NBI database and describes the specific data it contains. The sub-set of bridges extracted from the NBI for NYS is described along with the strategy used to back calculate the geometric characteristics of bridges.
- In Chapter 4, the models used for evaluating the resistance of bridges are presented and the assumptions made for performing the structural analysis are explained. Also, the probabilistic resistance deterioration model calculated from load rating historical values is described.
- Chapter 5 deals with the calibration of a live load model suitable for system reliability analysis of bridges. A methodology is proposed to calibrate the live load model using Weigh-In-Motion (WIM) traffic data.
- In Chapter 6, structural reliability analysis concepts are outlined along with the methods used to calculate the reliability index for structural systems.
- In Chapter 7, the cost of failure is estimated by means of information obtained from the literature including direct (demolition, repair and reconstruction) and indirect costs (traffic delay, environmental impact and accident costs). A step-by-step procedure is proposed to conveniently apply the calculation for practical application.
- In Chapter 8, the risk-based approach is applied for a representative set of NYS composite steel bridges to obtain the recommended inspection interval. The method is presented as a step-by-step procedure for practical application. A numerical example is presented to provide guidance on the application of the method. The results obtained for a large population of real bridges is presented and discussed. Finally, the results obtained in the Thesis are summarized and possible future research directions are highlighted.
- Finally, in Chapter 9, the results obtained in the Thesis are summarized and possible future research directions are highlighted.

# 2 Review of the State of the Art

This chapter outlines the state of the art of the main important technical issues needed to achieve the objectives of this Thesis. The first part deals with inspection processes carried out by European countries and the US. The second part describes recent research on modeling structural system behavior. The last part reviews how risk-based methods were used in previous bridge engineering-related studies.

## 2.1 Overview of Bridge Condition Assessment

A survey was conducted a few years ago to compare bridge assessment procedures employed in different European countries (SAMARIS, 2006). The countries involved in the survey were Austria, Slovenia, Czech Republic, Norway, Poland and Hungary. In addition, the results of the survey were complemented by an extensive review of existing policies related to bridge assessment in Denmark, France, Germany, Spain, Switzerland and the United Kingdom. In these countries, in general, visual inspections are carried out every one or two years by maintenance personnel who are familiar with bridge data collection procedures but do not have special training in bridge structural behavior or structural safety assessment. Major follow-up inspections and structural assessments are subsequently carried out by bridge engineers every one to ten years. The survey noted that traffic data measurements, such as Weigh-In-Motion (WIM) data, were regularly recorded but not used for the safety assessment and that decisions on bridge maintenance and rehabilitation were more commonly based on the visual condition of bridge components rather than structural safety calculations. One of the weaknesses of the SAMARIS project (SAMARIS, 2006) was the lack of information from the remaining European countries. Furthermore, the information provided by the participating countries did not lead to a straight-forward comparison due to differences in bridge management practices. Although a common inspection protocol does not exist for all Europe and each country is using particular inspection and condition assessment procedures, a common feature divided the inspection process into three main levels: 1) routine inspection (around every 2 years), 2) major (around every 5 years) and 3) detailed inspection (when it becomes necessary). The lack of data and the absence of a common approach in Europe hinder at the moment the possibility of developing a full risk-based inspection program, and therefore other sources of information are sought in this Thesis. In COST 345 report, (Brady et al., 2004) point out that the systematic collection of information carried out by the private sector has led to the loss of valuable information that private companies have no incentive to provide to the administrations if not strictly required by contract. Specifically, the short-term view of the private sector may not be in the best interest of the long-term needs of the public sector especially when addressing assets with 50-200 years lifespan.

In the United States, bridge inspection regulations are established by each state's Department of Transportation (DOT) to comply with minimum requirements outlined by the Federal Highway Administration (FHWA) as set in the National Bridge Inspection Standards (NBIS 2004, 2009). The regulations usually require that routine inspections of every bridge be undertaken every two years. The data

recorded for each bridge are then assembled into the NBI to generate a comprehensive database for all US bridges for use to properly plan bridge maintenance strategies (FHWA, 1995). Recently, the Moving Ahead for Progress in the 21st Century Act (MAP-21, 2012) set the objectives for bridge inspection long term policies and the FHWA proposed an update of the NBIS, to meet the MAP-21 requirements. These objectives include a proposal for departments of transportations to use different bridge inspection intervals based on a bridge's level of risk.

Bridge inspection standard procedures have evolved in the US since the institution of NBIS in 1971, when the bases of inspection policies were first established. A comprehensive summary of the bridge inspection program history in the US is presented by Ryan et al. (2012). Different types of inspections are established with different objectives and degrees of detail. The classification of inspections is commonly accepted in the entire US territory as demanded by the FHWA (T. W. Ryan et al., 2012) and adopted by each state inspection manual published by state departments of transportation to complement the specifications set by the AASHTO (American Association of State Highway and Transportation Officials) Manual for bridge evaluation (AASHTO, 2018). This latter document defines seven types of inspection along with their specific objectives. These consist of: inventory (or initial), routine, in-depth, fracture critical member, underwater, damage and special inspection. The focus of this work is on routine inspection. Routine inspections are performed periodically to monitor the trends of deteriorations pointed out in previous inspections, and to update the items in the NBI file related to each bridge. This inspection is generally performed with simple tools and relies on visual observation of the bridge's elements. Inspectors are also required to identify critical locations of the structure deserving special attention and in-depth inspection.

In order to show synthetically the basic standard practice of some European and American countries a summary of the findings is presented in Table 2-1. The objective of this table is to give a first impression of the comparison of the first level of bridge inspection approaches, mostly represented by visual inspection, being a full understanding of each country's policy reached by looking at the corresponding bibliographic reference. For a comprehensive review of the inspection standard practices carried out by different country authorities the reader can refer to SAMARIS (2006) and NCHRP 375 (Hearn, 2007).

**Table 2-1. Summary of visual inspection current practice in different countries.**

| Country | Current practice | Reference |
|---|---|---|
| USA | *Routine inspection*<br>2-year | *Bridge Inspector's Reference Manual*<br>(T. W. Ryan et al., 2012) |
| Canada (Ontario) | *Detailed visual inspection*<br>2-year | *Ontario structure inspection manual*<br>(Ontario Ministry of Transportation, 2008) |
| Spain | *Inspección Básica*<br>15 months | *Guía de inspecciones básicas de obras de paso*<br>(Dirección General de Carretera, 2009) |
| Italy | *Ispezione Ordinaria*<br>2-year | *Linee guida per la classificazione e gestione del rischio, la valutazione della sicurezza ed il monitoraggio dei ponti esistenti*<br>(Ministero delle Infrastrutture e dei Trasporti, 2020) |
| United Kingdom | *General Inspection*<br>2-year | *Inspection of highway structures (CS 450)*<br>(Highways England, 2020) |
| Germany | *Major Test* – 6-year, inspection of all components<br><br>*Minor Test* – 3 year after Major test | *Highway Structures Testing and Inspection (DIN 1076)*<br>(Deutschland Bundesministerium für Verkehr, 1999) |

Table 2-1 shows that a similar current practice based on a time interval between inspections of approximately 2 years based on condition state is observed more or less in most countries inspection programs. Therefore, although this Thesis is focused on US bridges, the concepts here developed can be seen in a broader perspective than just the case of USA.

The MAP-21 (2012) specifically mentions NCHRP (National Cooperative Highway Research Program) report 782 (Washer et al., 2014) as a starting point for a risk-based inspection program, whereas additional work has been published by the same research team (Washer, Connor, Nasrollahi, & Provines, 2016; Washer, Connor, Nasrollahi, & Reising, 2016). Washer et al. (2014) observed that the standard two-year inspection interval may be too conservative for newly constructed bridges in the first ten years of their lives, when they are likely to experience only minor defects, but that the two-year interval may be an

excessively large period for bridges approaching the end of their service lives. The research found that inspection intervals up to 72 months could be applied to bridges in particularly favorable condition in terms of their risk of failure. The work developed in NCHRP 782 defines occurrence factors (OF) as possible causes of failure and consequence factors (CF) as likely outcomes of damage to an element. Both OF and CF are assigned values between 1 and 4 and implemented into a risk matrix similar to the one shown in Figure 2-1 where the top right element has the highest risk and the lower left the lower risk.

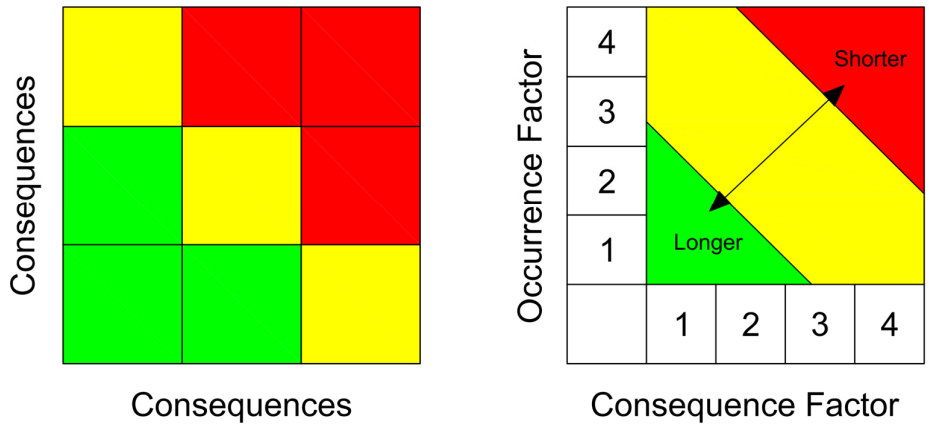


**Figure 2-1. Qualitative risk matrix (left) and inspection interval linked to the risk matrix (right).**

Thus, the NCHRP 782 report proposes a practical approach to relate typical causes of failure and their consequences in a qualitative fashion using condition rating as the basis for assessing risk and a subjective ranking proposed by a panel of experts. It is noted that the NBI condition rating assigns each bridge a value between 0 and 9 where a condition rating of 3 indicates that a bridge is in serious condition due to loss of section, deterioration, spalling, or significant cracking.

The relationship between condition rating historical data and inspection interval was further summarized by Nasrollahi and Washer (2015) who analyzed historical trends of condition ratings to assemble statistical relationships between inspection intervals and bridge condition ratings. They compared the probability of failure to a target probability of failure set by the authority. The link between OC and CF and their application to case studies is performed by Reliability Assessment Panels (RAP) as a group of experts familiar with the infrastructure under study and the inspection process. A main conclusion of Nasrollahi and Washer (2015) work was that the inspection interval could exceed the standard 24 months for those bridges showing good condition rating. An example application of this methodology is proposed for bridges in Chile by Valenzuela et al. (2010) where a RAP of 20 experts subjectively calibrated an equation to define an index of bridge risk-based on bridge condition.

While the Nasrollahi & Washer (2015) work can be suitable to set inspection time intervals by establishing a common target probability of failure for a network of bridges, the work can be improved by considering the consequences of failure so that the target can be set based on risk criteria in keeping with the MAP-21 (2012) requirements. Furthermore, Nasrollahi and Washer (2015) use the condition rating as the basis for defining bridge failure when in reality condition ratings are subjective indicators assigned based on visual inspection related to local deteriorations and damages. It is noted that the reduction in condition rating may indicate a possible reduction in member capacity but it cannot assess the actual capacity. Additionally, the approach does not consider the demand (or the load) on the structure, and relies on a non-objective evaluation of the structural consequences of the observed damage and the global structural safety. On the other hand, load ratings are the result of a structural analysis that takes into account the actual state of the bridge by considering the structural effects of loss of material, bearing misalignment, loss of foundation support, and other relevant factors into a structural analysis model, which gives each deterioration (intensity and location) the appropriate weight into the safety assessment procedure. It is therefore clear that condition rating is not a valid indicator of a bridge's structural safety and that load rating rather than condition rating should be used as the basis for applying risk-based inspection strategies.

Clause 4.2.4 of the AASHTO MBE (2018) mentions that states and the FHWA are responsible for assigning criteria to determine which bridges can have their inspection intervals reduced based on structural capacity and engineering judgment. Similarly, the FHWA Technical advisory T5140.21 (FHWA, 1988) allows increasing the inspection interval for bridges that present particularly favorable conditions (e.g. newly constructed bridges) following accepted engineering criteria. However, in current practice, the possibility of reducing the inspection interval is not normally considered because of the vague criteria of using "engineering judgement" which may be difficult to defend. It is expected that if more objective criteria are developed, the aforementioned recommendation to use of a risk-based approach for condition rating combined with the (FHWA, 1988) advisory would encourage engineers to use risk-based inspection methods for inspection program optimization

The USA infrastructure network currently includes a total of 616,096 bridges listed in the NBI database which combines data provided by every state. This database is public, available online for downloading (FHWA, 2019b) and it contains a specific file for each bridge in the American territory for each year since 1992. The information in each file includes each bridge's location, geometric properties, load rating, traffic data, critical characteristics, posting, inspection interval and condition rating among other useful items. A key information provided by the NBI is the load rating, measured in total tons of live load that the most critical member of the bridge can carry before the member's limit capacity is reached. This load rating can therefore be used to back calculate the structural capacity of the critical bridge member. Thus, as explained above, the load rating is considered to be a better indicator of the bridge's safety than the condition rating which is only a ranking of the apparent deterioration of the bridge members that does not reflect the

inherent capacity the bridge members to carry load. In particular, the evolution of the load rating over time would provide a good indicator of the effect of time-related deterioration on bridge safety.

## 2.2 Structural System Behavior of Bridges

Traditional bridge design and load rating procedures have focused on studying the safety of individual components without explicitly accounting for the reserve strength that the system may have and its ability to continue to carry load after the damage or even the complete failure of one or more components. In recent years, this ability has commonly been labelled as "structural redundancy". Researchers have proposed various definitions of structural redundancy and robustness and methods to quantify them as summarized by Anitori, Casas & Ghosn (2013) and Cavaco et al. (2013). The redundancy of superstructures was studied by Ghosn and Moses (1998) and Ghosn and Yang (2014) in NCHRP reports 406 and 776 who developed procedures to calibrate a system factor that can be incorporated in the design and load rating equations to adjust the resistance factors applied on the nominal resistance given by AASHTO MBE (2018) and AASHTO LRFD (2017). A similar study was carried out for bridge substructures by Liu et al. (2000) in NCHRP report 458. In the work by Ghosn and his colleagues, a redundant bridge is defined as a structure capable of resisting additional load after one of its main member fails by redistributing the load among the remaining members. The three aforementioned NCHRP studies outline deterministic and probabilistic approaches to numerically calculate the redundancy and robustness of bridge superstructures and substructures. For example, a quantification of redundancy can be achieved by defining redundancy as the additional structural reliability provided by the system compared to the reliability against first member failure. The reliability measure of redundancy is described by Equation 2-1:

$$\Delta\beta_u = \beta_{system} - \beta_{member} \tag{2-1}$$

where $\beta_{member}$ is the reliability index related to the failure of one member; $\beta_{system}$ is the reliability index related to the failure of the system.

In order to ensure that the bridge is able to carry a part of the load (for example emergency vehicles) while damaged an additional structural robustness measure is given in Equation 2-2:

$$\Delta\beta_d = \beta_{damaged} - \beta_{member} \tag{2-2}$$

where $\beta_{member}$ is the reliability index related to the failure of one member; $\beta_{damaged}$ is the reliability index related to the failure of a system in a damage state.

The relative reliability measures $\Delta\beta_u$ and $\Delta\beta_d$ are used to define redundant and non-redundant bridges by comparing the values calculated for an individual bridge structure to threshold levels labeled as target relative reliability indices. The relative reliabilities calculated for different bridge configurations are used to calibrate system factors that can be easily implemented by bridge engineers during design and load rating processes.

Because an accurate risk assessment requires the consideration of system failure rather than just member failure as traditional load rating processes do, similar concepts to those proposed in NCHRP reports 406 (Ghosn & Moses, 1998), 776 (Ghosn & Yang, 2014) and 458 (Liu et al., 2000) for accounting for system behavior and recognition of redundant structures should be used and implemented into the structural analysis process to define the risk of failure of bridges and help define an optimum inspection interval.

A risk-based assessment of bridges should also account for the fact that the nominal legal loads used for rating existing bridges in AASHTO MBE (2018) or the design loads set for new bridges or inventory ratings as set in AASHTO LRFD (2017) do to not accurately model the load demand on highway bridges. Live loads are intuitively the most uncertain and challenging parameters needed to model the global probabilistic safety of bridges evaluated using structural system reliability analysis. A comprehensive historical perspective of the evolution of nominal vehicular live loads in America can be found in the Transportation Research Board (TRB) circular E-C104 (2006). For the purposes of this work, it is worthwhile recalling that typical bridge designs before 1993 were performed using the HS-20 live load. In 1993, AASHTO introduced the HL93 live load to ensure that bridge member designs achieved a uniform level of reliability which the older specifications did not achieve.

Because the nominal live load models were meant to ensure that bridge designs achieve uniform reliability but by themselves do not reflect the actual maximum live loads applied on bridge structures, several researchers developed procedures to use vehicular monitoring instrumentations to collect data that can be used to update the code-specified live load models and to obtain a more accurate evaluation of the safety of existing structures. For example, Ghosn et al. (2011) and Sivakumar, Ghosn, and Moses (2011) provide guidelines describing how to collect weight in motion (WIM) data from traffic monitoring stations and use these to calibrate a probabilistic live load model to evaluate the safety and reliability of existing structures. Similar procedures can be implemented to include the statistical characterization of actual live load and be directly used in reliability analyses of bridges and risk assessment procedures. In particular, (Anitori, Casas, & Ghosn, 2017) developed models based on New York state WIM data that are appropriate for the advanced structural analysis and assessment of bridges including finite element based reliability analysis.

## 2.3 Risk-Based Methods in Bridge Engineering

Once the demand, in the form of live load, and the response, in the form of bridge capacity, are defined probabilistically the probability of failure of bridges can be calculated and linked with the consequences of failure to quantify the risk of a bridge's failure. Risk-based approaches are used in different fields of engineering to evaluate the efficacy of engineering processes in terms of meeting the expectation of society in a most optimum way. Risk analyses provide an answer to the intuitive concept which recognizes that even a structure that has a very small margin of safety with respect to the demand can still be acceptable if the consequences of its failure are small. For example, a bridge with little traffic volume serving a remote rural area should have a lower priority for future maintenance investment than a bridge with the same safety margin (or probability of failure) but located along a major route and thus associated with a failure with high impact in terms of economic losses for its users and the community it serves.

A challenging factor in calculating the risk associated with the failure of a structure is related to the evaluation of the consequences of failure. Several studies have been published about this topic for different engineering applications. For building structures, Janssen et al. (2012) set a list of consequences to consider when performing a risk-analysis and they give some guidance for calculating the associated cost. Imam and Conover (2012) outline a similar list for bridge structures which can be of value for bridge related risk assessment studies.

Tanner and Hingorani (2015) review the application of risk methods to building structures focused on European regulations, setting risk acceptance criteria related to individuals and society and distinguish between the risk of new and existing structures. In this context, the occupancy area of different types of buildings was divided into two groups: a) low occupancy buildings such as residential buildings, and b) high occupancy such as assembly halls, theaters, cinemas and grandstands. This classification was used to calculate the risk associated with different structural failure modes. The consequence of failure is represented by the number of fatalities linked to a specific occupied area in a type of building and is compared to a set of desirable risks to persons and to society to determine a non-subjective target reliability index value for each building class that can serve as a rational basis for code calibration.

Economic factors are considered by Steenbergen et al. (2015) for structures in general. They point out that risk analysis should be used to minimize the total service-life cost. They observed that economic losses may be of little importance when compared to the loss of life. Steenbergen's team (2015) also studied a database of bridge collapses, excluding failures during construction, and they proposed a linear equation to determine the number of fatalities as a function of span length. Specifically, they observed that reliability indices based on economic cost vary with time and decrease as the design life is approached. A minimum level of reliability is defined based on ensuring human safety.

Along the same line COST action 345 (Brady et al., 2004) provides a broad view of European countries infrastructure maintenance procedures and an estimation of bridge replacement and running costs.

Running costs include those due to maintenance, repair renewal, management and inspection. The qualitative risk matrix shown in Figure 2-2 is presented to link the consequences of failure and their likelihood and decide what level of inspection should be conducted.

| | | Probability of hazard occurring | | |
|---|---|---|---|---|
| | | Low | Medium | High |
| Consequence | Low (i.e. no risk to people or property) | Negligible risk Routine inspection | Low risk Routine inspection | Medium risk Increased frequency and/or detail of inspection |
| | Medium (i.e. minimal risk to people, but high cost of disruption) | Medium risk Routine inspection | Medium risk Increased frequency and/or detail of inspection | High risk Assessment required |
| | High (i.e. high risk to people or property, high cost of repair or disruption) | Medium risk Routine inspection | High risk Assessment required | Unacceptable risk Assessment and mitigation required |

**Figure 2-2. Risk matrix to determine the degree of inspection to apply to the structure.**

In the field of life cycle assessment, NCHRP report 483 (Hawk, 2003) provides a comprehensive approach for assessing the life cycle costs of bridges. These include agency cost, such as inspection, demolition, repair and reconstruction including materials, personnel and equipment costs, and user cost including those with detour, crash and bridge work. Life-cycle analyses deal mostly with long term evaluations in terms of structural performances using the reliability index or risk as criteria, therefore they rely on continuous updating of input data on the structure and its function. In the same line of life cycle cost benefit calculation but for a different engineering problem risk-based concepts were recently used by Ryan and Stewart (2020). This study aims at giving insight of the climate change related adaptation for timber power poles accounting for the regional variability of climate change in Australia. In this case, one of the cost elements is represented by the so called "risk reduction value" that is defined as the monetary risk brought by implementing the climate adaptation strategy for power poles. In other words it is recognized that risk can be treated as a cost that is properly scaled according to its probability of occurrence, and therefore be included into life-cycle analyses or cost-benefit of resources allocation as in this Thesis.

The estimation of user costs is of particular interest for the transportation sector, where bridges form key links of the network. In this sense, NCHRP report 824 (Hirschman, Da Silva, Strauss-Wieder, & Tompkins, 2016) assesses the cost of truck freight travel time. A detailed breakdown of transport costs is provided for truck trip alternative analysis where the major truck-related delay costs are identified and divided into direct variable truck transportation cost (hourly value of expected hours of delay), on-dock

penalties due to delivery delay, and cargo related supply chain. The latter set includes the cost of capital incurred from delays in getting intermediate inputs to production facilities, opportunity cost of delayed final sales, administration and management, insurance, product spoilage, reduced production efficiencies.

An interesting analysis of the consequences of failure was performed in NCHRP project 24-25 (Stein, 2007) for failures of bridges due to flood-induced foundation scour as these represent the main cause of bridge failures (Smith, 1976; Wardhana & Hadipriono, 2003). The study by (Stein, 2007) evaluates the consequences of failure using a homogenized economic approach, giving valuable numerical models for practical implementation. Models to obtain dollar amounts for user costs as a function of detour length for bridges exposed to different levels of Average Daily Traffic (ADT), vehicle occupancy, and average value of time for each user as well as direct costs in terms of repair, demolition and reconstruction are provided. It is interesting to observe that NCHRP project 24-25 (Stein, 2007) recognizes the ADT as the unique parameter linked to the number of fatalities unlike Steenbergen et al. (2015) that refers to bridge span length. It appears reasonable to conclude that, due to the small number of bridge failures, it is difficult to identify the main factors that determine the number of fatalities which probably depends on both factors as well as other factors such as the distribution of traffic in different seasons, days of the week, or the hours of the day.

Given the current emphasis on sustainability and the ramification on the health of the community affected by bridge failures and associated congestion and traffic disruptions, researchers have also included environmental costs in their assessment of the costs of bridge failures. Environmental costs are defined by the impact on human health and climate related to several pollutants that are introduced into the atmosphere after a failure event occurs and the associated increased traffic congestion and changes in detour paths. These pollutants are identified by Ahn et al. (2013) and guidance is provided on the economic impact on society in terms of monetary expense per travelled distance by the FHWA (2012) among other studies.

## 2.4 Chapter conclusion

Previous research efforts outlined in the different sections of this chapter highlight current work in both Europe and the US to develop inspection procedures based on rational risk-informed principles. In fact, researchers have already recommended procedures in that vein. In the US a database of bridges (NBI) is available in the public domain, which makes the research effort applicable to various structures rather than focused on individual bridges as usually done in Europe. This partly justifies the focus of this work on US bridges. However, even though much of the community agrees that a risk-based approach represents the most effective method to manage existing bridge inspection programs, its implementation in routine engineering practice remains a challenge that requires additional work. In fact, the basic concepts of risk analysis have been well known for a long time, but it is important for researchers to synthetize them, extract only the relevant parts and provide a simple tool that can be implemented in bridge management practice. The review of existing literature on the subject indicates that the following critical tasks still require special attention:

1) Assessment of likelihood of failure based on rational calculations instead of qualitative considerations.
2) Proposing a comprehensive quantitative assessment of failure consequences including environmental aspects for risk application.
3) A clear step-by-step procedure for the application of risk-based concepts for practicing engineers.

# 3 Analysis of Bridge Database

The NBI is a collection of files describing the most important characteristics of the bridges in the U.S. The number of bridges in the NBI database is approximately 600,000. The bridge data are recorded and updated annually by the state Departments of Transportation (DOT) and published by the Federal Highway Administration (FHWA) in a standardized format (FHWA, 1995). The file entries provide basic information (labelled as items) for each bridge including its location, type of service, traffic indices, detour length, geometry, topology, deterioration condition, and other inspection related data. The information is used by agencies to plan budget allocation and to keep bridge conditions under control. The backbone of each bridge entry is represented by the different reports, which are not in the public domain and thus not available for this work, that describe with high detail the operations carried out for each bridge during its service life. These reports include inspection reports, information on the repairs, element replacements and safety assessments performed over the years.

Bridge NBI annual updates are available for download (FHWA, 2019b) starting from the year 1992. This historical perspective allows for studying changes of bridge conditions over time, with the understanding that the causes of the changes for any bridge condition are usually difficult to assess. For example, condition ratings or load ratings may show an increase from one year to another year, and although one can assume that a repair or replacement has taken place for that specific bridge although no direct mention of the actual reasons for that performance increase is given in the NBI files. Likewise, bridge condition rating decreases may be assumed to be linked to deterioration but no explicit explanation is provided in the NBI entries.

Assessing the safety of bridges between inspection cycles requires an estimation of the level of additional deterioration that may take place in the short term and how this deterioration would reduce the load carrying capacity of these bridges. Because such information is not readily available, the objective of this chapter is to develop an approach that utilizes raw NBI bridge data to model a bridge's structural performance in terms of the system's load carrying capacity and its evolution over time due to the deterioration of its constituent materials.

## 3.1 Definition of Bridge Population Set

A set of bridges is extracted from the NBI database for New York state bridges (approximately 17,000 bridges) to meet the objectives of this work. The bridge selection criteria are divided in several parts:

1) Only bridges in the State of New York are considered. This work is focused on NY State bridges because the Weigh-In-Motion (WIM) truck traffic information available for this study had been collected at WIM stations in New York.
2) Only steel-concrete composite bridges are considered. This structural type is typical in the US in general and in NY State in particular.

3) Only bridges whose Load Factor Rating (LFR) is recorded in the NBI files are considered because they represent the majority of cases and allow for a uniform approach for calculations.
4) Only bridges for which photos are available are considered (source Google Maps Street view). These photos will help determine the number of main girders in the bridge to complement the dimension data available in the NBI database. In fact, in order to correctly calculate the structural capacity of a bridge it is necessary to know the number of beams of the superstructure from photos available on the internet. This requirement has imposed an important limitation on the number of bridges that can be studied. The picture extraction process is shown in detail in Appendix A for an example bridge.

After point 1 to 3 are applied to the database a set of 6412 bridges are filtered, and after point 4 a total of 279 bridges representative of the former group is extracted. In order to keep the representability of the full 6412 bridges a configuration analysis is performed. Specifically, it is of interest to ensure that all ranges of load rating, detour length, span length, ADTT and bridge width are covered. The general picture of these four variables in the bridge group is shown in the four subplots of Figure 3-1.

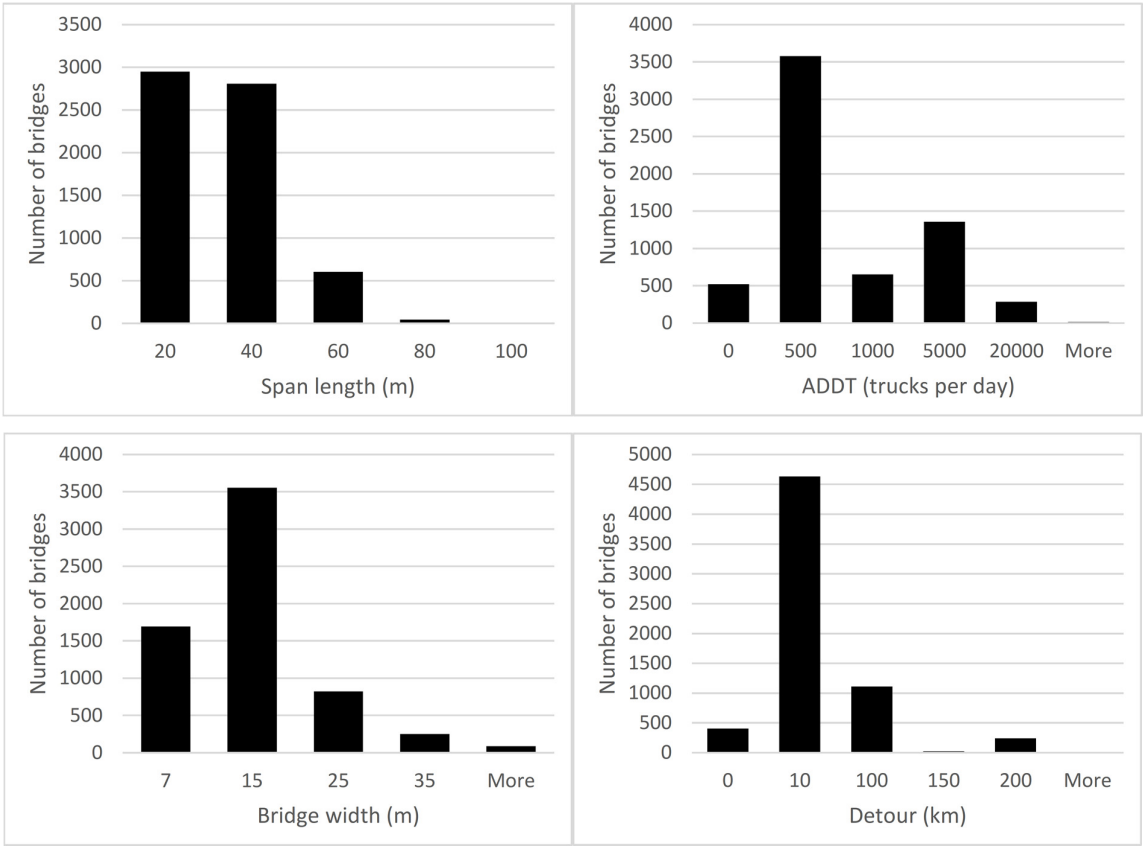


**Figure 3-1. Statistics for the 6412 bridge subset in terms of span length, ADDT, bridge width and detour length.**

Looking at these statistics the subset defined by applying the 4th filter of the former list to ensure that the new bridge set is defined as much as possible by the permutation of the parameters listed in Table 3-1, leading to a final subset of 279 bridges labelled as *set 1*. The statistics for the for *set 1* in terms of load rating, detour length, span length, ADTT and bridge width are shown in Figure 3-2.

**Table 3-1. Bridge properties permutation for the final filter.**

| Span length | ADDT | Width | Detour |
|---|---|---|---|
| m | trucks per day | m | km |
| 20 | 0 | 7 | 0 |
| 40 | 500 | 15 | 10 |
| 60 | 1000 | 25 | 100 |
| 80 | 5000 | 35 | 150 |
| 100 | 20000 | | 200 |

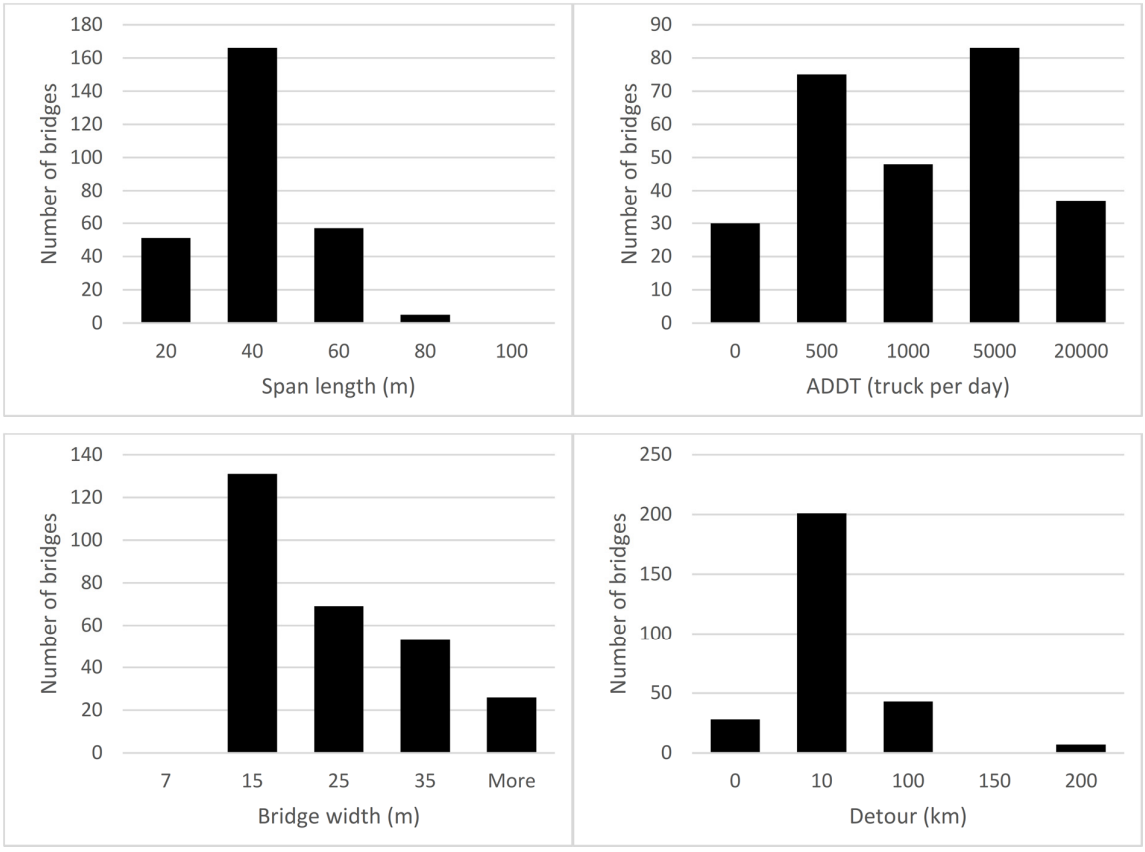


**Figure 3-2. Statistics for the 279 bridge subset in terms of span length, ADDT, bridge width and detour length.**

It is noted that is not the purpose of the filtering process to match the histograms of Figure 3-1 with the ones of Figure 3-2. Instead, the presence of at least one of each bridge configuration generated by the permutation of the parameters in Table 3-1 is ensured and for each of them pictures are found to determine the number of beams. Therefore, it must not surprise the difference in the percentage of bridges with 20 m span length, which is more dominant in the first set than in *set 1*.

As already mentioned, the last step of this database filtering process is represented by the online research of pictures from which the number of beams is determined. The geographical localization from latitude and longitude values along with the pictures found online with the corresponding sources is shown in Appendix A.

The load carrying capacity of each bridge in this subset is calculated and the cost of failure is estimated to finally determine the risk of its failure. It is noted that the database under study can be easily refined and expanded in future works as additional details on bridges of interest are made available.

## 3.2 Load Rating Methodology

In this work, the capacity of each bridge is calculated from the operating Rating Factors (RF) stored in NBI item 64. This parameter represents the capacity of the bridge in terms of the maximum permissible load level to which the structure may be subjected depending on the rating vehicle's configuration and is expressed in total mass in metric tons. The rating vehicle's classification is also expressed in metric tons where, for example, MS18 represents the HS-20 Legal truck having a total mass of 32.4 metric tons. It is recalled, that the truck number identifier for the HS- series gives the sum of the load of the drive axle plus the axle loads under the trailer. For the purpose of load rating the AASHTO Manual for Condition Evaluation of Bridges (AASHTO, 2003) allows different methods for load rating. These include the Load and Resistance Factor Rating (LRFR) method, in addition to the traditional Allowable Stress Rating (ASR) and Load Factor Rating (LFR) method (Mlynarski, Wassef, & Nowak, 2011). The Federal Highway Administration (1995) mentions that the Load Factor Rating (LFR) method is the preferred method even though it gives the option state agency to express load ratings in any other method and units, all of which are listed in item 65 of the NBI as outlined in Table 3-2.

**Table 3-2. Available rating methods.**

| Code | Description |
|---|---|
| 1 | Load factor (LFR) reported in metric tons using MS18 loading. |
| 2 | Allowable Stress (ASR) reported in metric tons using MS18 loading. |
| 3 | Load and Resistance Factor Rating (LRFR) reported in metric tons using MS18 loading. |
| 4 | Load testing reported in metric tons using equivalent MS18 loading. |
| 5 | No rating analysis performed. |
| 6 | Load Factor (LFR) rating reported by rating factor (RF) method using MS18 loading. |
| 7 | Allowable Stress (ASR) rating reported by rating factor (RF) method using MS18 loading. |
| 8 | Load and Resistance Factor Rating (LRFR) rating reported by rating factor (RF) method using HL-93 loading. |

Load Factor (LFR) rating method is described in AASHTO MBE (2018) Appendix A, both for intact and deteriorated bridges and consists of the following rules:

1) Both the live load $\gamma_{LL}$ and the dead load factor $\gamma_{DL}$ are 1.3.
2) A single MS-18 (HS-20) rating truck is used for the analysis weighing 325 kN.
3) The dynamic amplification is calculated with the expression $IM = 1 + \frac{50}{(0.3\,L+125)} \leq 1.3$ (with $L$ the span length in meters).
4) The lateral load distribution factor for most two-lane girder bridges is equal to $DF = S/1.7$ where $S$ is the spacing between main longitudinal beams (with $S$ expressed in meters).

Operating load rating ($RF$) and bridge capacity ($C$) are therefore related to each other by the Equation 3-1:

$$RF = \frac{C - \gamma_{DL} DL}{\gamma_{LL}\ LL\ \ IM\ \ DF} \tag{3-1}$$

where $DL$ is the dead load effect, $LL$ is the live load effect.

To find the capacity $C$ given the rating factor, RF, the live load LL, impact factor IM and distribution factor DF, it is necessary to know the dead load DL. The dead load itself depends on the member dimensions which are not provided in the NBI data files. The procedure can be represented in terms of minimizing a tolerance tol which gives the difference between the estimated capacity $C$ and the combination of factored dead and live loads where the dead loads are estimated based on member dimensions that are consistent with

the capacity $C$. This relationship can be represented as the minimization of the term $tol$ given in Equation 3-2:

$$C - (RF\ IM\ DF\ \gamma_{LL}LL + \gamma_{DL}DL) < tol \tag{3-2}$$

The calculation of the single terms of Equation 3-2 and the iterative calculation to solve it are described in the next section.

## 3.3 Back Calculation of Bridge Member Capacity

The objective of Equation 3-2 is to find a solution for the member capacity $C$ able to minimize the tolerance of the inequality.

The MS-18 rating vehicle has the configuration presented in Figure 3-4 where x gives the location of the front axle of the truck relative to the left end of the bridge. Xg gives the location of the center of gravity of the truck relative to the front of the truck. The live load effect $LL$ can be calculated with an MS-18 truck located on the influence line of the considered effect such as the one shown in Figure 3-3.

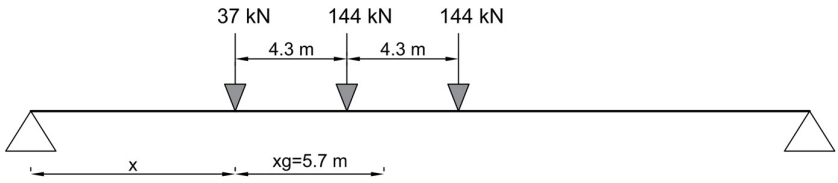


**Figure 3-3. Live load beam model.**

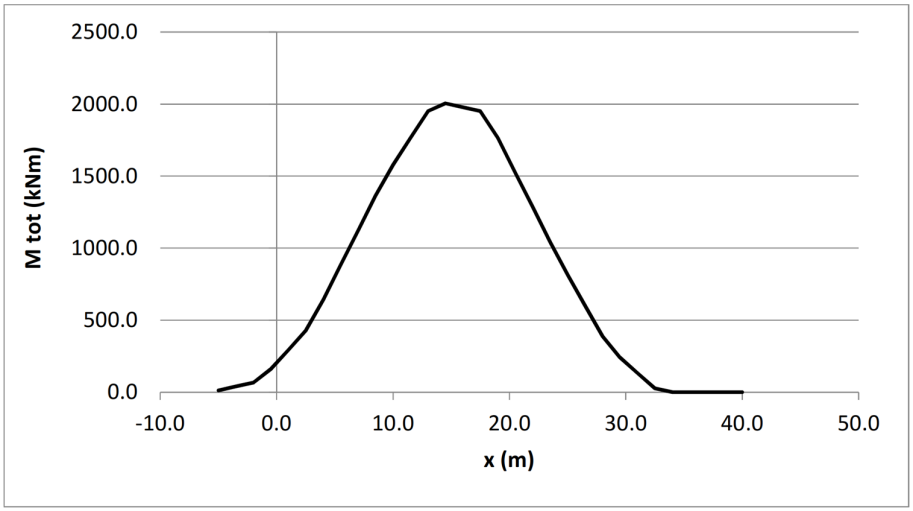


**Figure 3-4. Influence line example for a 30 m bridge.**

In order to automate the live load calculations these are repeated for a set of generic span lengths to give a curve of maximum live load moment effect versus span length as shown in Figure 3-5. The maximum moment load effects in Figure 3-5 are normalized relative to the maximum moment produced by a point load having the same weight of the MS-18 truck (325 kN).

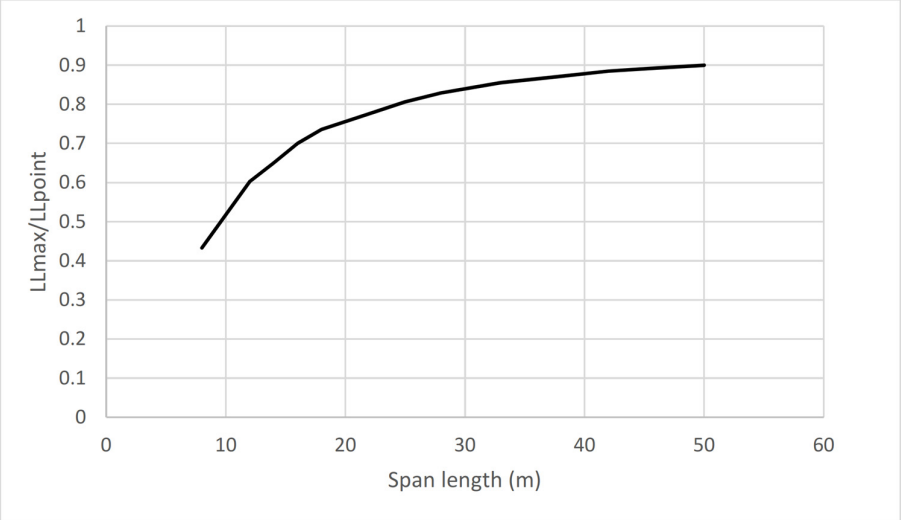


**Figure 3-5. Normalized MS-18 truck effect versus span length.**

The capacity term is calculated using the following simplified composite beam criteria.

- The slab thickness is 20 cm per experience of typical 8 in slab thickness observed in composite bridges. The material considered in this study for the concrete deck is 24 MPa (3.5 ksi).
- The ratio beam depth/span length $H/SL$ is kept between 0.033 and 0.036. The recommendation is taken from AASHTO LRFD (2017) Table 2.5.2.6.3-I.
- The web thickness is $w_t = H/150$. This recommendation is the minimum proportion to avoid local buckling in the web, and it is therefore used as a dimensioning criteria for unstiffened webs as per AASHTO LRFD (2017) 6.10.2.1.1.
- The flanges width is $b_t = b_c = H/2$. The flange width is established from engineering judgement being the code minimum recommended $b \geq H/6$ as per AASHTO LRFD (2017) 6.10.2.2-2.

- The top flange thickness is $t_c = H/24$. This value is recommended by AASHTO LRFD (2017) 6.10.2.2-1.
- The steel used for the calculation is 345 MPa yielding strength (50 ksi).

The bottom flange thickness $t_s$ is changed iteratively and both the capacity $C$ and the dead load $DL$ are updated at each iteration. The bottom flange thickness providing the smallest tolerance $tol$ is selected to represent the steel beam design. This back-calculation is used to regenerate the geometry of the steel beams of the set of bridges under study (*set* 1) that is not explicitly reported in the NBI database entry and is necessary to perform the structural analysis at all levels (system and member). A detailed example of the capacity calculation of the composite member is presented in Appendix C.

Separately, the transverse reinforcement of the concrete slab is designed according to AASHTO LRFD (2017). A detailed example of this calculation is provided in Appendix D.

## 3.4 Probabilistic Member Deterioration Model

The historical data withdrawn from the NBI database can be used to analyze the deterioration trend of bridges over the years. In this case the load rating recorded in *item 64* should include loss of steel thickness due to deterioration as well as other interventions such as repair or element replacement. A different set of bridges (different from *set 1*) is considered for the deterioration part. In fact, as will be shown in further sections, several bridge deterioration trend data cannot be used and *set 1* would result in a too small population. In the next sections the criteria to select *set 2* bridges and how they are used to come up with an annual deterioration ratio are explained.

### *3.4.1 Bridge data and Load Rating historic data*

The historical data extracted from the NBI database can be used to analyze the deterioration trend of bridges over the years. It is assumed that reduction in the load rating recorded in *item 64* of the NBI is primarily due to loss of steel thickness due to corrosion while increases in load ratings are due to interventions such as repair or element replacement. A different set of bridges than *set 1* is considered for modeling deterioration effect to consider a larger number of bridges. Therefore, a new *set 2* of bridges is selected as explained below.

### *3.4.2 Bridge data and Load Rating historic data*

The 2018 NBI database for NYS consists of 17521 bridges 2426 of which are simple span steel-concrete composite bridges. Load rating data are available for each of these bridges for every year since 1992. Figure 3-6 gives the load rating (LR) in metric tons for three example bridges over the years.

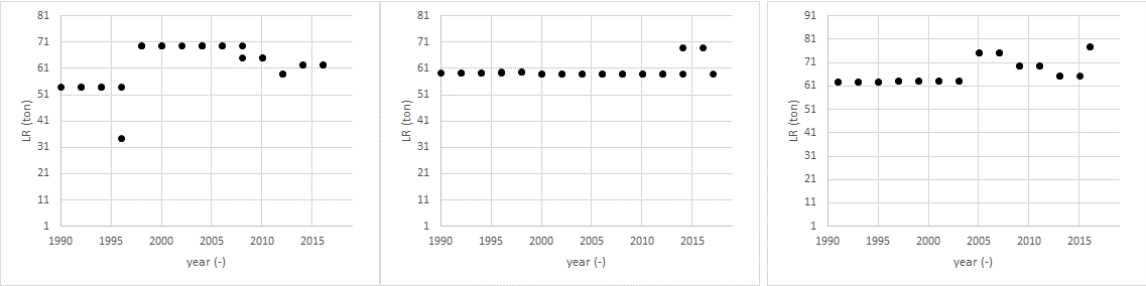


**Figure 3-6. Bridge 000000001001439 (left), bridge 000000001001639 (center) and bridge 000000001011240 load rating over year of inspection.**

Several observations can be made from the plots in Figure 3-6:

1. The load factor is often increasing. It is assumed that it is due to a repair which would improve member capacity.
2. More than one load rating are given for some years. For example, for the left plot (Figure 3-6) there are 2 values for the rating in 1996. Specifically, a value of 54 tons is recorded in the NBI data of 1997 and 34.4 tons in the data of 1998. There is not enough information to understand the reason behind this difference. It is possible that the 1996 inspection report information is reevaluated in subsequent years.
3. The load rating values remain constant for many consecutive years. This may indicate that even if deterioration is taking place, only significant levels of deterioration would lead to reduction in load rating.

The long periods of time during which the load rating remains essentially unchanged may represent what one may call “incubation periods” before the inception of serious degradation in the structural capacity of the bridge members. This incubation period may depend on many hard to quantify factors, such as the age of the bridge, the quality of the construction and the material properties, and the type of previous repairs if any. The data also show that once deterioration commences, it leads to a reasonably constant rate of reduction in the load rating (see Figure 3-6 left). Because it is difficult to determine the incubation period, for the purposes of this study, it is assumed that the risk assessment is being undertaken either at the onset of or during the course of degradation. Because of the observed constant rate of reduction in the load rating after the onset of deterioration, in this report the deterioration of bridges is quantified using an annual deterioration rate that represents the yearly decrease in load rating. Even though the reason for the decrease in the load rating is not available, it is further assumed that the most relevant deterioration process is that of the corrosion of the primary steel girders.

A preliminary filtering is needed to remove all the bridge entries that are not valid according to a set of criteria that are outlined next:

1) Different rating methods are used in the US and their associated load rating values are recorded in the NBI files. Because the most common rating method is that labeled as #1 in Table 3-2, only load factors calculated with that method are used in these calculations to maintain consistency.
2) Spikes in the load rating historic data are those that show a load rating value at time T, $LR(T)$, higher from those at time T+1, $LR(T+1)$ and time T-1, $LR(T-1)$ where $LR(T+1) = LR(T-1)$. This situation is illustrated in Figure 3-7, where the spiked observed in 2015 is considered as an erroneous entry.

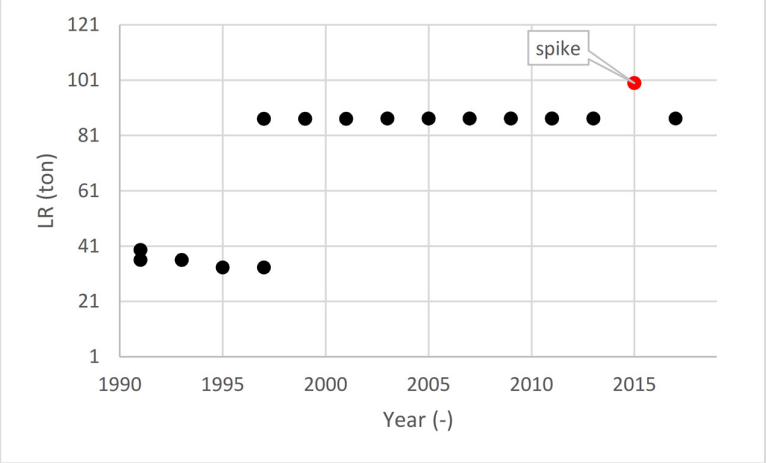


**Figure 3-7. Example of spike in load rating.**

3) If different load rating values are recorded in the NBI files for the same year, the average of these is considered for that year. For example, in the plot shown in Figure 3-8 the final load rating for the year 2008 value is calculated as (65.3+69.9)/2=67.6

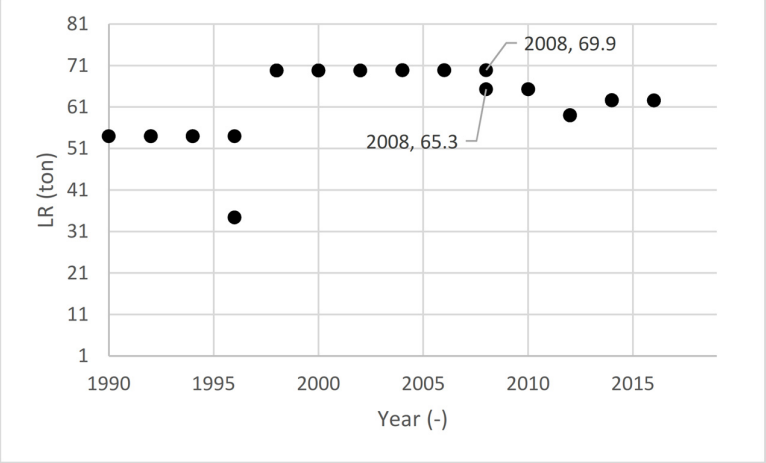


**Figure 3-8. Example of different Load Rating for the same year.**

4) The last acceptable data point $LR_n$ that ends a series of decreasing load rating values is the one rating $LR_n = LR(T)$ that is lower than the one that comes after it $LR(T+1) \geq LR(T) = LR_n$. An example is shown in Figure 3-9.

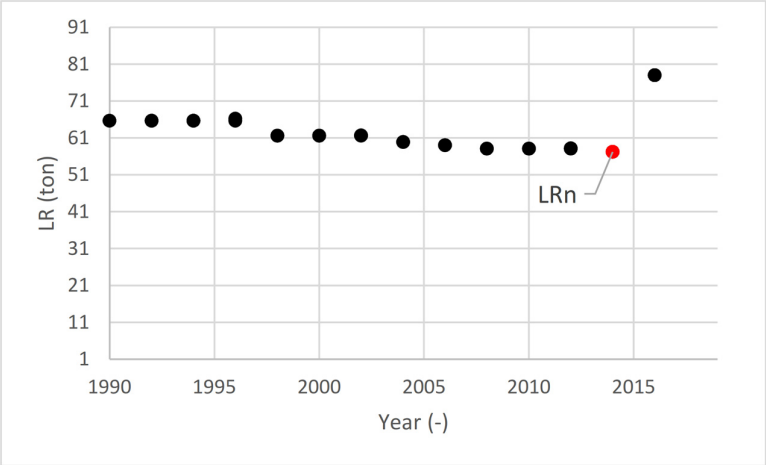


**Figure 3-9. Example of last valid point in the load rating historic series.**

5) The first acceptable point $LR_0 = LR(T)$ in a series is found going backwards from $LR_n$ until the following inequality is verified $LR(T-1) \leq LR(T) = LR_0$. An example is shown in Figure 3-10.

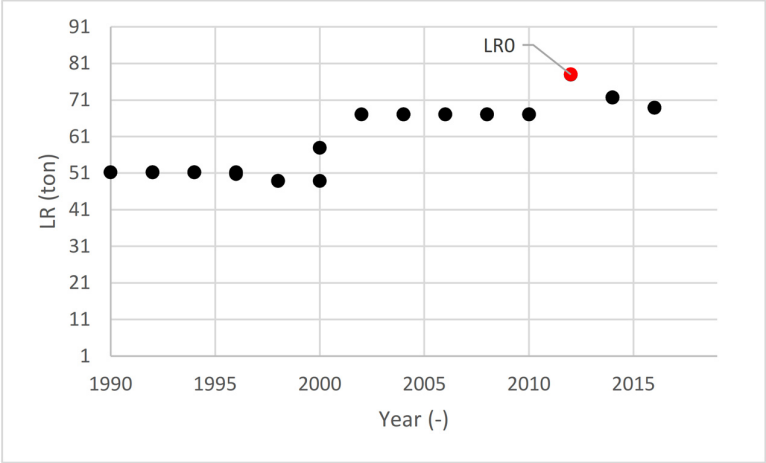


**Figure 3-10. Example of first valid point in the load rating historic series.**

6) Once $LR_n$ and $LR_0$ are identified, the values in between may be fitted with a straight line, as shown in Figure 3-11.

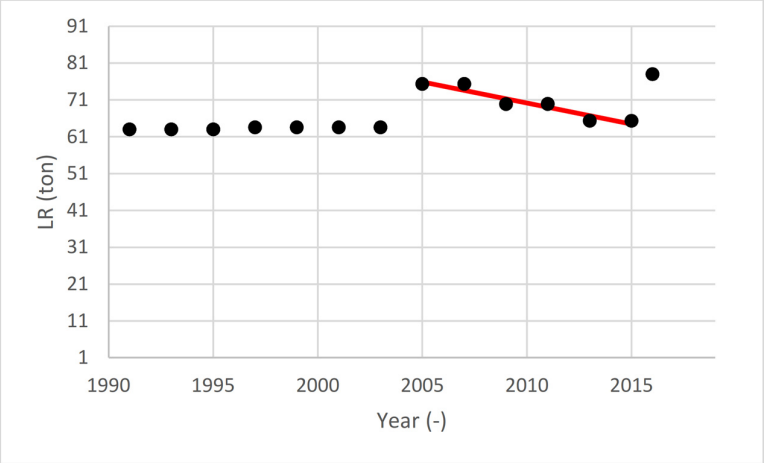


**Figure 3-11. Valid load rating range and linear fit.**

7) The minimum number of years over which the deterioration rate is calculated is 3 years because 2 data points are too few to establish a trend. For example, the load rating series plotted in Figure 3-12 is ignored.

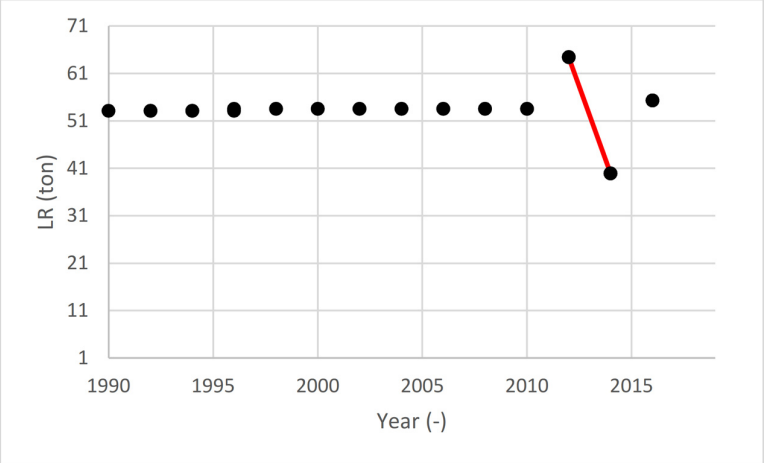


**Figure 3-12. Discharged data series (too few valid data).**

8) Once a valid set of deteriorating load rating values is established, deterioration rate is calculated from the slope of the linear fit. A calculation example is presented in Appendix B.

## 3.5 Multiple bridge data fitting

The filter described in the previous section is applied to the entire population of bridges in NYS to find the population of bridges with a valid deterioration ratio. From the original 2426 bridges, 1330 bridges present a valid decreasing load rating deterioration and can therefore be labeled as *set 2*. The results are

sorted and organized into a cumulative distribution plot in order to represent the deterioration ratio as a statistical variable (Figure 3-13).

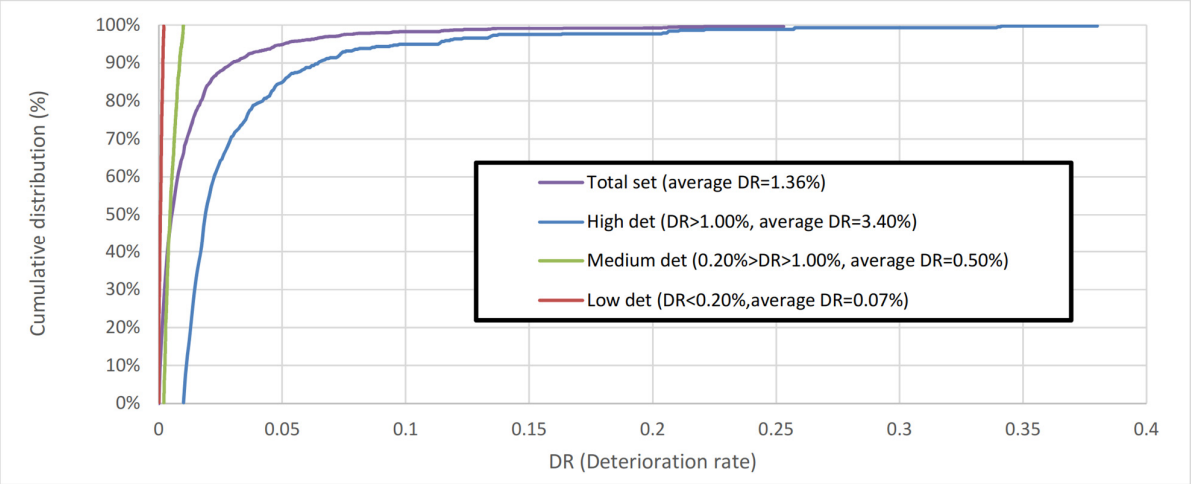


**Figure 3-13. Cumulative distribution of the deterioration Rate (DR).**

As can be seen from Figure 3-14, the purple line represents the cumulative distribution of the entire *set 2*, with an average DR=1.36%. However, it is found convenient to group the bridges into three groups of high (DR>1.00%, average DR=3.40%), medium (0.20%>DR>1.00%, average DR=0.50%) and low (DR<0.20%,average DR=0.07%) deterioration rate. The group boundaries can be better visualized by cutting off the values larger than 5% as shown in Figure 3-14.

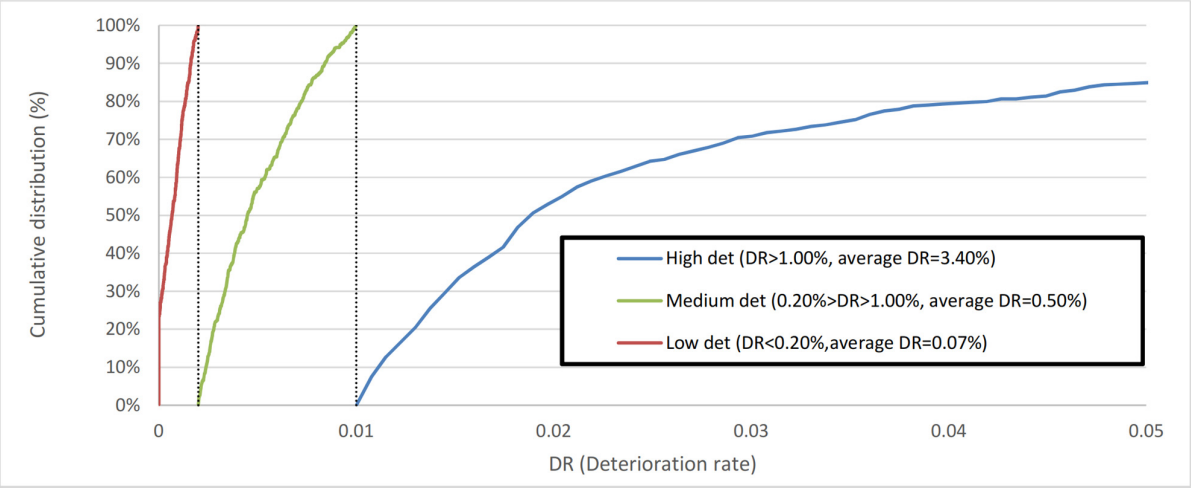


**Figure 3-14. Deterioration rate (zoom view of the x-axis) cumulative distribution and limit values for the deterioration ratio groups.**

As already mentioned, the number of valid bridges is 1330 and the three groups contain 34%, 40% and 31% of the total for the high, medium and low deterioration rate respectively.

The results obtained in this subsection are key for the definition of the response of bridge systems when deterioration is present. In fact, as will be explained in Chapter 4, the deterioration rates obtained will be inputted as random variables to perform a probabilistic simulation for the response of the bridge. Here, it is noted that the analytical description of the cumulative probability distribution of the variable (represented by appropriate probability functions) has been attempted by the author of this work, but no commonly used predefined probability function successfully fitted the distribution of the deterioration rate. For this reason, the input for the simulation process will be a cumulative probability function defined by the extracted discrete probability values.

## 3.6 Reliability of Bridge Inspection

The outcomes of bridge inspections are affected by uncertainties of different kinds and these uncertainties are dragged throughout the entire chain of calculation of the evaluation process. Generally speaking, inspection uncertainties can be divided into probability of detection and sizing accurateness. The probability of detection consists of using a certified result obtained with a precise detection method to compare it the performances of less precise tools. The results are typically presented in the form of true positive, true negative and false positive and false negative. The number of true positive calls divided by the total number of observations for a given defect may be considered an indicator of the probability of detection. Once the defect is known, the accurateness of the defect properties observed by different inspectors can also be statistically analyzed, treated as a regular random variable and described with a statistical distribution function and its parameters.

Also, performances can be evaluated at defect level or at index level. In case of defect level, the effectiveness of visual inspection is studied by looking at the shape and intensity of the defect within the member and it can be compared with inspection efficiencies of other disciplines, as aviation or mechanical engineering. On the other hand, if the performance of the inspection is studied with regard to indexes, there is less focus on the defect itself and more interest in the human interpretation of the observation and its translation into, for example, condition rating.

Phares et al. (2001) and Moore et al. (2001) studied the performances of 49 bridge inspectors from 25 states in the US inspecting six in-service and decommissioned highway bridges. The study was performed with a representative population of inspectors in terms of years of experience and without any knowledge of previous inspection reports or information about the bridges. The study was mostly focused on visual inspection in the context of standard Routine Inspection and concluded that 95% of main bridge elements condition rating may vary within two rating points of the average. The statistical characterization of the condition rating process performed over the six test bridges shows a bias of 1.06 and a COV of 15% for superstructures.

Similarly Tenžera et al. (2012) studied the reliability of visual inspection in the evaluation of bridge condition in Croatia. The difficulties linked to a uniform response in visual inspection is observed to be dependent on a number of psychological factors, such as expectations, attitude, type of education, quantity of information, motivation, sociocultural influences etc. While the effort of the latest inspection strategies is directed towards a reduction of the possible differences in the interpretation of bridge deterioration a relevant effort is still needed. The investigation was performed with 15 inspectors with considerable experience in visual inspection procedures according to the Croatian standards. Five bridges were rated according to a six-category scale from 0 (no damage) to 5 (extensive damage registered). Unlike other studies, where a baseline inspection is present from which a sort of bias factor can be calculated, in this study the baseline is the median of the rating provided by all the inspectors. Thus no bias factor can be calculated. While the study is carried out for different elements of each bridge, the interest of our work is on superstructure, where the standard deviations for the main girder are between 0.4 and 0.7, while for the entire superstructure ranges between 0.7 and 0.9.

It is noted that, while the probability of detection is constant for automated processes it is not observed to be constant for a visual inspection, where a given defect is often associated with a level of deterioration, as pointed out by Faber and Sorensen (2002). For example, fatigue cracks in steel elements can be associated with a probability of detection near to zero when they are almost nonexistent, to 25 mm, where a probability of detection of 0.8 is obtained (Kwon & Frangopol, 2011). In the context of life-cycle cost optimization of bridge elements affected by fatigue crack, Orcesi and Frangopol (2011) studied the contribution of Visual Inspection (VI), Magnetic Particle Inspection (MPI) and Ultrasonic Inspection (USI) and included their probability of detection. Specifically, unlike previously observed, they use a fix 60% for VI for the probability of detection of fatigue cracks.

A comprehensive evaluation of the inspection accuracy and efficiency is performed by Campbell et al. (2019) and further studied by Campbell et al. (2020) where several possible parameters influencing the inspection efficiency are studied for a set of representative inspectors. The following conclusions are highlighted:

- Detection rate mostly increases with increasing time of inspection (but not in some cases). In fact, after many inspections performed on the same bridge and detecting always the same damage pattern, the attention of the inspector to old damages (more severe than the current ones) decreases. This is why rotating inspectors is important but may not be enough if the inspector has access to previous inspection reports.
- Cracks in steel are infrequent and difficult to detect, while corrosion is easier to detect in general. However, it depends on the accessibility of the defect from the inspector.
- The most important factors for inspection accuracy are found to be related with the characteristics of the individual performing it (not in some cases though).

- It is not clear if experience in inspector is a positive or negative feature for damage detection.
- Other factors are temperature and ambient lighting.
- In the paper 30 inspectors were tested. The real damage state of the different structures were a-priori perfectly known.
- The detection rate of fatigue cracks was between 31% and 86%. The mean was 65% and standard deviation 14%.

The state of the art about this topic is still not particularly developed to be applied conveniently in calculations. In fact, these studies should be repeated, several times up to a point where results reproducibility could be reasonably guaranteed, and all the variables into play correctly identified and characterized for a wide population of bridges and bridge types and structural details. In addition, the safety calculations are seldom based on synthetic indices, as load rating in the present work, for which no uncertainty indication is found in literature.

In this work, the statistics obtained by Phares et al. (2001) and Moore et al. (2001) for the condition rating are used as an uncertainty factor for the member capacity inspection. It is noted that also Santamaria et al. (2020) used this information to predict performance of concrete bridges and include numerically the subjectivity of the inspectors. The relationship between condition rating and member capacity are based on the guidelines provided by the Illinois Department of Transportation (2016), where loss of section due to corrosion is linked to condition rating (Figure 3-15).

**CONDITION RATING GUIDES FOR SPECIFIC SUPERSTRUCTURE MATERIALS**

**STEEL SUPERSTRUCTURE**

| Code | Description |
|---|---|
| 8 | VERY GOOD. No visible rust. |
| 7 | GOOD. Some rust may be present but without any section loss. |
| 6 | SATISFACTORY. Initial section loss (minor pitting, scaling, or flaking) up to 2% section loss. |
| 5 | FAIR. Initial section loss up to 10% in critical areas, fatigue or out-of-plane bending cracks may be present in secondary members, arrested fatigue cracks may be present in primary members, hinges may be showing minor corrosion problems, anchor bolt(s) may be missing. |
| 4 | POOR. Section loss up to 30% in critical area, fatigue or out-of-plane bending cracks may be present in primary members, previously arrested fatigue cracks propagating beyond arresting holes in primary members, fatigue cracks in secondary members throughout the bridge, anchor bolts broken on rocker bearings with movement off bearing plate. |
| 3 | SERIOUS. Advanced section loss up to 50%, extensive perpendicular to stress fatigue or out of plane bending cracks in primary members. |
| 2 | CRITICAL. Severe section loss over 50% requires special inspections, temporary supports or repairs may be required to remain open to traffic. The Bureau of Bridges and Structures shall be notified immediately. |

**Figure 3-15. Condition Rating linked to corrosion level as per the Illinois Department of Transportation (2016).**

A linear relationship between these values is built and shown in Figure 3-16.

| CR | corrosion (Illinois DOT) | corrosion (linear fit) |
|---|---|---|
| 6 | 2.0% | 1.2% |
| 5 | 10.0% | 13.8% |
| 4 | 30.0% | 26.4% |
| 3 | 40.0% | 39.0% |
| 2 | 50.0% | 51.6% |

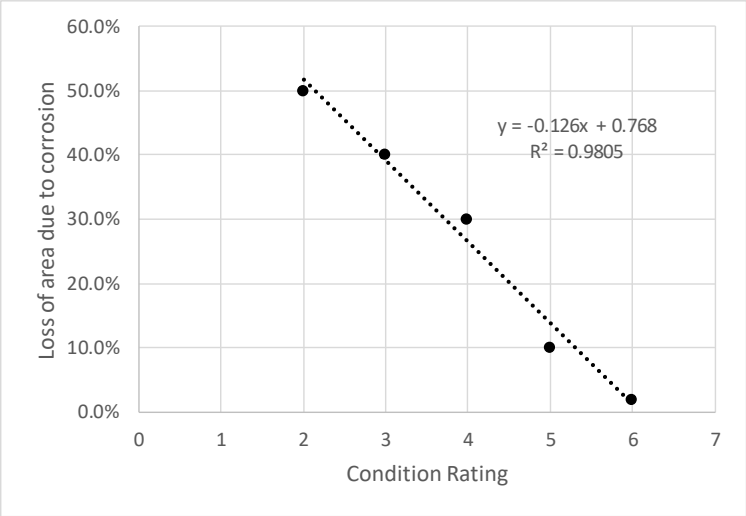


**Figure 3-16. Linear relationship between corrosion level and condition rating.**

The loss of sectional capacity is found by sectional analysis of all bridges in *set 1* to convert the uncertainties in condition rating into uncertainty in member capacity as shown in Table 3-3.

**Table 3-3. Conversion of condition rating bias to capacity bias.**

| CR nominal | CR mean (bias=1.06) | Corrosion nominal (from linear fit) | Corrosion mean (from linear fit) | Capacity bias (from sectional analysis) |
|---|---|---|---|---|
| 1 | 1.06 | 64% | 63% | 0.97 |
| 2 | 2.12 | 52% | 50% | 0.97 |
| 3 | 3.18 | 39% | 37% | 0.97 |
| 4 | 4.24 | 26% | 23% | 0.96 |
| 5 | 5.3 | 14% | 10% | 0.95 |

The results show that the 1.06 bias factor, showing that inspectors tend to overestimate the condition rating by 6% can be represented by a capacity reduction ranging between 0.95 to 0.97. This very narrow range can be conservatively simplified for all levels of corrosion with a single 0.95 factor applied to sectional capacity. This calculation shows that the inspection uncertainties and capacity are linearly related, allowing to extend the same COV=15% observed for condition rating to sectional capacity.

## 3.7 Chapter conclusion

In this chapter, the National Bridge Inventory data were presented with particular focus on the specific entries of interest for this work. It is important to notice that the choice of publishing this large and reasonably

complete amount of data by the US authority, unlike the common practice of most of other countries, increases the volume of research studies on studying the long term performance of the highway infrastructure network with great advantage for the US community.

The bridge entries were filtered to identify a suitable set of bridges for the risk analysis process carried out in this work. Ideally, it would be desirable to analyze the full set of over 600'000 bridges present in the USA. However, the selection of a smaller dataset has several technical reasons. Firstly, the bridge types need to be restricted, because the objective of the study is to develop a framework for the risk analysis of bridges. Because the development of a new framework requires an iterative process that explores various options, it is easier to work with a limited set of data and the process can be eventually implemented for all types of bridges. Also, because the parametric structural analysis needs to be automated and only bridge systems with common characteristics (but different configurations) can be modeled this way a selection is needed. In this case, we have selected to illustrate the proposed framework on simple span bridges, which form a very common type for composite steel girder-concrete deck resisting systems. Another reason is that in this work, as will be explained in Chapter 5, the traffic loads are specialized for the New York state bridge network. Thus, only bridges of this region were considered for consistency. The results of these concepts are the definition of the bridge population labelled as *set 1*.

This chapter proposed an approach for quantifying the reduced performance of bridges over time by studying the load rating historical data available from the NBI database data. It must be noted that the load rating value by itself is an extremely synthetic metric, which needs several assumptions to back calculate the corresponding geometry but can be conveniently used for very common type bridges such as composite steel girders with concrete decks. The results obtained in this chapter will be used to set different inspection intervals based on each of the three deterioration levels. The deterioration rate represents one of the parameters that will be used carry out the calculations for the evaluation of the inspection interval, and therefore the practicing engineer will be required to identify which of the three levels of deterioration is more adequate for the bridge under study. The engineer has the freedom to assess the deterioration category based on the environmental exposure of the bridge to aggressive chemicals, exposure to deicing salts or indirectly to level of snow precipitation. However, in case the data to assess the deterioration rate are not available, the deterioration rate may be estimated from the NBI database historic load rating series as explained in Appendix B.

Finally, a brief description of the state of the art in terms of estimation of the uncertainties associated with the inspection process is outlined for its application in Chapter 6 to the reliability calculation.

# 4 Bridge System Capacity

In order to perform the structural analysis and therefore to calculate the safety of bridges a model to describe the response of the structure resisting the demand of the acting loads must be defined. Structural models may be defined with different degrees of complexity depending on the objective of the calculation, the available structure's data and the availability of computational power, among other factors.

Specifically, simplified line analysis procedures have been routinely applied in the US to study the response of multi-girder bridges, where the distribution of the live load to the most critical longitudinal member can be conservatively defined by simplified formulas such as those provided in AASHTO LRFD (2017) specifications for design and evaluation purposes. A more accurate approach to describe the response of these kind of bridges is the use of finite element models, based on 1-D, 2-D or 3-D elements or a combination of them to give different degrees of detail of the local behavior of the structural elements as well as the overall bridge response. A most typical solution used by structural engineers is to use simple 1-D elements to model the main load carrying components (e.g. longitudinal girders, substructure), and 2-D and 3-D elements for specific critical components, such as connections, bearings and regions of concentrated loads. Furthermore, engineers may have to decide whether to employ simple linear elastic material or more complex non-linear material models. Similarly, the analysis can assume small deformations whereby the initial geometry is essentially maintained throughout the analysis process or a more complex geometric non-linear approach where the geometry of the structures is updated as the load increases.

In this work, bridge superstructures are modeled by means of frame elements organized in a 2-D grillage, where it has been observed that material non-linearity must be included to correctly represent the interaction among members defining the system behavior and geometric non-linearity can be ignored since the deformations of the structure are not large enough to modify the behavior of the structure even up to failure. This approach was found to give accurate results to determine the failure load of typical multi-girder bridges when compared to more advanced 3-D finite element models and experimental test results (Linzhong Deng, Ghosn, Znidaric, & Casas, 2001; Ghosn & Casas, 1996; Ghosn, Casas, & Xu, 1996)

The structural analysis is carried out using the calculation core provided by the OPENSEES framework (McKenna, 2011) and additional TCL (Tool Command Language) code (https://www.tcl.tk/) for pre- and post-processing of the analysis.

To obtain the structural reliability of the bridge systems the nonlinear analysis program is implemented into a simulation algorithm that considers the uncertainties in the input variables and assembles the results in probability distribution functions.

## 4.1 Grillage Analysis Model

The structural analysis carried out in this work is based on the plane frame grillage model. The grillage model consists of a set of orthogonal longitudinal and transverse frame elements each representing a specific load transfer mechanism within the bridge system. The grillage method is developed for composite steel-concrete bridges and the mechanical properties of each element of the grillage are assigned based on the recommendations of Hambly (1991). The different parts of the grillage are shown in Figure 4-1, where the longitudinal and transverse elements are identified.

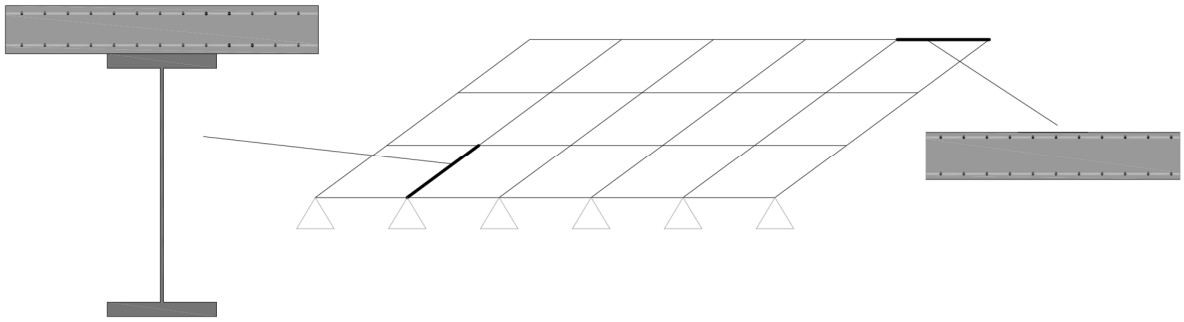

**Figure 4-1. Typical Grillage model for a multi-girder bridge.**

**a) Longitudinal members model the Composite action of the girder and slab;**
**b) Additional transverse member model the effect of cross beams and diaphragms.**

Longitudinal elements are used to represent the flexural behavior of the main longitudinal girders along with the composite action of the concrete slab on top of it, while transverse elements are used to describe the behavior of the slab distributing the load among the longitudinal elements according to their stiffness. A ratio between longitudinal and transverse elements between 0.5 and 2.0 is employed as suggested by Hambly (1991). Multi-girder bridges usually include intermediate cross-frames for the temporary bracing of the girders during construction. The effect of these temporary elements on the behavior of global behavior of the bridge can be generally ignored according to Hambly (1991) and according to an additional check performed in this work. Typical cross-frame steel configurations and their design can be found in Appendix E and their influence in a full bridge model is shown to be negligible as further explained in Appendix F.

Since live loads are usually defined by a group of point loads that can be located anywhere on the bridge surface and the valid load input for the grillage is represented by concentrated loads at the nodes, auxiliary elements can be implemented to connect the actual load application point to the nearest available grillage node, making sure that the stiffness of these elements is small enough to avoid any interference with the bridge element frames (Figure 4-2).

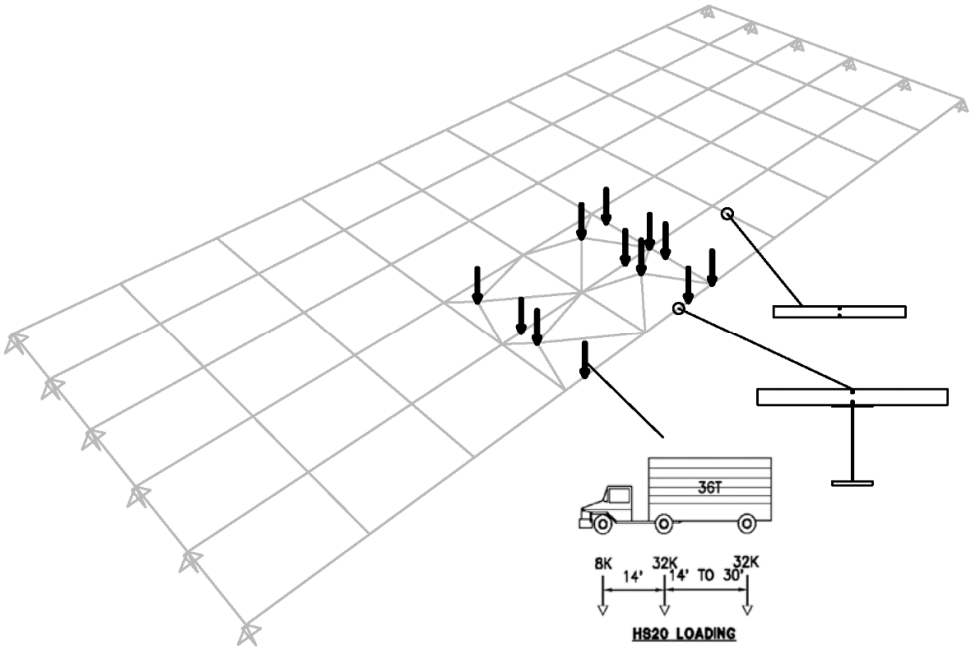


**Figure 4-2. Auxiliary elements for live load application at grillage nodes.**

The initial stiffness of the elements are calculated by the moment of inertia of each frame element's cross section including the composite effect of different materials within the section (steel, concrete, rebar) where necessary. However, as explained in the next section, the initial stiffness of each element is modified as the materials enter their nonlinear ranges to define the evolution of these stiffnesses as the load increases.

## 4.2 Non-linear Behavior of Bridge Members

The linear elastic grillage defined in the initial stages of analysis is a standard tool for bridge design and evaluation, familiar for many engineers Hambly (1991). However, one of the goals of this work is to include an accurate representation of the system behavior of the bridge in the non-linear range of deformation. Specifically, in the push-down analysis that will be explained in the next section, the longitudinal elements yield as the live load increases reducing their stiffness which causes a larger proportion of the load is expected to transfer to other longitudinal elements because of their still large stiffness. Likewise, transverse elements

allow the load transfer from one element to the other and their efficiency depends on the state of their materials that can also undergo non-linear deformations.

The first step to define the non-linear stiffness that will be inputted into the grillage model is to define the non-linear behavior at the material level. Concrete, structural steel and steel rebar stress strain constitutive models are defined, as shown in Figure 4-3.

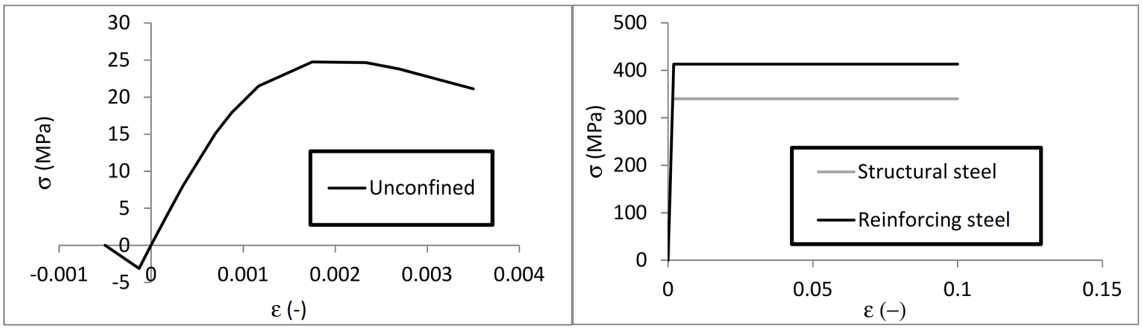


**Figure 4-3. Concrete (left), reinforcing steel and structural steel (right) constitutive models.**

The concrete stress-strain relationship in compression is obtained by the equations proposed by Popovics (1973) as presented in Equation 4-1:

$$f_{ci} = f'_c \left(\frac{\varepsilon_{ci}}{\varepsilon_c}\right) \frac{n}{n - 1 + \left(\frac{\varepsilon_{ci}}{\varepsilon_c}\right)^n} \tag{4-1}$$

Where $f'_c$ is the nominal concrete compressive strength (24 MPa or 3,500 Psi in this work), $f_{ci}$ is the concrete strain at any strain $\varepsilon_{ci}$, $\varepsilon_c$ is the peak strain (0.002 in this work) and $n$ is a parameter depending on the values of the tangent $E_c$ and secant $E_{sec}$ stiffnesses, as specified in Equations 4-2, 4-3 and 4-4.

$$n = \frac{E_c}{E_c - E_{sec}} \tag{4-2}$$

$$E_c = 4700\sqrt{f'_c} \tag{4-3}$$

$$E_{sec} = \frac{f'_c}{\varepsilon_c} \tag{4-4}$$

In Equation 4-3, the tangent stiffness $E_c$ and the concrete strength $f'_c$ must be taken in MPa.

The tensile branch of the stress-strain curve is taken as linear up to the tensile stress $f'_{ct}$ calculated according to AASHTO LRFD (2017) as presented in Equation 4-5:

$$f'_{ct} = 0.62\sqrt{f'_c} \tag{4-5}$$

On the other hand a bilinear symmetric stress-strain curve for steel is used with an elastic stiffness of $E_s = 210{,}000$ MPa, a yielding stress of 340 MPa (50 ksi) for structural steel and of 413 MPa (60 ksi) for rebar steel, and a horizontal plastic range with a ultimate strain of 0.10.

Moment curvature ($M - \varphi$) curves such as that shown in Figure 4-4 are preliminarily calculated to determine the variation of the flexural stiffness of longitudinal and transverse frame elements as they undergo plastic deformation following the stress-strain relationship of the material constituents already described (Figure 4-4).

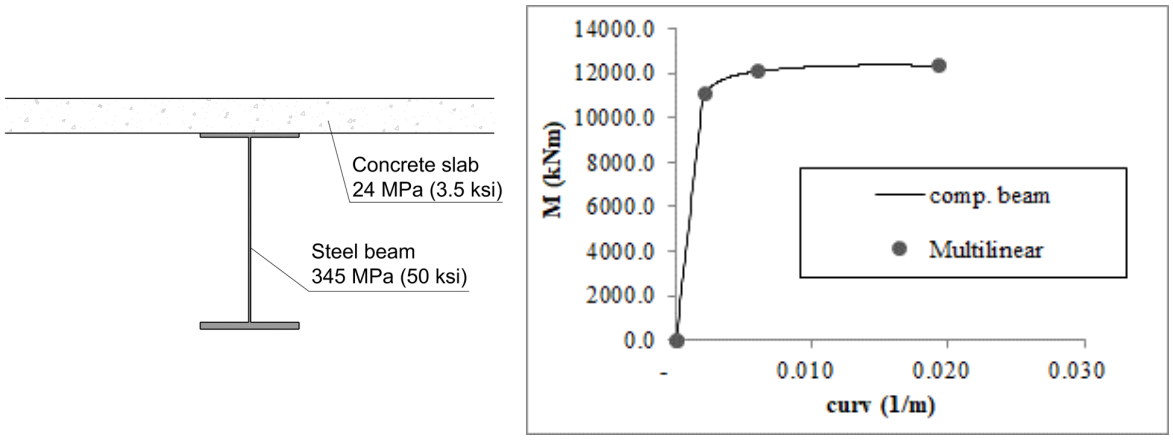


**Figure 4-4. Sectional analysis of the main longitudinal elements.**

Only the positive moments (sagging moments) are considered in the $M - \varphi$ since only simple span bridges are analyzed in this work. However, for members far from the load application where negative moments (hogging moments) may appear, the linear negative stiffness will still be valid since it is expected that these

moments will be small. The $M - \varphi$ curve is simplified to speed up the analysis into three lines defined by the origin and three additional points according to the following criteria:

1) The first point is located where the bottom edge of the beam reaches the yielding strain
2) The last point of the curve is located where one of the materials (usually the concrete) reaches its ultimate strain (0.035 for concrete or 0.10 for steel)
3) Once the first and last points are defined, an intermediate point is located to better approximate the theoretical $M - \varphi$ curve. The intermediate point is iteratively changed to find the optimum position that provides the minimum difference between the area bounded by the theoretical curve and the multilinear curve in the post-yielding range.

While the moment curvature curve correctly describes the flexural behavior of the longitudinal members throughout their length, transverse element present a slightly more complex mechanism. In fact, both positive and negative non-linear behavior must be considered and even though sectional analysis can be performed at the cracked section, the rest of the uncracked member and its tension stiffening effect must be considered. Three stages can be recognized in the flexural behavior of transverse reinforced concrete members as shown in Figure 4-5.

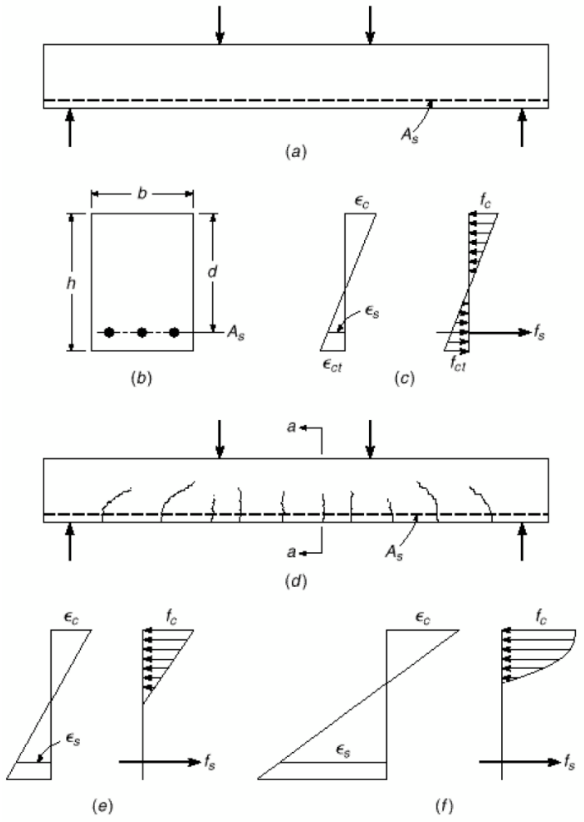


**Figure 4-5. Typical sectional behavior of a cracked section within a reinforced concrete section. Extracted from Nilson (2011).**

Referring to Figure 4-5, it can be observed that in the first loading stage (Figure 4-5 a) the member is still uncracked and every section's (shown in Figure 4-5 b) flexural stiffness can be modeled using the elastic moment of inertia of the gross concrete section so that the stresses in the concrete follow a linear distribution augmented by the contribution of the steel reinforcement (as shown in Figure 4-5 c). As the load increases, equally spaced cracks start to form at the bottom (tension side) of the member (Figure 4-5 d) when the tensile stress of the concrete reaches the modulus of rupture in those sections. The strain and the stress distribution appear as shown in Figure 4-5 e, while between cracks uncracked zones are still present. When the crack develops the bottom reinforcing steel has to absorb the force previously resisted by the concrete in tension but the strains of the concrete in compression are still in the linear range of the concrete stress-strain curve. In the last stage (Figure 4-5 f), as the load on the member increases, the reinforcing steel yields and the compression stresses in the concrete have a non-linear profile up to the failure point that is reached when the top compression concrete strain its limit value.

The flexural stiffness of slab elements, as already mentioned, is a key element to correctly model the force distribution among longitudinal members. For this reason, it is recognized that an equivalent moment of inertia $I_e$ must be considered when some of the sections are cracked while other are not according to the Equation 4-6 (Branson, 1977):

$$I_e = \left(\frac{M_{cr}}{M_a}\right)^3 I_g + \left[1 - \left(\frac{M_{cr}}{M_a}\right)^3\right] I_{cr} \leq I_g \tag{4-6}$$

Where $M_a$ is the moment level under consideration related to the equivalent stiffness, $M_{cr}$ is the cracking moment, $I_g$ is the section gross inertia, $I_{cr}$ is the inertia of the cracked section.

The moment of inertia of the gross section $I_g$ can be found by applying Equation 4-7:

$$I_g = \frac{1}{12} bh^3 + n\left(A_{s,top} y_g^2 + A_{s,bot} y_g^2\right) \tag{4-7}$$

Where $b$ and $h$ are the base and height of the rectangular cross section, $A_{s,top}$ and $A_{s,bot}$ are the top and bottom steel areas respectively and $y_g$ is the centroid of the cross section.

The cracking moment $M_{cr}$ can be found by applying Equation 4-8:

$$M_{cr} = \frac{f'_{ct} I_g}{y_g} \tag{4-8}$$

In order to find the cracked moment of inertia, the neutral axis must be found first from Equation 4-9 determined by the equilibrium of the cross section in the second stage (Figure 4-5 e) including the top reinforcement.

$$x = \frac{-E_s(A_{s,top} + A_{s,bot}) + \sqrt{E_s^2(A_{s,top} + A_{s,bot})^2 + 2E_c E_s b(dA_{s,bot} + c_u A_{s,top})}}{E_c b} \tag{4-9}$$

Where $d$ is the effective depth of the section, hence the distance from the top edge to the centroid of the bottom reinforcing steel, and $c_u$ is the distance from the top edge to the centroid of the top reinforcing steel.

The cracked stiffness is therefore calculated with Equation 4-10:

$$E_c I_{cr} = E_s A_{s,top}(d - x)\left(d - \frac{1}{3}x\right) \tag{4-10}$$

These equations are applied to the slab elements obtaining moment curvature relationships as shown in Figure 4-6.

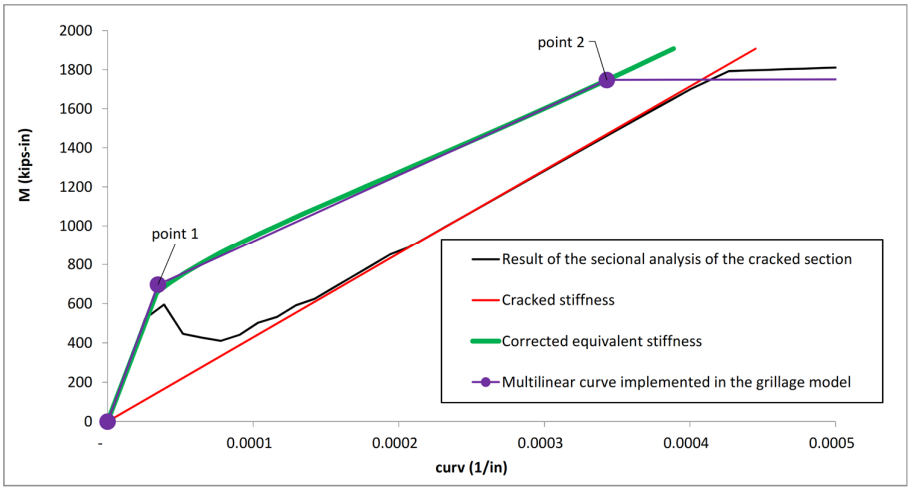


**Figure 4-6. Moment curvature curve for the second stage to account for the equivalent stiffness of the cracked member (zoom on the first part of the curve, the plastic deformation part is not shown for clarity).**

Referring to Figure 4-6, the direct result of the sectional analysis of the cracked section is shown in black line, the analytical cracked stiffness calculated with Equation 4-10 matches the numerical results in the second stage (after the crack has formed) and the green curve shows the equivalent stiffness that takes into account cracked and uncracked sections along the length of member. In order to improve the efficiency, a trilinear curve is used to describe each concrete member's $M - \varphi$ curve calculated with the following steps:

1) The initial slope starting at the origin corresponds to the uncracked stiffness.
2) The second point moment represents the yielding of the reinforcing steel and the third and the last point represents the crushing of the concrete (ultimate concrete strain 0.035).
3) The curvature at which yielding occurs is calculated with the yielding moment and the equivalent stiffness defined in Equation 4-10. Therefore, the third slope of the curve is known.
4) The stiffness of the second segment is found by calculating the tangent of Equation 4-10 at the yielding moment (tangent of the green line at the yielding moment).
5) Since the first slope and the second slope are known the resulting first point is known.

An example of a complete moment curvature curve is shown in Figure 4-7.

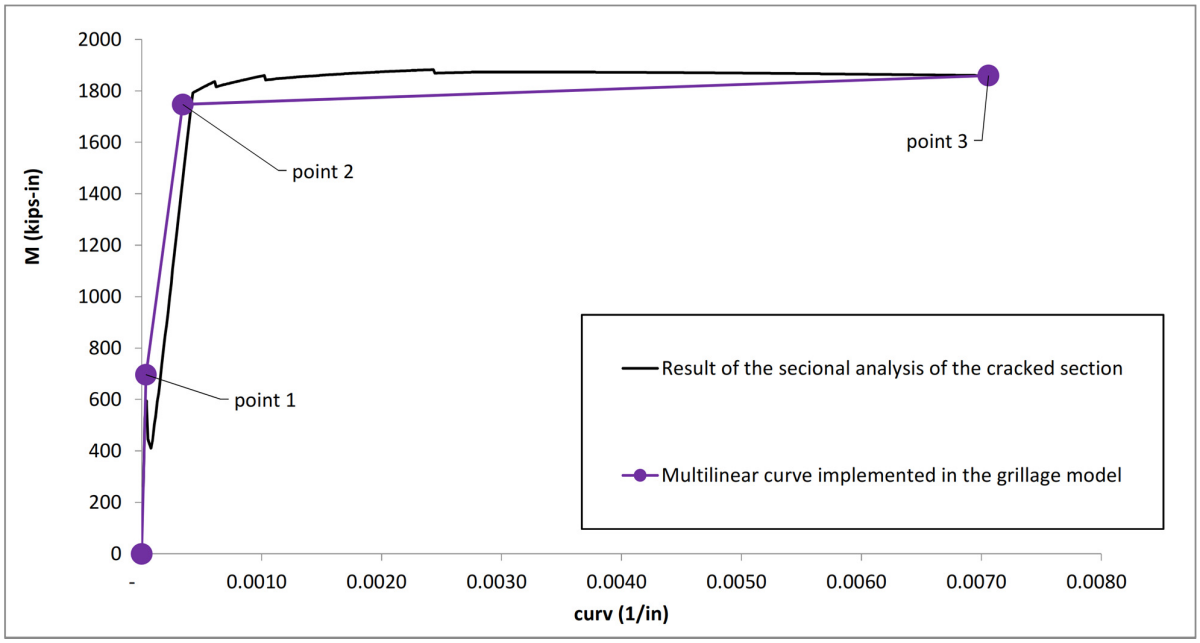


**Figure 4-7. Moment curvature curve of the cracked section and 3-point curve implemented in the grillage model.**

Non-linear $M - \varphi$ curves are placed at five intermediate nodes of the bridge model each with a specific integration length according to the Legendre quadrature rule (Neuenhofer & Filippou, 1998) for each longitudinal and transverse frame element.

## 4.3 Structural Analysis

The objective of the structural analysis is to calculate the load carrying of each bridge by means of a push-down analysis in which the dead load is applied first, and the live load is applied incrementally, while updating every member's stiffenss according to its $M-\varphi$ curve at each load increment up to the failure of one main longitudinal element. It is noted that the load increments need to be applied sequentially since the superposition of loads valid for linear elastic analysis is not valid for non-linear analysis. As already mentioned, only material nonlinearities are considered because the effects of the geometric non-linearity have been shown to be of little consequence for simply supported bridges and for small spans. In fact, failure is normally reached when concrete crushes, and at this load stage, normally, the deflection is small enough to prevent any second order effect and to allow a small-displacement analysis.

The mathematical representation of the equilibrium between external and internal forces at any load level is expressed by Equation 4-11:

$$[K] \cdot \Delta \mathrm{r} = \Delta \mathrm{R} \tag{4-11}$$

Where $[K]$ is the global stiffness matrix of the structural system, $\Delta \mathrm{r}$ is the vector of the displacement increments and $\Delta \mathrm{R}$ is the vector of load increments. The global stiffness matrix, which itself is non-linear depending on the load level, is formed by assembling the contributions of the different frame elements. Therefore, in order to obtain the non-linear response of the structure, an iterative incremental step-by step analysis is performed using standard numerical analysis tools (Taylor, Hinton, Owen, & Oñate, 1984). For example the Newton Raphson method consists in numerical iterations through the equilibrium Equations 4-12 and 4-13:

$$[K_T]^k \cdot \Delta \mathrm{r}_n^k = \Delta \mathrm{R}_n^{k-1} = (\Delta R_E)_n - (\Delta R_E)^{k-1} \tag{4-12}$$

and

$$\mathrm{r}_n^k = \mathrm{r}_{n+1}^{k-1} + \Delta \mathrm{r}_n^k \tag{4-13}$$

Where the subscript $n$ refers to the load step while $k$ refers to the iteration within a specific load step. $(\Delta R_E)_n$ is the vector of externally applied load increments at step $n$ and $(\Delta R_E)^{k-1}$ is the internal resisting load increments.

A correct initial and subsequent slope of each iteration step is of interest to increase the efficiency of the algorithm. The simplest approach is to determine the tangent slope and update it at the beginning of each step (Figure 4-8) and is labeled as Standard Newton Raphson (SNR) method.

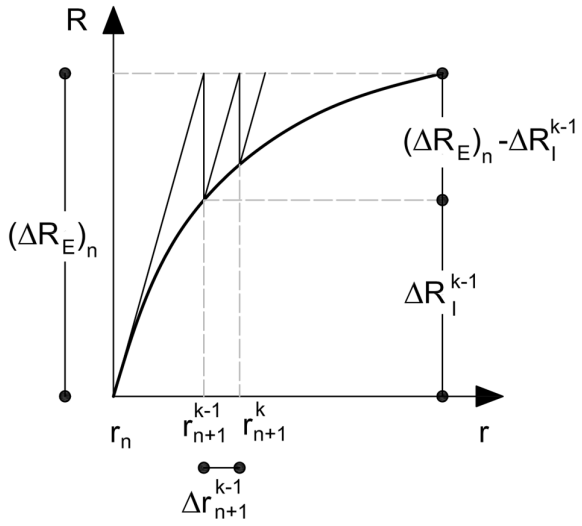


**Figure 4-8. Standard Newton-Raphson (SNR) procedure for non-linear solution algorithms**

An alternative approach is keep the slope of the iteration curve based on the initial tangent slope. This method is labeled as Modified Newton-Raphson (MNR) (Figure 4-9).

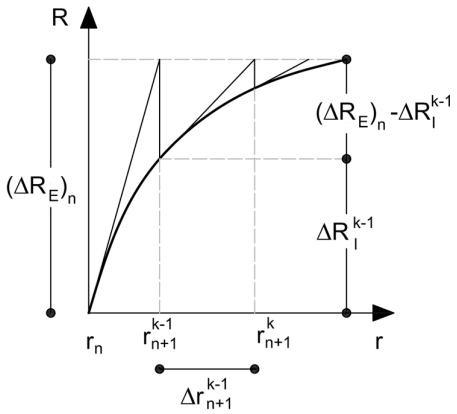


**Figure 4-9. Modified Newton-Raphson (MNR) procedure for non-linear solution algorithms**

While the MNR method allows faster but a large number of iterations, the SNR method allows slower but fewer iterations. In general, a good compromise it to employ the MNR method for the first few iterations, where there is a chance that the initial elastic behavior of structures may well be modelled by a solver where the change of slope will not be critical, and switching to SNR method when the change of slope on the non-linear algorithm becomes critical.

The non-linear analysis can be carried out by force control or displacement control procedures Figure 4-10. The force control option consists of finding the displacement vector $\Delta r_n^k$ which produces an internal force vector $(\Delta R_E)^{k-1}$ balancing the applied force increment $(\Delta R_E)^{k-1}$ while the displacement control option consists of finding the internal force vector $(\Delta R_E)^{k-1}$ balancing the applied force $(\Delta R_E)^{k-1}$ which produces an applied displacement increment $\Delta r_n^k$.

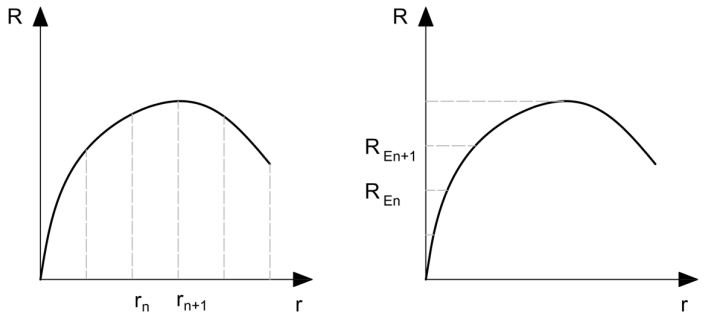


**Figure 4-10. Displacement (left) and load (right) control procedure.**

The non-linear solver methods outlined in this section are implemented in the software OPENSEES (McKenna, 2011) and used in this work to carry out the non-linear structural analysis of the bridges under

study. In this work, several tests have been carried out to select the most efficient algorithm among SNR, MNR and different combinations of both methods since it very important to reduce the time to analyzes as much as possible which in this case was kept on the other of 1 to 2 seconds. The results show that using the SNR method led to a slight (e.g. 3%) improvement in calculation time compared to that of the MNR method and is therefore used for the calculations both of the preliminary sectional analysis and for the consequent system structural analysis.

Even though the displacement control may lead to a better estimation of the maximum displacement of a bridge system, force control method are able to provide acceptable convergence to the ultimate load carrying capacity of the system. On the other hand, the displacement control algorithm is able to reach a displacement slightly larger than the displacement at ultimate capacity which can be used to back calculate (with interpolation) the correct value of the ultimate capacity.

## 4.4 Validation of the numerical model

The validity of grillage models for linear elastic systems has been extensively studied by Hambly (1991) and O'Brien and Keogh (1999) while Ghosn and Casas (1996) demonstrated their validity for the non-linear analysis of multi-girder bridges. The document *Evaluation of existing highway bridge systems* by Ghosn and Casas (1996) compares the results of several bridge load tests to numerical analyses with based on the simplified non-linear grillage concluding that this model is valid to evaluate the overall behavior of most of common bridge types. The aforementioned document was used as the basis for the nonlinear modelling applied in this work. A comparison between the results of a FEM model of a bridge configuration which is very similar to the ones used in this work is provided by Gheitasi and Harris (2015) to load test results performed by Kathol et al. (1995).

In this document, the results of the full-scale laboratory test of a simply supported three-beam bridge spanning 21.3 m as provided by Kathol et al. (1995) are compared to those obtained using the grillage analysis. The cross section of the bridge under study is shown in Figure 4-11.

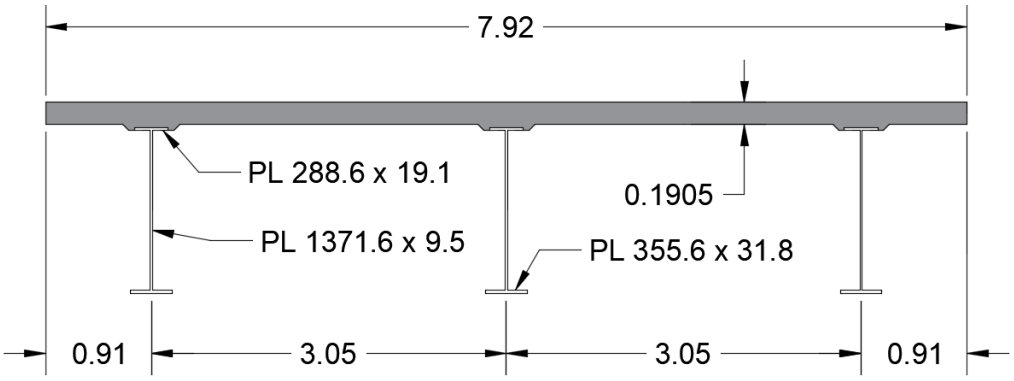


**Figure 4-11. Kathol et al. (1995) test bridge cross section (units are in meters).**

The live load is applied to approximate the effect of two side-by-side HS-20 trucks (with a slight change to the axle spacing) as shown in Figure 4-12. The point loads are applied by 12 post-tensioned rods fastened to 12 steel plates with dimensions of 500 X 200 mm on the top surface of the bridge deck and passed through the floor of the structural deck and individually connected to hydraulic rams.

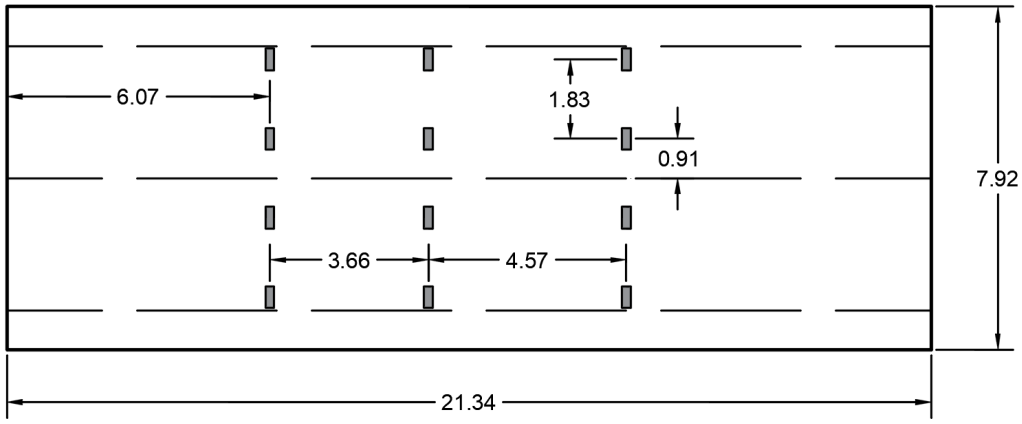


**Figure 4-12. Kathol et al. (1995) test bridge system off loads.**

The bridge's material properties are summarized inTable 4-1.

**Table 4-1. Material properties for the tested bridge.**

| | | | |
|---|---|---|---|
| **concrete** | | | |
| concrete strength | $f'_c$ | MPa | 39.0 |
| tensile stress | $f'_c$ | MPa | 2.3 |
| secant stiffness modulus | $E_c$ | MPa | 29564 |
| | | | |
| **structural steel** | | | |
| yielding stress | $f_{sy}$ | MPa | 248.2 |
| ultimate stress | $f_{su}$ | MPa | 400.0 |
| Young's modulus | $E_{ss}$ | MPa | 200000 |
| | | | |
| **reinforcing steel** | | | |
| yielding stress | $f_{ry}$ | MPa | 496.4 |
| ultimate stress | $f_{ru}$ | MPa | 827.4 |
| Young's modulus | $E_{rs}$ | MPa | 200000 |

The results are shown in Figure 4-13, where the applied load versus the center beam's deflection is plotted for the original test, the FEM model and the grillage model proposed for this work.

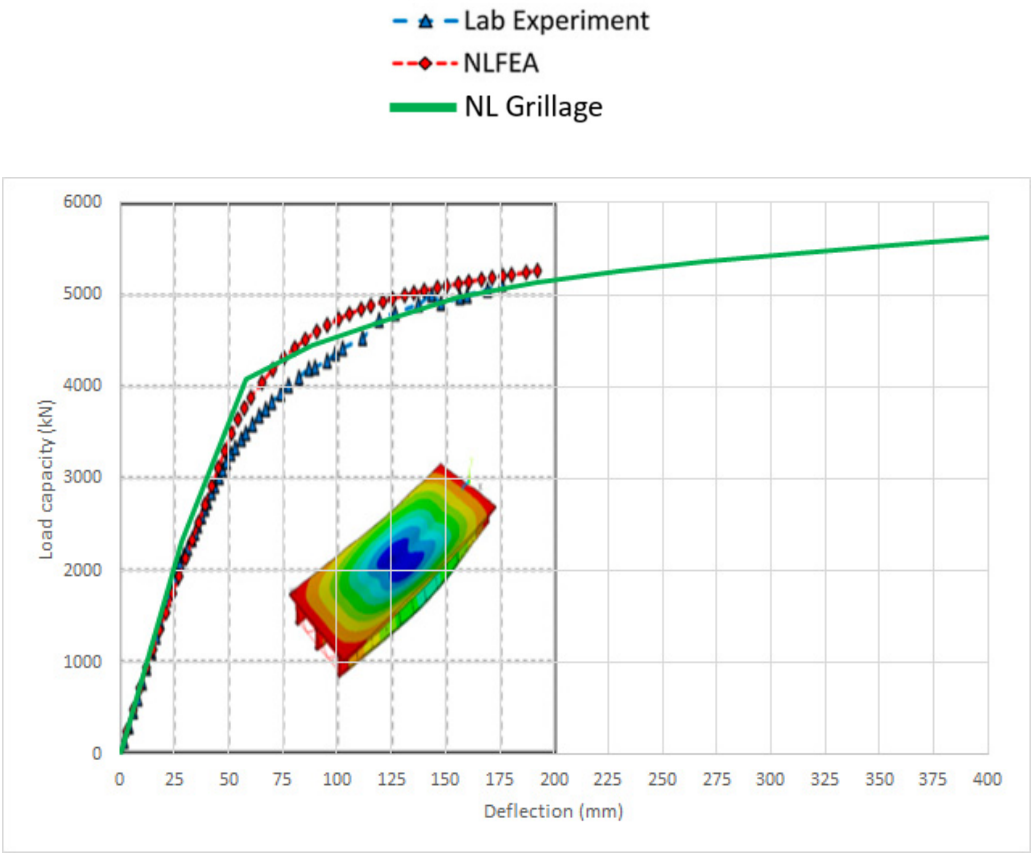


**Figure 4-13. Load capacity versus deflection of the central beam. Adapted from Gheitatsi and Harris (2015).**

The prediction of the overall response of the bridge as a result of the simplified grillage analysis shows acceptable agreement with the detailed Finite Element Method and the test results. This means that for evaluating the overall response of the bridge, specifically the ultimate load carrying capacity the grillage model is valid. In fact, the calculations performed by Ghosn and Casas (1996) are expected to be extended to practically all types of bridges after identifying the properties of the longitudinal and transverse sections. It is clear though that the FEM model is able to provide more details than the grillage model such as local stress distributions, local nonlinearities, lateral displacement of bottom flanges, that cannot be calculated with the grillage model. However, such details are not of interest in this work. As a matter of fact, Kathol et al. (1995) explains that the test was stopped due to a localized failure of the concrete deck in the central part of the slab due to the concentrated loads which prevented the bridge from developing its full global failure mechanism that is the actual objective of this work. In fact, local deck failures, which will certainly inconvenience traffic on the bridge, do not lead to the collapse of the structure.

## 4.5 Probabilistic Model of System Resistance

The non-linear analysis performed in this study is capable of calculating the load carrying capacity of a bridge expressed in terms of the live load multiplier which when applied to the basic nominal live load causes the bridge to fail when the bridge member properties are set at their nominal resistance values. However, one main objective of this work is to account for the uncertainties in estimating the values of the parameters that determine a bridge's load carrying capacity and developing a probabilistic approach to quantify the bridge's safety in terms of its structural reliability as will be further explained in Chapter 6.

The description of the system resistance in statistical terms is based on defining a joint random variable $R - DL$ ($R$ =System resistance, $DL$ =Dead Load), which gives the capacity in terms of the maximum live load that the bridge can carry. The statistical characterization of $R - DL$ is performed by generating a set of bridges for analysis where each bridge is characterized by a combination of randomly generated input variables that meet their known statistical properties. The outcome of all the analyses are assembled into histograms of $R - DL$ that help determine the statistical distribution function of the bridge capacity and related parameters.

The uncertainties used in determining the dead load $DL$ are summarized in Table 4-2 as extracted from Sivakumar et al. (2011).

**Table 4-2. Random variables for dead load Sivakumar et al. (2011).**

| Random variable | Bias | COV | Distribution |
|---|---|---|---|
| Steel weight | 1.03 | 5.0% | Normal |
| Concrete weight | 1.05 | 10.0% | Normal |
| Asphalt weight | 1.00 | 25.0% | Normal |
| Barrier weight | 1.03 | 5.0% | Normal |

The statistical variables relevant for the definition of the resistance $R$, depend on the variability of the material mechanical properties as obtained by Nowak and Collins (2013) and summarized in Table 4-3. The inspection uncertainties are taken from Phares et al. (2001) and Moore et al. (2001) as explained in Section 3.6.

**Table 4-3. Resistance uncertainties for longitudinal and transverse elements.**

| Random variable | Bias | COV | Distribution |
|---|---|---|---|
| Composite concrete steel longitudinal members | | | |
| Concrete strength | 1.21 | 15.5% | Log-normal |
| Steel yielding stress | 1.05 | 10.0% | Normal |
| Material and fabrication | 1.07 | 8.0% | Normal |
| Analysis factor | 1.05 | 6.0% | Normal |
| Inspection uncertainties | 0.95 | 15% | Normal |
| Reinforced concrete transverse members | | | |
| Concrete strength | 1.21 | 15.5% | Log-normal |
| Reinforcing steel yielding stress | 1.13 | 3.0% | Normal |
| Material and fabrication | 1.12 | 12% | Normal |
| Analysis factor | 1.00 | 6.0% | Normal |

For the analysis of deteriorated bridges, the moment curvature curves are modified according to the deterioration rates and their statistical descriptions determined in section 3 of this Thesis (Figure 3-13). The modification of the moment curvature curve is applied by scaling the ultimate moment and the associated plastic branch, and defining a new intercept with the linear branch which remains unchanged as described in Figure 4-14.

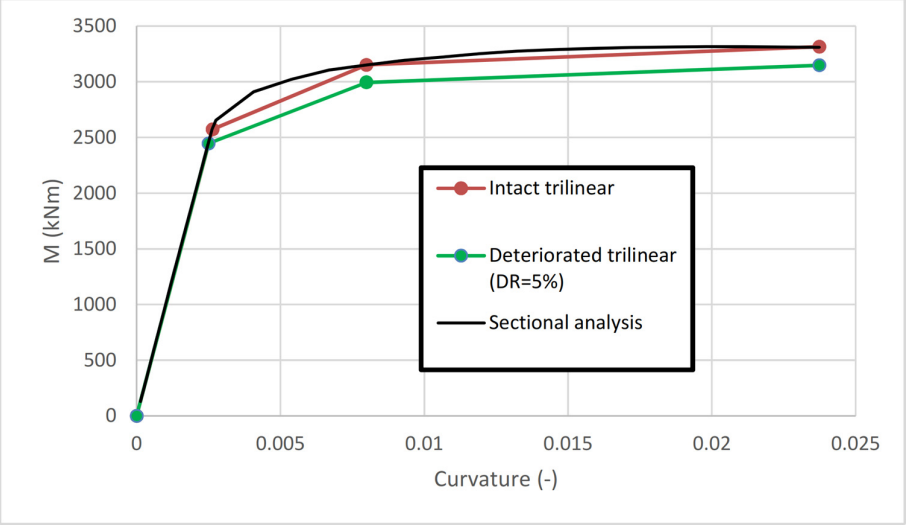


**Figure 4-14. Modification of the moment curvature curve to account for deterioration in bridge member capacity.**

In order to find the probability distribution, which describes the random variable $R - DL$ along with its parameters, a simulation process must be carried out. The simulation process consists of generating a set of $n$ samples of one bridge representing (each identified with the subscript $i$) a possible scenario of $m$ input variables (each identified with the subscript $j$) that lead to a possible output response of the bridge (Figure 4-15).

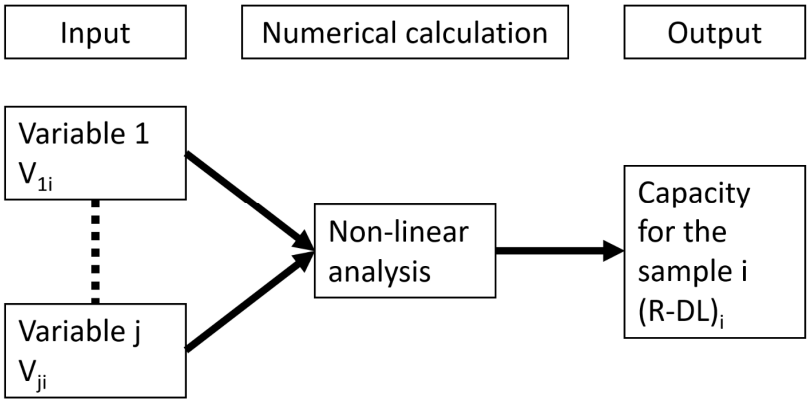


**Figure 4-15. Generation of input data and calculation of output for bridge sample.**

The most straightforward method to generate a set of $n$ bridge samples is through a Monte Carlo Simulation (MCS), where a realization of each variable $j$ is randomly generated based on its statistical properties for each bridge sample $i$. This process itself is repeated $n$ times to create $n$ bridge samples. The number of bridge samples does not need to be defined a priori but the sampling is continued until the statistical properties of the output converge to a stable outcome. For example, the bridge's live load carrying capacity represented by the $R - DL$ variable can be described by a normal probability distribution and therefore the mean and standard deviation updated after calculating the result of every sample until the parameters reach stable values. Although MCS has the advantage of being theoretically simple and easy to implement its major drawback is the high computational cost due to the high number of samples needed to obtain stable results.

One of the alternatives to MCS is the use of stratified-random sampling usually labeled as Latin Hypercube Simulation (LHS) which consists of extracting $n$ values from each of the $m$ random variables equal to the total number of samples (Iman & Conover, 1982). A value for each parameter is selected randomly from each interval generating a matrix of $nxm$ random variables as shown in Equation 4-14.

$$[V_1 \quad \cdots \quad V_j \quad \cdots \quad V_m] = \begin{bmatrix} v_{11} & \cdots & v_{1j} & \cdots & v_{1m} \\ \vdots & \ddots & \vdots & & \\ v_{i1} & \cdots & v_{ij} & & \\ \vdots & & & \ddots & \\ v_{n1} & & & & v_{nm} \end{bmatrix} \tag{4-14}$$

Where $V_j$ is the $n$-dimensional vector describing the $j$-th random variable set of $n$ realizations, and $v_{ij}$ are the $V_j$ vector elements at the generic $i$-th realization.

A visualization of the selected process of selecting values for each random variable from each cumulative probability distribution for a two-dimension problem where $n = 5$ and $m = 2$ is shown in Figure 4-16.

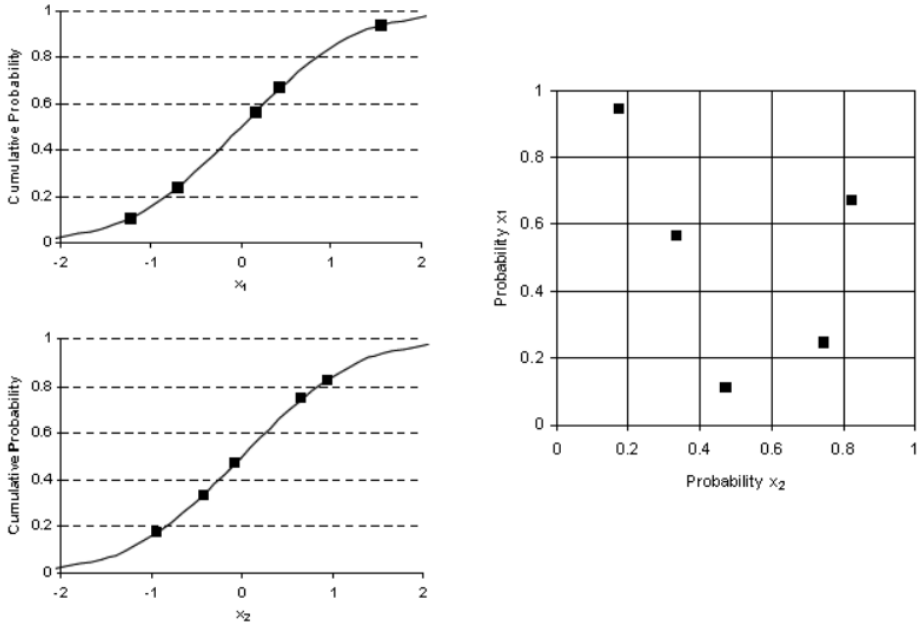


**Figure 4-16. LHS variable values for an example simulation with where $n = 5$ and $m = 2$.**

The two plots on the left in Figure 4-16 represent the two random variables of the example and the stratification of each of them into five sub-domains from which each sample value is extracted. Therefore, the extracted values are organized into a matrix as shown in the right matrix in Figure 4-16. This matrix shows how the two sets of extracted values are paired to cover the whole area of the matrix as much as possible and no point appears in each line or column twice.

The generic pairing of the random variable samples is associated with a correlation between each couple of random variables $V_I$ and $V_{II}$ defined by Equation 4-15:

$$\rho(V_I, V_{II}) = \frac{\sum_{i=1}^{n}(v_{I,i} - \bar{V}_I)(v_{II,i} - \bar{V}_{II})}{\sqrt{\sum_{i=1}^{n}(v_{I,i} - \bar{V}_I)^2 (v_{II,i} - \bar{V}_{II})^2}} \tag{4-15}$$

Where the vinculum sign indicates mean value. The different correlations between the various random variables can be organized into a symmetric $mxm$ correlation matrix P shown in Equation 4-16

$$\mathrm{P} = \begin{bmatrix} 1 & & \\ & \ddots & Sym \\ \rho(V_I, V_{II}) & 1 & \ddots \\ & & 1 \end{bmatrix} \tag{4-16}$$

The correlation between two variables indicates systematic dependency with a coefficient of $\rho = 1$ for a strong increasing correlation and $\rho = -1$ for a strong decreasing correlation. As shown in Figure 4-17, the noisier the correlation is the lower is, the absolute value of $\rho$ and a coefficient $\rho = 0$ indicating uncorrelated variables. In other words, the correlation coefficient indicates the noisiness and direction of a linear relationship, but it does not give the slope nor other characteristics of non-linear relationships between each pair of random variables (Figure 4-17).

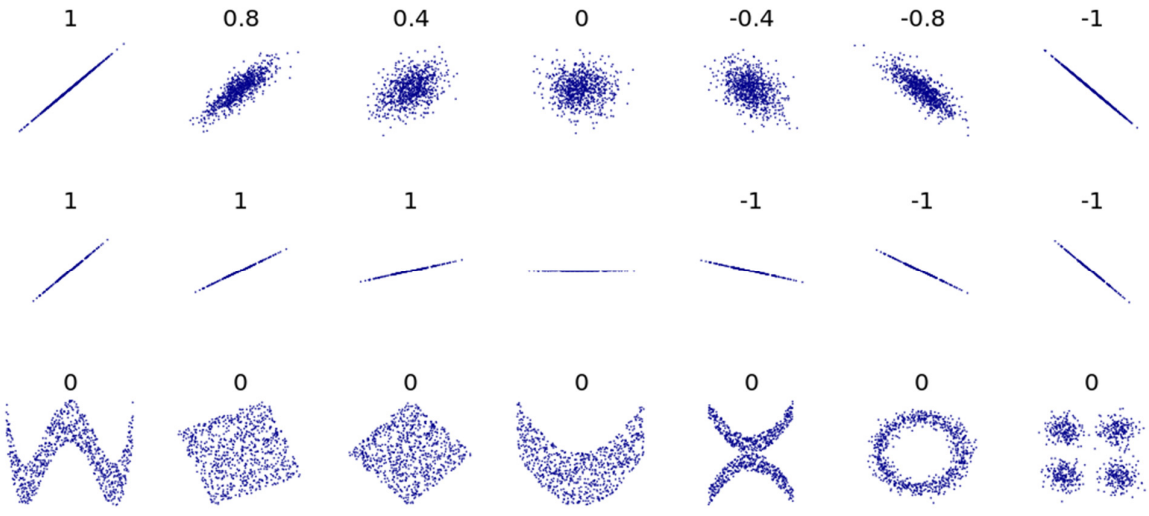


**Figure 4-17. Several sets of couples of variables with the related correlation coefficient (extracted from https://en.wikipedia.org/wiki/Correlation_and_dependence).**

For example, the correlation between the strength of different materials must be set to 0.0, because the value of one variable is independent of the value of the other. On the other hand, the strength of concrete cast at different locations is likely to present some dependency with a correlation coefficient greater than 0.0, even though, generally speaking, it is reasonable to assume that the material properties are homogenous within the concrete volume, reducing the concrete strength to one unique variable.

In principle, the correlation matrix obtained by the random pairing of the different sample input values in LHS may not provide an acceptable correlation matrix. Therefore, a mathematical algorithm may be used to change the pairing of the variable values with the objective of matching the correlation matrix obtained from the sampling process to a desired correlation matrix. A full description of the restricted pairing process may be found in the work by Iman and Conover (1982).

In this work a correlation $\rho = 0$ is considered between each pair of random variables summarized in Table 4-2 and Table 4-3 because they have no physical dependency between each other. It is noted, that the concrete strength applied to the slab for the transverse and longitudinal elements could be treated as two random variables with perfect correlation. However, in this analysis, we use a unique concrete strength random variable and, assign the same concrete strength value to the longitudinal and transverse elements at each simulation run because this option is computationally more efficient than having two perfectly correlated variables.

Therefore, the objective correlation matrix for the restricted pairing process is represented by the identity matrix with dimensions $m$x$m$ where $m = 13$ is equal to the total number of random variables.

## 4.6 Example Probabilistic Analysis of Bridge System Capacity

An example probabilistic analysis of a bridge system is performed in this section to illustrate the simulation procedure and extract some useful results for latter implementation in the risk analysis process. The capacity of the bridge system analyzed in this study is conveniently represented by the joint variable *R-DL*, (where *R*=system resistance, *DL*=dead load). The statistical properties of this joint variable automatically account for the uncertainties in all the random variables that control the load carrying capacity of the bridge system including the distribution of the applied load among the bridge members.

The probabilistic study of the system capacity is first performed with a full Monte Carlo simulation, where the random variables outlined in Table 4-3 are applied to one of the bridges of *set 1*. The bridge, identified in the NBI data file by the label 000000001006922, carries 2 traffic lanes, its span length is 38.1 m, and, its total width is 13.0 m. It is composed of 5 parallel longitudinal beams spaced 2.60 m center to center. A simulation campaign is performed to study the convergence of the statistical parameters that describe the *R-DL* variable at failure. The total calculation time for a $10^6$ simulation runs is 160 hours making the average calculation time for a non linear analysis of one bridge sample approximately equal to 0.5 seconds. It must be noted that these 0.5 seconds include pre and post processing times as well as the time

for storing the results. This low analysis time, reflects the high optimization that has been obtained in the structural analysis code, since no standard calculation program would be able to perform this non-linear calculation in such a short interval. Specifically, the code for pre and post processing and storage is programmed and optimized in Tlc/tk language in the context of this work, while the structural calculation algorithm is taken from the OPENSEES framework which is reasonably fast.

The statistical parameters of the *R-DL* variable for this bridge are evaluated by plotting the histogram of the MCS output on a normal probability plot, after observing that a normal probability gives the best fit among many probability distribution functions (Figure 4-18).

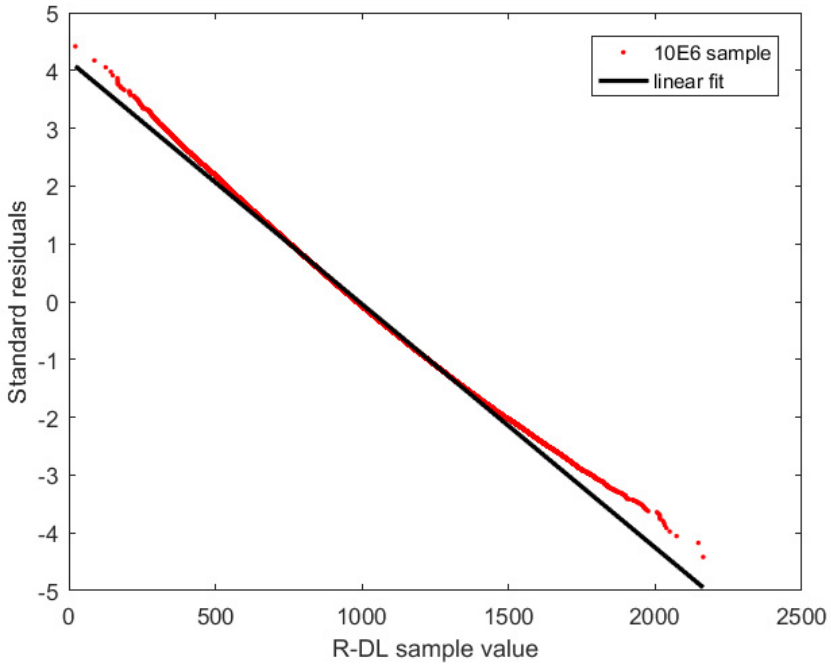


**Figure 4-18. Probability plot for the $10^6$ sample simulation of the random variable *R-DL*.**

The same curve fit process is performed with different number of simulation runs providing different degrees of precision of the probability distribution parameters (bias and coefficient of variation) as outlined in Figure 4-19.

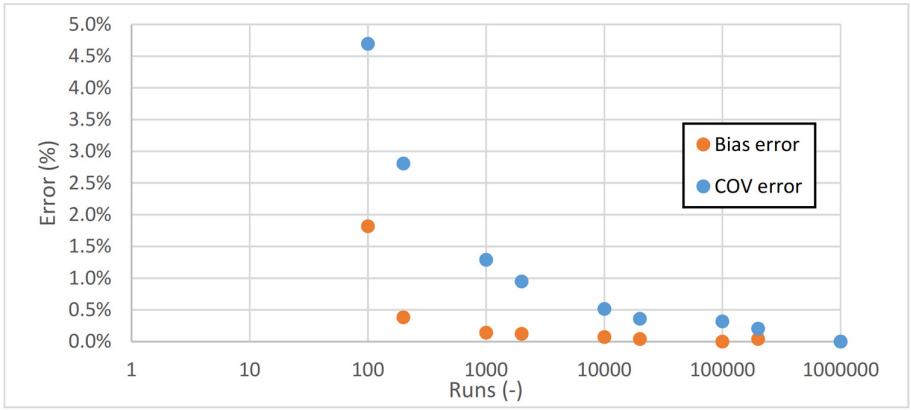


**Figure 4-19. Convergence of bias and coefficient of variation of system capacity of example bridge with number of Monte Carlo simulations.**

The maximum number of MCS runs is preset to $10^6$ simulations to define the baseline for the values of COV of the *R-DL* random variable and are used to compare the results of other simulations and check accuracy. The relations between the number of runs and the percent difference from the values obtained with $10^6$ runs are shown in Figure 4-19 where the bias factor (orange dots) converges faster than the COV (blue dots). Convergence will be considered to have been achieved when the absolute value of the error in the bias factor is smaller than 1%, and the error in the COV is smaller than 5%.

The converged values of the average *R-DL* (fitted in the normal probability plot with a coefficient of regression $R^2$=0.99 as shown in Figure 4-18) is 989.4 kNm with a standard deviation of 237.4 kNm. The mean is compared to the nominal value of 846.6 kNm (deterministic value) indicating that the bias is 1.17 and the coefficient of variation is 24%. This result can be compared to the typical bias for member capacity, as for example, given by Nowak and Lind (1987) for evaluating the moment capacity of composite steel girders equal to 1.12 with a COV=10%. Similarly, Bhattacharya et al. (2009) use a bias of 1.11 and a COV 12%. It is noted, that the typical values that are provided in the literature are for member resistance and do not include inspection uncertainties, while the simulation in this study gives the random variable of the entire system *R-DL* and includes inspection uncertainties.

The same sensitivity analysis performed with the Monte Carlo simulation is performed with the simplified Latin Hypercube Simulation described in Section 4.5. The LHS calculations are calculated to simulate the capacity of the bridge system for different deterioration rates and time intervals as shown in Figure 4-20.

| Nominal capacity (kNm) |
|---|
| 846.6 |

**Mean value**

| Years of exposure | deterioration rate: high | medium | low |
|---|---|---|---|
| 1 | 952.3 | 982.4 | 988.9 |
| 2 | 915.0 | 976.6 | 988.9 |
| 4 | 856.6 | 965.1 | 988.8 |
| 6 | 807.1 | 953.6 | 988.7 |

**Bias**

| Years of exposure | deterioration rate: high | medium | low |
|---|---|---|---|
| 1 | 1.12 | 1.16 | 1.17 |
| 2 | 1.08 | 1.15 | 1.17 |
| 4 | 1.01 | 1.14 | 1.17 |
| 6 | 0.95 | 1.13 | 1.17 |

**Standard deviation**

| Years of exposure | deterioration rate: high | medium | low |
|---|---|---|---|
| 1 | 239.0 | 237.4 | 238.3 |
| 2 | 247.0 | 236.6 | 238.3 |
| 4 | 255.0 | 234.8 | 238.3 |
| 6 | 243.2 | 232.6 | 238.3 |

**COV**

| Years of exposure | deterioration rate: high | medium | low |
|---|---|---|---|
| 1 | 25% | 24% | 24% |
| 2 | 27% | 24% | 24% |
| 4 | 30% | 24% | 24% |
| 6 | 30% | 24% | 24% |

**Figure 4-20. Statistical parameters for the system capacity for different deterioration rates and exposure periods.**

The top part of Figure 4-20 presents the nominal *R-DL* value already calculated (deterministic value) while the bottom four matrices give mean values, bias factors, standard deviations and coefficients of variations for each case analyzed. Each 4x3 matrix represents the change of the variable *R-DL* resulting from three levels of deterioration (high, medium and low) and different years of deterioration. The deterioration rates are included in the calculation by adding a 14$^{th}$ random variable representing the statistical variation of the cumulative histograms plotted in Figure 3-13 for each deterioration rate. The percent reduction in member capacity for a given time period $DR(T)$ is calculated as $DR \times T$ where $DR$ is the annual deterioration rate and $T$ is the time interval in years.

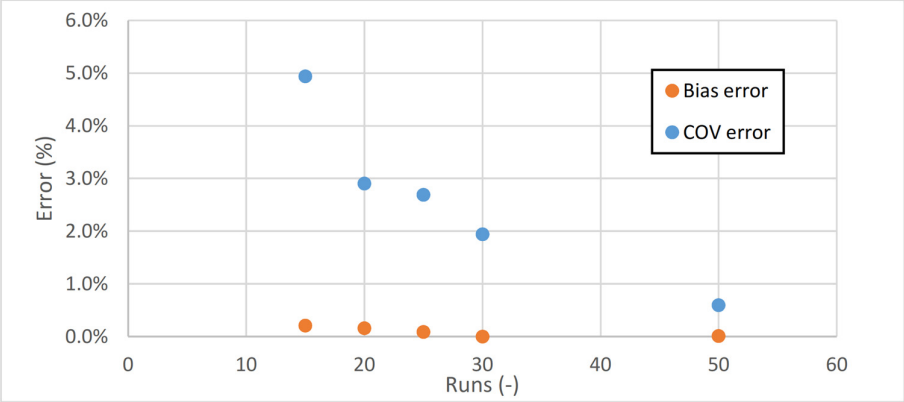


**Figure 4-21. Sensitivity of the *R-DL* parameter for the example bridge executed with LHS for different number of runs.**

The calculation of the random variable *R-DL* is performed for each bridge with the aforementioned LHS to reduce the computation effort compared to a crude MCS. Figure 4-21 shows how fast the statistical parameters obtained using LHS converge to the final results of $10^6$ MCS runs. Specifically Figure 4-21 shows that the error in determining the COV is more sensitive to the number of LHS runs compared to the bias factor. However, the effectiveness of the LHS is remarkable, considering that with close to 20 runs the error is around 3%. The results obtained in the LHS sensitivity analysis are reported in Table 4-4 to provide a better sense of the order of magnitude of the errors obtained. The sensitivity analysis demonstrates that for this specific case a LHS with 15 runs may already provide acceptable values with the aforementioned target errors of 5% for the COV and 1% for the bias factor. It is noted that the limitations in the LHS algorithm are such that not much improvement can be achieved in the bias with a higher number of simulations but that the COV can be reduced significantly to an error of 0.6% by doubling the number of simulations to 50. In any case, the results shown in Table 4-4 confirm that for both the bias and for the COV the precision obtained by the number of runs confirms that the 25 runs LHS found in the previous case provides acceptable errors in terms of COV and bias factor.

**Table 4-4. Sensitivity of the *R-DL* parameter for the example bridge executed with LHS for different number of runs.**

| # of sample | nominal | mean | st dev | bias | COV | err bias | err COV |
|---|---|---|---|---|---|---|---|
| | kN | kN | kN | - | - | - | - |
| 15 | 846.6 | 991.4 | 249.6 | 1.17 | 0.25 | 0.2% | 4.9% |
| 20 | 846.6 | 991.0 | 244.7 | 1.17 | 0.25 | 0.2% | 2.9% |
| 25 | 846.6 | 990.3 | 244.0 | 1.17 | 0.25 | 0.1% | 2.7% |
| 30 | 846.6 | 989.4 | 242.0 | 1.17 | 0.24 | 0.0% | 1.9% |
| 50 | 846.6 | 989.5 | 236.0 | 1.17 | 0.24 | 0.0% | 0.6% |

Another interesting parameter to be studied is the influence of the live load pattern on the *R-DL* parameter since the calculations shown so far are performed with two side-by-side trucks where nominal weight of the AASHTO Legal Load truck is used for the internal truck and a truck having the configuration of the Legal Load is used for the external truck but with an amplified weight equal to 2.4. The explanation on how the weights are determined will be explained in Chapter 5. The bridge capacity (*R-DL*) is obtained by incrementing the applied loads until bridge superstructure system failure *R-DL* is equal to the total incremented weight on the bridge. The simulation process is also repeated with only one Legal truck on the bridge.

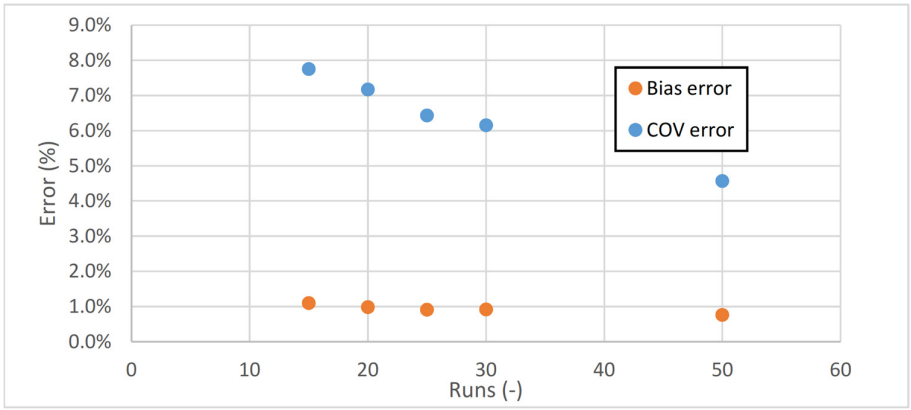


**Figure 4-22. Sensitivity of the *R-DL* parameter for the example bridge executed with LHS for different number of runs. 1-truck configuration.**

**Table 4-5. Sensitivity of the *R-DL* parameter for the example bridge executed with LHS for different number of runs. 1-truck configuration.**

| n_sample | nominal | mean | st dev | bias | COV | err bias | err COV |
|---|---|---|---|---|---|---|---|
| | kN | kN | kN | - | - | - | - |
| 15 | 738.0 | 872.0 | 193.0 | 1.18 | 0.22 | 1.1% | 7.8% |
| 20 | 738.0 | 871.0 | 194.0 | 1.18 | 0.22 | 1.0% | 7.2% |
| 25 | 738.0 | 870.4 | 195.4 | 1.18 | 0.22 | 0.9% | 6.4% |
| 30 | 738.0 | 870.4 | 196.0 | 1.18 | 0.23 | 0.9% | 6.2% |
| 50 | 738.0 | 869.1 | 199.0 | 1.18 | 0.23 | 0.8% | 4.6% |

The results for the one-truck loading plotted in Figure 4-22 and listed in Table 4-5 show that the convergence of the *R-DL* statistical parameters presents acceptable precision with an error smaller than 5% after 50 runs. Furthermore, the bias factor of 1.18 and the COV of 0.23 is consistent with the results obtained with the two-lane load pattern. The conclusion is that the dependency of the system capacity statistical parameters on the load pattern (1 or 2 trucks) is negligible.

Thus, for the rest of the study LHS is performed for each bridge with 50 LHS runs, because the results shown in Figure 4-21 and 4-22 and Table 4-4 and 4-5 show that this number of runs provides sufficient degree of precision. The results obtained for the different bridge configurations can be visualized by observing their dependency to the ratio $M_{DL}/M_u$ (nominal dead load moment of the member over nominal member capacity)

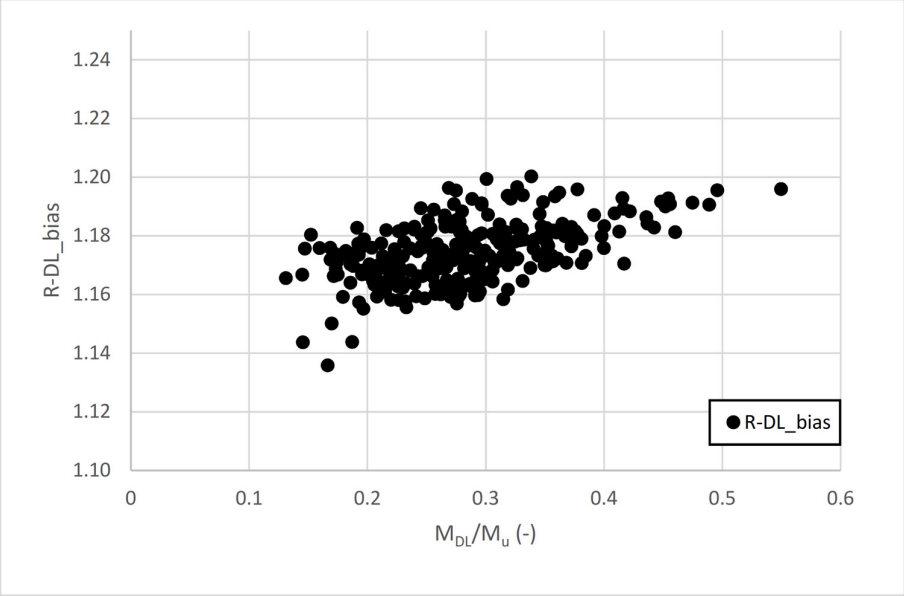


**Figure 4-23. Bias factor of the *R-DL* (or equivalently *LL* in the y-axis) versus the ratio between dead load moment and ultimate moment of a member for the full *set 1* of bridges.**

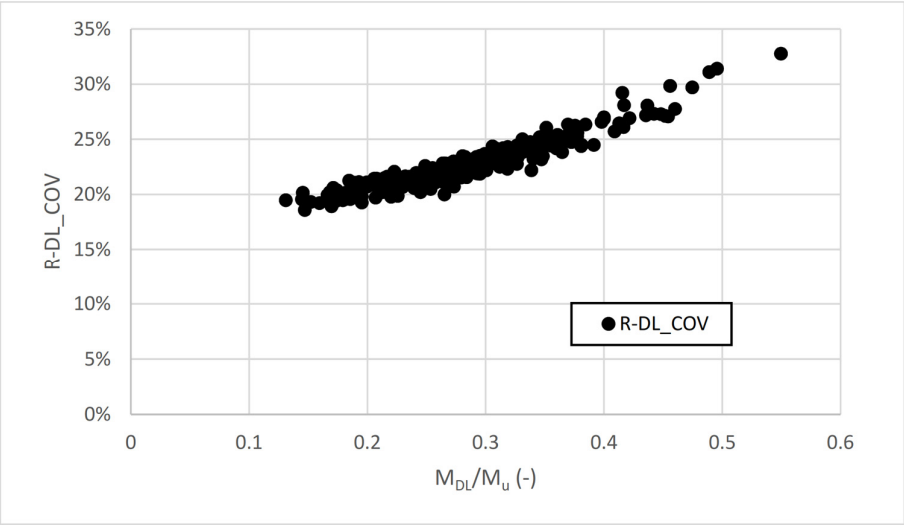


**Figure 4-24. COV of the *R-DL* versus the ratio between dead load moment and ultimate moment of a member for the full *set 1* of bridges.**

Figure 4-23 shows how the bias factor of the system *R-DL* varies versus the ratio between dead load moment and ultimate moment of a member for the full *set 1* of bridges. Figure 4-24 gives the COV of the system *R-DL* versus the member $M_{DL}/M_u$ ratio.

Figures 4-23 and 4-24 show that bridges where the dead load is more predominant in relation to the capacity of the bridge members have a higher bias factor and a higher COV for the system *R-DL*. The explanation of this trend depends on the relation between the margin R-DL available to carry the live load. In general, at low values of applied live load the bridge response remains in the linear range and progressively moves into non-linear range as the applied live load increases. It must be recalled that, as shown in Figure 4-14, the uncertainties are higher in the non-linear range of the response. Therefore, when the bridge has very little capacity left for live load, the a higher proportion of the live load is applied when the bridge is in the non-linear stage where the uncertainties are higher than for the early stages of loading. On the other hand, when a large amount of live load is applied when the bridge is still in its linear elastic range the uncertainties in estimating the response are on the low end. Likewise, the trend in the bias factor is directly related to the proportions of *R* and *DL* in the *R-DL* random variable as shown in the values given in Figure 4-20, the bias in member resistance, *R,* is higher than the bias in member dead load, *DL* and thus in *R* and *DL* of the system. In other words, *R-DL* bias and COV are smaller for those bridges where a large part of the capacity is consumed by the dead load, as expected.

Another interesting trend to observe is the relationship between the bias and COV of the load carrying capacity of the bridge member and the load carrying capacity of the system represented by the *R-DL* of the member and system respectively. This is achieved by the plot shown in Figure 4-25 where the bias factor of the member ultimate moment minus dead load moment ($M_u - M_{DL}$) on the x-axis is compared to the bias

factor of the system capacity minus total dead load ($R - DL$) on the y-axis. Figure 4-25 shows that there is an approximate linear relationship between member and system results both in terms of bias factor and COV although the linear relationship is not perfect because of the different bridge configurations effect on system behavior including the nonlinear cracking and yielding of the slab in the transverse direction.

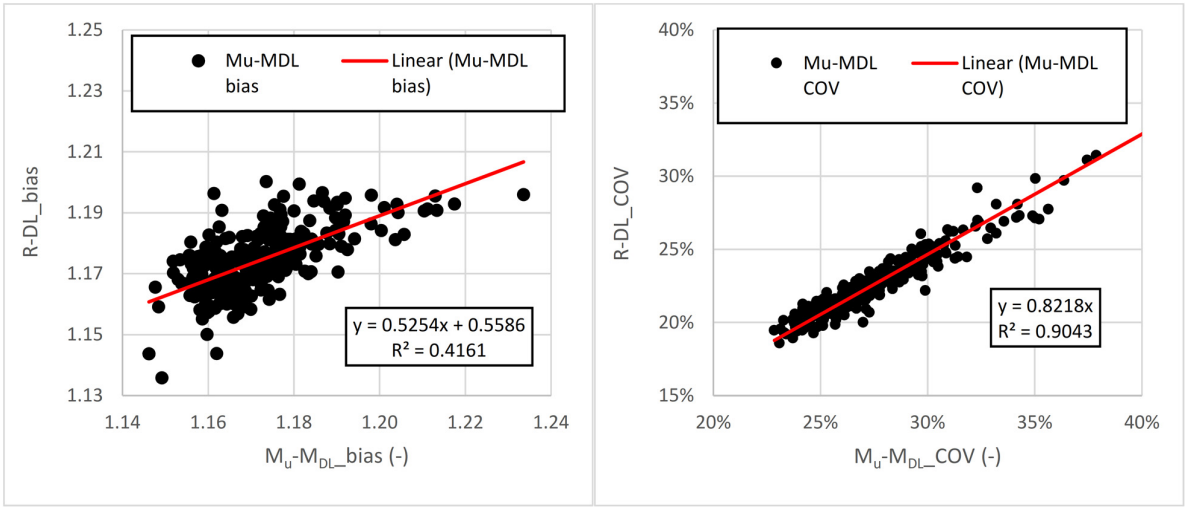


**Figure 4-25. Bias factor (left) and COV (right) of the member ultimate moment minus dead load moment ($M_u$-$M_{DL}$) versus bias factor (left) and COV (right) of the system capacity minus total dead load ($R$-$DL$) on the y-axis.**

## 4.7 Chapter conclusion

In this chapter, the resistance side of the bridge system's safety equation has been assessed along with its full description as a random variable to allow its implementation in a reliability analysis. The analysis is implemented to a nonlinear grillage model of the bridge to assess its system behavior, hence accounting for its ability to redistribute loads after one or more members exhibit nonlinear deformation.

While many different strategies are available in the literature to calculate system capacity to assess the reliability of bridges, this work requires extremely efficient and fast algorithms because a large number of calculations need to be performed to find the statistics of system resistances of several different bridges each with a different configuration, each of which must be evaluated for different deterioration rates and for different exposure periods. For these reasons, a simplified and fast nonlinear grillage analysis is adopted to study the global response of bridges as an alternative to a more precise but computationally demanding FEM model. The grillage results are determined to be accurate for the purposes of this study where the local response of each detail of the bridge is not needed.

Furthermore, the statistics of the system capacity are assessed for later implementation in a simplified system reliability analysis. This key element is first calculated with a MCS for a specific example bridge, and afterwards compared with the more efficient LHS. A suitable number of LHS runs is established by observing that after 50 runs, the statistical parameters of the calculated load carrying capacity of the bridge system reach acceptable converged values. LHS is therefore used for the system reliability analysis of the full *set 1* of bridges (279 bridges).

A review of the results of the simulations shows how the system *R-DL* random variable relates to the ratio of member dead load to member ultimate capacity. The trend observed shows higher values of bias factor and COV for those bridges with a high level of dead load. For the bridges of *set 1*, it is observed that the bias ranges between 1.1 and 1.2 and the COV ranges between 20 to 30%. This information will be used in Chapter 6 to develop a simplified reliability analysis process for use in the practical probabilistic risk analysis process.

# 5 Live load model

The calculation of the probability of failure of bridge systems is based on the numerical representation of the response of the bridge as well as the demand over it in terms of applied load. In the previous chapter described the dead load model adopted for this study. This chapter is dedicated to the probabilistic modeling of the live load intensity and its effects on structural members. Live loads for bridges are represented by the maximum load occurring over a specific period of exposure that depends on the type of analysis being carried out. Structural codes (AASHTO, 2017; CEN, 2003) provide guidance to determine the traffic live load using a widely used deterministic approach in combination with live-load safety factors. However, the assumptions made for the code-calibrated nominal live loads and associated load factors may not be applicable for all types of bridges and analysis procedures. Furthermore, when, as is the case in this work, a more accurate probabilistic analysis is required, a recalibration of the live loads may be necessary to better account for the uncertainties associated with estimating the critical vehicle weights and other live load characteristics.

The recalibration of the live load model requires input traffic data collected at stations that give accurate representation of actual traffic over bridges. In this work, traffic data recorded using weigh-in-motion (WIM) technology at representative stations in NYS are used to model the live load.

The data are used to calibrate a live load model suitable for structural analysis, in particular for analyzing composite steel girder-concrete slab bridges taking into consideration the structural configuration of the bridge including span length, number of beams and beam spacing. The model will include statistical parameters applicable for reliability analyses.

Most of the contents of this chapter have been published in the papers by Anitori et al. (2013; 2016).

## 5.1 WIM Database

The weigh-in-motion (WIM) data used in this work are the result of a one-year long monitoring campaign carried out at 20 WIM stations spread around the New York State highway network and analyzed by Ghosn et al. (2015) after applying filtering protocols proposed by Sivakumar et al. (2011) to eliminate unreliable data. For each WIM station's set of data, a number of traffic characteristics was determined, including the total number of vehicles recorded at each site, the average daily truck traffic ADTT, defined as the number of trucks per day recorded at each site averaged over one year of measurements, and the number of overweight (OW) trucks, defined as the number of trucks that exceed the legal weight limits applicable to the state of New York. Additional details on these topics can be found in Fiorillo and Ghosn (2014) and in Ghosn et al. (2015). Table 5-1 lists each station's traffic characteristics.

**Table 5-1. Traffic characteristics for each WIM station.**

| Station ID | No. of vehicles | % OW | ADTT |
|---|---|---|---|
| 1281 | 27221 | 19.2 | 76 |
| 1400 | 652304 | 18.6 | 1832 |
| 1800 | 305100 | 22.6 | 851 |
| 2680 | 154740 | 24.4 | 429 |
| 3311 | 1225061 | 18.4 | 3481 |
| 4342 | 477552 | 14.2 | 1329 |
| 4483 | 113220 | 16.3 | 322 |
| 5183 | 467485 | 21.2 | 1298 |
| 5281 | 114761 | 26.4 | 317 |
| 6282 | 67350 | 21.3 | 186 |
| 6340 | 107884 | 20.1 | 335 |
| 6482 | 822958 | 17.3 | 2299 |
| 7100 | 454588 | 23.3 | 1293 |
| 7181 | 149752 | 26.6 | 414 |
| 7381 | 273144 | 12.4 | 779 |
| 8280 | 1733022 | 11.7 | 4804 |
| 8382 | 1277280 | 14.3 | 3605 |
| 9121 | 1149657 | 15.2 | 3861 |
| 9580 | 561431 | 21 | 1555 |
| 9631 | 226993 | 25.5 | 651 |

## 5.2 Effects of Truck Loads on Short to Medium Span Bridges

Based on the dimensions of typical truck configurations in the database and the type of bridges and span length being analyzed, it has been observed that there is a low probability of fitting two consecutive trucks in the same lane. Therefore, for short to medium span bridges (15 to 60 m) under consideration, the maximum load effect is governed by the presence of a single truck per lane. As already mentioned, this work focuses on the analysis of simple span steel-concrete composite bridges which represent a very common structural type in many countries and within the United States, especially in the state of New York. A set of 100 configurations representative of the existing steel-concrete composite bridge population having the combination of the geometric parameters listed in Table 5-2 was established for analysis.

**Table 5-2. Bridge configurations for structural analysis.**

| | |
|---|---|
| Span length (m) | 15, 20, 30, 40, 60 |
| Number of beams | 4, 6, 8, 10 |
| Beam spacing (m) | 1.2, 1.8, 2.4, 3.0, 3.6 |

The set of bridges in Table 5-2 is analyzed to find the load effect in terms of bending moment for each of the trucks in the WIM database. Each truck's data include the number of axles, the axle spacings and the axle weights. The design of the bridge members is performed using the same criteria described in Chapter 4.

Due to the large number of analyses to be performed for each vehicle and for the different possible positions of the vehicle along the longitudinal axis of the lane and lateral position, the analysis is performed using a set of influence surfaces. The influence surfaces are found by placing a unit point load at a specific node of the grillage representing the main members of the bridge and recording the corresponding moment produced at the midspan of the bridge, which is the most critical location for a point load over a simple span. . The process is repeated by moving the point load to every node of the grillage to define a contour diagram where the ordinate in the map at a specific point represents the moment effect of a unit point load at the most critical location of a specific member. The influence surfaces are plotted using normalized node coordinates; both longitudinally (normalized with respect to span length) and transversally (normalized with respect to bridge width). As an example, Figure 5-1 shows the influence surface for the two members of a multi-girder bridge, where member 1 is the edge girder and member 2 is the next girder. In the example shown in Figure 5-1 the effect of a point load (-1.0 kN) applied at the location of the red arrow produces a moment on the external member of 12 kN.m.

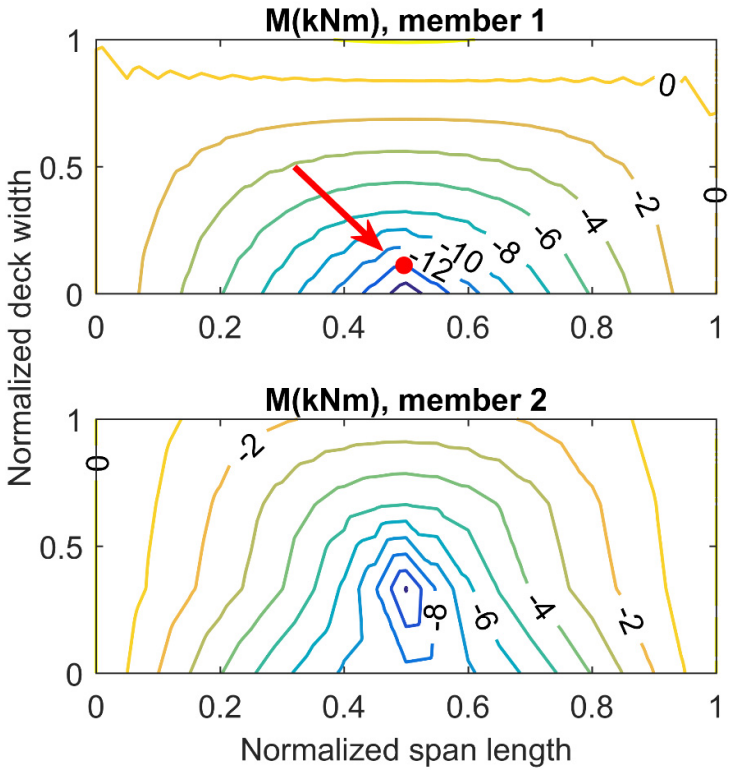


**Figure 5-1. Example of moment influence surfaces for the section at midspan of a 30 m four-girder bridge with 1.8 m beam spacing, for the (a) first and (b) second member.**

Once the influence surfaces are drawn, the maximum bending moment is determined by positioning each truck's axle at the appropriate node of the influence surface and by multiplying the ordinate at each node by the weight of the axle at that node and superposing the effects of all the axles.

For example, consider a single or two side-by-side AASHTO HL-93 design trucks moving along a path where the exterior wheel is half way between the two external girders over the 30 m four-girder bridge with 1.8 m beam spacing whose influence surfaces are depicted in Figure 5-1. The fraction of the load effect of one truck carried by the most loaded internal girder is 0.34 and it is 0.50 for the external member for the case where one lane only is loaded by the HL-93 truck. The fraction of the loads carried by the internal girder is 0.54 and that carried by the external girder is 0.57 for the for the 2-lane loaded case. These are compared to the AASHTO distribution factors that would be equal to 0.32 for the internal and 0.50 for the external member when the bridge is loaded by a single lane after removing the multiple lane factor, and 0.45 for the internal and 0.55 for the external member for the 2-lane case. The relatively small differences in the results may be due to the specific characteristics of the bridge analyzed in this example and the positioning of the loads. The AASHTO LRFD load distribution factors are calibrated by fitting equations through the results of hundreds of bridge grillage analyses similar to the analyses performed in this work. The accuracy

of the grillage models was verified by comparing the results of a number of cases with those of more advanced 3-D finite element analyses and field test results (Zokaie, Mish, & Imbsen, 1995).

## 5.3 Load effect on bridge members from single lane traffic

The moment effects for all the vehicles in the WIM database, were collected and organized in histograms similar to the ones shown in Figures 5-2 and 5-3.

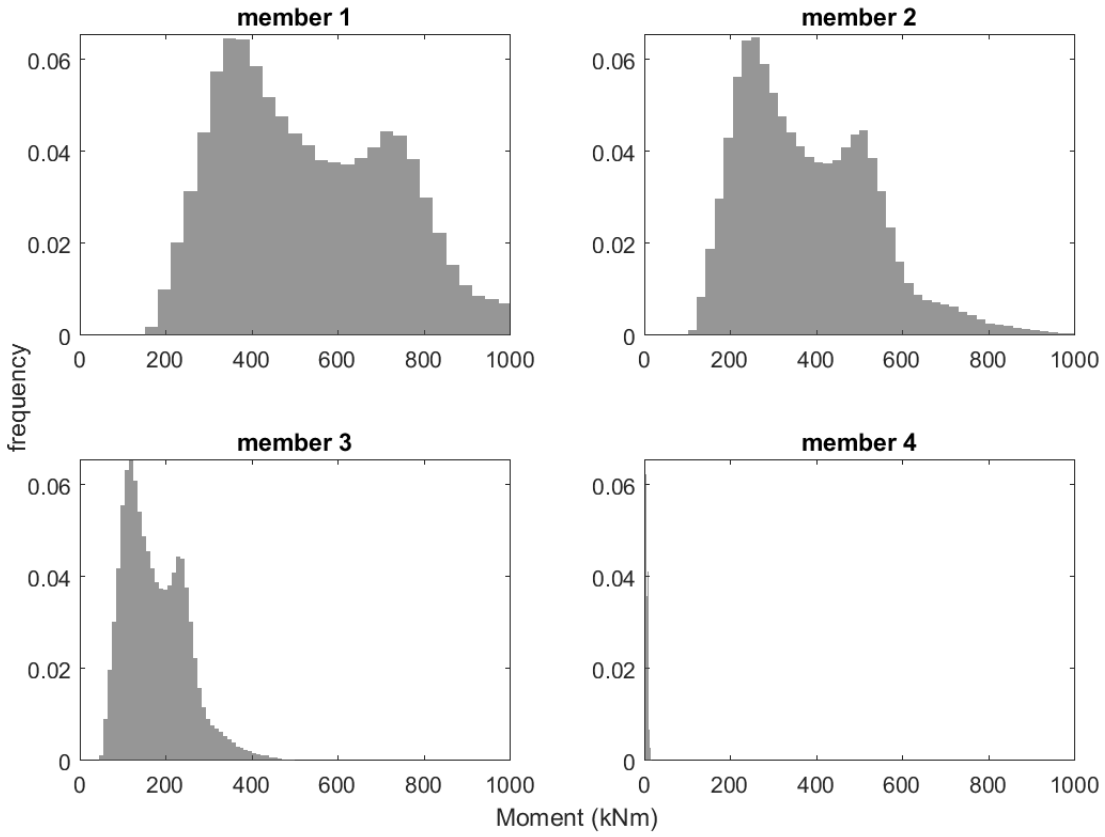


**Figure 5-2. Histograms of maximum moment in the first four longitudinal members from the edge due to traffic load in lane 1 of a 30 m bridge with 10 beams at 1.8 m.**

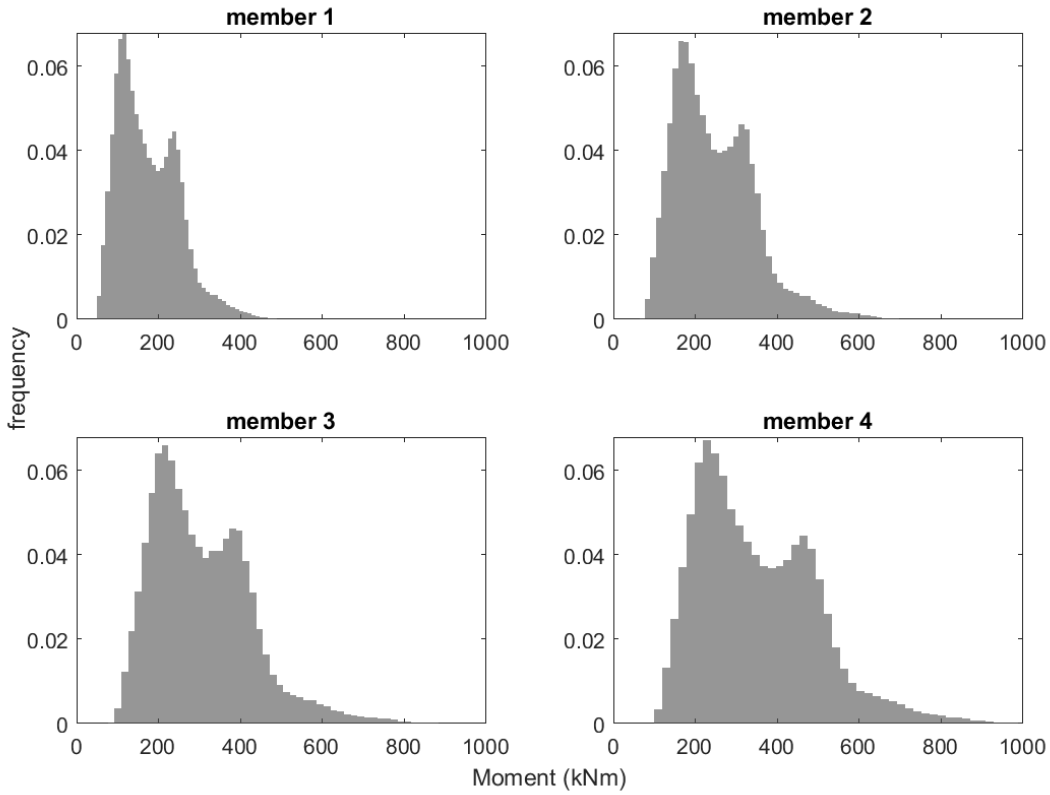


**Figure 5-3. Histograms of maximum moment in the first four longitudinal members from the edge due to traffic load in lane 2 of a 30 m bridge with 10 beams at 1.8 m.**

From Figures 5-2 and 5-3 and the analyses of the other bridges, it is observed that the moment effect of the vehicles passing over the most external lane is primarily carried by the external girder and the load effect on the interior girder decreases so that the fourth girder carries negligible fraction of the total moment effect. On the other hand, the effect of vehicles passing over an internal lane (say the passing lane) is more widely distributed among the first four members of the bridge as shown in Figure 5-3.

## 5.4 Statistical Analysis of Load Effect

The extrapolation of the load effect histograms to calibrate a nominal live load model for application during the design of bridges has been used by Nowak (1999) and implemented in the AASHTO LRFD. In that study, Nowak (1999) employed a simple method to extrapolate the maximum load effect from truck data collected during a survey undertaken in 1975 in Ontario Canada. The simple method was found to be reasonable because the Ontario data available at the time was biased toward the heaviest 20% of the trucks crossing the survey site. The approach may not be necessarily accurate for other data sets although it was widely used in other research projects (Jo, Onoufriou, & Crocombe, 2005; Khorasani, 2010). According to Nowak's method, the load effect data are assumed to fit a normal distribution. Assuming a certain number,

N, of trucks crossing the bridge during the reference period, the expected maximum load effect is obtained using the 1/N fractile of the standard normal probability function. This truck weight fractile provides the number of standard deviations by which the maximum load exceeds the mean value. However, other researchers (Ghosn, Sivakumar, & Miao, 2013; Sivakumar et al., 2011; Soriano, Casas, & Ghosn, 2017) observed that the entire data set does not follow a normal distribution but that the upper tail of the load effect distribution (heaviest vehicles) can have the statistical characteristics of the upper tail of a fictitious standard distribution curve. In particular, it was found that the upper 5% of the sample load effect data could be fitted with the tail end of a normal distribution. For example, as shown in Figure 5-4, the tail end of the load effect cumulative histogram, matches very well with that of normal cumulative probability distribution. It is noted that in Figure 5-4, the cumulative distrbutions are plotted on a normal probability scale for a 40 m bridge.

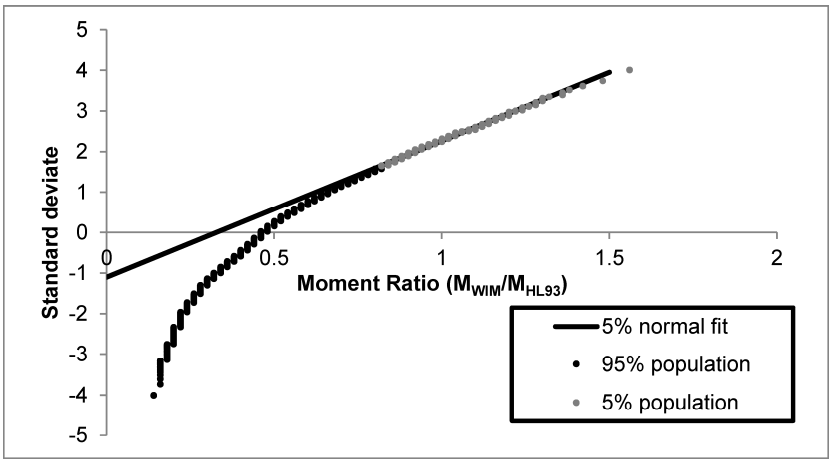


**Figure 5-4. Normal distribution probability plot and linear fit of the 5% upper tail.**

The abscissa in Figure 5-4 gives the ratio of the moment effect of the vehicles in the WIM database and the effect of the AASHTO HL-93 design load, while the ordinate gives the normal deviate corresponding to the probability of exceeding a given load effect value as assembled from histograms similar to those in Figures 5-2 and 5-3. The probability plot would give a straight line when the data plotted follow a normal distribution. In the case of Figure 5-4, the entire population of data does not follow a straight line, but the upper 5% population does. The regression analysis used to find the best parameters of the fitting line for the upper 5% shows a coefficient of regression $R^2 = 0.99$, where a coefficient of 1.00 indicates a perfect fit. Similar results in terms of goodness of fit are obtained for the set of bridges analyzed in this work as discussed in section 5.2 and in other cases analyzed by Sivakumar et al. (2011) confirming that the 5% upper tail of the load effect data can be well described by the upper 5% of a normal distribution. Fitting the tail end by that of a hypothetical normal distribution will facilitate the projection of the data to estimate the expected maximum load over a bridge's service period as will be presented further in this document.

The fitting of the upper 5% tail of load effect calculated from WIM data with that of a normal distribution is repeated for the full set of bridges presented in section 5.2 and for the first four members of each bridge. For example, Table 5-3 lists the mean values and the standard deviations of the equivalent normal probability distributions of the moment load effects in the most loaded beams of bridges of different span-lengths. These statistics are for equivalent normal distributions whose tail ends match the upper 5% of the load effects of the vehicle population collected at New York *WIM* site 9121. This *WIM* station recorded more than one million vehicles over a 1-year period.

**Table 5-3. Normal distribution parameters for the upper 5% of the load effect for the most external member for bridges of different span length.**

| Span length (m) | Mean of normal distribution that fits the upper tail of $\mathbf{M_{WIM}/M_{HL93}}$ histogram | Standard Deviation of normal distribution that fits the upper tail of $\mathbf{M_{WIM}/M_{HL93}}$ histogram |
|---|---|---|
| 15 | -0.01 | 0.39 |
| 20 | -0.03 | 0.34 |
| 30 | -0.02 | 0.36 |
| 40 | -0.01 | 0.37 |
| 60 | 0.00 | 0.34 |

From Table 5-3, it is observed that the load effect divided by that of the HL-93 design load the mean value of is close to zero and the standard deviation ranges between 0.34 to 0.39 for all cases considered. However, these results need to be projected to give the maximum effect in an exposure period such as the 75-year exposure for new designs as specified by the AASTHO LRFD or a 100-year exposure as specified by the Eurocodes. Alternatively, a smaller exposure time used for evaluation analyses according to AASHTO MBE. In this work, different exposure periods are considered for different intervals between inspections as will be explained in sections 5.8 and 5.9.

## 5.5 Multiple presence of trucks

In general, it has been observed that the maximum load effect in a single lane of a simply supported bridge is governed by individual trucks when the bridge is less than approximately 60 m (200 ft) in length as noted by Nowak (1999), Ghosn et al. (2013), Fu et al. (2013), Ghasemi et al. (2016). However, for multi-lane bridges and longer and continuous spans, the analysis must take into account the probability that the maximum effect may be due to the presence of more than one truck in different lanes, different spans or within the same lane when the span length is long. For example, the work carried out by O'Brien and Enright (2011) where the traffic load effect was obtained by the analysis of traffic data from bridges in the Netherlands and Czech Republic concluded that for bridges with span lengths greater than 45 m, high lane

distribution factors and very high traffic volumes, the governing load scenario consists of the presence of more than a single truck per lane. Due to the different truck characteristics observed in the *WIM* dataset analyzed in this work, which shows that the heaviest trucks are significantly longer than those observed in the Netherlands or the Czech Republic, and also due to the different lane distribution factors observed for the types of multi-girder bridges studied as compared to the values assumed by O'Brien and Enright (2011), it is herein assumed that the case of one truck per lane or two side-by-side trucks govern as also recommended by Nowak (1999), Fu et al. (2013), Ghasemi et al. (2016).

The plot in Figure 5-5 shows the frequency distribution of the normalized total moment at the mid-span of a 60 *m* long single span when one lane of the bridge is loaded and compares it to that obtained when the traffic is occupying two lanes.

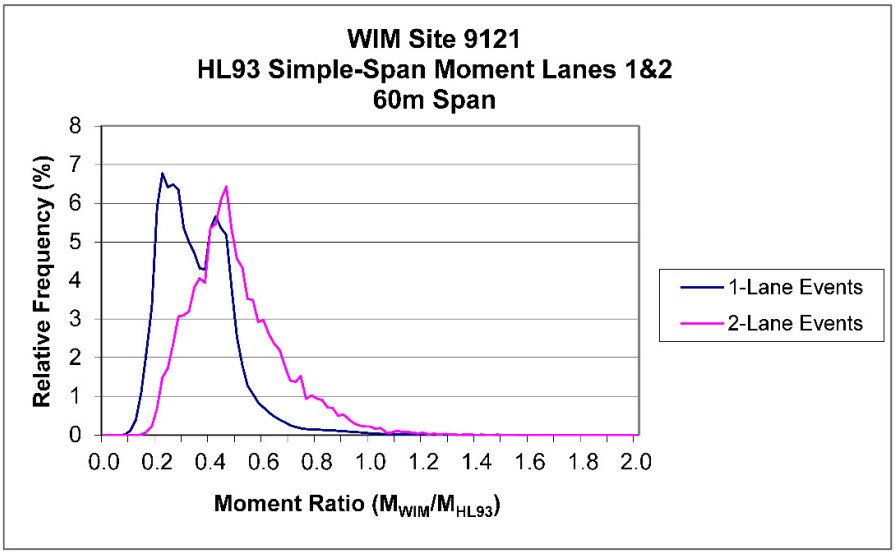


**Figure 5-5. Normalized moment histogram for a 60 m (200 ft) span bridge.**

The effect of multi-lane vehicular load was considered by Ghosn and Moses (1985), Ghosn and Moses (1986), Nowak (1999) and more recently by O'Brien and Enright (2011). The approach followed by Nowak (1999) is based on the observation that there is a correlation between the weights of trucks in two adjacent lanes, where a coefficient of correlation smaller than 1.00 indicates that the moment effect due to two trucks cannot simply be represented by two equal trucks with the same Gross Vehicle Weights (GVW) although it is not excluded a priori. A correlation coefficient equal to 1.00 indicates that the moment effect due to multi-presence of two trucks is always caused by two similar trucks with the same weight. Specifically, full correlation is represented by ρ=1.00, partial correlation by ρ=0.50 and no correlation by ρ=0.00. The results listed in Table 5-4 provide the parameter $Z$ which is the normal standard deviate of the probability of occurrence for a given number of simultaneous occurrences, N, such that $Z = -\Phi^{-1}(1/N)$. The return period, T, given in the last column of Table 5-4 for each value of Z is found by extrapolating the load effect

database assuming a normal distribution. These return periods can then be used to determine which truck weight should be used in each lane to simulate the maximum load effect.

**Table 5-4. Return periods, T, for different correlation coefficients in two-lane load events.**

| Number of lanes loaded | | | *N* (number of events) | *Z* (st. norm. variate) | *T* |
|---|---|---|---|---|---|
| One | | | 20 000 000 | 5.33 | 75 years |
| Two | $\rho$=0.00 | Lane 1 | 1 500 000 | 4.83 | 5 years |
| | | Lane 2 | 1 | 0.00 | average |
| | $\rho$=0.50 | Lane 1 | 150 000 | 4.36 | 6 months |
| | | Lane 2 | 1 000 | 3.09 | 1 day |
| | $\rho$=1.00 | Lane 1 | 50 000 | 4.11 | 2 months |
| | | Lane 2 | 50 000 | 4.11 | 2 months |

Following the results in Table 5-4, Nowak (1999) assumed that trucks in side-by-side configurations represent 1/15 of the truck loading events, truck weights in side-by-side events are correlated and thus the maximum 75-year load effect can be simulated by placing the maximum 2-month truck in each lane. However, these assumptions that are based on the limited data available at the time, may not be always valid. In fact, analyzing large numbers of *WIM* sites in New York, Sivakumar et al. (2011) observed that:

1) As already explained earlier and shown in Figure 5-4, the load effects of heavy trucks do not generally follow normal probability distributions but that only the upper 5% in the tail end matches that of fictitious normal distribution;
2) The percentage of trucks involved in multi-presence events vary with the truck traffic volume represented by the Average Daily Truck Traffic (*ADTT*); and
3) The weights of trucks in side-by-side or closely following configurations are uncorrelated.

Using a limited set of European traffic data, O'Brien and Enright (2011) observed that in some cases the weights of closely spaced trucks show low levels of correlation. Thus, they demonstrated that, in some cases the loading of two-lane bridges up to 45 *m* in length is governed by either one truck in only one lane or two side-by-side trucks, but that in other cases the governing scenario is a mixture of both event types, and that for longer spans in the range of 35 to 45 *m*, simulations showed that one truck in one lane in combination with two trucks in the other lane produce bending moments close to the characteristic 1000-year load. Thus, O'Brien and Enright conclude that "the characteristic 1000-year load shows that for bridges with low lateral transfer, the critical loading event for bending moment is typically an extremely heavy vehicle in the slow lane (80% to 90% of the 1000-year GVW), sometimes with a standard vehicle (in the range 30 to

50 t) in the fast lane – which is consistent with Turkstra's load combination rule (1980). For bending moments in bridges with high lateral distributions, the characteristic load can be represented by a very heavy vehicle (60% to 80% of 1000-year GVW) in the slow lane with a moderately heavy vehicle (50 to 60 *t*) in the fast lane.

However, the observations made by O'Brien and Enright may not be consistent with the data collected in other countries or other sites. *WIM* data analyzed by Sivakumar et al. (2011) have shown that the percentage of trucks that arrive at a site side-by-side ranges between 1% to 2% for short to medium span bridges up to 60 *m* in length, with a high value of 6% for long span bridges with heavy truck volumes. In this work, it is assumed that 2% of the trucks cross a bridge side-by-side with another truck which is consistent with a typical *ADTT* of 2000.

## 5.6 Analytical approach for multiple presence of trucks

The assumption of lack of correlation between consecutive vehicles is demonstrated in Figure 5-6 for NYS data, where the weight of each vehicle is compared to the weight of the subsequent or adjacent one, showing no particular trend (2015). Similar observations were made in NCHRP 12-83 (Wassef, Kulicki, Nassif, Mertz, & Nowak, 2014) where data from different sites were showed that some level of correlation was observed for closely travelling trucks of medium weight but no correlation was noted between the weights of closely travelling very heavy trucks.

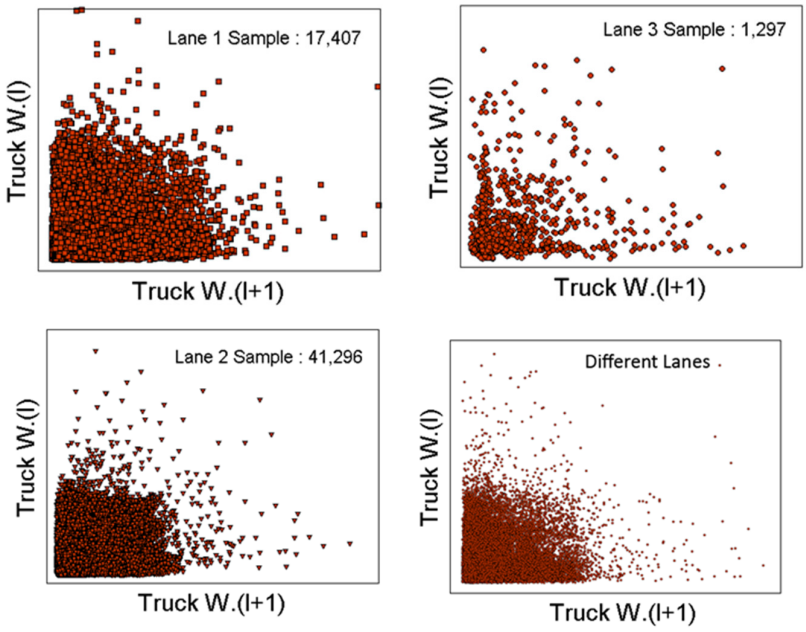


**Figure 5-6. Correlation of consecutive trucks in lane 1, 2 and 3 and in different lanes (adopted from Ghosn et al., 2015).**

Therefore, given the probability distribution of the load effect of each truck in a side-by-side configuration, the probability density function of the effect of two trucks can be calculated with Equation 5-1 as:

$$f_s(S) = \int_{-\infty}^{+\infty} f_{x2}(S + x_1)\, f_{x1}(x_1) dx_1 \tag{5-1}$$

where $x_1$ is the effect of the truck in lane 1 and $x_2$ is the effect of the truck in lane 2, $f_s(S)$ is the probability distribution function of the multi-lane effects for the joint event $S = x_1 + x_2$, $f_{x1}(\dots)$ is the probability distribution function of the effects of the trucks in lane 1 and $f_{x2}(\dots)$ is the probability distribution function of the effects of trucks in lane 2. It was observed by Ghosn et al. (2013) and Sivakumar et al. (2011), that in many cases, the frequency distributions of the truck weights in different lanes are similar and, therefore, the same distribution function can be assumed for $f_{x1}(\dots)$ and $f_{x2}(\dots)$. Because many WIM datasets do not provide information on which lane a truck occupies when the data was recorded, the assumption of same load histograms for all lanes has also been adopted in previous research by Fiorillo (2015) and Ghosn et al. (2015).

Other than the input parameters, the main difference between the multi-presence approach adopted by Sivakumar et al. (2011) and Ghosn et al. (2013) and subsequently by Soriano et al. (2017) compared to that of Nowak (1999) is that the latter calculates the truck load effect independently for each lane, then assumes different correlations between the weights of the trucks in side-by-side configurations. The approach adopted here finds the load effect of two-lane loads using Equation 5-1 and then executes the projection using the expected number of multiple-presence events, *N*, within the service life, *T*.

If the tail of the load effect distribution is modeled as the combined effect of two independent normal distributions, as it can be certainly done when dealing with the upper 5 % maximum effects as explained earlier, then the convolution approach of Equation 5-1 simplifies and the resulting probability distribution can be described by the tail of a new normal distribution with the statistical parameters calculated with Equations 5-2 and 5-3:

$$\mu_S = \mu_{x1} + \mu_{x2} \tag{5-2}$$

$$\sigma_S = \sqrt{(\sigma_{x1})^2 + (\sigma_{x2})^2} \tag{5-3}$$

where $\mu_{x1}$ and $\mu_{x2}$ are the mean values of the normal distributions that fit the upper 5% of the actual distributions of the load effects of the trucks in lane 1 and 2 respectively and $\sigma_{x1}$ and $\sigma_{x2}$ are the associated standard deviations; $\mu_S$ and $\sigma_S$ are the mean and standard deviation of the distribution that fits the tail end of the combined load effect.

## 5.7 Statistical Projection of Extreme Load Effect

The histograms of the load effects of the entire population of trucks shown in Figures 5-2 and 5-3 are based on one-year observation for each WIM station. However, the load effect needs to be adapted to the exposure time of the bridge under study representing the service or design life the structure to consider the possibility that the maximum load is not captured by the WIM data collected. The statistical projection approach proposed by Sivakumar et al. (2011) and implemented by Ghosn et al. (2013) and Soriano et al. (2017) is adopted in this study. The approach assumes that the *WIM* data gathered during the monitoring period is representative of the truck population over the entire service life of the bridge and that the bridge loading process remains stationary over time. Therefore, it is very important that the data collection period be carefully planned to collect a substantial amount of data that provide an adequate statistical representation of the extreme trucks through ensuring a high confidence levels in the statistics of the upper 5% of the data.

While the effects of individual trucks or a combination of trucks may be represented by histograms such as those in Figure 5-5 or presented in mathematical expressions such as Equation 5-1, bridge engineers are interested in ensuring the safety of bridges when they are exposed to the maximum possible loads that may take place within their service lives. The projection of the load effect to find the maximum load in a specific time interval requires the application of extreme value theory which can be greatly simplified if the upper 5% of the load effect histograms can be represented by a normal distribution as demonstrated in section 5.4. In fact, the maximum load effect of data that fit a normal distribution is known to follow an Extreme Value Type I (Gumbel) distribution, the statistical parameters of which are obtained by means of Equations 5-4 and 5-5 (Ang & Tang, 2007):

$$\alpha_N = \frac{\sqrt{2ln(N)}}{\sigma_{event}} \tag{5-4}$$

$$u_N = \mu_{event} + \sigma_{event}\left(\sqrt{2ln(N)} - \frac{ln(ln(N))+ln(4\pi)}{2\sqrt{2ln(N)}}\right) \tag{5-5}$$

where $\alpha_N$ and $u_N$ are the inverse measure of dispersion and the most probable value of the Type I distribution; The mean value of the load effect for one event is $\mu_{event} = \mu_s$ and its standard deviation $\sigma_{event} = \sigma_s$ for two-lane loadings or $\mu_{event} = \mu_{sx1}$ and $\sigma_{event} = \sigma_{x1}$ for one-lane loading are the mean value and the standard deviation of the normal distribution that produces a tail end that matches the upper 5% the truck load effect data; $N$ is the number of load repetitions expected during the bridge's service life.

The statistics of the Type I extreme value distribution $\alpha_N$ and $u_N$ are subsequently used to find the mean of the maximum load effect, $L_{max}$, its standard deviation, $\sigma_{Lmax}$ and its coefficient of variation $V_{Lmax}$

for any reference service life during which $N$ load repetitions are expected, by means of Equations 5-6, 5-7 and 5-8:

$$L_{max} = \mu_{max} = u_N \frac{0.577216}{\alpha_N} \tag{5-6}$$

$$\sigma_{Lmax} = \frac{\pi}{\sqrt{6}\alpha_N} \tag{5-7}$$

$$V_{Lmax} = \frac{\sigma_{Lmax}}{L_{max}} \tag{5-8}$$

The procedure described in this section can be directly implemented to study the safety of a particular bridge if a set of representative *WIM* data is available for the bridge site. However, the analysis may be tedious and demanding especially if an entire set of bridges needs to be analyzed. Therefore, a calibration process is performed in the next section to provide a synthetic representation of the live load effect for more straightforward use.

## 5.8 Live Load Model

The results obtained by the application of Equations 5-6, 5-7 and 5-8 may be directly used to calculate the safety of bridge systems in a probabilistic methodology. However, a simplified formulation is proposed in this work where the live load model is described by a set of point loads similar to the nominal live loads used in design and evaluation processes. The objective is to reproduce the same maximum load effect on bridge members calculated in Section 5.7 with a set of forces linked to a typical truck configuration. It is noted that the same load effect can be obtained by different truck load configurations with different nominal weights of each axle, but it is convenient to adopt configurations from the AASHTO standard trucks to provide a live load model that engineers and researchers are familiar with. In this sense, Ghosn et al. (2015, 2011, 2013) showed that 3-S2 semi-trailers form the vast majority of trucks traveling on US highways and that these trucks produce the largest load effects on the main members of medium span bridges. Similarly, the effects of heavy trucks on short span bridges (less than 30 m) are mostly governed by single unit trucks, which can best be modeled by AASHTO Type 3 legal trucks. For these reasons, it is proposed that the maximum load effects on short to medium span single lane and two-lane bridges be simulated by analyzing the combined effects of either one or two side-by-side trucks having the configurations of the AASHTO 3-S2 or Type 3 Legal Trucks shown in Figure 5-7.

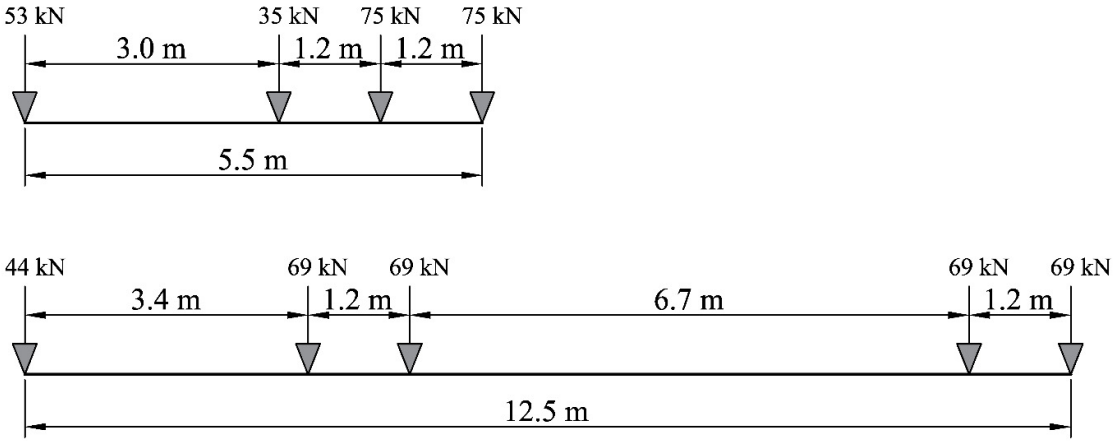


**Figure 5-7. AASHTO Type 3 and 3-S2 Legal Truck configurations and corresponding nominal axle weight.**

Because the nominal axle weight used shown in Figure 5-7 provide a lower load effect than the one calculated with the mean value of the projected load effect as obtained from Equations 5-6, 5-7 and 5-8, a correction factor $\alpha$ is calibrated to adjust the AASHTO truck weights as shown in Figure 5-8.

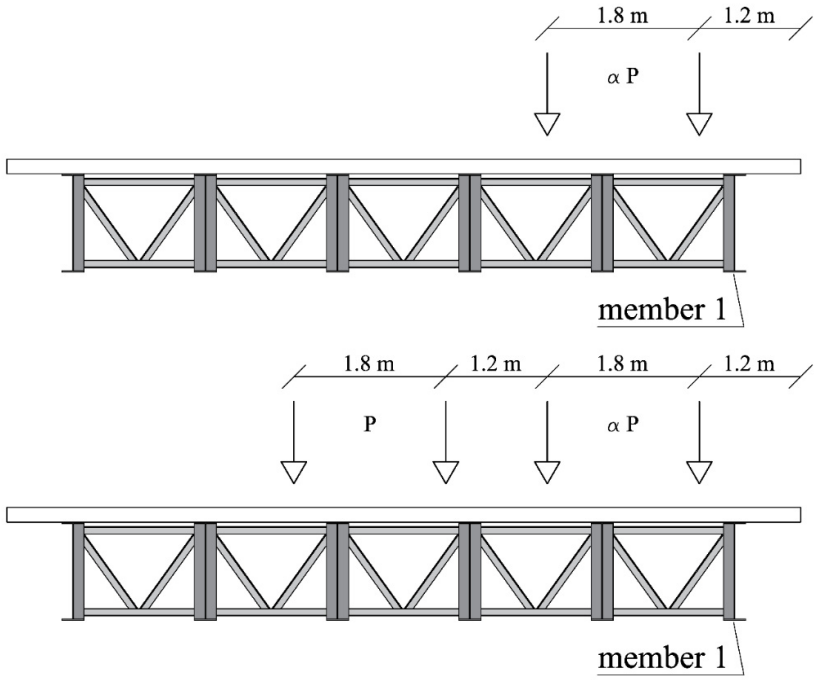


**Figure 5-8. Section view of side-by-side truck loading pattern.**

Two different load patterns are proposed: the first is represented by one eccentric truck multiplied by the factor $\alpha$ and the second represented by two side-by-side trucks where the most external truck is multiplied

by the factor $\alpha$ while the internal truck is used with its nominal weight. The proposed $\alpha$ factor serves both as a multiple presence factor and an overweight factor. The calibration of the parameter $\alpha$ is executed such that the maximum load effect produced by the single AASHTO legal truck of weight $\alpha P$ or two side-by-side trucks of weights $P$ and $\alpha P$ on the most critical main member is equal to the maximum load effect obtained from Equation 5-6 for the member.

During the structural analyses performed in this study, the following assumptions are made regarding the transverse placement of the trucks to simulate the worst loading conditions:

- The distance between the most external wheel and the edge of the deck is 1.2 m (barrier + curb + clearance).
- The truck wheels are spaced at 1.8 m.
- For the two-truck cases, the transversal distance between trucks is 1.2 m, unless the deck width is smaller than 7.2 m in which case the distance between trucks is reduced to satisfy the distance from the edge criteria set in the first bullet.

The longitudinal position of the trucks to be employed during the analysis is the one that produces the highest value for the load effect and it has to be calculated for each truck in its own lane separately. The calibration of $\alpha$ is carried out by equating the mean of the maximum load effect produced by Equation 5-6 to the legal truck load effect using Equation 5-9:

$$\alpha = \frac{L_{max,1}}{E_1^{legal}} \tag{5-9}$$

For two-lane loadings, the parameter $\alpha$ of the legal truck in the main drive lane is obtained according to Equation 5-10:

$$\alpha = \frac{L_{max,2} - E_2^{legal}}{E_1^{legal}} \tag{5-10}$$

where $L_{max,k}$ is the mean value of the maximum load effect obtained from Equation 5-6 over $k$ loaded traffic lanes, and $E_i^{legal}$ is the effect of the legal truck (3-S2 or type 3) located in such a way as to produce the maximum effect position in lane $i$.

The calibration process consists of calculating $L_{max}$ using Equation 5-6 for all the combinations of the bridge configurations listed in Table 5-2 repeated for each of the truck records collected from the twenty

WIM stations. $L_{max}$ and the corresponding parameter α are calculated for bending moments for exposure periods, T= 1, 2, 3, 4, 5 and 6 years.

The results obtained from Equations 5-9 and 5-10 are approximated with a simplified polynomial expression, as proposed by Anitori et al. (2017) as a function of beam spacing, number of beams and span length of the bridge under study, and described by Equation 5-11:

$$\alpha_{eq.} = J + a_1 \frac{SL}{30.5} + b_1 \frac{BS}{1.8} + c_1 \frac{NB}{6} + a_2 \left(\frac{SL}{30.5}\right)^2 + b_2 \left(\frac{BS}{1.8}\right)^2 + c_2 \left(\frac{NB}{6}\right)^2 \quad (5\text{-}11)$$

The symbols in Equation 5-11 are defined as: $SL$ is the span length, $BS$ is the beam spacing, $NB$ is the number of beams, $J$ is a constant coefficient and $a_1$ ... $c_2$ are regression coefficients.

The coefficient $J$ in Equation 5-11 depends on the exposure time and is defined for 1-lane and 2-lane load patterns as well as for Type 3 and 3-S2 truck configurations. The values of $J$ for each case are listed in Table 5-5.

**Table 5-5. Values of the constant *J* for different exposure intervals, one and two lane load pattern and 3-S2 and Type 3 truck configurations.**

| | 3-S2 | | Type 3 | |
|---|---|---|---|---|
| Exposure (years) | 1-lane | 2-lane | 1-lane | 2-lane |
| 1 | 2.19 | 1.35 | 1.15 | 0.89 |
| 2 | 2.25 | 1.44 | 1.21 | 0.99 |
| 3 | 2.29 | 1.50 | 1.24 | 1.05 |
| 4 | 2.31 | 1.54 | 1.27 | 1.09 |
| 5 | 2.34 | 1.57 | 1.30 | 1.11 |
| 6 | 2.35 | 1.60 | 1.31 | 1.14 |

The coefficients $a_1$ ... $c_2$ are regression coefficients that give different weights for each bridge parameters. The values are listed in Table 5-6.

**Table 5-6. Coefficients of Equation 5-11 for analysis of shear and moments under one-lane and two-lane loadings for 3-S2 and Type 3 truck configurations.**

| | 3-S2 | | Type 3 | |
|---|---|---|---|---|
| | 1 Lane | 2 Lanes | 1 Lane | 2 Lanes |
| $a_1$ | 0.263 | 0.38 | 1.828 | 1.378 |
| $b_1$ | 0.001 | 0.066 | 0.047 | 0.152 |
| $c_1$ | 0.245 | 0.178 | 0.908 | 0.273 |
| $a_2$ | -0.086 | -0.112 | -0.074 | -0.017 |
| $b_2$ | 0.001 | -0.006 | -0.016 | -0.051 |
| $c_2$ | -0.103 | -0.059 | -0.389 | -0.113 |

## 5.9 Probabilistic Live Load Model

While the coefficients and constants in Tables 5-5 and 5-6 are sufficient for performing deterministic bridge analyses, a probabilistic format for the live load model is needed if the engineer decides to carry out a reliability analysis of a bridge structure. Specifically, the probabilistic format must account for the variability in the applied load and the associated modeling uncertainties (Ghosn et al., 2011, 2013). Therefore, the load effect in a reliability analysis using the results for the α parameter generated in this paper or similar simulations can be represented as the product of the following random variables for the two-lane loading case, as shown in Equation 5-12:

$$LL_{2-lane} = W_{truck} \cdot (1 + \alpha \cdot StS) \cdot Mod \cdot Dyn \tag{5-12}$$

or using Equation 5-13 for the one-lane case

$$LL_{2-lane} = W_{truck} \cdot \alpha \cdot StS \cdot Mod \cdot Dyn \tag{5-13}$$

where $W_{truck}$ is the deterministic load effect of the nominal weight of the AASHTO 3-S2 Legal Truck having a total weight equal to 320 kN or the Type 3 Legal Truck with a gross weight equal to 222 kN; $Mod$ is the load effect model uncertainties, $StS$ is the site to site variability accounting for the uncertainty in defining a load value representing different WIM stations, $LL$ is the total live load effect intensity. Detailed statistics of the random variables in Equations 5-12 and 5-13 are provided in Table 5-7.

**Table 5-7. Random variables associated with the parameter α.**

| Symbol | Random variable | Mean | COV | Distribution | Reference |
|---|---|---|---|---|---|
| $\alpha$ | Weight multiplier of the truck on main drive lane | From Equations 5-9 and 5-10 | 1-lane loading 4.0%<br>2-lane loading 8.0% | Gumbel | Present study |
| $StS$ | Site to site variability from different WIM stations | 1.00 | Mean 15.0%<br>Low, Medium and High OW 6.0% | Normal | Present study |
| $Dyn$ | Dynamic amplification due to moving vehicles | 1-lane loading 1.13<br>2-lane loading 1.10 | 1-lane loading 9.0%<br>2-lane loading 5.5% | Normal | (Nowak, 1999) |
| $Mod$ | Load effect model (grillage) | 1.00 | 8.0% | Normal | (Sivakumar & Ghosn, 2011) |

The statistical values for the dynamic amplification factors listed in Table 5-7 as suggested by Nowak (1999) are found to be in line with the ones proposed by numerical studies and experimental investigations (Lu Deng, Cai, & Barbato, 2011; Ghosn & Moses, 1985, 1986; Ghosn, Moses, & Gobieski, 1986; González, 2010; O'Brien, González, & Žnidarič, 2012).

## 5.10 Chapter conclusion

In this chapter, a methodology is developed to define a live load model for the refined analysis of multi-girder bridge systems. This methodology was implemented to calibrate a live load model using WIM data recorded at several New York State locations. This live load has the great advantage to be convenient for system reliability analysis because it accounts for all relevant load related variables and parameters.

This live load will be used in this work to represent the live load demand of the basic safety equation. It must be recalled that bridge structures are not only threatened by traffic overload, but by several other sources of extreme events such as foundation scour, vessel or vehicle impact, earthquakes or winds. While the probability of failure linked with these other extreme events may be relevant for specific cases, supporting traffic load is the main purposes of highway bridges and thus is the focus of this work.

The live load defined in this chapter is specifically used for the system reliability analysis that will be explained in Chapter 6 which is main component of risk assessment as will be further explained in Chapter 8.

# 6 Reliability Analysis of Bridge Structural Systems

Establishing the safety of a structure is usually assured by following design criteria and guidelines published at the national or regional levels. Engineers are familiar with procedures for analyzing typical engineered structures and design these to meet pre-set criteria. However, in order to ensure that established criteria and safety factors provide sufficiently safe designs, code writers usually calibrate these to meet target levels of structural reliability or safety. In other words, the structural code committees quantify the requirements of the society in terms of safety to people and economic efficiency, and translate them into usable engineering models associated with appropriate safety factors and criteria for design purposes. Similar approaches are proposed in this study for developing a method for determining adequate bridge inspection intervals based on risk assessment criteria. Risk-based methods require the definition of limit state equations and numerical analysis methods for determining the reliability of a bridge structure which subsequently will be combined with the consequences of failure. This chapter describes the reliability analysis procedure implemented in this study as a main component of the risk analysis process.

## 6.1 Reliability analysis

A set of terms must first be defined to familiarize the reader with the reliability analysis framework. The definitions used herein follow the concepts explained by Nowak and Szersezen (2001). The first term to be defined is failure. A structure fails when it does not fulfill its original purpose after some external perturbation is applied. It is therefore clear that there cannot be a unique definition of failure but it is simply related to a specific loss of performance. The point at which the loss of performance occurs is defined as a limit state and is normally preceded by an adjective (e.g. ultimate, serviceability, fatigue) that specifies the nature of the loss of performance. The limit state is further defined by a set of possible structure and external perturbation (actions) conditions leading to the limit state. Therefore, the limit state can be imagined as a curve separating the acceptable range of structural performances from the unacceptable range. In other words, the limit state curve is a boundary between the set of safe and unsafe performances. The reason why different configurations of the structure and actions exist is due to the fact that structure and actions are modeled with certain degrees of uncertainty, allowing infinite definitions of the problem with different probabilities of occurrence whose study is defined as probabilistic analysis.

In order to better explain the bases of the probabilistic analysis a simple case of a beam with resistance moment $R$ (capacity) loaded by a point load representing a truck that produces a moment $Q$ (demand). The uncertainties of the resistance $R$ and the demand $Q$ can be mathematically represented by a probability distribution curve as shown in Figure 6-1.

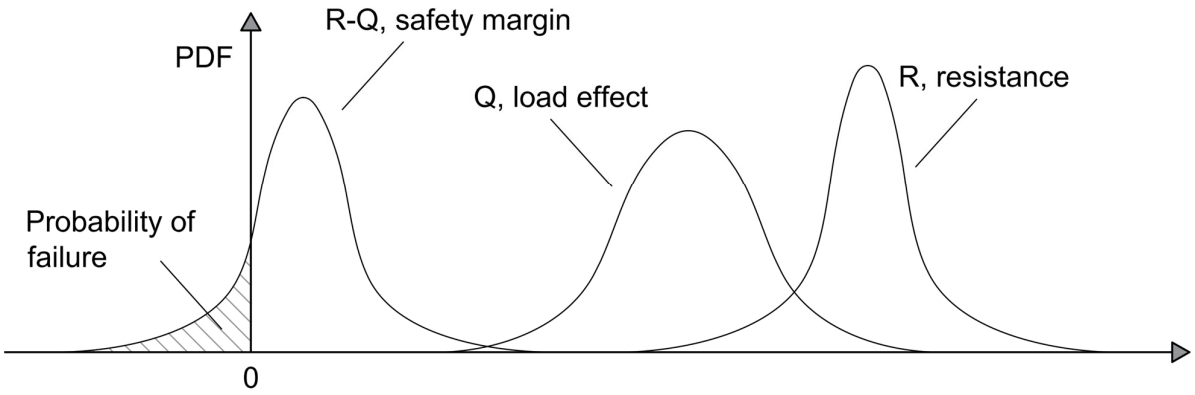


**Figure 6-1. Limit state function, safety margin and probability of failure definitions (extracted from Novak (2001)).**

As can be seen from the figure, many realization of the resistance have higher values than those of the load, meaning that in many situations there is additional resistance than strictly required. In addition, it is normal to observe a higher uncertainty in the load effect rather than the resistance values and this is observed by looking at the corresponding spreads of the probability distributions. If the load effect is subtracted from the resistance, the resulting limit state is expressed in terms of the variable $Z = R - Q$ defined a probabilistic measure of the margin of safety.

The variable $Z$ assumes negative values for unsafe bridges (shaded area of Figure 6-1) and positive values in the safe region. The probability of failure is defined by Equation 6-1:

$$P_f = P(Z < 0) = \int_{-\infty}^{0} f(x_n)\, dx \tag{6-1}$$

where $f(x_n)$ is the joint density function defined as the limit state equation of the $n$ random variables that define the variable $Z$.

The probability of survival is usually described mathematically through the reliability index $\beta$ based on the assumption that the limit state function $Z$ follows a normal distribution, according to Equation 6-2:

$$\beta = -\Phi^{-1}(P_f) \tag{6-2}$$

Where $\beta$ is the reliability index, $\Phi^{-1}(\cdot)$ is the inverse function of the standard normal cumulative distribution.

A convenient interpretation of the reliability index $\beta$ is that it represents the distance (specifically, the number of standard deviations) the mean of the margin of safety $Z$ is away from failure when $Z = 0$.

## 6.2 Limit State Equation

The limit state equation $Z = f(x_n)$ is the combination of different random variables both for the demand $Q$ and for the response part $R$. However, for the sake of simplicity, the 2-variable example (demand $Q$ and capacity $R$) used in the previous section are still used to define the space of state variables as the limit state equation curve defined by the function $f(Q, R)$ in the $Q, R$ coordinate system as shown in Figure 6-2.

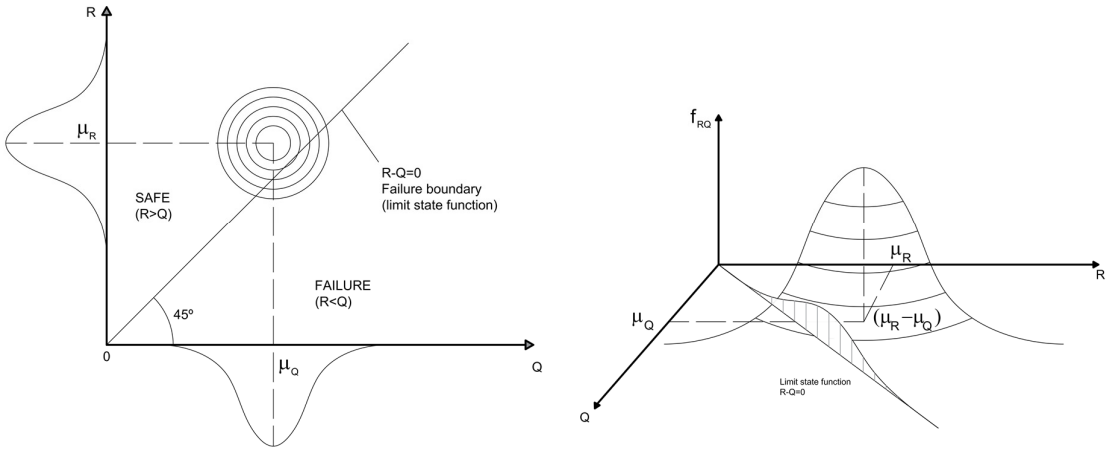


**Figure 6-2 Space of state variables for the simple 2-variable case (extracted from Novak (2001). In the 2-dimensional (left) and in the 3-dimensional space (right).**

The probability of failure can be visualized graphically as the integral of the joint density function (a surface in a 2-dimensional space) in the failure zone, as expressed by Equation 6-1.

In the present work the number of variables are more than two and a graphical representation is not possible. The system safety is represented by the limit state inequality shown in Equation 6-3:

$$(R - DL) - LL(1 + \alpha) \cdot Mod \cdot Dyn \cdot StS \geq 0 \tag{6-3}$$

Where $R - DL$ is the joint random variable representing the available capacity after subtracting the dead load part which can be estimated as explained in Chapter 4 of this Thesis. The demand $Q$ is expanded as explained in Chapter 5 where $LL$ is the truck load effect (3-S2 truck with base line weight equal to 320 kN or the Type 3 truck with base line weight equal to 222 kN), $Dyn$ is the dynamic amplification due to moving vehicles, $Mod$ load effect model uncertainty (grillage) and $StS$ is the site-to-site variability of the traffic load

(refer to  for the numerical values and probability distribution type and parameters). Equation 6-3 is valid for a two-lane model. The one-lane live load equation is obtained by substituting the term $(1+\alpha)$ with $\alpha$ defined in Equation 5-9.

The objective of the reliability analysis is to find the probability that $Z > 0$ as expanded in Equation 6-1 condition to be false.

## 6.3 Solution method for reliability

The calculation the reliability index for the simple case of two normally distributed random variables $(Q, R)$, assuming a simple limit state equation as shown in Figure 6-1, can be solved in closed form by the simple Equation 6-4:

$$\beta = \frac{\mu_R - \mu_Q}{\sqrt{\sigma_R^2 + \sigma_Q^2}} \tag{6-4}$$

Where $\mu_R$ and $\mu_Q$ are the mean and $\sigma_R^2$ and $\sigma_Q^2$ the standard deviations of the random variables $R$ and $Q$. The probability of failure would be easily calculated by applying inversely Equation 6-2. However, for more complex limit state equations, a closed form equation may not be available and numerical methods need to be used such as the crude Monte Carlo Simulation (MCS) or the Latin Hypercube Simulation (LHS) described in Chapter 4 of this Thesis. Other available methods include the Importance Sampling technique, First Order Reliability Method (FORM), Second Order Reliability Method (SORM) among others. While MCS and LHS are used for sampling the $R - DL$ variable in Chapter 4, a comprehensive understanding of these methods may be obtained in Nowak and Szersezen (2001), Ang and Tang (2007) and Lui and Chen (2005).

In this work, the probability of failure associated with Equation 6-3 is calculated with the FORM method that allows the calculation of the reliability index given the distributions and the corresponding parameters of each terms of the limit state equation. According to FORM, any random variable $x_i$ that does not follow a normal distribution is first transformed into an equivalent variable that follows a normal distribution depending on the value of the realization at which it is being evaluated according to any of the different methods available in literature, such as the Simple (Paloheimo & Hannus, 1974). Normal Tail (Ditlevsen, 1981) or the Rosenblatt (Rosenblatt, 1952) or the Nataf (Nataf, 1962) Transformation. For a comprehensive description of these transformation methods and their comparison refer to Melchers and Beck (2018). Subsequently, each normal (or normalized) probability random variable is further transformed into a reduced variable $u_i$, having zero mean and a unit standard deviation, using the Equation 6-5:

$$u_i = \frac{X_i - \mu x_i}{\sigma x_i} \tag{6-5}$$

The transformed limit state equation $f(x_i, \dots, x_n)$ becomes $f(u_i, \dots, u_n)$. The space corresponding to the reduced variables is described, for the simple case of two random variables, with concentric circles of equiprobability Figure 6-3. The space of the reduced variables can be visualized in two dimensions in the graph shown in Figure 6-3, where the limit state function in the normalized space, $f(u_i, \dots, u_n)$ is shown along with the tangent to the equipotential circle defining the minimum distance between the origin and the limit state design function. Figure 6-3 allows to graphically visualize the definition of the reliability as the shortest distance from the origin in reduced space to the limit state surface.

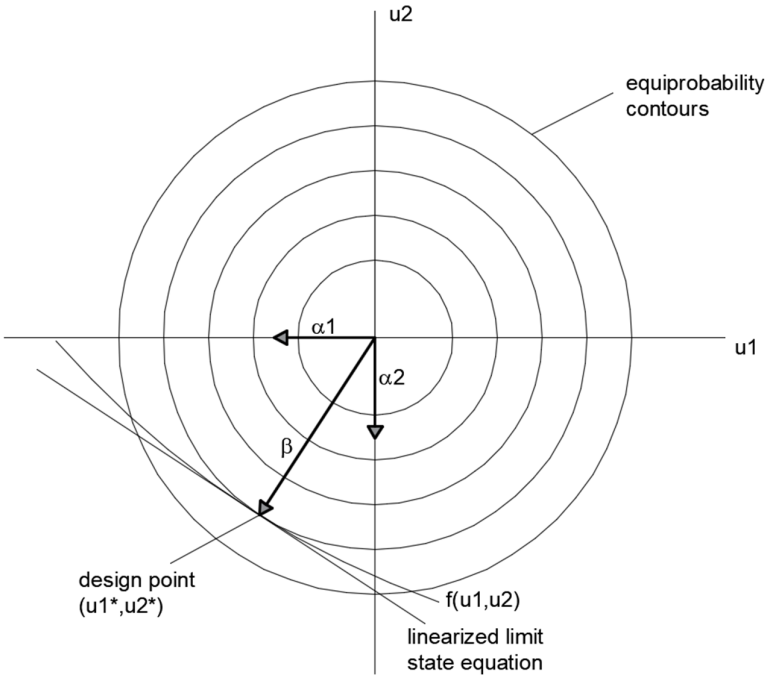


**Figure 6-3. Reliability analysis formulation in the reduced variable space. Adapted from Ellingwood et al.(1980).**

As shown in Figure 6-3, the point $(u_i^*, \dots, u_n^*)$ on the limit state surface, that corresponds to the aforementioned minimum distance, can be determined by solving the set of Equations 6-6, 6-7 and 6-8:

$$\alpha_i = \frac{\frac{\partial f}{\partial u_i}}{\sqrt{\sum_i \left(\frac{\partial f}{\partial u_i}\right)^2}} \tag{6-6}$$

$$u_i^* = -\alpha_i \beta \tag{6-7}$$

$$f(u_i^*, \dots, u_n^*) = 0 \tag{6-8}$$

where $\alpha_i$ is the unit directional vector of the $i-th$ random variable in the normalized space and $\beta$ is the reliability index.

The solution is found by changing the values of the factors $\alpha_i$ to obtain the minimum distance from the linearized limit state equation and the origin in the reduced space. The design point, defined as the point that gives the shortest distance to the origin on the reduced space, corresponds to the point in the original random variable space by means of Equation 6-9:

$$X_i^* = \mu x_i \left(1 - \alpha_i \beta V_{X_i}\right) \tag{6-9}$$

Such that $f(u_i^*, \dots, u_n^*) = 0$.

The FORM algorithm described above is available in the reliability analysis module of the software OPENSEES and detailed information for its implementation are described by Haukaas and Der Kiureghian (2004).

## 6.4 Reliability analysis results

The FORM algorithm described in the previous subsection is used to calculate the reliability index of the 279 bridges contained in *set 1*. The limit state equation that defines the border between safe and unsafe designs has already been defined by Equation 6-3 and the possible values of the random variables are summarized in Table 5-7 for the demand with the live load definition provided in Chapter 5 and in the values shown in Figure 4-20 with the capacity and dead load statistical characterization provided in Chapter 4. The full explanation and relevant sources behind the statistics of each random variable and its distribution function are provided in Chapter 4 and Chapter 5 for capacity/dead load and live load respectively and summarized in Table 6-1.

**Table 6-1. Input for the FORM reliability algorithm.**

| **Variable** | probability distribution | nominal value | bias | COV |
|---|---|---|---|---|
| Capacity (*R-DL*) | normal | depends on: -result of system nonlinear analysis | depends on: -bridge configuration -deterioration rate -exposure years (e.g.Figure 4-23) | depends on: -deterioration rate -exposure years (e.g. Figure 4-24) |
| Demand ($\alpha$-*LL*) | gumbel | depends on: -span length (Figure 5-7) | depends on: -bridge configuration -exposure time (Equation 5-11, Table 5-5 and Table 5-6) | depends on: -number of traffic lanes (Table 5-7) |
| Site to site variability | normal | 1.00 (Table 5-7) | 1.00 (Table 5-7) | 15.0% (Table 5-7) |
| Dynamic amplification factor | normal | 1.00 (Table 5-7) | depends on: -number of traffic lanes (Table 5-7) | depends on: -number of traffic lanes (Table 5-7) |
| Model (grillage) | normal | 1.00 (Table 5-7) | 1.00 (Table 5-7) | 8.0% (Table 5-7) |

The capacity random variable parameters depend on the result of the structural analysis, and on the deterioration rate that also increases as the exposure time does. In other words, for each bridge, a set of matrices similar to the ones shown in Figure 4-20 for an example bridge is calculated. On the demand side of the equation the nominal truck configuration is Type 3 for span lengths shorter than 30 m and 3-S2 Legal for bridges spanning more than 30 m. The transformation from nominal to average maximum live load, including site to site variability, dynamic amplification and model uncertainties is calculated according to the concepts explained in Chapter 5 and summarized in Table 5-7.

The 279 results obtained by applying the FORM algorithm can be better visualized to study the range of reliability indices obtained by observing some of the trends that have been found to be relevant in Figures 6-4 to 6-11.

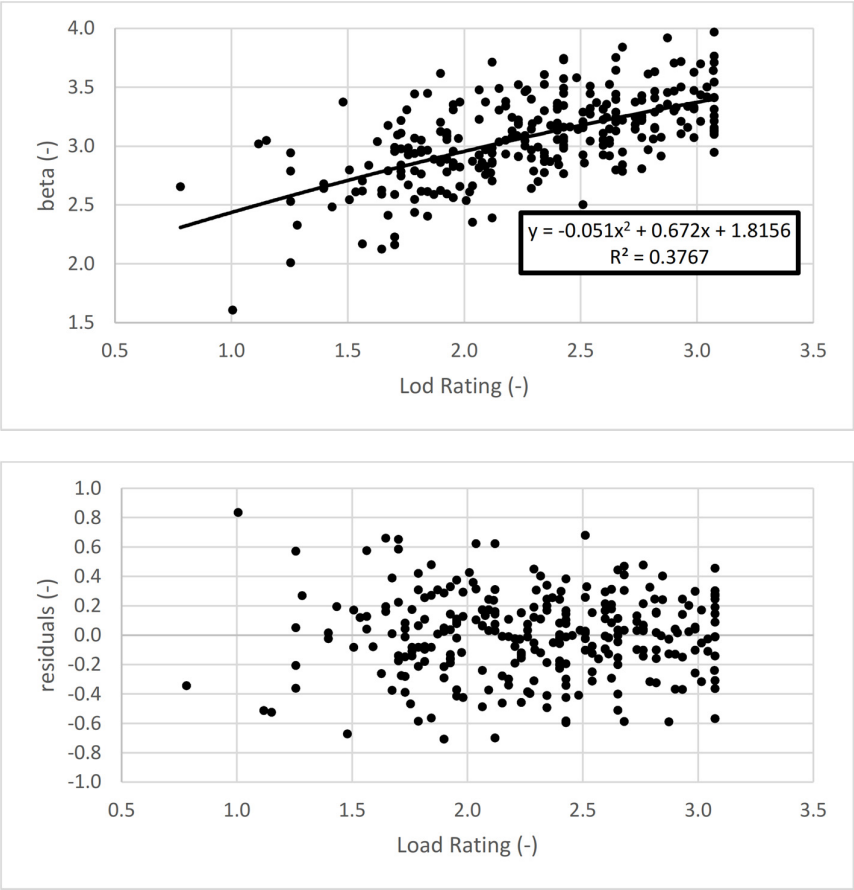


**Figure 6-4. System reliability index vs. Load Rating (top) and residuals plot (bottom).**

The first plot shown in Figure 6-4 relates the reliability index calculated in this Chapter with the LFR Legal Load Rating provided in the NBI database. As expected, the data plotted in Figure 6-4 (top) shows that, the reliability index increases as the load rating increases. For the purpose of following the trend, the plot of residuals is also provided in Figure 6-4 (bottom). The residuals plot shows that for a fixed load rating value the reliability index can vary within a range of plus/minus 1.0 with a standard deviation of 0.28. The spread in the residuals is related because the load rating assesses the member capacity, while the reliability index, as calculated in this study, assesses the system's capacity and thus for structures with an equal load rating the ones with a better system behavior (more redundancy) have a higher reliability index. Hence, neither the LFR nor the LRFR methods are expected to provide perfect relationship between the reliability index and Load Rating, even though the latter has been calibrated with member reliability criteria. For this reason, the trends do not lay along perfect curves but always present some degree of scatter.

Other than the relation between reliability index and load rating depicted in Figure 6-4, it has been difficult to establish relations between the system reliability index and other specific structural properties or, physical characteristics (such as beam spacing, span length or number of beams). This is because each bridge

is associated with different values of load ratings that is the main controlling factor of the bridge capacity. Therefore, in the next set of plots a third variable is plotted in different colors to help put into context the effect of other parameters on the relation between the reliability indices and the load rating.

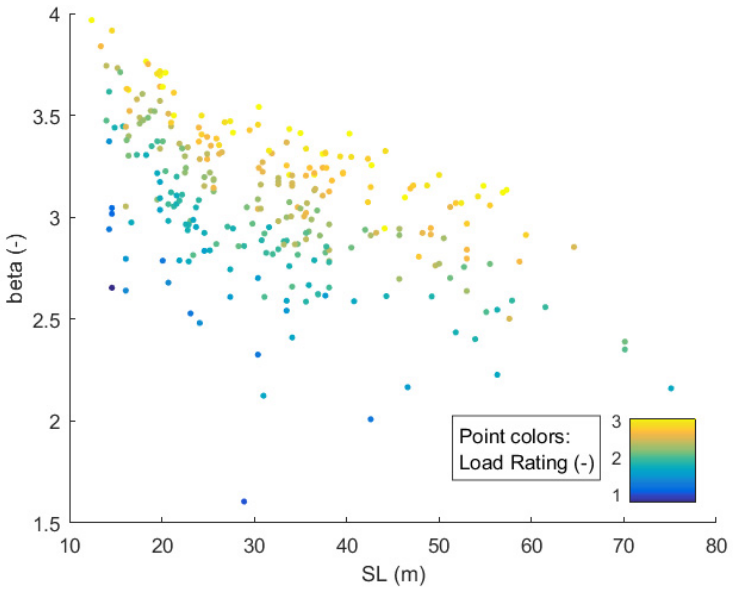


**Figure 6-5. System reliability index vs. span length and point colors representing Load Rating (Operational).**

The plot shown in Figure 6-5 puts into relation the reliability index with the span length and helps understand that the reliability index decreases as the span length increases for the same load rating values. It is observed that the influence of the other parameters cause a variation of about plus/minus 1.0 in the beta values. However, the spread around the trend line for the reliability indices of bridges with high load rating (yellowish points) indicating that the influence of parameters other than span length is relatively smaller than for bridges with low load ratings (bluish points). On the other hand, the reliability index seems to be less dependent on the number of beams as illustrated in Figure 6-6, while beam spacing is an important parameter and its influence on the reliability index is noticeable, as shown in Figure 6-7.

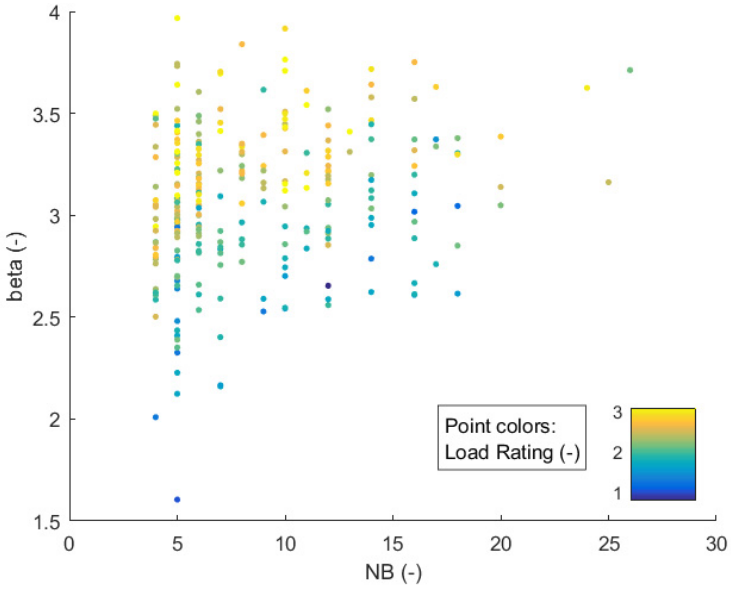


**Figure 6-6. System reliability index vs. Number of beams and point colors representing Load Rating (Operational).**

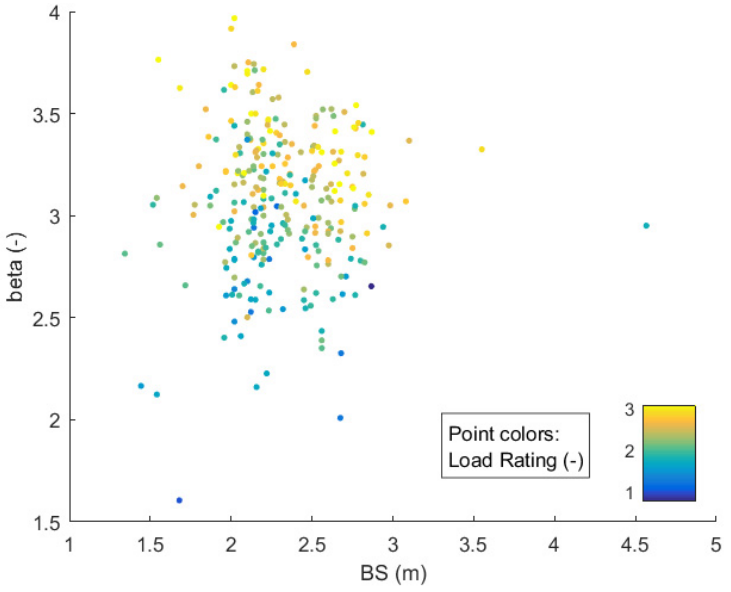


**Figure 6-7. System reliability index vs. Beam spacing and point colors representing Load Rating (Operational).**

In Figure 6-7, the effect of beam spacing by itself may be difficult to observe. However, it may be more relevant to look at the bridge's aspect ratio defined as the beam spacing divided by the span length (BS/SL).

The resulting plot is shown in Figure 6-8 illustrating the increasing trend in reliability index as the beam spacing increase and as the span length decreases.

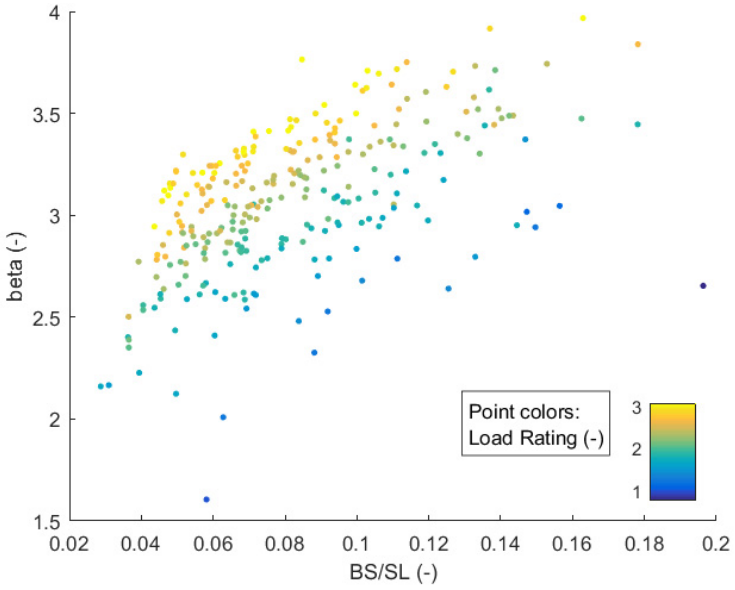


**Figure 6-8. System reliability index vs. aspect ratio and Load Rating (Operational).**

To further study the effect of a bridge's aspect ratio (span length and beam spacing) and load rating on the reliability index a sensitivity analysis is performed on a generic bridge rather than bridges in *set 1* varying only one variable at the time. The sensitivity analysis is performed on a base bridge having a span length of 30 m formed by 6 beams spaced 2.5 m having Operating Load Rating RF=1.2 according to the LFR rating method.

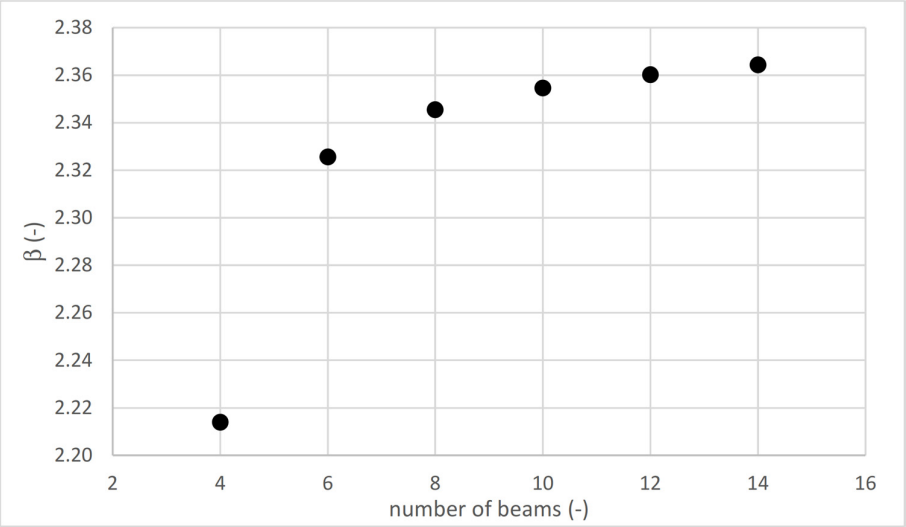


**Figure 6-9. Sensitivity analysis of reliability index versus number of beams.**

The first sensitivity analysis is performed over bridges with increasing widths obtained by increasing the different number of beams as shown in Figure 6-9 showing that the reliability index increases asymptotically as the number of beams increases as expected. This is because even though the additional beams are located far from the application of the traffic load, it is still possible to observe significant load transfer laterally for the smaller number of beams, due to the transverse load stiffness provided by the deck. However, as the number of beams increases, the improvement in the reliability index is minimal because the additional beams are less effective when they are farther away from the applied traffic load.

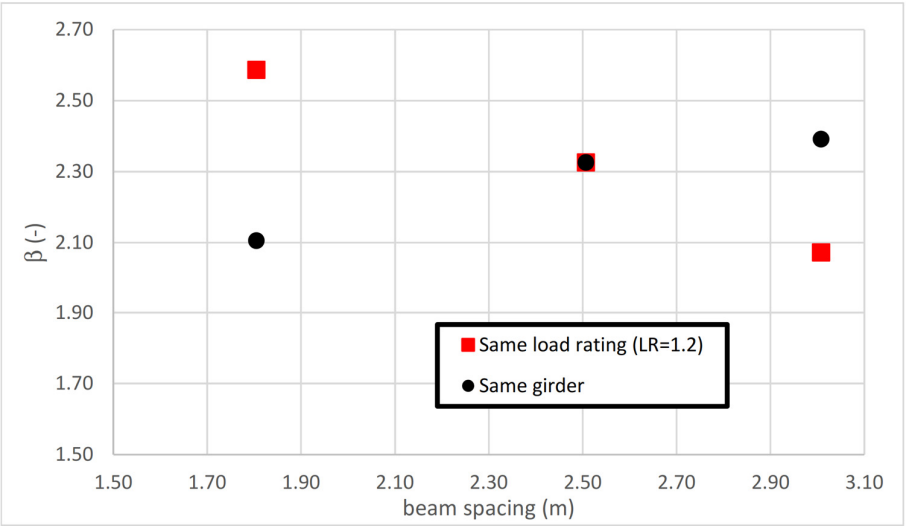


**Figure 6-10. Sensitivity analysis of reliability index versus beam spacing.**

The second sensitivity analysis is performed to study the effect of beam spacing as shown in in Figure 6-10. The series identified with red squares in Figure 6-10 show that increasing the beam spacing increases the reliability of the bridge. In this case, the load rating of the member is kept constant at a value of RF=1.2 by readjusting the girder design (bottom flange thickness). In addition, a change in the slab width inevitably implies that the dead load is also changed accordingly. In this case, the increase in member capacity due to the increase in slab width and girder dimensions is more relevant than the increase of the dead load and the increase in tributary live load on the most critical beam, explaining the increase in system capacity.

The series identified with the black dots, however, demonstrates that, if the beam designed with the 2.5 m spacing configuration is kept unchanged for the bridges with 1.75 m and 3.0 m, the reliability decreases as the beam spacing increases. In this case, the increase in member capacity is relatively small (only due to the increase in slab width) and the increase in dead load and tributary live load on the most critical member explain the decrease in system capacity.

One should note that the case, where only the beam spacing is changed without changing the beam capacity (black dots in Figure 6-10) is not realistic because beam design accounts for beam spacing. This case is analyzed to only study the trends.

The third sensitivity analysis is executed to study how the transverse slab properties affect the system reliability index. The sensitivity analysis is performed on the base bridge (span length of 30 m, 6 beams spaced 2.5 m and Operating LFR Load Rating of RF=1.2) after multiplying the slab stiffness and reinforcing steel area (top and bottom) by different ratios. The results are listed in Table 6-2 and a graphic visualization of the trends is shown in Figure 6-11.

**Table 6-2. Sensitivity of the reliability index to slab stiffness and slab resistance (rebar area).**

| | | Stiffness multiplyier | | | | | |
|---|---|---|---|---|---|---|---|
| | | 0.1 | 0.5 | 1.0 | 2.0 | 5.0 | 10.0 |
| Steel area multiplyer | 0.50 | 2.253 | 2.286 | 2.291 | 2.294 | 2.298 | 2.301 |
| | 0.80 | 2.256 | 2.301 | 2.316 | 2.326 | 2.333 | 2.338 |
| | 1.00 | 2.257 | 2.302 | 2.326 | 2.344 | 2.355 | 2.360 |
| | 1.25 | 2.247 | 2.303 | 2.328 | 2.354 | 2.357 | 2.364 |
| | 2.00 | 2.235 | 2.304 | 2.338 | 2.370 | 2.383 | 2.392 |
| | 5.00 | 2.255 | 2.336 | 2.369 | 2.380 | 2.400 | 2.419 |

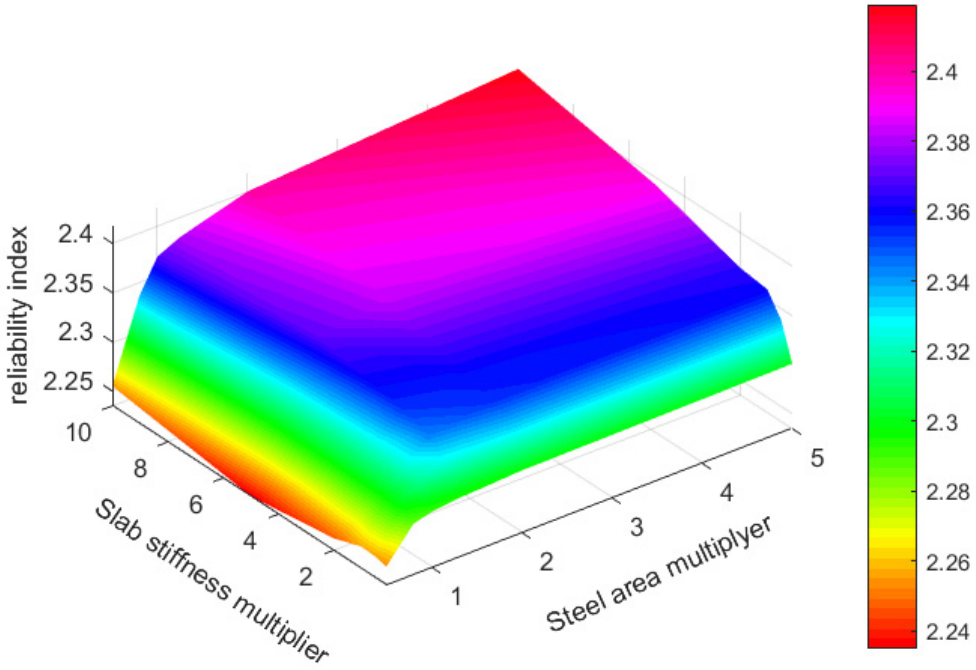


**Figure 6-11. Sensitivity of the reliability index to slab stiffness and slab resistance (rebar area).**

While in the first stages of the load increment the bridge all elements, including the slab, will be in its linear elastic range of internal stresses, the bridge elements undergo non-linear stresses as the load increases. The results show that, as expected, the reliability decreases as the stiffness and rebar area multipliers decrease, since these two characteristics influence the system ability to redistribute loads. However, as the two multipliers increase the subsequent increase in system reliability is slower reaching a plateau for high values of slab stiffness and resistance due to the fact that the transverse behavior of the bridge cannot be improved because a very high transverse beam stiffness will spread the load equally to all the beams even when the live load is located on an the extreme lane of the bridge. This will cause all the beams to fail simultaneously producing an upper limit for the bridge system capacity.

## 6.5 Chapter conclusion

After defining the statistical characteristics of the resistance and load demand for bridges as described in Chapters 4 and 5 respectively, a system reliability analysis process can be performed for any composite steel girder bridge following the procedure outlined in this chapter. The reliability index is a direct measure of the safety of bridge structural systems and is calculated for all the 279 bridges in *set 1*.

A sensitivity analysis showed that the Operating load rating and the span length have major effects on the reliability index of multi-girder composite steel bridges. Factors that have a lesser influence on the reliability index include the beam spacing and the number of beams.

The reliability analysis will determine a bridge's probability of failure, which when multiplied by the consequences of failure will provide a measure of the risk associated with each bridge and how it changes with the level of deterioration over time. As will be seen in the next two chapters, the information extracted from the reliability analysis will help determine an optimum, inspection interval which is the main objective of this work.

# 7 Cost analysis of Failure Consequences

In this section, the cost of bridge failure is estimated and monetized in terms of dollar amounts and used as a comprehensive measure of the consequences of a bridge's failure and its impact on society. The cost of bridge failure has been studied by many authors (Fiorillo, 2015; Frangopol, Dong, & Sabatino, 2017; Neves & Frangopol, 2005) with particular focus on bridge life-cycle assessment and maintenance. In general, assessing a cost of failure in absolute terms is a difficult task because of the uncertainties in evaluating the specific factors that must be considered and associate these with dollar amount. For these reasons, cost analyses are best used for comparing design alternatives and for decisions involving prioritization of a single bridge or a group of bridges, which could be parts of a bridge network or a sub-population. In such cases, the cost acts as a uniform and rational attribute for a bridge or a design alternative. In this work, the cost of failure is used to quantify the risk after determining the probability of failure as will be demonstrated in Chapter 8.

## 7.1 Characterization of the Cost of Failure for Highway Infrastructures

The quantification of the risk associated with an event is, from a general point of view, dependent on the consequences of the occurrence of that event. While the term consequences is a general term, one can refer to the cost of losses, which provides a quantification of the consequences of a failure of an infrastructure facility such as those of bridges assessed in this work. The term cost may be assumed to entirely depend on the valuation of the benefit or losses associated with a certain product as noted by Lee (1995). In addition, cost refers to the tradeoffs between uses of resources, that in general can be related to money, time, land, loss of an opportunity to enjoy a benefit, or loss of lives (Litman, 2009).

The definition of cost is also associated with political decision processes, which are by their very nature part of the political debate itself. For example, Tanner and Hingorani (2015) associates the cost of building failure, in a broad sense, with the loss of human life because as he states "the risk to personal integrity takes precedence over all others". While this approach may be acceptable for problems where there are a constrained set of consequences as may be assumed for residential buildings, it may be overly simplified for infrastructure problems that affect different sets of constituents ranging from the single user to the general community and the environment. Therefore, many researchers used different approaches even for buildings. For example, Steenbergen et al. (2015) separates the consequences of failures in buildings and other structures considering the economic value of the loss as one item and the loss of lives as a second separate item. However, it is more practical to avoid dealing with two different parameters, and to assign a single risk value for each structure under study. In this sense, Steenbergen et al. (2015) pointed out that a problem arises when using a unique cost evaluation which mixes measurable market costs of products to non-market costs, such as human loss of lives or decrease of life quality including psychological impact or anxiety which in the views of some researchers may be considered unethical. For example, from a political and mass

communication point of view, it may not be acceptable to value human lives and vehicle fuel in a same basket, since the audience is probably going to reject this approach even though at a global scale, that is what a political decision making process is about. In this work the approach used by several researchers in this field (Frangopol et al., 2017; Hawk, 2003; D. B. Lee, 1995), consisting of adopting a unique cost value linked to a bridge collapse is used for simplicity since it correctly reflects the value consumers place on applying resources to alternative options.

To obtain an estimated of the cost of failure, a categorization of the different consequences to take into account is necessary. The losses resulting from the failure of a bridge represented by their monetary costs, are the sum of the costs related to the structure itself and to the bridge owner labeled as direct or agency costs and the costs to the community labelled as indirect or society costs. The total Direct Cost ($C_D$) includes those of demolition, repair or reconstruction of partially or totally failed structures. On the other hand, the Indirect Costs are those due to vehicle congestion and delays ($C_{I1}$), accidents due to detour ($C_{I2}$), environmental impact ($C_{I3}$) and fatalities and injuries ($C_{I4}$). It must be noted that parts of the indirect costs, which are considered in this study, already exist regardless of whether the bridge fails or not. Such costs include those related to vehicle ownership, operational maintenance cost of running a vehicle. Therefore, this study will only consider the additional part of these costs that come about due to the failure of the bridge.

Furthermore, even though the total cost of failure is borne by society as a whole, there is a part of the cost borne by the government that are imposed indirectly even on non-users through taxes and tolls and will be labeled as external. Other costs such as vehicle operation costs that are borne by bridge users directly affected by the bridge failure will be labelled as internal costs. Other costs such as health issues from environmental air pollution due to congestion may be borne both by society at large and the users. For example, Zhang and Batterman (2013) observed that increased health problems due to traffic congestion affects mostly the vehicle users directly and the population living at about 100 m distance from the roadway during a congestion event. Therefore, one part of the cost may be borne by the individuals privately, such as medicines, private health insurance increased rates or loss of productivity (affecting the individual salaries) while other costs may be borne by the public health system, loss of productivity (affecting the efficiencies of economic units or public agencies) being carried by society as a whole. Determining if a cost is internal or external is not a straight forward task and several examples of costs that can be either internal or external depending on the point of view of the researcher conducting the study (Delucchi, 1997).

Another characterization of costs is whether they are fixed or variable. Conventional transport mode cost estimation considers as variable those costs that increase as a result of the occurrence of a certain event and that automatically decrease as the event occurrence reduces. Fixed costs are not affected by consumption, and can be further subdivided into past unrecoverable costs (such as an alternative design study that is never going to be built) and programmed costs (such as programmed road surface maintenance). However, this classification depends on the perspective of the problem under study and the definition of fixed and variable

cost used in this work are adapted to the bridge failure event. Therefore, it is recognized that after a bridge failure the user is required to bypass the missing infrastructure link by increasing its expenditure with a direct proportion (and thus variable) to the extra route needed to get to the same previously planned destination. On the other hand, fixed costs will be associated uniquely with the actual failed structure and are not dependent on the traffic volume or the disruption time of the infrastructure link under examination.

Another classification of the costs involved in the field of infrastructure is market or non-market cost. Some goods, such as structural materials, vehicle fuel or maintenance are part of competitive market and are used to establish their price and their cost. On the other hand, non-market costs are associated with those goods or events whose consequences of vehicle emissions on health (as the costs of a car accident) are not regularly traded in a market.

Finally, in a more philosophical way, the cost of the occurrence of an event is not independent on the point of view from which this is established. In fact, a lower cost may be considered by an individual not aware of the elements making up the full cost of an event and being the scope of the cost estimation a way to determine the consequences of an event, it may be of interest to take into account the perceived cost instead of the actual cost. For example, vehicle users tend to consider the cost of the vehicle itself as the perceived cost, being the actual cost a much more complex sum of factors as insurance, fuel, maintenance etc. In particular cases such as bridge failures, the cost estimation may be performed at different levels: from the point of view of citizens, of the technical engineer responsible of the infrastructure budget allocation or of the public administration. Assuming that the engineer is able to determine the correct actual cost, the public administration should adopt this point of view without filters, while the cost perception of the regular citizen may be biased by the way the information is conveyed and by the different possible political views and ethical values that may give the impression of a different cost from the actual and therefore to a perceived cost. It is noted that the perceived cost is not necessarily lower than the actual cost. In fact, the consequences of the occurrence of an event may be perceived as larger than the actual ones. For example, when taking into account the delay of a bridge inspection that, even if rationally justified by engineering calculation, may led to an increase in people anxiety and its consequent cost on society, meaning that the delay on a policy towards the possibility that a bridge may fail, brings to a large perceived cost, that contributes to even higher health related costs.

As a last point, the costs considered in this chapter must be quantifiable in order to be summed to the total cost. For this reason, the different costs considered in the next subsections are the results found in published literature documents from different fields. In this sense, for instance, the estimation of market costs is more reliable than non-market values. Market costs are associated with events that occur much more frequently than events linked to non-market values. It can therefore be stated that the quality of a cost estimation depends on the frequency of occurrence of that event or likewise in the probability that past similar events costs are estimated with sufficient precision to be extrapolated for future events.

## 7.2 Time dependent aspects of cost

Several economic factors influence the variation of costs over time. These include the discount rate, inflation/deflation and price elasticity (Stein, 2007). The discount rate defines the interest rate charged to banks from central banks (e.g. Federal Reserve in the US and Central European Bank in Europe) to finance loans for final users. The discount rate has fluctuated over the years depending on economic conditions. As shown in Figure 7-1, the discount rate at which the US Federal Reserve has been financing banks fell to almost zero immediately after the latest financial crises of 2008 only to rise slightly to about 2% over the last few years, with an average rate in 2019 of 2.16%. (The Federal Reserve, 2020). The projected discount rate for the year 2020 is expected to be 1.75% (The Federal Reserve, 2019a). The discount rate allows for an objective comparison of costs incurred at different points in time by considering the opportunity value of time. The opportunity value of time reflects the economic return that could be earned if funds were applied for alternatives other than for the activity being considered (e.g., the funds could be earning interest) or the compensation that must be paid to induce people to defer an action to later. Adjusting for the opportunity value of time is known as discounting (Demos, 2006).

Inflation and deflation are respectively the increase and decrease of prices over time as a result of supply and demand in an economic system. A steady 2-3% annual inflation rate is considered desirable by American and European authorities to propel consumption and ensure a value of savings over time (Central European Bank, 2020; The Federal Reserve, 2019b). However, in a free market economy, the central bank authorities cannot easily achieve the target inflation rate, but can only stimulate the economic response of citizens by adjusting the discount rate and controlling the money supply. Nevertheless, as shown in Figure 7-2 over the last few years, the US inflation rate has remained within the target value averaging about 2.0% over the last 3 years.

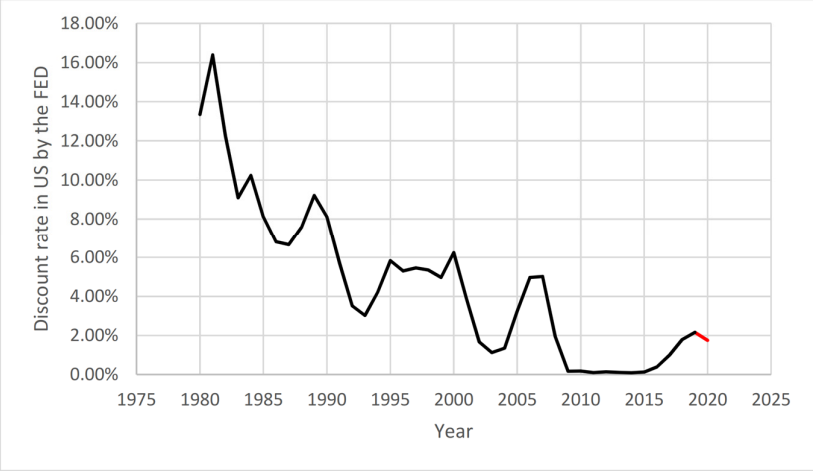


**Figure 7-1. Discount rate in the US established by the Federal Reserve.**

The estimated future costs must, therefore, be adjusted based on expected inflation rate and a discount from the actual price of a good must be taken when the investor is using federal funds.

Price elasticity is defined as the percentage change in the consumption of a good caused by a one-percent change in its price. Prices of goods can be categorized, with different levels of degrees, as elastic or non-elastic depending on the sensitivity of consumers to the price of a good. This concept is useful to determine the uncertainties in calculating the cost of failures for cost-benefit studies over an appropriate time interval.

In this work, the costs of failure are updated from the year they are established to the present (2020) considering the inflation rate of previous years. Future costs are adjusted based on an expected inflation rate of 2% and a discount rate equal to 1.75% as forecast by the Federal Reserve. However, possible changes in consumer behavior due to price elasticity is not considered as suggested in NCHRP 24-25 (Stein, 2007) where it is stated that given an estimated price elasticity on the order of 3% no significant effect on consumer surplus is expected.

As stated by Demos (2006), analytical "adjustments for inflation and discounting are entirely separate concerns, and they should not be confused by attempting to calculate both at once". Instead, future costs and benefits of a project should be expressed in constant dollars and then discounted to the present at a discount rate that reflects only the opportunity value of time (known as a real discount rate). This is because public sector project benefits should be dependent only upon real gains (cost savings or expanded output), rather than purely price effects. According to Demos (2006) one commonly used approach for discounting is based on the "Relocation in Time". According to this approach, a single figure can be "moved" (transformed into an equivalent value) backward or forward in time. The comparison can be made using the present worth $PW(\ \ )$ which can be calculated with Equation 7-1:

$$PW(year_{out}) = FV(year_{in}) \prod_{year_{in}}^{year_{out}} \left(\frac{1}{1 + I_d}\right) \tag{7-1}$$

Where $I_d$ is the expected discount rate for each year under consideration and $FV(\ \ )$ is the future known value, $year_{out}$ is the year to which the value is being updated from the original known value in $year_{in}$ year.

In this work, the effect of inflation is considered in two ways: to adjust historic data to current costs, or to study how costs will be affected if actions are deferred. The costs of failure extracted from available literature are used in this work after updating these to 2020 dollars using real inflation historic data (thebalance.com, 2020) by means of Equation 7-2 and the values plotted in Figure 7-2 for each US dollar record year. The costs for deferring actions, will use the same equation but with a projected interest rate of 2%.

$$PW(year_{out}) = PV(year_{in}) \prod_{year_{in}}^{year_{out}} (1 + I_i) \tag{7-2}$$

The function $PV(\cdot)$ in Equation 7-2 stands for monetary value in $year_{in}$ and $I_i$ is the inflation rate for each $i$ year obtained from historical data.

Future cost projection can therefore be calculated in a single equation considering a real discount rate ($I_{real}$) as the difference between inflation and discount rate and considering this difference as a constant value for the next $n$ years, leading to Equation 7-3:

$$PW = PV \left(\frac{1}{1 + I_{real}}\right)^n \tag{7-3}$$

The suggested value for the real discount rate used by Demos (2006) was 4%, as historically used in Colorado Department of Transportation (CDOT) calculations, but that was before the economic crisis of 2008 took place. For this reason, at present time, and considering that in this work no time projections for periods longer than 6 years are made and assuming that public funds are borrowed from a central bank institution, it seems reasonable to use a 0% real discount rate, since both inflation and discount rate are expected to be around 2%, simplifying Equation 7-3 to $PW = PV$ meaning that the present cost is equivalent to the projected cost.

The sections that follow will provide models for estimating the costs of bridge failures as documented in the literature over previous years and will update these to the year 2020 based on the inflation data shown in Figure 7-2.

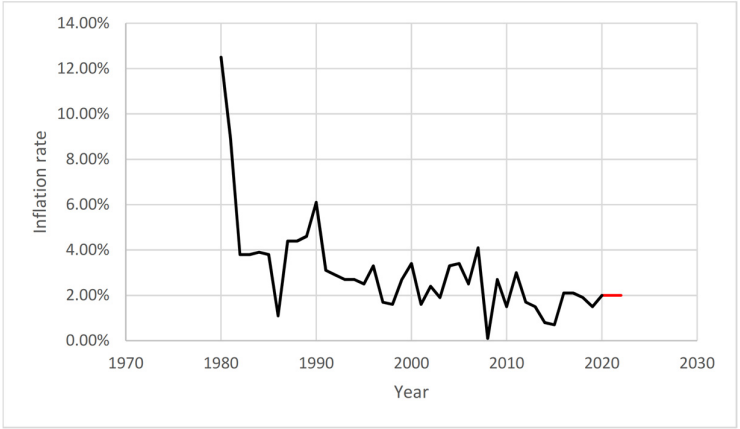


**Figure 7-2. Historic inflation rate for US economy.**

## 7.3 Cost Models

### *7.3.1 Direct Cost*

Direct (or agency) costs are costs associated with the repair of the damaged parts of a bridge or the demolition and reconstruction of an entire bridge after a bridge failure. A construction cost of $1679.17\ \$/m^2$ is calculated by Fiorillo (2015) using the unit costs for construction contained in RSMeans database (2009) as a function of the bridge total surface. A demolition cost of $31.78\ \$/m^3$ is used according to the Federal Emergency Agency (FEMA, 2010) as a function of the bridge material total volume. These values calculated for 2015 are further updated to 2020 leading to a construction cost of $1859.58\ \$/m^2$ and a demolition cost of $35.2\ \$/m^3$ including disposal of construction waste and recycling.

### *7.3.2 Cost of Operating Vehicles*

Disruption time is the length of time the bridge is expected to be out of service due to its failure. Specifically, disruption time, expressed in day of closure, $T$, gives the time for the repair or demolition and reconstruction operations required to restore a bridge to its previous service condition. It can be approximated as a function of the construction cost according to Jiang and Wu (2004) who established a regression model based on 102 bridges in Indiana, described by Equation 7-4:

$$T = \alpha\ \ln[C_C] - \gamma \tag{7-4}$$

Where $C_C$ is the expected construction cost in US dollars, $\alpha$ and $\gamma$ are calibrated coefficients of the regression model that are related to the construction and road type.

**Table 7-1. Coefficients α and γ for Disruption Time (Jiang & Wu, 2004)**

| Construction Type | $\alpha$ | $\gamma$ |
|---|---|---|
| Superstructure Repair | 26.67 | 259 |
| Bridge Replacement Interstate | 41.26 | 445 |
| Bridge Replacement State | 30.86 | 310 |

The disruption time is of great interest for life-cycle calculations as well as for design alternative evaluation when bridge availability is a requirement. For example, the recent trend of employing Accelerated Bridge Construction (ABC) focuses on design approaches where the cost of the project includes a wide range of factors other than mere construction cost. In this sense, vehicle operating costs sustained by infrastructure users are estimated with the equation and values suggested by Khan (2015) for ABC projects where vehicle

operating cost $C_{I1}$ is calculated as the sum of the cost due to the detour length and the cost due to the users´ time loss are modeled as shown in Equation 7-5:

$$C_{I1} = C_3\ D\ ADT\ T + \left[C_4\ O\ \left(1 - \frac{\rho}{100}\right) + C_5\ \frac{\rho}{100}\right]\frac{D\ ADT\ T}{S} \tag{7-5}$$

Where $C_3$ is the unit cost of running a vehicle per km (0.366 $ per km); $D$ is the detour length in kilometers, which can be obtained from the NBI database; $C_4$ is the value of time per adult (13.46 $ per hour); $O$ is the average occupancy rate per vehicle (1.35); $\rho$ is the ratio of $ADTT/ADT$ in percent; $C_5$ is the value of time per truck (26.93 $ per hour); and $S$ is the average detour speed in congested condition is 20.92 km/h according to Sjödin et al. (1998). The proportion between light-weight and heavy vehicles is the difference between Average Daily Traffic (ADT, NBI item 29) and Average Daily Truck Traffic (ADTT, NBI item 109). A similar equation is also used by Thompson (2017) for the analysis of risk during the life-cycle cost analysis in the AASHTOware bridge management system.

### *7.3.3 Cost of Accidents due to Detour*

After a bridge is closed to traffic, an additional cost is imposed on the users due to the longer route that they have to drive to bypass the failed bridge. Additionally, the increased travel distance implies an increase in the total number of accidents.

The accident rate related to the standard use of the infrastructure network in the United States may be found in several studies carried out by the National Highway Traffic Safety Administration (NHTSA). Both fatality and injury rates are measured in *Vehicle per Mile Travelled* (VMT), and normally it is expressed in terms of 100 Million VMT. Accordingly, the values used in this work are set at 1.13 fatalities per 100 Million VMT as per 2018 data (NHTSA, 2019) and 77 injured per 100 Million VMT as per the latest available data of 2015 (NHTSA, 2016). The number of fatalities ($n_{fatalities}$) and injured ($n_{injured}$) is therefore calculated with Equations 7-6 and 7-7:

$$n_{fatalities} = \frac{1.13}{10^8} ADT\ \ T\ D\ \ \frac{1}{1.609} \tag{7-6}$$

$$n_{injured} = \frac{77.00}{10^8} ADT\ \ T\ D\ \ \frac{1}{1.609} \tag{7-7}$$

Where 1.609 is the factor to convert miles to kilometers.

The number of vehicles involved ($n_{vehicle}$) in an accident for calculating the cost of property damage estimated by Equation 7-8:

$$n_{vehicle} = \frac{n_{fatalities} + n_{injured}}{O} \tag{7-8}$$

Where $O$ is the average vehicle occupancy.

The next step is the calculation of the economic cost of each accident item. A first attempt to this problem is assessed by Lee (1995), observing that the cost of loss of life for society can be approximately estimated to be $ 1 million by comparing it to the usual amount covered by insurances to compensate the beneficiaries of life insurances. It is understood, that this is an average number, since usually insurance companies provide different compensation based on the consequence of a fatality, as for instance, age of the deceased individual and the condition of dependents, such as a spouse, children, or elderly live-in relatives. A more detailed and recent study for evaluating the costs of accidents was carried out by Blincoe et al. (2015) for the National Highway Traffic Safety Administration recognizing different kinds of accidents and different degrees of injury as well as property damage (PDO) for estimating the consequences of motor vehicle crashes in the US. The cost of each fatality was found to be $ 1,393,169 per person while the cost for property damage was found to be $ 2,785 per vehicle in 2010 US dollars. The severity of injury is classified into six levels (Gennarelli & Wodzin, 2008) listed in Table 7-2. These costs and the breakdown of the different factors are listed in Table 7-3.

**Table 7-2. AIS-code for severity of injuries (Gennarelli & Wodzin, 2008).**

| AIS-Code | Injury | Example | AIS % prob. of death |
|---|---|---|---|
| 1 | Minor | Superficial laceration | 0 |
| 2 | Moderate | Fractured sternum | 1 – 2 |
| 3 | Serious | Open fracture of humerus | 8 – 10 |
| 4 | Severe | Perforated trachea | 5 – 50 |
| 5 | Critical | Ruptured liver with tissue loss | 5 – 50 |
| 6 | Maximum | Total severance of aorta | 100 |

**Table 7-3. Summary of unit costs of crashes in 2010 dollars (Gennarelli & Wodzin, 2008).**

| | PDO Vehicle $/vehicle | MAIS0 $/person | MAIS1 $/person | MAIS2 $/person | MAIS3 $/person | MAIS4 $/person | MAIS5 $/person | Fatal $/person |
|---|---|---|---|---|---|---|---|---|
| Medical Care | 0 | 0 | 2,799 | 11,453 | 48,620 | 136,317 | 384,273 | 11,317 |
| EMS | 28 | 21 | 89 | 194 | 416 | 838 | 855 | 902 |
| Market Prod. | 0 | 0 | 2,726 | 19,359 | 64,338 | 140,816 | 337,607 | 933,262 |
| Household Prod. | 60 | 45 | 862 | 7,106 | 22,688 | 37,541 | 95,407 | 289,910 |
| Insurance Adm. | 191 | 143 | 3,298 | 4,659 | 15,371 | 28,228 | 72,525 | 28,322 |
| Workplace Costs | 62 | 46 | 341 | 2,644 | 5,776 | 6,361 | 11,091 | 11,783 |
| Legal Costs | 0 | 0 | 1,182 | 3,351 | 12,402 | 26,668 | 82,710 | 106,488 |
| Prop. Damage | 2,444 | 1,828 | 5,404 | 5,778 | 10,882 | 16,328 | 15,092 | 11,212 |
| Total | 2,785 | 2,083 | 16,701 | 54,544 | 180,493 | 393,097 | 999,560 | 1,393,196 |

The composite cost of injury per person is calculated from the proportion of each injury severity over the total as shown in Table 7-4, resulting in $ 13,691 per person in 2010 US dollars.

**Table 7-4. Cost of injuries.**

| injury severity | n. people injured | percentage | total cost of injuries $ | injury cost $/person |
|---|---|---|---|---|
| MAIS0 | 4,583,265 | 53.9% | 2,083 | 1,123 |
| MAIS1 | 3,459,200 | 40.7% | 16,701 | 6,793 |
| MAIS2 | 338,730 | 4.0% | 54,544 | 2,172 |
| MAIS3 | 100,740 | 1.2% | 180,493 | 2,138 |
| MAIS4 | 17,086 | 0.2% | 393,097 | 790 |
| MAIS5 | 5,749 | 0.1% | 999,560 | 676 |
| total | 8,504,770 | | | 13,691 |

The costs updated to 2020 are $ 1,678,357 per fatality, $ 16,493 per person for injury and $ 3,355 per vehicle for property damage.

### *7.3.4 Environmental Cost*

The costs related to the impact of gas emissions of vehicles during the disruption of traffic due to bridge failure are defined as environmental costs. A comprehensive summary of the different emissions can be found in USEPA (1996) for different transportation modes. The most important emissions pointed out by Ahn et al. (2013) are listed as:

- Carbon monoxide ($CO$): which is a toxic gas caused by incomplete combustion emitted by vehicle tailpipes damaging human health and contributing to climate change.
- Dioxide ($CO_2$): which is a product of combustion emitted during the production of the fuel itself and from vehicle tailpipes damaging human health and contributing to climate change. Dioxides dissipate in

the environment and have more global impact than Carbon monoxide, that is more responsible for the costs near the emission source.

- Volatile organic compounds ($VOC$) such as hydrocarbon (HC), which are mostly related to fuel production and vehicle tailpipes and have an impact on human health besides being ozone precursors.
- Nitrogen oxides ($NO_x$) and nitrous oxide ($NO_2$) which are different types of compounds, some of which are toxic, and have an impact on human health besides being ozone precursors. Their source is vehicle tailpipes.
- Fine particulate matter ($PM_x$). These inhalable particles are defined by their diameter in micrometers. Typically $PM_{10}$ or $PM_{2.5}$ with particle diameters of 10 and 2.5 micrometers respectively are emitted by vehicle tailpipes but are also the product of brake and tire wear and road dust and affect directly human health.

The different contaminants can be divided into exhaust emissions from tailpipes and non-exhaust emissions, for instance, from tire and break wear. In general, the compound environmental costs caused by the aforementioned emissions are responsible for damage to human health including shortness of breath, respiratory and other diseases and death, and include, among the non-health damage, structural deterioration, decreased visibility and ecological degradation. A more detailed description of the exposure and health effects of the pollutants can be found in HEI (2010) and Read (1994). The evaluation of the cost of emissions is performed by many researchers at very different levels of precision. Usually, complex emission models are used to estimate the emission given a certain number of boundary conditions. A popular model developed by the USEPA (United States Environmental Protection Agency) are the MOBILE (USEPA, 2003) model or the more modern MOVES (USEPA, 2015). The latter model allows to realistically consider vehicle speed within a simulation unlike the former where only average speed may be inputted. The importance of this latest model refinement is shown, in Figure 7-3 and is of particular importance for saturated traffic conditions (congestion). It can be shown that both very low and very high speeds increase the emissions significantly recognizing the range of speeds for which vehicle are expected to be efficient and those speeds that are expected to be reached with less frequently.

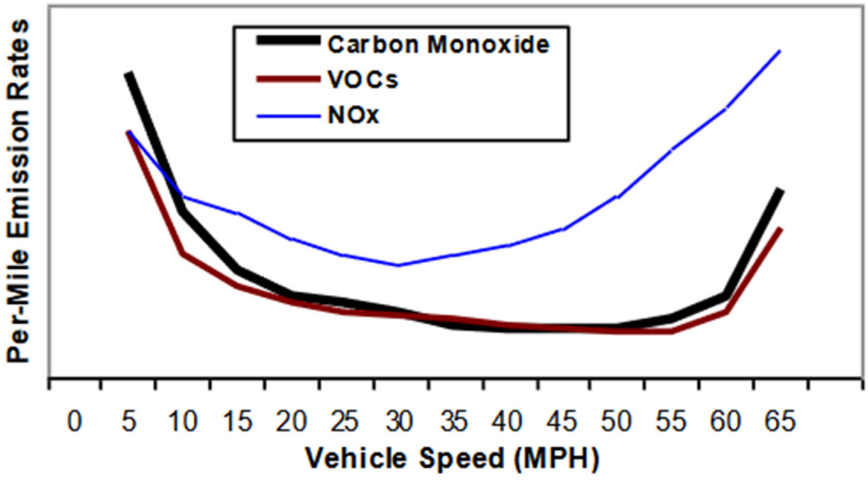


**Figure 7-3. Vehicle emission by speed (Figure taken from Litman (2009) with the results obtained by TRB (1995)).**

Zhang and Batterman (2013) studied the impact of air pollution on people exposed to contamination due to vehicle emissions such as driving commuters or individuals living near major roadways. Zhang and Batterman (2013) distinguished between the length of time of congestion when the capacity of the roadway is exceeded. In this sense, the emissions occurring during normal traffic conditions are merely proportional to the number of vehicles in the normal traffic flow. On the other hand, when congestion takes place a non-linear and more severe increase in air pollutants is observed. Specifically, these congestion increases are related to the lower average speed (involving frequent "speedups and slowdowns" and "starts and stops"), which increases travel time and exposure on a per vehicle basis and reduces the dispersion of the pollutants due to reduced air turbulence that increases the concentration of the pollutants.

In this work, the additional detour length needed to by-pass a failed or closed bridge is considered to be congested. It cannot be determined a priori if the unavailability of a bridge within a network will occur in congestion conditions. However, it is reasonable to assume that the alternative path, which is supporting its own traffic volume is unlikely to have been designed for the additional volume detoured from the failed structure which may lead to exceeding its traffic capacity. Therefore, the alternative path will be in congestion condition during much of the bridge's disruption time.

The amount of each pollutant and therefore its cost is defined for cars, light trucks and heavy trucks. The percentage of heavy trucks is calculated by Fiorillo (2015) to be 87% of the total of the total ADTT on NYS highway network based on WIM traffic data. The environmental impact cost ($C_{I3}$) can be calculated according to Equation 7-9:

$$C_{I3} = \Big((ADT - ADTT)\, C_{pc} + 0.87\, ADTT\, C_{pht} + 0.13\, ADTT\, C_{plt}\Big)\, T \quad (7\text{-}9)$$

Where $C_{pc}$ $C_{pht}$ and $C_{plt}$ is the sum of the costs of all the pollutants for cars, light trucks and heavy trucks respectively. It is noted that the part of the air pollution generated in rural areas is expected to be less relevant that the one in urban areas, because some of the cost is borne by the individuals living in the vicinity of the roadway and rural areas have a smaller population density than urban areas. Instead, costs linked to green house gas emissions are similar for rural and urban environments.

The relationship between urban and rural average environmental cost is estimated as 1.16 considering normal traffic conditions according to FHWA (2012) and as 10.0 according to Litman (2009) and Maiback et. al (2008) as a demonstration of the large differences that can be observed from different researchers as a result of the many different calculation uncertainties in these kinds of cost models.

Finally, the congestion regime of traffic is expected to increase the environmental cost per unit length travelled. The ratio between congested and free flow cost conditions is also affected by differences deriving from the traffic and location circumstances being a factor of 2.0 a reference value provided by Zhang et al. (2011).

The final cost rates used in this study are found in the comprehensive study carried out by Litman (2009), updated to 2020 dollars and are multiplied by 2.0 to consider the traffic congestion regime and are summarized in Table 7-5.

**Table 7-5. Environmental unit cost ($ per vehicle per kilometer travelled) based on Litman (2009).**

| | Non GHG environmental rural | Non GHG environmental urban | Greenhouse Gas Costs rural | Greenhouse Gas Costs urban |
|---|---|---|---|---|
| Vehicle | 0.010 | 0.160 | 0.039 | 0.049 |
| Light Truck | 0.018 | 0.289 | 0.054 | 0.067 |
| Heavy Truck | 0.034 | 0.477 | 0.243 | 0.199 |

The average cost per VMT (Vehicle per mile travelled) is variable depending the proportion of trucks and other vehicles for each bridge analyzed in *set 1* ranging from 5.0 to 10.0 cents of dollar for rural areas and from 25 to 30 cents for urban areas as shown in the histogram of Figure 7-4. The classification of rural or urban environment is based on the bridge location as indicated in NBI item 26.

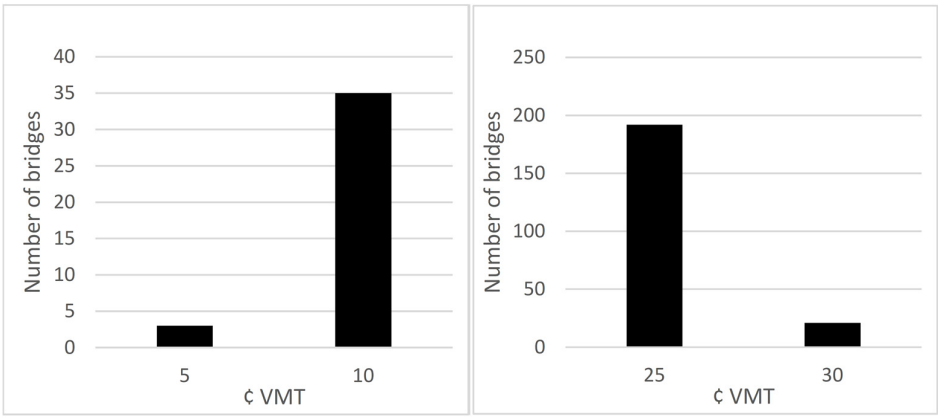


**Figure 7-4. Environmental cost (in cents of dollar per VMT) versus number of bridges in *set 1*.**

Additional detail on the assumptions and methods utilized to determine these costs and in general how the considerable debate around this topic can be found in the EPA report *The Benefits and Costs of the Clean Air Act, 1990 – 2020* (2011).

### *7.3.5 Quantifying Fatalities and Injuries due to Bridge Collapse*

Finally, the cost of fatalities and injured after a bridge failure is considered as the number of occurrence multiplied by its related cost. For example, NCHRP document 107 (Stein, 2007) established a relationship between the number of fatalities due to bridge failures and average daily traffic volume expressed in terms of ADT (Table 7-6).

**Table 7-6. Number of lives lost in bridge failure (Stein, 2007).**

| Average Daily Traffic (ADT) | Number of Lives Lost |
|---|---|
| ADT<100 | 0 |
| 100≤ADT<500 | 1 |
| 500≤ADT<1000 | 2 |
| 1000≤ADT<5000 | 2 |
| ADT≥5000 (Not an interstate or arterial) | 5 |
| ADT≥5000 (interstate or arterial) | 10 |

Another practical approach for the estimation of the cost due to loss of lives is linking it to the cost of construction. For example Saydam (2013) calculates the total cost of loss of lives due to bridge collapse as five times the construction cost of the bridge. This approach has the advantage of the ease of application and the number of fatalities doesn't need to be quantified, but it may look an over simplification since the same construction cost can be assigned to a quite different type of bridge being the shape of the bridge and its type necessarily sensitive properties.

For this reason, several researchers attempted at relating the number of fatalities to some structural parameters, as span length. In this sense, Imam and Chryssanthopoulos (2012) states that there is only a weak correlation between number of fatalities and span length, while Caspeele et al. (2016) and Steenbergen et al. (2015) show more optimistic relationships.

It must be emphasized though, that not necessarily all bridge failures imply fatalities or injured. In fact, Spector and Gifford (1986) found that an average of 100 small bridges fall every year without fatalities, or very few as observed by Lee at al. (2013) and that the fatalities are concentrated in a small number of failure events (Wardhana & Hadipriono, 2003). For these reasons, the parameter under study is more precisely the number of fatalities conditional on the probability of getting at least one in a bridge failure (probability of casualty or mortality). For instance, the approach followed by Caspeele et al. (2016) for residential buildings is based on the definition of three consequence classes CC1, CC2 and CC3 associated with the increasing conditional probability of casualty 0.01, 0.05, and 0.20 respectively, whereas a fixed value of 0.055 is suggested for bridges. These values are used in conjunction with the probability of failure to calculate the number of casualties, or likewise to set a reliability index once the expected number of fatalities is found.

Another approach is presented by Steenbergen et al. (2015) and Caspeele et al. (2016), who relate the number of fatalities to bridge span length by means of linear regression of a set of real data, coming up with an average value of 0.09 times the span length. The dataset of bridges used has span lengths up to 500 m as shown in Figure 7-5 (left plot). For completeness the same bridge data set analyzed by Steenbergen et al. (2015) are also analyzed in this study for number of injuries in Figure 7-5 (right plot) obtaining a linear fit of -0.022 $SL$+25.872 with a negative slope indicating a counterintuitive decrease of injured as span length increases and an R-squared coefficient as low as 0.006 indicating practically no correlation between data and model. This means that the linear regression cannot be used for injuries as is or at least it is not an acceptable representation for this set of bridge collapse events.

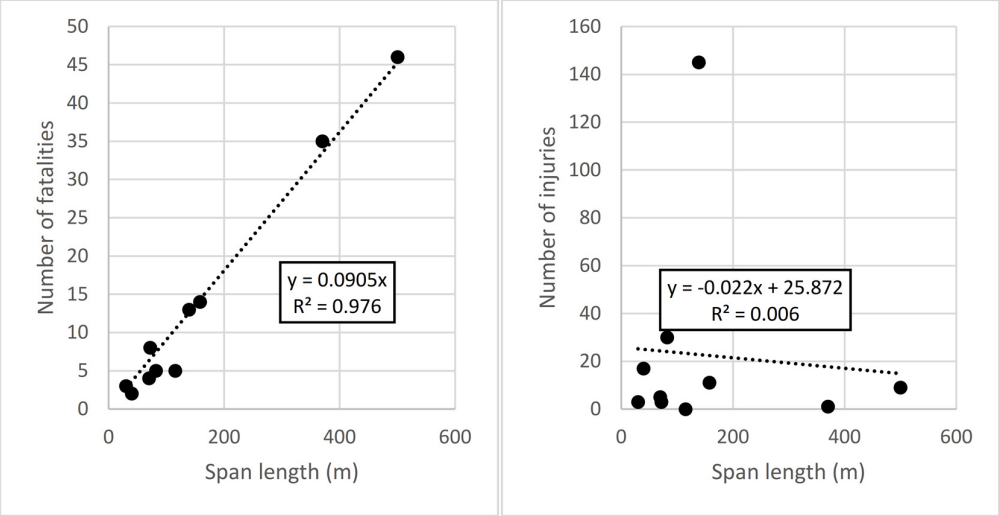


**Figure 7-5. Number of fatalities versus span length on the left (Steenbergen et al., 2015). Number of injured versus span length on the right (Present study).**

The comparison of these estimation models with real failure event can be performed for two cases for which data are available. For instance, the I-35W Mississippi River Bridge collapse in 2007 caused 13 fatalities and 145 injuries. In this specific case, the severity of the injuries have been made public by the National Transportation Safety Board (NTSB, 2007) indicating that 34 injuries were classified as "serious", 111 as "minor" and 32 additional cases as "none or unknown". Since the main span length of this bridge is 139 m, the aforementioned linear regressions defined in Figure 7-5 provides an expected number of 12.6 fatalities. The comparison to the model suggested above show that the number of fatalities is equivalent to that predicted by the regression. Similarly, the application of Table 7-6 criteria to this failure event led to 10 fatalities, given that an ADT 14'000 and considering that the bridge is located in Interstate 35W. So, again, this alternative criteria to obtain the number of fatalities based on amount of traffic gives good results for the I-35 W bridge.

Another example is represented by the Mianus River Bridge collapsed in 1983 after the failure of a critical connection (pin and hanger) in a main load bearing element due to intrinsic difficulties in the inspection of these elements in a this bridge's non-redundant structural configuration, led to 3 fatalities and 3 serious injured (Scheer, 2010), Given a main span length of 30 m, the linear regression in Figure 7-5 provides an expected number of 2.7 fatalities which are on the same order as those observed from the collapse event. Also, the application of Table 7-6 criteria to this bridge leads to 5 fatalities, given that an ADT 9'100 is obtained considering that the bridge is located in Connecticut route 104. Again, the two criteria based on span length or ADT result in quite good predictions.

The more recent work carried out by Proske (2020), attempts at estimating the number of fatalities per year due to bridge collapses, besides giving a quite complete global view and state of the art on this topic. In this paper, the number of fatalities $N$ is estimated according Equation 7-10:

$$N = \sum U_i k_i N_E \tag{7-10}$$

Where $k_i$ is the conditional probability of getting at least one fatality given a bridge collapse and are dependent on the $i_{th}$ cause of collapse, $U_i$ is the probability of failure and $N_E$ is the maximum expected number of fatalities which is found by the author to be 3.03 for road bridges, 180 for railway bridges and 92 for the general case after performing a statistical analysis on a bridge population of 235 severe bridge collapse. The summation sign over the $i_{th}$ addends represent different possible modes of failure.

For what the application of these figures to this work, the number of fatalities can be estimated multiplying the $k_i N_E$ for road bridges. The values of $k_i$ can be 0.8 for bridge overload, while the expected number of fatalities can be 3.03 for road bridges or 92 for the general case as suggested by Proske (2020) resulting in an upper bound of 73.6 and a lower bound of 2.4 expected fatalities given any bridge collapse, irrespective of its geometry or type. In the context of this Thesis the minimum and maximum span lengths of *set 1* is 12 m and 75 m leading to a minimum and maximum number of fatalities (according to Figure 7-5 left) of 1.1 and 6.8 which is in the low range of the results obtained with Proske's (2020) proposal and close enough to the expected number of fatalities for road bridges (3.03).

The failure events suggested by Steenbergen et al. (2015) are incremented with new cases taken from Scheer (2010) getting to 22 cases as presented in Table 7-7.

**Table 7-7. Bridge failure cases for fatalities/injured statistics (Scheer, 2010; Steenbergen et al., 2015).**

| Bridge | Country | Year | Span/ length (m) | Fatalities | Injured |
|---|---|---|---|---|---|
| Duplessis Bridge | Montreal - Canada | 1951 | 55 | 4 | 0 |
| Naga city | Philippines | 1972 | 40 | 145 | 200 |
| Reichs bridge | Austria | 1976 | 241 | 1 | 0 |
| Poulding country culvert | Ohio - USA | 1983 | 10 | 5 | 4 |
| Sungsu truss bridge | Korea | 1994 | 120 | 32 | 17 |
| Koror Babelhuap bridge | Palau | 1996 | 241 | 2 | 4 |
| Amsterdam bridge | New York - USA | 1987 | 34 | 10 | 0 |
| Kaohsiung | Taiwan | 2000 | 91 | 1 | 22 |
| East of Porto bridge | Portugal | 2001 | 200 | 70 | 0 |
| Northern bypass bridge | Pakistan | 2007 | 70 | 6 | 0 |
| Brooklyn bridge (Harrodsburg) | Kentuky - USA | 1953 | 76 | 0 | 1 |
| Ariccia | Italy | 1967 | 312 | 2 | 0 |
| Silver Bridge | Ohio - USA | 1967 | 500 | 46 | 9 |
| Sunshine Skyway Bridge | Florida - USA | 1980 | 370 | 35 | 1 |
| Queen Isabella | Texas - USA | 1996 | 72 | 8 | 3 |
| I40 | Oklahoma - USA | 2002 | 158 | 14 | 11 |
| I35, Minneapolis | Minnesota - USA | 2007 | 139 | 13 | 145 |
| Tarcoles | Costa Rica | 2009 | 82 | 5 | 30 |
| E313 Viersel | Belgium | | 40 | 2 | 17 |
| Mianus River Bridge | Connecticut - USA | 1983 | 30 | 3 | 3 |
| Cleddau Bridge | Wales | 1970 | 70 | 4 | 5 |
| Severn River Bridge | UK | 1960 | 115 | 5 | 0 |

Similar results as those obtained by Steenbergen et al. (2015) are obtained in this work for a different set of events more suited for the bridge population under study. The fitting population is found by removing from Table 7-7 data span lengths longer than 85 m similar to the span length used in *set 1*, by removing cases with zero injured or fatalities, and by removing the Naga City and Amsterdam bridge as they are considered outliers. The removal of those cases with zero fatalities and injured is explained because this estimation model is conditional on the presence of a fatality in the collapse event. In a further step, the estimation will be corrected to take into account of the presence of bridge collapses without fatalities (probability of mortality).

The linear regression shown in Figure 7-6 and executed to determine the relationship between fatalities and span length of $0.09SL$ found by Steenbergen et al. (2015) and already shown in Figure 7-5 slightly decreases to $0.076\,SL$. Similarly the relationship between number of injured and span length is found to be $0.154SL$.

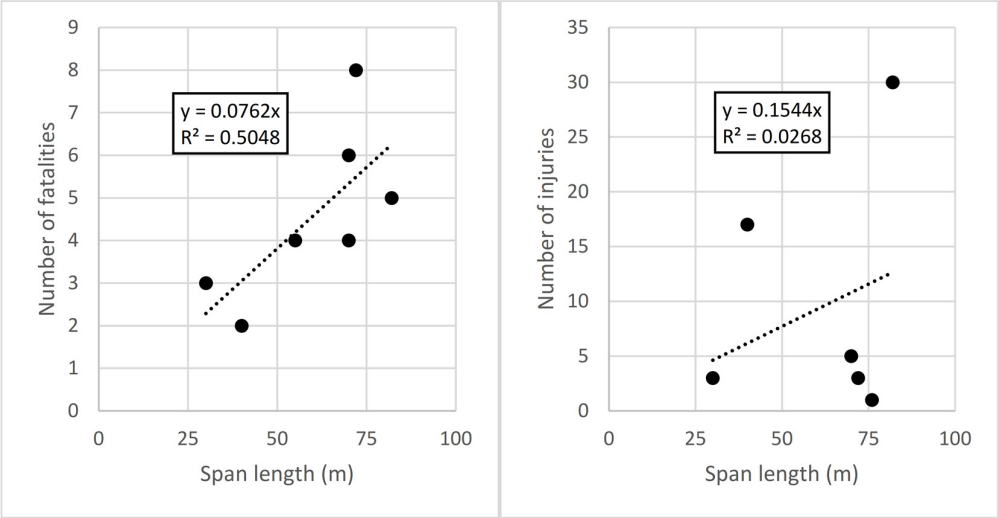


**Figure 7-6. Relation between number of casualties (left) or injuries (right) versus span length smaller than 85 m.**

As can be observed by looking at the R-square fitting coefficients, the correlation between fatalities and span length shows relatively strong fit, while a weaker fit is observed in the case of injuries. Nevertheless, the high level of uncertainties linked to the presence of vehicles during a bridge collapse is not expected to lead to higher confidence as those provided by the other methods outlined earlier.

It is recalled that these estimation models are conditional to the presence of fatalities in the bridge collapse event (probability of mortality or casuality). This means that the number of fatalities need to be reduced to take into account those events of bridge collapse without fatalities. Therefore, the expected number of fatalities and injured must be multiplied by the probability of mortality expressed by many authors for different circumstances and comprehensively presented by Proske (2020). As already mentioned, a coefficient of 0.8 is suggested by Proske (2020) for overload failure modes and 0.055 from Caspeele et al. (2016) for the general case. The latter value (0.055) seems more suitable for the general case treated in this work and will therefore be adopted.

Some additional remarks are due to the evaluation of the ratio of injuries to fatalities as previously found in Figure 7-6 (right) to be 2.0. Previous studies on building population subjected to severe seismic events in Japan show ratios of 48 in the decade of the 50s and 60s and a decrease to 7 in the 80s 90s as observed by Wyss and Trendafiloski (2011). Likewise, the FWSI (fatalities and weighted serious injuries) is used for railway accidents being 0.1 for severe injury and 0.01 for minor injury. This derives in ratios of 10 and 100 respectively. It is recalled that a ratio of 77/1.13=68.14 is used in Subsection 7.3.3 for road vehicle crashes. However, in the case of bridge collapse a smaller ratio is observed. For instance, the work presented by Garg et al. (2020), outlines that the proportion of injuries to fatalities in bridge collapses in India, shown in a year wise plot (Figure 7-7), results in a rough proportion of 1.5:1.

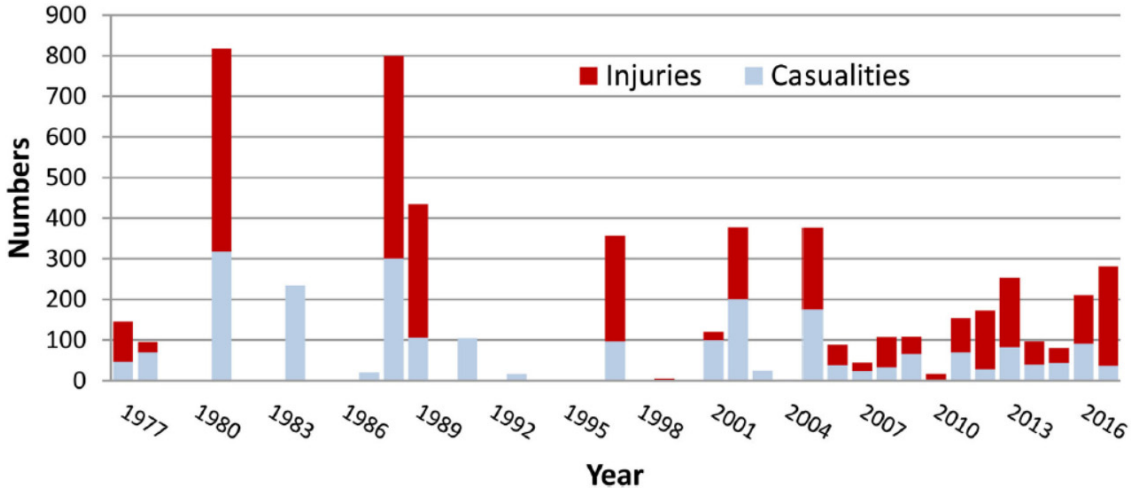


**Figure 7-7. Injuries and fatalities from bridge failure events in India (Garg et al., 2020).**

Again, the authors of the paper highlight the high contribution of railway bridge collapses in the count of fatalities and injuries that in general involve higher numbers of fatalities and injured than road bridges. In addition, being the paper focused on solely Indian bridges, a direct extrapolation to American or European bridges may not be straightforward. Despite the results obtained in these cases, road bridge failures may present different singularities, and again, the amount of data available in literature is poor. A trend investigation of the aforementioned ratio from 1850 to the present presented by Proske (2020) for bridge collapses in general, showing that higher values of the ratio injured/fatalities of the order of 1.0 or 2.0 should be used for road bridges. It must be emphasized that the injuries regression analysis alone, due to the scarcity of the data, may not be rigorous enough to be used as a prediction tool. However, the ratio obtained with the regression shown in Figure 7-6 of injured over fatalities of 2.0 is in good agreement with the results obtained by Garg et al. (2020) of 1.5 and with the aforementioned range suggested by Proske (2020) consistently observed in each author's datasets.

The specific circumstances related to the collapse of the I-35 and Mianus bridges explained previously each of these two bridges are a clear example of how difficult is to find a correlation between a specific bridge parameter or traffic properties and number of casualties. For this reason, it would be reasonable to hypothesize that casualties would be related to ADTT, bridge length or the combination of both. One can also hypothesize that loading patterns, bridge elevation and other geometric configurations, or specific circumstances occurring during the failure, as special maintenance operations may influence the numbers and severity of casualties. It should also be mentioned that the fluctuations of the traffic volume during the day lead to different degrees of occupancy of the bridge, therefore a bridge with a high ADT does not necessarily cause a high fatalities and injured toll if the failure occurs at a time of the day with a low traffic

volume. Unfortunately, the limited database currently available is not sufficiently broad to perfectly model the effects of all potential factors.

Once the number of events (fatalities and injured) is found, the corresponding unit costs need to be estimated and associated to each of the two items. The cost of fatalities is easier to establish because there are no degrees of severity involved and its value can be taken as the one calculated for car crashes in Table 7-4 as $ 1,393,196 in 2010 and $ 1,678,357 updated to 2020 US dollars. On the other hand, defining the cost of injuries is a much harder task for several reasons. First, most of the bridge toll information is provided in the form fatalities/injuries, without a specification of the degree of severity of the injured, unlike car crashes that are a much more frequent events and injured are well documented. Second, many minor injuries may be documented but still contributing very little to the total cost of toll, and sometimes, when only the total number of injured is available and an average cost of injuries is calculated, an unrealistic cost is found. For the same reason minor injuries are more likely to be undocumented.

One of the few bridge collapse that provides a reasonable amount of information about injuries is the aforementioned case of the Mississipi river bridge. The compensation settlement related to each fatality and injury are publicly available. For this particular bridge the average compensation for each of the 11 fatalities was $ 760,000, (for a partial total of 8,360,000 $ which is 23.8% of the total cost) and for each of the 34 severe injured was $ 723,000 (for a partial total of $ 24,582,000 which is 70.0% of the total cost) and for each of the 111 who suffered minor injury was $ 19,500 (for a partial total of $ 2,164,500 which is 6.2% of the total cost). Looking at these figures it can be concluded that, the fatalities and severe injuries essentially make up the total cost of toll. Additionally, while at first sight the aforementioned proportion between injuries and fatalities of 1:1 or 2:1 may be strongly out, it can be observed that, from the economical point of view, and if only the severe injured are considered, the proportion obtained is 3:1, which is only slightly off the rough proportion suggested earlier. The cost of fatality and severe injury found for this bridge are smaller than the ones found for car crashes, but still on the same order of magnitude.

For the Mianus bridge collapse, only the total amount of the compensation is available, being $ 7,800,000. If the proportion found for the Mississipi bridge between fatality and sever injury cost of 1.05 is assumed the cost of each of the 3 fatality is $ 1,330,000 and the cost of each of the 3 injured is $ 1,270,000 which is reasonably in the range of expected costs compared to the values presented in Table 7-4.

In this work, the cost of injury is assumed as 0.95 the cost of fatality (1/1.05 found above), being it the best estimate available to the knowledge of the author of this work and as a consequence of the data available, bearing in mind that further research should be carried out in the future for an improvement of the these figures.

### *7.3.6 Cost of Inspection*

Besides the consequences of bridge failure calculated in terms of cost to society the last cost to be evaluated is the cost of routine inspection. The different parts composing the total cost of inspection are estimated as provided by Hassan S. (personal communication, December 22, 2019):

- Field inspection hours: 14 hours for Team Leader (senior engineer with Professional Engineer's License, at a rate of 60.00 $/hour) and 14 hours for Assistant Team Leader (junior engineer, rate 35.00 $/hour).
- Expenses: $ 2,500 for a bucket truck to access the bridge
- Load rating hours: for the multi-girder configuration analyzed in this work 12 hours for load rating engineer (rate 45.00 $/hour) and 4 hours for load rating reviewer (rate 60.00 $/hour).
- Salary overhead: An average multiplier of 2.6 is assumed on salaries.

The resulting cost of inspection is $ 8,000, with 75% of the cost being due to the visual inspection and 25% to the post-processing of the data collected. These values are in agreement with the cost range between $ 4,500 to 10,000 reported by Zulfiqar et al. (2014).

## 7.4 Summary and calculation example

The summary of the models and equations obtained through the chapter and further used in this work is presented in Table 7-8.

**Table 7-8. Models and equations used in this work to define the total cost of bridge failure.**

| Cost Item | Equation | source |
|---|---|---|
| Demolition | $35\ V$ | (FEMA, 2010) |
| Reconstruction | $1860\ S$ | (RSMeans, 2009) |
| Congestion and delay | Equation 7-5 | (Khan, 2015) |
| Accidents due to detour | Equations 7-6, 7-7, and 7-8 | (NHTSA, 2019) (Blincoe et al., 2015) |
| Environmental | Equation 7-9 | (FHWA, 2012) |
| Fatalities | $F = 0.0762SL \times 0.055$ | (NHTSA, 2019) (Present study) |
| Injuries | $2.0\ F$ | (Garg et al., 2020; NHTSA, 2018; Proske, 2020) (Present study) |

The following symbols are used in Table 7-8: $V$ bridge volume, $S$ bridge surface, $SL$ bridge span length, and $F$ number of fatalities.

In order to better understand the calculation process, all the figures involved in the calculation and the application of the equations summarized in Table 7-8 a calculation example is performed with one of the bridges of *set 1* in Appendix G.

## 7.5 Final Remarks on the Cost of Bridge Failure

The total cost $C$ is the sum of the direct cost $C_D$ and the indirect costs $C_{I1}$, $C_{I2}$, $C_{I3}$and $C_{I4}$. The different studies referenced above clearly demonstrate the difficulties in establishing absolute cost estimates for each cost category due to the lack of sufficient numbers of case studies. It is therefore noted that the models adopted in this work for the cost estimation are as accurate as the available literature allows and a word of caution must be given for the use of these values in other contexts different from the one pursued in this work.

Likewise, for a better understanding of the importance of the different cost items within the 279 bridges of *set 1* a histogram of cost percentages is presented in Figure 7-8 sorted by ascending ADT and Figure 7-9 sorted by ascending detour length.

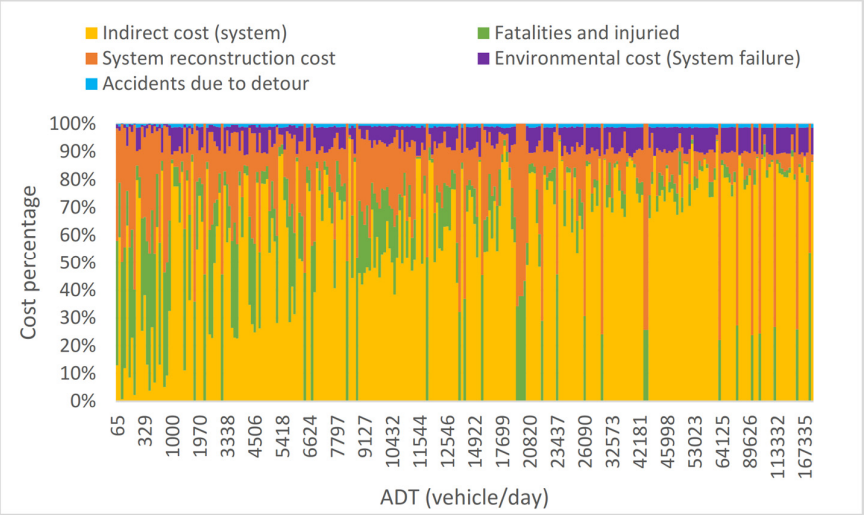


**Figure 7-8. Relative cost contribution for each of the 279 bridges of *set 1* (bridges sorted by ascending ADT).**

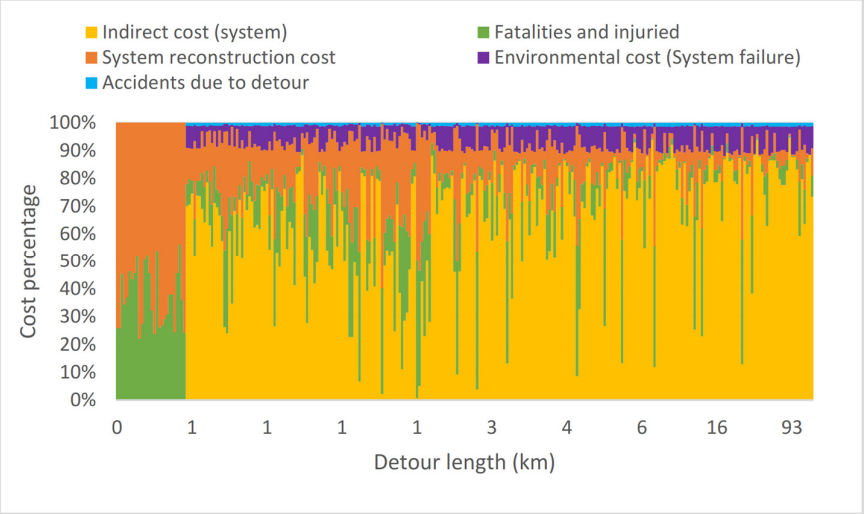


**Figure 7-9. Relative cost contribution for each of the 279 bridges of *set 1* (bridges sorted by ascending detour length).**

In general, it can be observed that the indirect cost importance increases as the ADT and Detour length increase. However, the trend is not strong and clean when the two parameters are checked alone. In order to overcome this problem the bin x-axis of the histogram is more conveniently represented with the joint parameter Detour length times ADT as shown in Figure 7-10

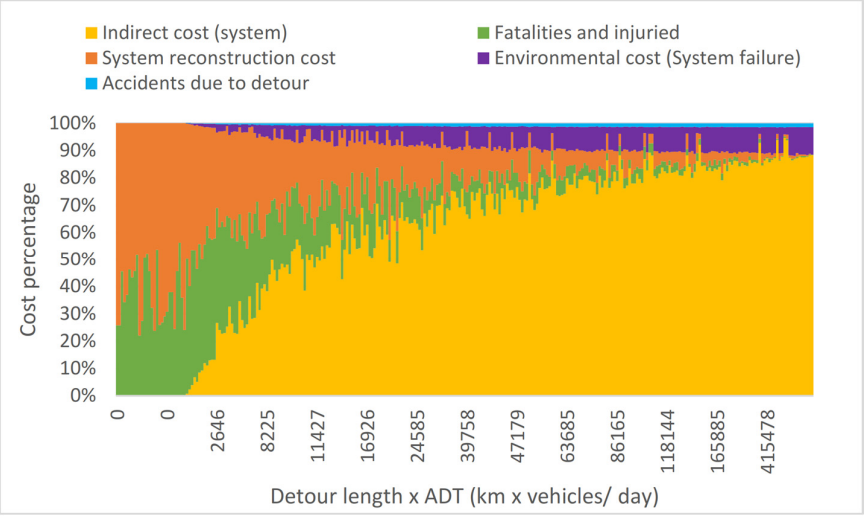


**Figure 7-10. Relative cost contribution for each of the 279 bridges of *set 1* (bridges sorted by ascending detour length by ADT).**

From these figures, the maximum and minimum contribution to the total cost and therefore the possible relevance of each cost item is presented in Table 7-9.

**Table 7-9. Maximum and minimum percentage of cost by cost type for the bridges under study (*set 1*).**

| | min | max |
|---|---|---|
| System reconstruction cost | 0.1% | 78.0% |
| Environmental cost | 0.0% | 10.6% |
| Indirect cost | 0.0% | 94.7% |
| Cost of accidents due to detour | 0.0% | 1.6% |
| Cost of fatalities and injured due to failure | 0.0% | 56.2% |

The following conclusions can be drawn from the observation of the cost calculated for *set 1* and the analysis of Table 7-9, Figures 7-8, 7-9 and 7-10:

1) The accidents occurring during the disruption time along the detour are observed to be in general small compared to other costs.
2) The environmental and the indirect costs increase in importance as the detour length or the ADT increase, as expected even though the environmental costs are less relevant.
3) The cost of failure of those bridges with zero detour length (e.g. twin bridges) is composed of demolition and reconstruction, and fatalities and injured in a fairly equal proportion.

The costs estimated in this chapter are used to calculate the risk of bridges by its combination with the results obtained in previous chapters and especially with the probability of failure obtained in Chapter 6.

# 8 Risk-based Optimization of Inspection Intervals

The purpose of bridge inspection programs is to assess the load carrying capacity of existing bridge structures and identify those that are at high risk of failure in order for the authorities to take necessary actions to reduce that risk. Thus, risk optimization implicitly is the main purpose of bridge inspection processes even though risk assessment is not explicitly formulated in current procedures. The quantification of risk in engineering applications aims to provide a measure of the consequences of a potential hazard or a set of hazards that an engineered system could possibly be vulnerable to. In this work, the hazard of interest is the failure of a deteriorating bridge structure, calculated with the methods outlined in Chapter 6, whose structural capacity, evaluated as explained in Chapter 4, is vulnerable to the effects of heavy live loads, estimated for a specific exposure period as explained in Chapter 5, where the consequences of failure on society is monetized using the models proposed in Chapter 7. The combination of these factors provides a quantified measure of the risk associated with the failure of a specific bridge in a state of deterioration exposed to heavy truck traffic. While the quantification of risk is possible using the tools developed in the previous chapters, the determination of an optimum bridge inspection schedule requires the establishment of acceptable criteria that reflects the specific characteristics of each bridge susceptible to failure from the effects of heavy truck loads.

It has been argued that the mandatory biennial routine inspection of all US bridges has expended a significant proportion of the limited funds available for maintaining the US infrastructure. According to current practice, a biennial inspection is performed even for bridges that have been recently built, rehabilitated or have otherwise shown very good condition during recent inspections and thus are known to present very low risk of failure. As already mentioned in Chapter 2, to reduce the efforts of the cost of inspections, the Federal Highway Administration is working on modifying the National Bridge Inspection Standards (NBIS) to allow for more flexible bridge inspection practices including the increase of inspection intervals when possible (FHWA, 2019b). The approach that the FHWA is implementing is based on an assessment of the risk with a certain degree of subjectivity and without an explicit consideration of factors that control this risk as mentioned in Section 2.1. In fact, the FHWA procedure uses condition rating as the basis for defining bridge failure when in reality condition ratings are subjective indicators assigned based on visual inspection related to local deterioration and damage. The condition rating does not distinguish between the risk associated with a deteriorated overdesigned bridge which can still carry significant load or that of an underdesigned bridge that does not meet minimum safety criteria even undamaged. On the other hand, load ratings, as used in this work, are more suitable metrics to evaluate the capacity and therefore the probability of failure of bridges.

To address the inherent limitations of the FHWA procedure and enhance its efficacy, this study has set as its objective the development of a more robust risk procedure. The proposed methodology would help determine an optimum bridge inspection interval based on an objective risk assessment process that utilizes a well-established and widely accepted methodology and relevant data that are readily available to the

engineering community. Another advantage of the present method is that it determines the inspection interval can in bridge-by-bridge basis, overcoming the difficulties of a network-based analysis similar to one of the methods proposed by Thompson et al.(2012). In fact, by combining all the structures of a network one loses focus on individual bridges and may "sacrifice" individual bridges for the global benefit and ignoring the importance of each bridge to the particular community it serves. Furthermore, from a practical point of view, obtaining the necessary information for a risk-based determination of an optimum inspection interval of a single bridge is easier than gathering information of an entire infrastructure network.

For application in engineering practice of the method proposed in this Dissertation, the evaluating engineer requires all usual information related to the bridge characteristics (geometry and materials and other information available from the NBI database). Additionally, an estimation of the annual reduction in the bridge load carrying capacity as established from previously performed field inspections and load rating calculations (which can be easily extracted from NBI files from multiple previous years) is needed.

The sections of this chapter will first establish risk-based criteria for determining the optimal inspection interval followed by a description of the proposed methodology which will be illustrated using convenient examples and results presentation and discussion.

## 8.1 Inspection Interval Criteria

Let us assume that a bridge has been inspected at time $T_0$ and, based on its load rating calculations, it was found to have a risk estimated to be equal to $R_0$. Due to its deterioration over time and possible increases in the expected maximum live load that it will be exposed to as its service life increases, its risk will increase over time as illustrated in the curve labelled A in Figure 8-1. Curve A represents the assessed risk accounting for the large aleatory and epistemic uncertainties in modeling future maximum loads on the bridge, the response of the bridge to these loads including the effect of future deterioration. The uncertainties related to the deterioration implied in Curve A are relatively large because they are based on the statistics of a large population of bridges that have the same general characteristics of the bridge being evaluated as explained in Chapter 2. In reality, the risk associated with this particular bridge represents only one realization from the entire population of bridges. Therefore, the bridge-specific risk can be represented by another curve that can be obtained by vastly reducing the uncertainties related to bridge deterioration. The bridge-specific curve can be obtained by focusing the evaluation of the deterioration rate on observations made on previous years' load ratings of this specific bridge. Hence, the expected bridge-specific risk over time may increase at a slower rate than the general risk curve. This can be modelled using the curve labelled B in Figure 8-1. In particular, improving the estimate of the bridge-specific risk can be achieved by performing regular inspections or monitoring which provide improved assessments of the bridge's load carrying capacity and its evolution over time. Therefore, at any point of time, the difference between the general risk curve A and the expected bridge specific curve B, depicted in Figure 8-1 by $\Delta R$, represents the reduction in the uncertainties

in the load carrying capacity of the bridge obtained by an improved estimate of the deterioration state of the bridge.

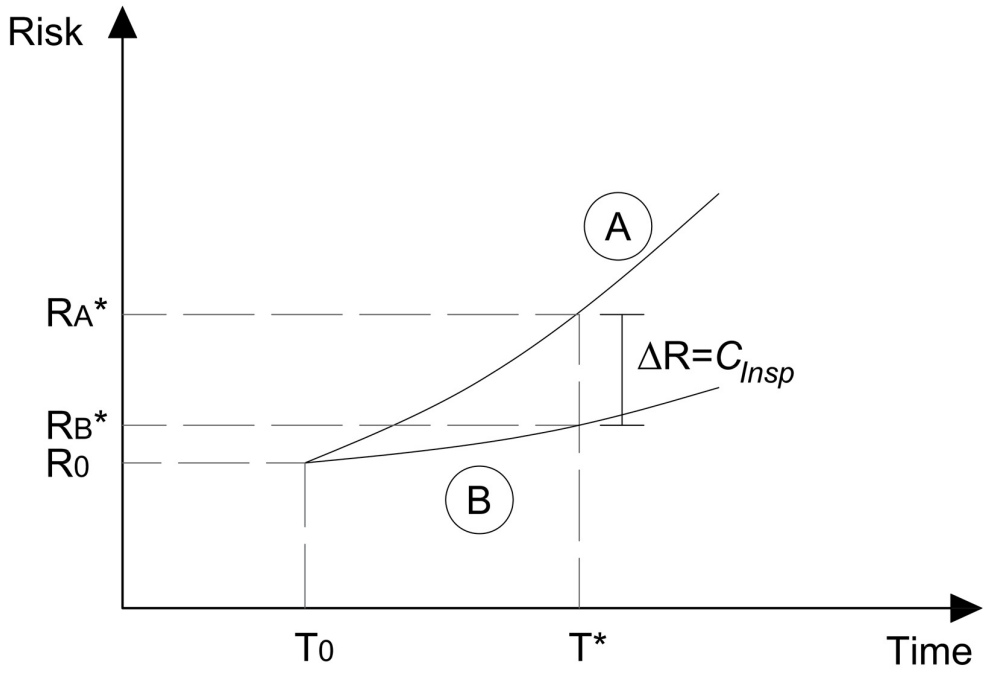


**Figure 8-1. Determination of inspection time interval.**

The additional cost ΔR that society pays to delay the inspection process, can only be tolerated if it is lower than the cost associated with obtaining an improved assessment of the risk that would ease "the fears" of the society with regard to the safety of using this bridge. Improving the estimate of the risk requires the performance of field inspection. Therefore, it is clear that incurring the cost of performing an inspection pays off when the difference between the estimated general risk exceeds the expected bridge-specific risk by the cost of performing a bridge inspection. Therefore, the optimum time to perform an inspection depicted in Figure 8-1 by T* is when the reduction in estimating the risk is equal to the cost of inspecting the bridge or when $\Delta R=C_{insp}$.

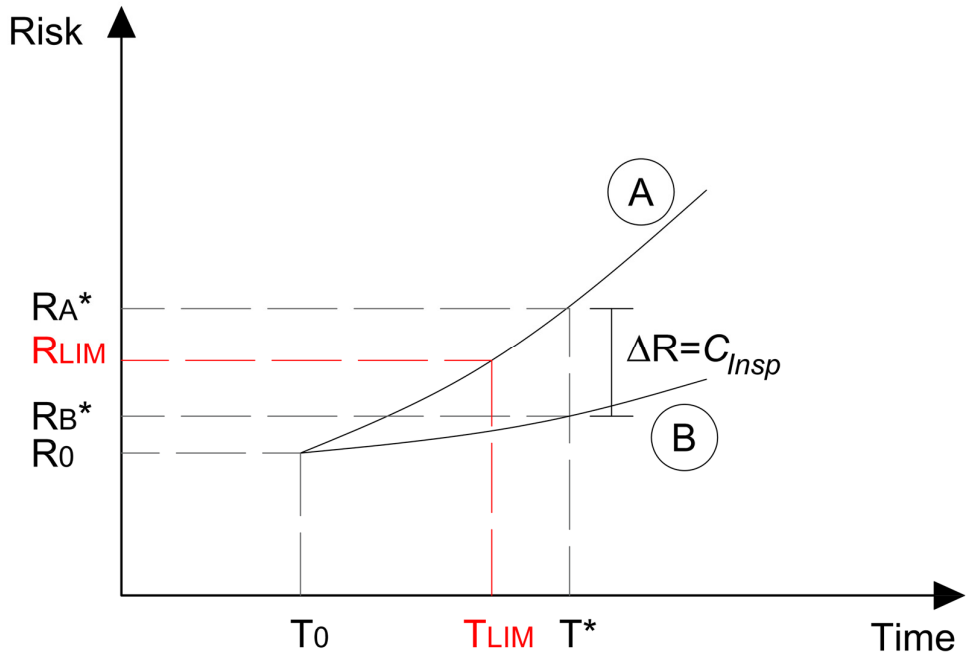


**Figure 8-2. Inspection interval limited by the $R_{LIM}$.**

Naturally, even though T* would be the optimum time to inspect the bridge from a cost-benefit perspective, the risk should not exceed society's pre-established level of risk-tolerance as represented by an upper limit value $R_{LIM}$. For example, $R_{LIM}$ may represent the risk associated with a rating factor RF=1.0 which historically has been used as the criterion for deciding on posting or rehabilitating bridges. Therefore, in this Thesis the time to perform a bridge inspection is proposed to be set at the lower of T* (when the general estimate of risk is equal to the cost of inspection) or $T_{LIM}$ which is the time when the general estimate of the risk on (curve A) exceeds a limit risk ($R_{LIM}$) associated with a rating factor smaller than 1.0, as shown in Figure 8-2.

The $T_{LIM}$ limitation is needed to avoid that the inspection interval becomes too large for weaker bridges, even if they are experiencing slow deterioration rates. In this sense, since this limitation is applied to curve A, that accounts for the uncertainties associated with estimating the deterioration rate based on a large population of bridges (as analyzed in section 3.5), the proposed approach for determining the optimum inspection interval includes a safety factor against unexpected deterioration rates different from the one observed at the specific bridge under study.

Even though in most cases performing the bridge inspection at the time calculated using this proposed procedure may reveal that the actual risk is lower than that originally estimated, in some instances it may reveal that it is higher than the originally estimated risk (e.g. curve B may have shifted upward at a faster rate

than expected). In the latter case and depending on the results of the improved risk assessment, the owners may decide to keep the bridge open, perform necessary maintenance, load post, or rehabilitate the bridge. The cost of performing the inspection is justified in either case i.e. whether the improved estimate is lower than the previously estimated risk (thus easing the fear of the public) and even more so if the risk is found to be higher so that necessary actions may be taken. It is possible that the proposed risk-based determination of the inspection interval may indicate that inspection be performed at more frequent intervals than the usual two years.

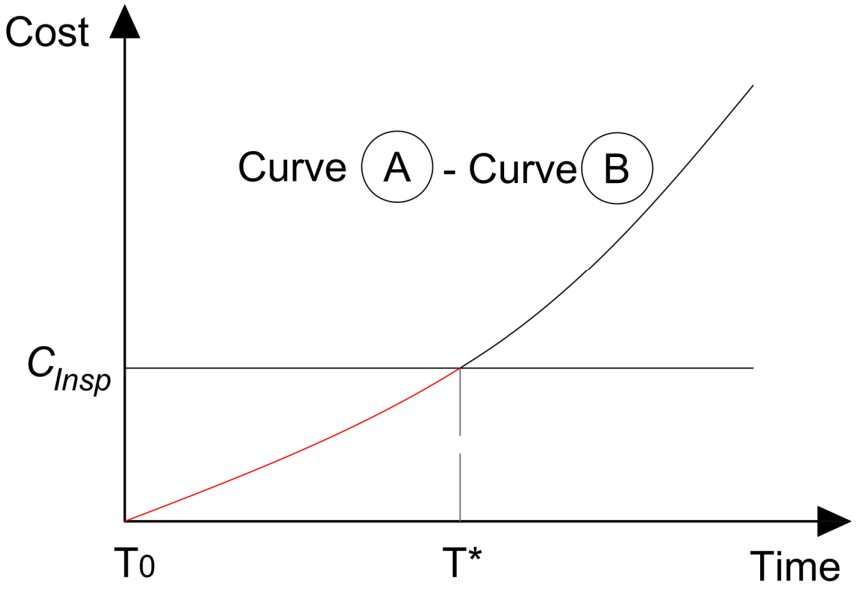


**Figure 8-3. Inspection interval based on inspection cost.**

In order to better visualize how the inspection interval defined earlier is optimum, the "delayed inspection" curve and the cut-off inspection cost are plotted in Figure 8-3. The red curve of the figure shows that until the cost of delaying the inspection is smaller than the inspection cost, it would be cost-effective to delay the inspection. When the cost of delaying the inspection increases above the inspection cost, delaying the inspection is no longer cost-efficient.

It is reasonable to expect that the proposed approach that would lead to delayed inspections would increase the anxiety of a society accustomed to the regular two-year inspection cycle. While it is not possible to quantify this aspect at the moment and include it in the present calculations, several researchers have conceptually discussed issues related to risk tolerance and risk perception which may require further study

before possible implementation in structural risk analysis processes. The reader may refer to Bell et al. (2006) and Nowak and Collins (2013) for further information.

The direct application of the concepts explained in this section is next described and labeled as "full-fledged method", while a "simplified procedure" is proposed further for a more practical calculation of the inspection intervals.

## 8.2 Full-fledged Method Example

The application of the method developed in the previous section is illustrated using an example bridge before applying to all the bridges in *set 1*. The first step of the routine inspection process consists of performing the inspection report on the specific type of location of the defects and assigning a condition rating for the bridge. The second step is performed by the evaluation engineer who receives the inspection report and studies the type, extent and location of the defects, then projects their effect on the structural properties of the components. The evaluation engineer performs the load rating following the guidelines as set in the state regulations or AASHTO MBE (2018). Furthermore, the information is entered into the NBI data file and collected by the FHWA at the national level.

The additional steps necessary to apply the method developed in this work would be performed in conjunction with the load rating calculation process.

Let us apply the process to bridge ID 1000871 of *set 1* as an example. This bridge is formed by 7 parallel beams spaced 2.5 m and spanning 24.6 m. The load rating assigned to this bridge is RF=2.5.

First, the deterioration rate needs to be calculated. Since the engineer in charge of the evaluation has access to the historical inspection reports and previous load rating calculations, the trend in the loss of load carrying capacity can be calculated. However, in case the information is insufficient the procedure described in Appendix B can be used. It is recalled that the deterioration rate is calculated for the member capacity, not for the load rating. In this example, it is assumed that after inspection and assessment of the type of deterioration, the engineer found a deterioration rate in member capacity equal to 2.0%. Following the grouping given in Chapter 3, high deterioration rate is defined as 3.4% and the medium deterioration rate is defined as 0.5% thus the bridge under study falls between these two categories. However, it is here recommended to classify bridges conservatively, especially if the deterioration rate is based on unprecise data as is often the case. Therefore, in this example the bridge is classified using the high deterioration rate group.

Thus, the risk is calculated following the calculation process described in this Thesis in Chapters 4-5-6 for the probability of failure and the cost calculation as performed in Chapter 7. The risk calculation is developed for:

1) A range of six years considering the deterioration uncertainties obtained by the statistical analysis performed in section 3.5. This would lead to curve A in Figure 8-1.
2) The same six-year range but assuming that the deterioration rate is deterministic which in this case conservatively assumes 3.4% reduction in member strength capacity per year (Figure 8-1 curve B)
3) Finally, the calculation of the risk threshold is obtained assuming a load rating equal to 1.0.

The results of the application of the steps 1) and 2) are reported in Table 8-1 and plotted in Figure 8-4.

**Table 8-1. Risk and relative risk over time for example bridge.**

| | Risk | | ΔRisk |
|---|---|---|---|
| | $ x 1000 | | |
| year | Curve A | Curve B | Curve A-Curve B |
| 0 | 2.8 | 2.8 | 0.0 |
| 1 | 4.9 | 3.6 | 1.3 |
| 2 | 10.7 | 4.5 | 6.2 |
| 4 | 23.9 | 6.1 | 17.9 |
| 6 | 33.2 | 8.0 | 25.2 |

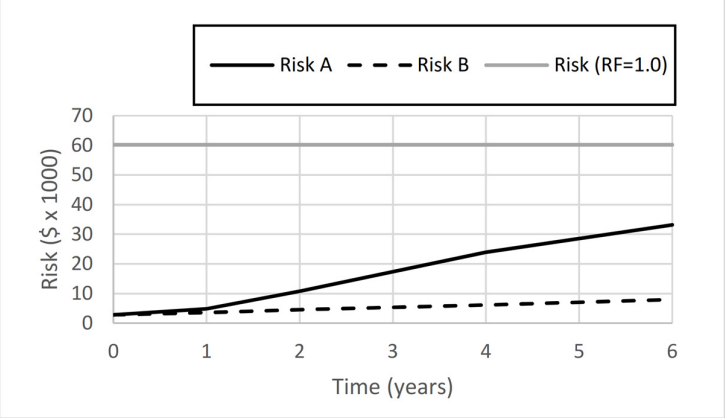


**Figure 8-4. Risk and relative risk over time for the example bridge.**

Because the risk threshold calculated in step 3), which is found to be $ 60,200 is higher than any risk projected in the next six years as calculated from step 1) it does not control the inspection period. Hence, the inspection interval can be calculated as a function of the inspection cost. The differences between the risk values calculated in steps 1) and 2) (Figure 8-4 black line minus dashed black line) for the period of 0 to 6 years are plotted in Figure 8-5. Assuming that the cost of inspection is $ 20,000, a horizontal straight line

can be drawn to intercept the relative risk curve at that level which would indicate that the optimum inspection time is of 4.6 years, that is conservatively rounded down to 4 years.

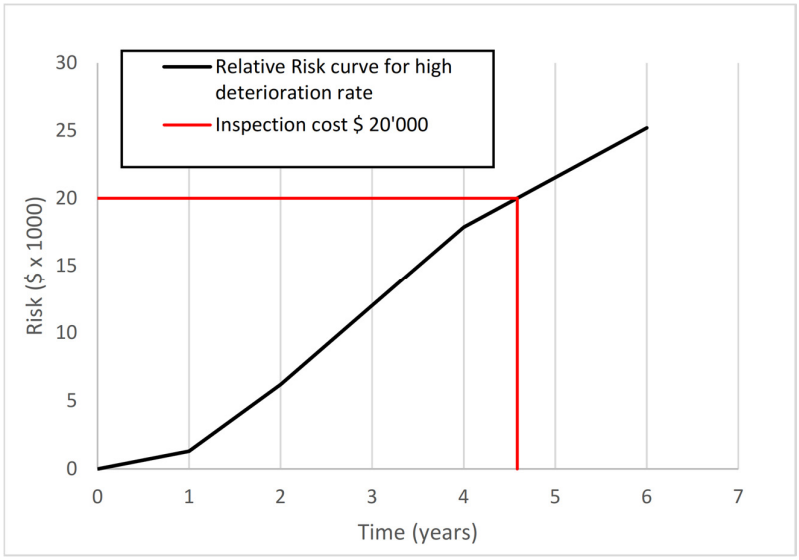


**Figure 8-5. Inspection time calculation for high deterioration rate and inspection cost equal to $ 20'000.**

A sensitivity analysis compares the optimum inspection period assuming different inspection costs (from $ 4,000 to $ 40,000) and three possible deterioration rates (high, medium and low). These results are summarized in the column chart of Figure 8-6.

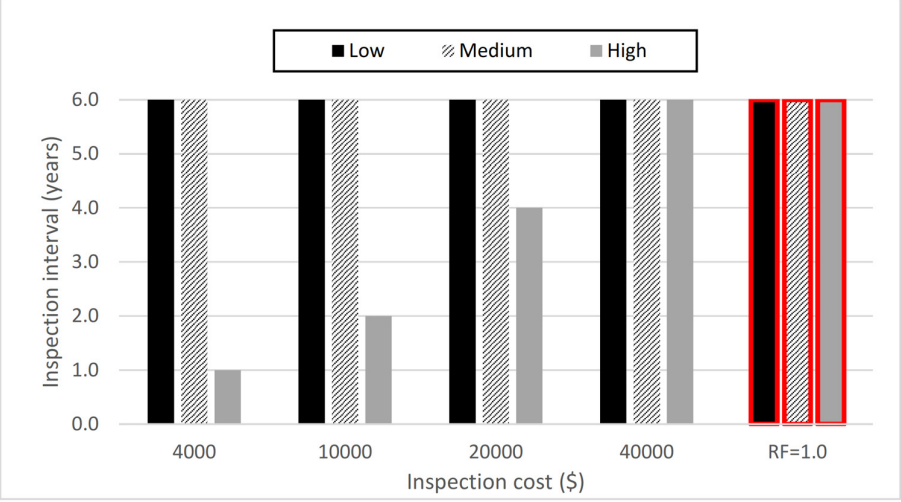


**Figure 8-6. Inspection interval as a function of inspection cost and deterioration rate for bridge ID 1000871 of set 1.**

The column chart of Figure 8-6 shows that in the case of low and medium deterioration, the inspection interval can be safely set at 6 years. If the bridge is experiencing high deterioration rate, the inspection interval would range between 6 years if the inspection cost exceeds $ 40,000 down to 2 years if the inspection cost is on the order of $ 10,000 and even one-year interval would be justified if the inspection cost is less than $ 4,000.

The calculations are repeated for bridge 1001429 with 5 beams spaced at 2.5 m spanning 31.0 m. In this case, the load rating is 1.7 meaning that the threshold risk linked to a load rating equal to 1.0 is more likely to limit the inspection interval compared to the previous bridge example. The results are summarized in the column chart of Figure 8-7.

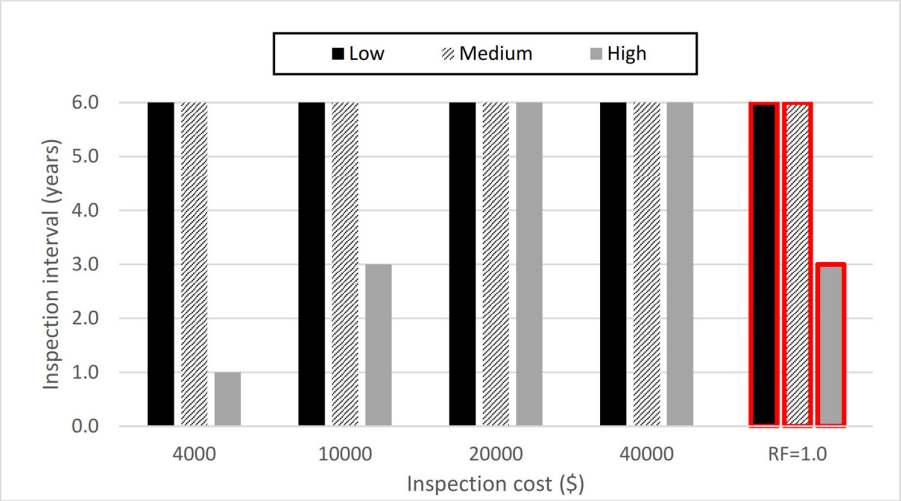


**Figure 8-7. Inspection interval as a function of inspection cost and deterioration rate for bridge ID 1001429 of set 1.**

As can be seen from Figure 8-7, for high deterioration rates and high inspection costs, the cost-effectiveness criterion to establish the inspection interval cannot be applied. Instead, the inspection time is limited (accounting for a proper safety margin as explained in Section 8.1) to 3 years to avoid that the bridge capacity falls below acceptable values between inspections. On the other hand, for low and medium deterioration rates the inspection interval can be safely set to 6 years.

## 8.3 Analysis of a Set of Bridges

In this section, the inspection interval is calculated for the entire population of bridges in *set 1*. As done in Section 8.2, the results of the risk analysis are rounded for practical purposes. The first modification limits the inspection interval to 6 years in those cases where the inspection interval is larger than 6. In other cases, the inspection intervals are conservatively rounded down to the lower integer. Finally, the inspection

interval that should theoretically be performed in an interval of less than 1 year are rounded up to 1 year. In fact, this latter circumstance presents itself when the capacity of the bridge is very sensitive to deterioration and assigning this bridge a 1-year routine inspection interval is essentially raising a flag to alert the authorities of the high risk it causes. For this reason, inspection intervals smaller than 1-year should be set on the basis of bridge specific condition and in those cases, the need for more in-depth inspections should be considered if the bridge has not been already scheduled for rehabilitation.

**Table 8-2. Percentage of bridges and their corresponding inspection intervals based on deterioration rate and cost of inspection.**

| | High deterioration rate (3.4%) | | | | Medium deterioration rate (0.5%) | | | | Low deterioration rate (0.07%) | | | |
|---|---|---|---|---|---|---|---|---|---|---|---|---|
| Inspection cost ($) | 4k | 10k | 20k | 40k | 4k | 10k | 20k | 40k | 4k | 10k | 20k | 40k |
| 1 | 77% | 56% | 41% | 26% | 18% | 7% | 3% | 1% | 1% | 0% | 0% | 0% |
| 2 | 11% | 19% | 14% | 16% | 7% | 4% | 1% | 1% | 0% | 0% | 0% | 0% |
| 3 | 5% | 7% | 17% | 14% | 5% | 4% | 3% | 1% | 0% | 0% | 0% | 0% |
| 4 | 4% | 8% | 9% | 11% | 6% | 5% | 3% | 1% | 0% | 0% | 0% | 0% |
| 5 | 0% | 3% | 3% | 5% | 3% | 4% | 3% | 1% | 0% | 0% | 0% | 0% |
| > 6 | 2% | 9% | 16% | 28% | 61% | 77% | 88% | 95% | 99% | 100% | 100% | 100% |

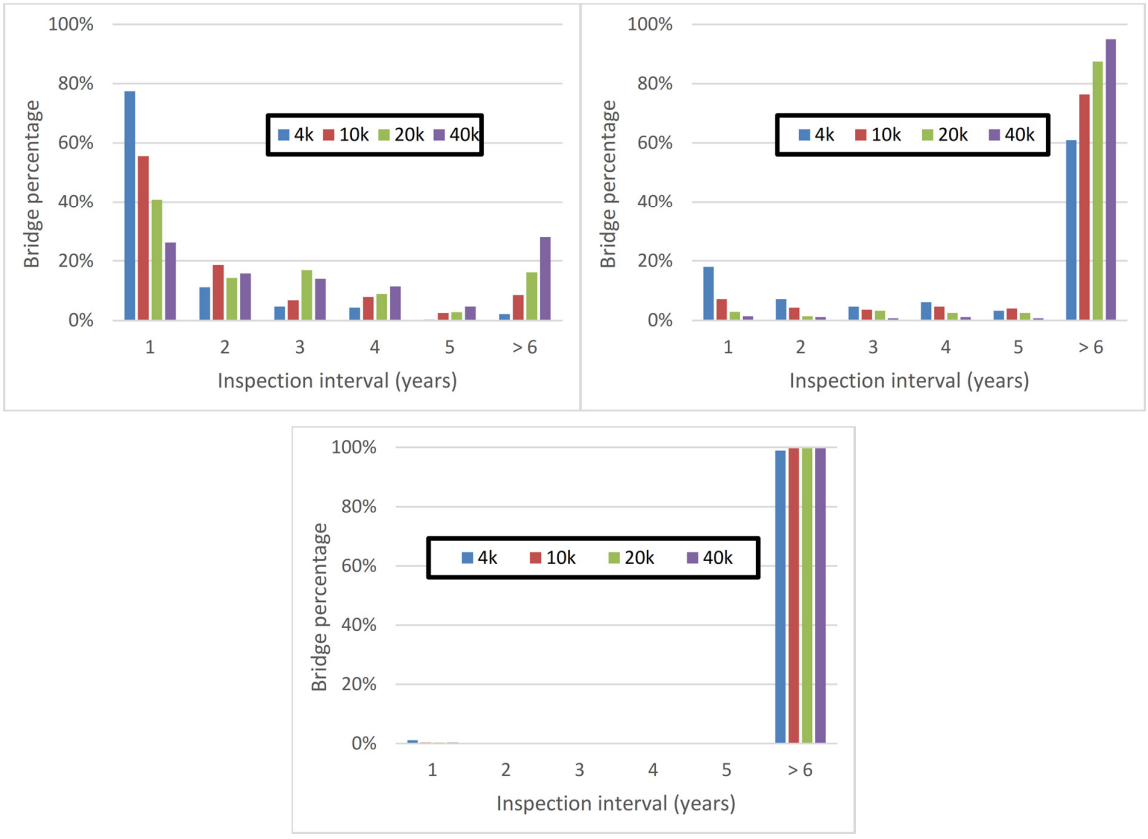


**Figure 8-8. Percentage of bridges and their corresponding inspection interval based on deterioration rate and cost of inspection. High, medium and low deterioration rates clockwise.**

While the full list of results for *set 1* bridges is presented in Appendix H the corresponding statistics are synthesized in Table 8-2 and Figure 8-8. The results are calculated assuming three categories of deterioration rates for the entire *set 1* of bridge population. For example, the histogram shown in Figure 8-8 (upper-left) shows that if all the bridges are subject to the deterioration rates and the inspection cost is $ 4,000, 80% of the bridges would show that it would be cost-effective to inspect them within a one-year period. The percentage of bridges for which a one-year inspection would decrease as the cost of inspection increases. When the cost of inspection is $ 10,000 the percentage is about 60%, when the cost $ 20,000 the percentage of bridges is 40% and when the cost is $ 40,000 the percentage is 25%.

Similarly, lower bridge percentages are associated with larger inspection periods. On the other hand, for medium and low deterioration rates (Figure 8-8 upper right corner and lower row) larger percentages of bridges would need to be inspected with a larger inspection interval. One of the conclusions that can be drawn from Figure 8-8 (down) is that a 6-year interval can be used for almost all bridges if they show low deterioration trends over the previous recent years.

**Table 8-3. Percentage of bridges showing an optimum inspection interval smaller larger or equal to the standard 2-year interval.**

| | High deterioration rate (3.4%) | | | | Medium deterioration rate (0.5%) | | | | Low deterioration rate (0.07%) | | | |
|---|---|---|---|---|---|---|---|---|---|---|---|---|
| Inspection cost ($) | 4k | 10k | 20k | 40k | 4k | 10k | 20k | 40k | 4k | 10k | 20k | 40k |
| <2 | 77% | 56% | 41% | 26% | 18% | 7% | 3% | 1% | 1% | 0% | 0% | 0% |
| 2 | 11% | 19% | 14% | 16% | 7% | 4% | 1% | 1% | 0% | 0% | 0% | 0% |
| >2 | 11% | 26% | 45% | 58% | 75% | 89% | 96% | 98% | 99% | 100% | 100% | 100% |

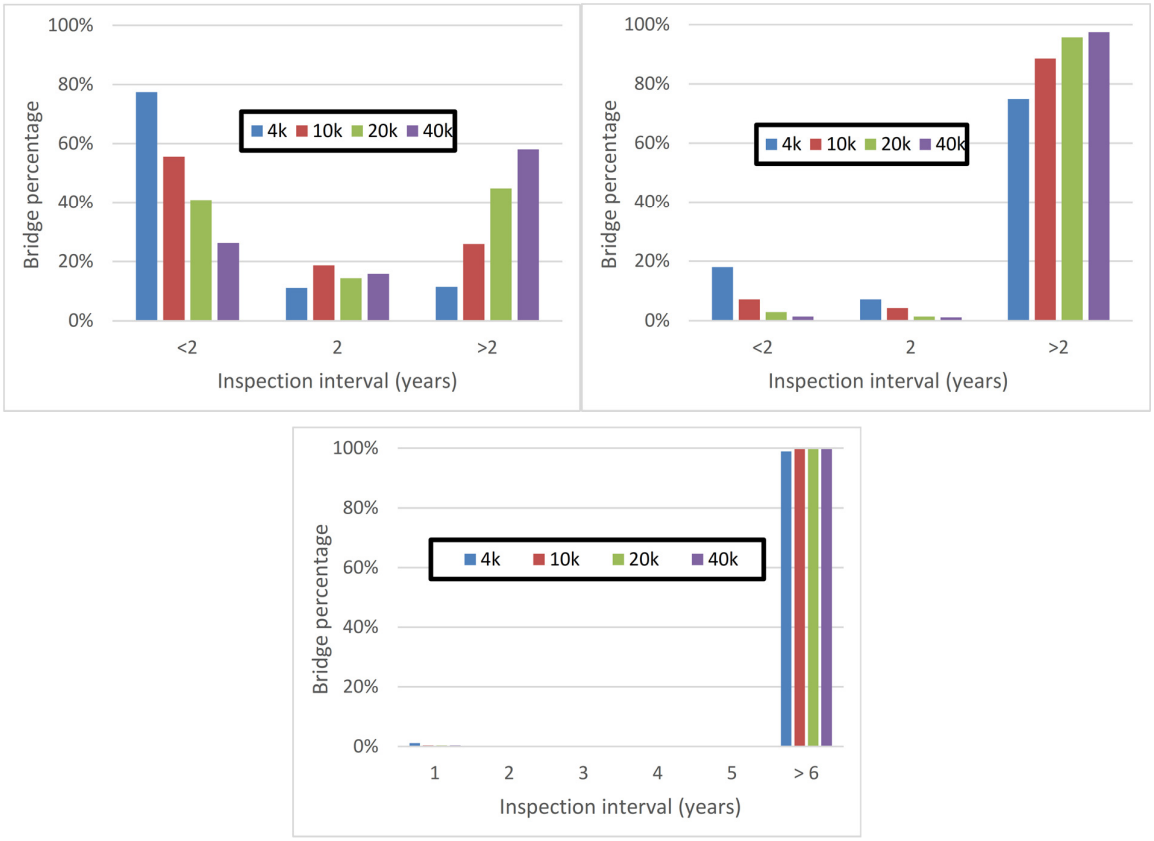


**Figure 8-9. Percentage of bridges showing an optimum inspection interval smaller, larger or equal to the standard 2-year interval. High, medium and low deterioration rates clockwise.**

The inspection intervals can also be compared to the standard two-year inspection interval currently used by the State DOTs. Table 8-3 and Figure 8-9 show the percentage of bridges for which the inspection interval is shorter equal or longer than two years respectively. The results presented in the histogram of Figure 8-9 (top-left) show that even in the most conservative situation where bridges are exposed to high deterioration rates, a significant percentage of bridges can be inspected in intervals longer than the standard 2-year interval. This percentage ranges between 15% to 55% as the inspection cost increases from $ 4,000 to $ 4,000. However, for this high deterioration rate, a large number of bridges also shows the necessity of being inspected in less than 2 years. In the case of medium and low deterioration rates, between 65 and 100% would need to be inspected within a time interval larger than two years.

**Table 8-4. Percentage of bridges for which the condition RF=1.0 is governing. Only for high deterioration rate.**

| Inspection cost ($) | 4k | 10k | 20k | 40k |
|---|---|---|---|---|
| 1 | 0% | 1% | 1% | 2% |
| 2 | 0% | 1% | 0% | 1% |
| 3 | 0% | 2% | 2% | 3% |
| 4 | 0% | 0% | 1% | 2% |
| 5 | 0% | 0% | 0% | 0% |
| total | 1% | 4% | 4% | 8% |

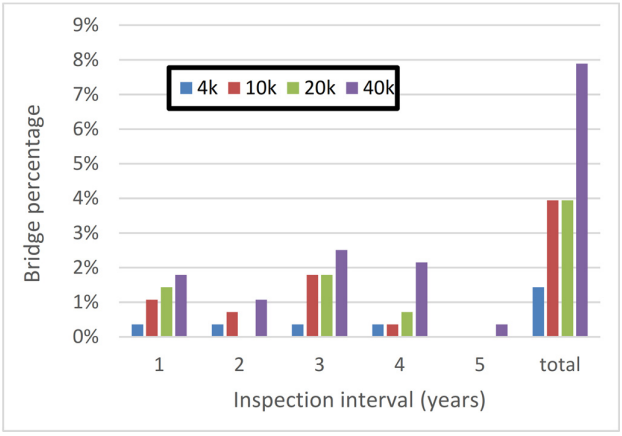


**Figure 8-10. Percentage of bridges for which the condition RF=1.0 is governing as a function of inspection cost for high deterioration rate. In the bin axis the inspection interval that is imposed by such condition.**

It is also interesting to show the influence of the limitation of the risk linked to a rating factor RF=1.0 (Table 8-4 and Figure 8-10). The results presented in Table 8-4 and Figure 8-10 are based on the assumption that all the bridges are experiencing a high level of deterioration rate that is because for medium and low deterioration rates the inspection interval of none of the bridges analyzed is controlled by the maximum risk threshold corresponding to a rating factor RF=1.0. It is recalled that a load rating RF=1.0 guarantees a certain margin of safety determined by the rating method employed. However, the authority may set a more stringent risk threshold based on a load rating larger than 1.0, which corresponds to increasing the global safety factor, with the consequence of more bridges being limited by this condition requiring lower inspection intervals for those bridges. As a conclusion, the current rating factor limit of 1.0 governs the inspection interval for 8% of the bridges assuming the most adverse conditions (high deterioration rates an inspection cost equal to $ 40'000 as can be seen by the last bin of Figure 8-10 labeled as "total").

The last result to be presented is an economical evaluation of the current 2-year standard inspection interval in the context of the present work. In fact, while the proposed method is able to calculate the inspection time given a cost of inspection, the optimum inspection cost given a fixed inspection interval can also be calculated. Therefore, it is possible to evaluate for each bridge of *set 1* what is the maximum inspection cost that would be optimum according to the risk-based method assuming that the standard 2-year inspection interval cannot be modified (Table 8-5 and Figure 8-11).

**Table 8-5. Percentage of bridge in different inspection costs worth 2-year inspection cost categories assuming a fixed 2-year inspection.**

| Inspection cost ($) | <4k | >4k <10k | >10k <20k | >20k <40k | >40k |
|---|---|---|---|---|---|
| High deterioration rate (3.4%) | 11% | 15% | 19% | 16% | 39% |
| Medium deterioration rate (0.5%) | 29% | 23% | 13% | 11% | 23% |
| Low deterioration rate (0.07%) | 36% | 22% | 10% | 11% | 21% |

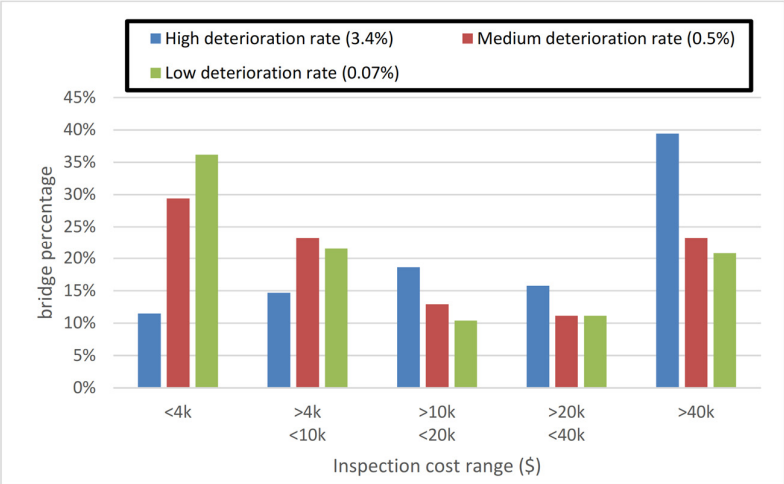


**Figure 8-11. Bridge percentages associated with inspection costs worth 2-year inspection for the three deterioration rate scenarios.**

For example, Figure 8-11, shows that in the case of high deterioration rate (blue column), 11% of bridges would require inspection every 2-year if their inspection cost is lower than $ 4'000. On the other hand 15% of the bridge population would require a 2-year inspection interval if the cost of inspection ranges between $ 4'000 and $ 10'000 and so on. Obviously, assuming less severe deterioration rates (medium in red and low in green) the 2-year inspection interval would be required for cheaper inspection costs than if the deterioration rate is high.

## 8.4 Simplified Risk Analysis Procedure

### *8.4.1 Conceptual approach*

The calculations performed in the previous section to determine the optimum inspection time interval involve a complex analysis that may be difficult to perform on a regular basis in engineering practice. A simplified procedure is therefore necessary to provide engineers with a practical method to calculate the recommended inspection time interval. In order to do that, a simple and familiar format is proposed, taking standard format similar to that commonly used in engineering practice (Washer, Connor, Nasrollahi, & Provines, 2016) but unlike those previously recommended studies, the proposed approach is calibrated using the results of the advanced risk assessments presented in the previous sections of this chapter. It is noted that the method proposed in this work is not based on absolute risk, but is formed by a cost–benefit analysis combined with a risk acceptance threshold corresponding to a minimum load rating value RF=1.0. Accordingly, the standard definition of the risk in Equation 8-1 must be adapted to the simplified procedure proposed in this chapter. The standard format for the calculation of risk is based on the following conceptual definition of risk described in Equation 8-1:

$$Risk = Hazard\ Likelihood \times Vulnerability \times Robustness \times Consequences \quad (8\text{-}1)$$

$Hazard\ Likelihood$ represents the probability of occurrence of a specific hazard or a set of simultaneous hazards in a specific period of time. In this work the hazard is the combination of maximum expected live load obtained in Chapter 5 and the environmental deterioration of the bridge as calculated in Chapter 3. While in the full-fledged method the live load is adapted to the structural configuration as explained in Chapter 5, in the simplified procedure there is no specific input dedicated to the live load due to it's small influence in the final results. On the other hand, the deterioration rate is entered as an explicit input that is based on the classification of the bridge into three categories of high, medium or low deterioration rate, as explained in Chapter 3 and will be further explained for the simplified procedure

$Vulnerability$ represents the susceptibility of a structure to suffer a local damage after the hazard is triggered. In this work the vulnerability of the bridge is represented by the resistance of the bridge (Chapter 4) and will be considered as an explicit input in the simplified procedure.

$Robustness$ represents the capability of the structure to carry the load in a deteriorated state using the system behavior that includes the load transfer among different elements after damage. In other words, it is the ability of a structure to withstand events like fire, explosions, impact or consequences of human error, without being damaged to an extent disproportionate to the original cause. In the simplified procedure this term is considered to be dependent on the bridge configuration as observed from the results obtained in Chapter 6.

$Consequences$ of failure represent the impact of the bridge's failure on the bridge users. The community the bridge is intended to serve in terms of economic losses, disruption of community functions and impact on the environment as explained in Chapter 7. However, because the determination of optimum inspection interval is based on a comparison between the cost of failure and the cost of inspection as explained in Section 8.1 it is herein proposed to represent the consequences in terms of the ratio of the cost of failure over the cost of inspection $C/C_I$.

It is noted that the approach used in this work for the full risk analysis method unifies the $Hazard\ Likelihood$, $Vulnerability$ and $Robustness$ into the probability of system failure, since the deterioration level as well as the live load configuration and load distribution are all included in the reliability analysis as explained in Chapter 3. The simplified approach will separate these terms for practical implementation to avoid the need to perform a full-fledged reliability analysis.

### *8.4.2 Calibration of the simplified procedure (general outline)*

As a result of the previous subsection, the simplified procedure seeks to provide a way to assess the four parameters recalling those of Equation 8-1:

I. The deterioration rate (to represent the $Hazard\ Likelihood$).
II. The load rating (RF) (to represent the $Vulnerability$).
III. The structural configuration which is reflected by SL=Span length and BS=beam spacing (to represent the $Robustness$).
IV. The relationship between cost of bridge failure and cost of inspection $k = C/C_I$ (to represent the $Consequences$).

The calibration process is based on the following steps (labelled as *calibration steps*) that are outlined briefly below and will be explained in detail further in this section:

1) All the bridges of *set 1* are redesigned for a uniform level of syetem reliability. The target value used in this case is the average value of system reliability index obtained for the whole set of bridges under study.
2) A load rating is back calculated for each redesigned bridge and defined as reference load rating $RF_R$.
3) The relative Risk over time curves (difference between curve A and B shown in Figure 8-5) are recalculated for the redesigned bridges. Furthermore, the values in the y-axis are normalized with the cost of failure $C$. These normalized curves are calculated for all bridges and the average curve is calculated. The average curves are calculated for the three deterioration rates as conceptually shown in Figure 8-12.

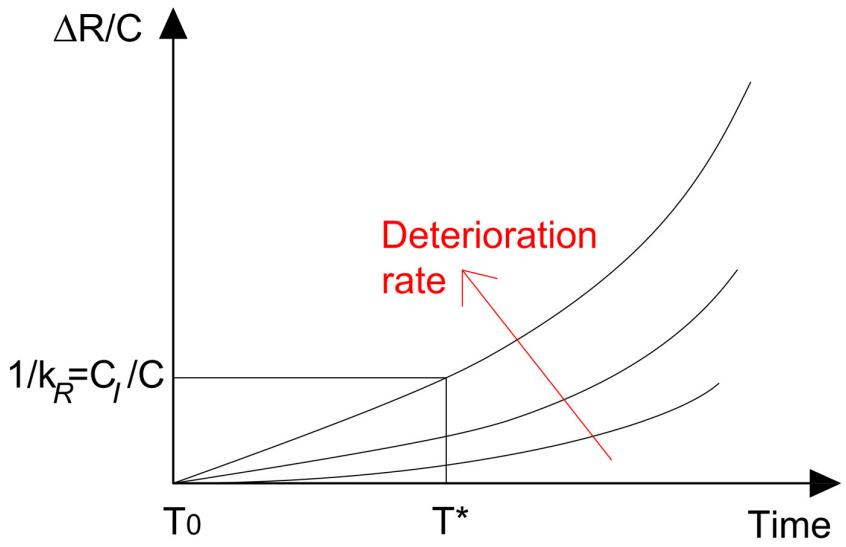


**Figure 8-12. Relationship between inspection interval and the normalized value $C_I/C$. Each curve is the average of all *set 1* bridges for each corresponding deterioration rate.**

4) The value of $k_R$ is calculated for the inspection intervals 1, 2, 4 and 6 years and organized in table format as conceptually shown in Table 8-6.

**Table 8-6. Inspection interval as a function of the deterioration rate and the ratio $k_R=(C/C_I)_R$, for bridges with a uniform reliability level (associated with the reference load rating).**

| | Inspection interval | | | |
|---|---|---|---|---|
| | 1 | 2 | 4 | 6 |
| High deterioration rate | $k_R = (C/C_I)_R$ | | | |
| Medium deterioration rate | | | | |
| Low deterioration rate | | | | |

The rows in Table 8-6 represent the deterioration rates, the columns represent the inspection intervals and the coefficients of the table represent the values of the reference ratio $k_R = (C/C_I)_R$ for bridges with a uniform level of reliability (the subscript R stands for reference).

At this point, the inspection interval is found for bridges with a uniform level of reliability. Likewise, it can be stated that the inspection interval can be found for bridges with a load rating matching the reference load rating. However, real bridges are associated with different system reliability levels depending on their member based load rating and on their structural configuration. Therefore, the inspection interval calculated in the previous calibration steps must be corrected for different reliability levels. Since the final user of the simplified procedure cannot easily calculate the reliability index the bridge under study, the parameter used herein is the relationship between the real load rating (as found in the NBI database) and the reference load rating defined in point 2).

5) The reference load rating calculated in point 2) is shown to depend on the bridge configuration; therefore, a functional equation is defined to relate the structural configuration with the reference load rating.

Once the reference load rating is defined for each bridge it is necessary to investigate how the ratio between the actual load rating and the reference load rating influences the elements of the Table 8-6. For this purpose the ratio $\omega$ between the actual load rating and the reference load rating is considered as shown in Equation 8-2:

$$\omega = \frac{RF}{RF_R} \tag{8-2}$$

Likewise, the ratio $\theta$ between the reference $C/C_I$ and the $C/C_I$ effectively found for the bridge under study is defined in Equation 8-3:

$$\theta = \frac{(C/C_I)_R}{C/C_I} = \frac{k_R}{k} \tag{8-3}$$

6) A sensitivity analysis of $\theta$ depending on the different possible values of $\omega$ for all deterioration rates is performed. As a result, a functional equation is found to define $\theta$ as a function of $\omega$.

In summary, a general calibration is carried out for bridges with a uniform level of reliability and for each deterioration ratio from point 1) to 4) and the results are adapted to each structural configuration and load rating value in points 5) and 6). In the next subsection the calibration process is presented with further detail.

### *8.4.3 Calibration of the simplified procedure (step details)*

In this subsection the calibration steps are analyzed in detail and more information is given on the simplifications applied.

*Calibration step 1*

In this step the bridges of *set 1* are redesigned to meet a uniform reliability level. The redesign process is iterative, and consists of changing the load rating until the reliability index equals the reference one. The value used for the reference reliability index is not of crucial importance, as it only represents a base point. However, it is convenient to use a reasonable value shown to be as common as possible within the bridges of *set 1*. For this reason a reliability index $\beta_{system} = 3.0$ is chosen since it is the average value of *set 1*. The

iterative process leading to the required reliability index can be visualized in the example of Figure 8-13 where the convergence is reached in 6 steps.

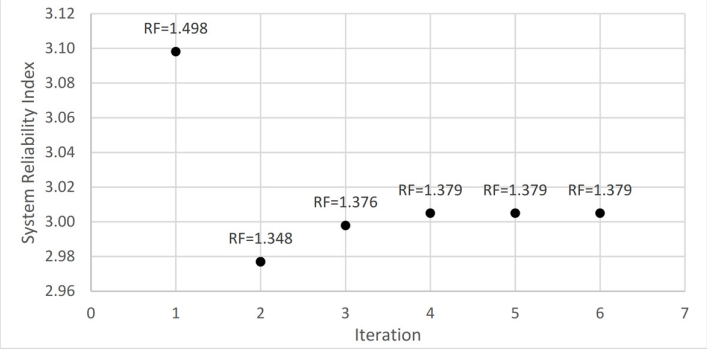


**Figure 8-13. Convergence in 6 steps of the required reliability index and calculation of the reference load rating.**

*Calibration step 2*

The load rating associated with this reliability index, different for each of the 279 bridges is defined as reference load rating (the results are shown in calibration step 5). It is noted that the uniform level of reliability is set at system level, while the reference load rating is still calculated with the standard rules of the LFR rating method and therefore at member level. The plot in Figure 8-14 shows the lack of uniformity in the reference load ratings, which is an indirect manifestation of the different system behaviors (robustness) that can be observed for each bridge.

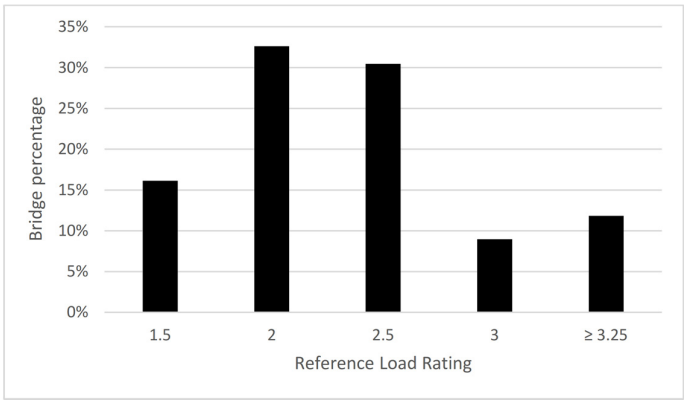


**Figure 8-14. Distribution of reference load rating for *set 1*.**

*Calibration step 3*

After the bridges are redesigned for a uniform system reliability index in calibration step 1 the risk analysis is performed. Specifically, the curve A-curve B (as in Figure 8-2) over time relationship is calculated. The resulting relative risk curve over time (similar to the one shown in Figure 8-5) is calculated and then the y-axis divided by the total cost $C$. This curve is calculated for all bridges of *set 1* and for high, medium and low deterioration rates. Figures 8-15, 8-16 and 8-17 show for each deterioration rate, the average curve (black line) along with the lower and upper bound (red markers) of all the bridges of *set 1*.

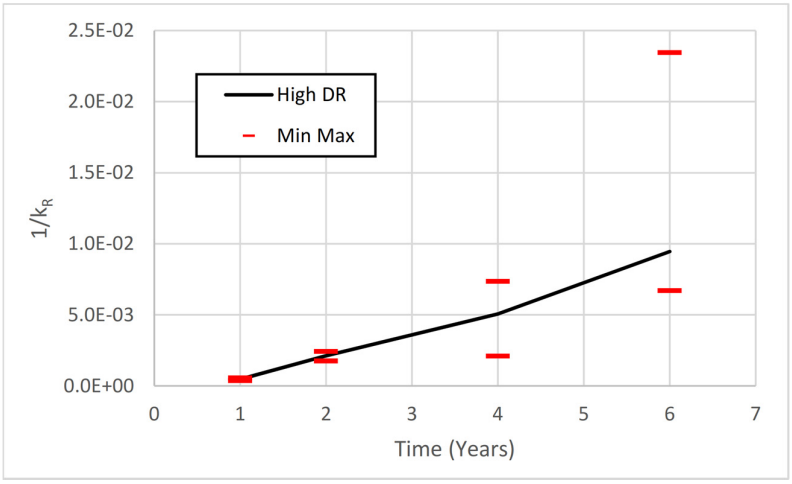


**Figure 8-15. *1/$k_R$* over time for high deterioration rate. The black line represents the average value of the curve and the red markers show the maximum and minimum value of the curve for the entire *set 1*.**

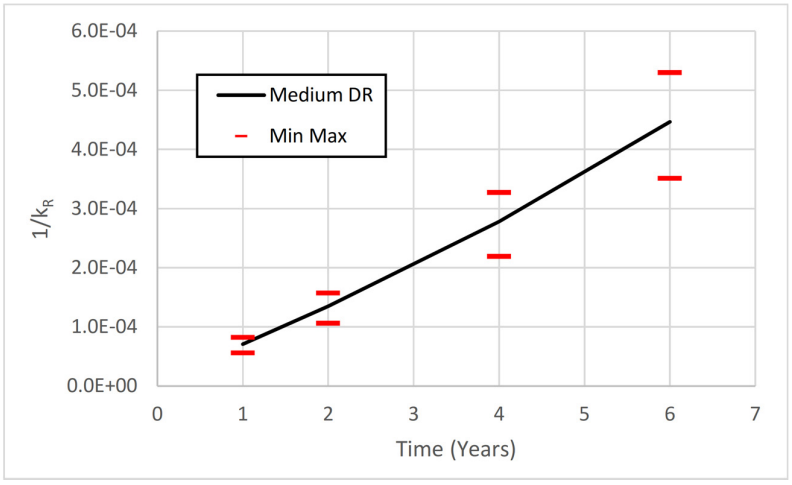


**Figure 8-16. *1/$k_R$* over time for medium deterioration rate. The black line represents the average value of the curve and the red markers show the maximum and minimum value of the curve for the entire *set 1*.**

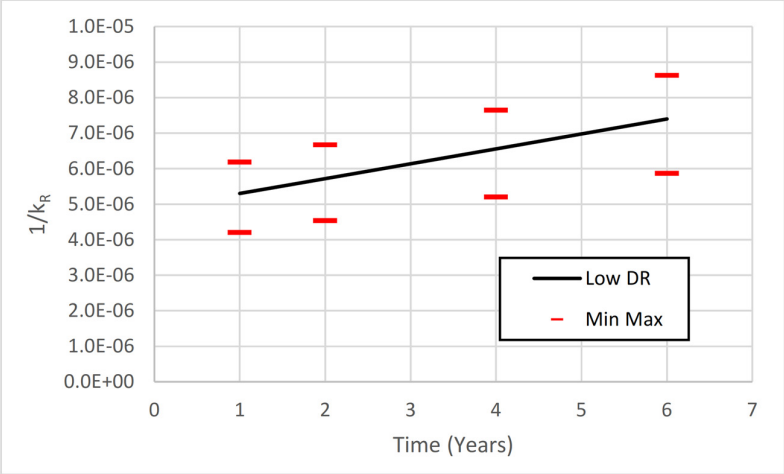


**Figure 8-17. *1/$k_R$* over time for low deterioration rate. The black line represents the average value of the curve and the red markers show the maximum and minimum value of the curve for the entire *set 1*.**

*Calibration step 4*

As shown in the previous step, the curve $1/k_R$ over time is different for each bridge. The simplification applied in the previous step is that the average curve over all bridges of *set 1* are considered. In fact, it can be seen from Figures 8-15, 8-16 and 8-17 that while the curves may range inside the red markers for *set 1* bridges, the average value is plotted with a black line. Therefore the recommended inspection interval for bridges designed with a uniform level of system reliability is shown in Table 8-7 as a function of the deterioration rate and the coefficient $k_R$.

**Table 8-7. Recommended inspection interval based on deterioration rate and on *$k_R$*.**

| | Inspection interval | | | |
|---|---|---|---|---|
| | 1 | 2 | 4 | 6 |
| High deterioration rate | 1.8.E+03 | 4.1.E+02 | 1.7.E+02 | 1.1.E+02 |
| Medium deterioration rate | 1.1.E+04 | 6.1.E+03 | 3.0.E+03 | 1.9.E+03 |
| Low deterioration rate | 1.5.E+05 | 1.4.E+05 | 1.2.E+05 | 1.1.E+05 |

A table similar to Table 8-7 will be used by the final user to establish the inspection interval. However, this table is defined for bridges with a system reliability index $\beta_{system} = 3.0$, therefore, the next two steps are dedicated to correct the table values depending on the specific characteristics of each bridge.

*Calibration step 5*

In this calibration step the relationship between the system reliability index (kept as constant) and the corresponding reference load rating is studied (as defined in calibration step 2). If this system reliability index is kept constant the resulting reference load rating will be as high as the robustness of the bridge is low.

Consequently, it is expected that different structural configurations lead to different values of reference load rating. Furthermore, a functional relationship between some structural parameters and the reference load rating is needed to calculate the reference load rating in a straightforward way, avoiding the system reliability calculation, difficult to perform for practicing engineers. For these reasons, several combinations of structural parameters have been analyzed in this work, in relation with the relative load rating, with the conclusion that the best configuration parameter is the aspect ratio span length over beam spacing $SL/BS$, as shown in Figure 8-18.

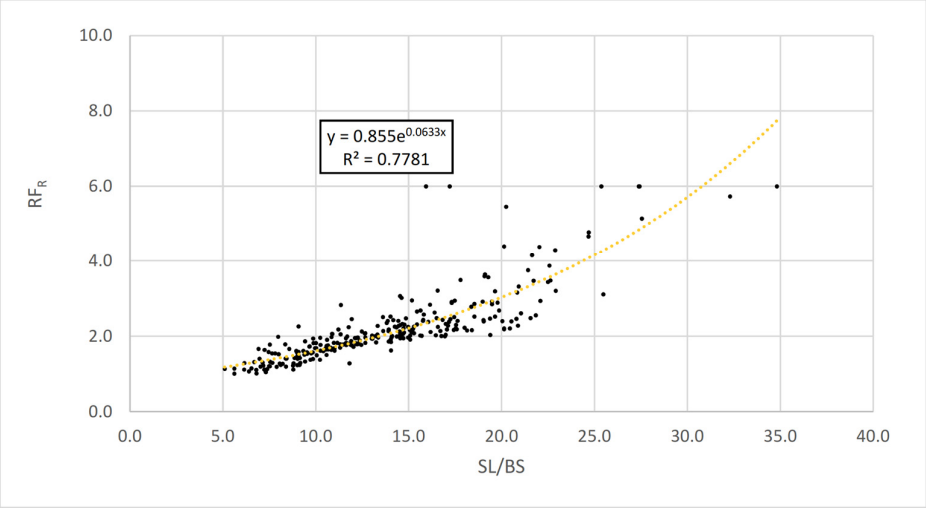


**Figure 8-18. Reference load *RF$_R$* rating versus beam spacing over span length (SL/BS) plot.**

The aforementioned relationship is shown to be very well described by an exponential function described in Equation 8-4:

$$RF_R = a_R \, e^{SL/BS \times b_R} \tag{8-4}$$

Where $a_R = 0.855$ and $b_R = 0.0633$.

The $R^2$ factor is found to be 0.7781, where 1.0 is a perfect fit. While all other fitting attempts have lead to a smaller $R^2$ factor, the goodness of this approximation will be studied in the next subsection, with the total error in estimating the inspection interval, when the coefficients will be part of an optimization process.

*Calibration step 6*

Once the relative load rating is found from step 5, it must be put into relation with the real load rating as reported in the NBI database or found by the structural analysist in the evaluation process by means of the

ratio $\omega$ defined in Equation 8-2. Therefore, this parameter is compared with the variation of relative cost $k = C/C_I$ from the reference design to the actual bridge. For this reason the parameter $\theta$ is defined in Equation 8-3. In other words, the objective is to find a functional relationship between $\omega$ and $\theta$.

For this purpose, a sensitivity analysis is performed with different values of $\omega$. It is recalled that $\omega = 1.0$ is exactly the condition where the load rating of the bridge is equal to the reference load rating, which implies a uniform system reliability index of 3.0 for all bridge configurations. Besides the aforementioned $\omega = 1.0$, the ratios considered are 0.5, 0.8, 1.2 and 2.0. For each case analyzed, the resulting $k$ from Equation 8-2 is found and, as a consequence, $\theta$ from Equation 8-3. The relationship between $\omega$ and $\theta$ is plotted in Figure 8-19 for high deterioration rate and for 1–year inspection interval which corresponds to the first row and first column element of Table 8-7.

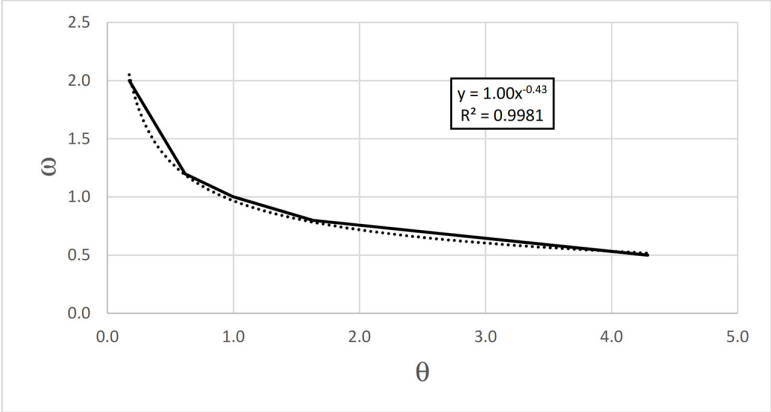


**Figure 8-19. Example of relationship between ω and θ.**

The power function is found to provide the better fit and maximum $R^2$ factor suggesting a relationship of the form described by Equation 8-5:

$$\omega = a_M \, \theta^{b_M} \tag{8-5}$$

The curve plotted in Figure 8-19 is also plotted for all bridges in set 1, for all deterioration rates and for all inspection intervals obtaining a global average value of $a_M = 1.0$ and $b_M = -0.5$. Again, the goodness of this simplification will be studied in the next subsection and be part of an optimization process.

**Table 8-8. Parametrical study of Equation 8-4 for *set 1*.**

| | $a_M$ | $b_M$ |
|---|---|---|
| min | 0.64 | -1.66 |
| max | 1.56 | -0.14 |
| mean | 1.00 | -0.50 |

### *8.4.4 Verification of the simplified method with bridge set 1*

In this subsection, the inaccuracies of the simplified procedure compared to the full-fledged method to calculate the inspection interval as per Section 8.3 are evaluated. It is important to mention that a simplified method is inevitably associated with a certain degree of inaccuracy or error, which is the price to pay for a less expensive and less cumbersome calculation. While several fitting coefficients are reported during the calibration steps outlined in subsection 8.4.3, it is found practical to just assume these as starting values, look at the errors between simplified and full-fledged method and eventually optimize the coefficients found during the calibration steps.

In order to carry out the comparison, the simplified procedure calibrated in subsection 8.4.3 is applied to the same cases developed in section 8.3. Therefore the same matrix made of 3 (deterioration rates) x 4 (inspection cost) x 279 (bridges) elements reported in Appendix H for the full-fledged method is calculated for the simplified procedure for a total of 3348 inspection interval calculation cases.

Conceptually, it is important to maximize the number of cases where the inspection interval calculated with the simplified procedure matches the one calculated with the full-fledged method. Additionally, the number of cases where the inspection interval suggested with the simplified method is larger than the one calculated with the full-fledged method (meaning that the simplified method is providing unconservative results) should be minimized, and be as close as possible to zero. The first condition is described by Equation 8-6:

$$err_1 = \frac{n_0 + n_1}{3348} \times 100 \tag{8-6}$$

Where $n_0$ is the number of cases where the full-fledged method results match with no error the simplified procedure and $n_1$ the still acceptable case where the results of the simplified procedure are only 1 year off the full-fledged method result, but on the safe side. On the other hand, the second condition is expressed by Equation 8-7:

$$err_2 = \frac{\sum n_i}{3348} \times 100 \tag{8-7}$$

Where $n_i$ is the number of cases where the results are unconservative and therefore $i$ is a negative value. For example, the expression $n_{-2} = 3$ would mean that the simplified method gives an inspection interval 2 years larger than the full-fledged method (for example 2 years versus 5 years respectively).

From this point, the simplified procedure can be seen as a mathematical optimization problem. In fact, a set of input parameters (load rating, structural configuration, deterioration rate, cost of inspection and cost of failure) and output values (inspection intervals) are linked to each other by a set of functions (Equations 8-4, 8-5 and Table 8-7) whose coefficients ($a_R$ and $b_R$ for Equation 8-4, $a_M$ and $b_M$ for Equation 8-5 and the 12 $k_R$ coefficients in Table 8-7) must be optimized to meet the required performances (maximize $err_1$ and minimize $err_2$). The starting point of the optimization process with the coefficients calibrated in subsection 8.4.3 are $err_1 = 92.7\%$ and $err_2 = 3.6\%$.

As a result of a trial and error process as well as coefficient sensitivity studies the following modifications are found to be effective:

1) The following values are used for the calculation coefficients $b_M = -0.476$, $a_R = 0.880$ and $b_R = 0.600$ instead of $-0.500$, $0.855$ and $0.633$ respectively. These values are found by analyzing the sensitivity of the errors to their variation and obtaining the most convenient set of coefficients.
2) For high deterioration rates the inspection interval must be limited to 2 years if the load rating is smaller than 1.8. Similarly, for medium deterioration rates the inspection interval must be limited to 3 years if the load rating is smaller than 1.3.
3) The values of Table 8-7 are decreased as per Table 8-9.

**Table 8-9. Inspection interval based on deterioration rate and on $k_R$ after the optimization process.**

| | Inspection interval | | | |
|---|---|---|---|---|
| | 1 | 2 | 4 | 6 |
| High deterioration rate | 1.8.E+03 | 2.4.E+02 | 8.7.E+01 | 5.3.E+01 |
| Medium deterioration rate | 1.2.E+04 | 3.6.E+03 | 1.6.E+03 | 9.1.E+02 |
| Low deterioration rate | 1.6.E+05 | 1.4.E+05 | 1.3.E+05 | 1.1.E+05 |

The results of applying these rules are $err_1 = 88.2\%$ and $err_2 = 0.0\%$. It is noted that this optimization problem cannot be solved mathematically but rather judging the different values of $err_1$ and $err_2$ critically at each change of coefficients. In fact, even though the initial value of $err_2 = 3.6\%$ was already small, it was clear that an additional effort was needed to further reduce the unsafe outcomes of the simplified

procedure to zero, even though the price to pay would be to reduce the accuracy of the method (from 92.7% to 88.2%). The fulfilment of this requirement implies that for the remaining 7.8% of the cases the recommended inspection interval is equal or greater than two year compared to the full-fledged method results. The final errors calculated and the aforementioned modifications to coefficients and equations which replace the initial values found in subsection 8.4.3 are considered sufficiently accurate and in the few cases where the simplified procedure provides inaccurate results they are on the safe side. In order to better visualize the final calibration results for *set 1* bridge population a column chart is plotted where the vertical columns represent the result of the simplified procedure and the red line represents the full-fledged method outcome.

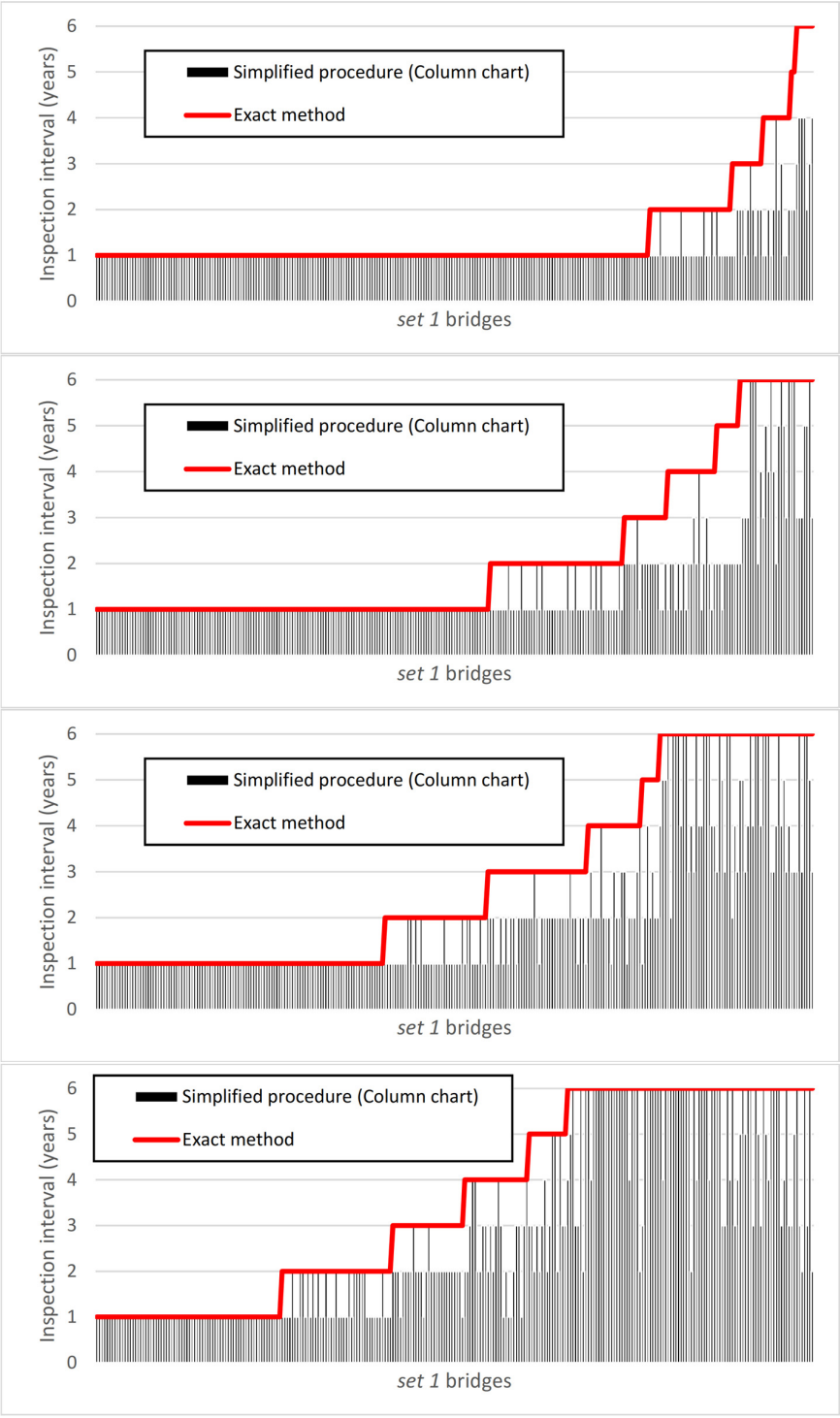


**Figure 8-20. Inspection interval calculated with the simplified procedure (column chart) and full-fledged method (red line for the high deterioration rate. Plot a), b), c) and d) (from top to bottom) represent an inspection cost of $ 4,000, $ 10,000, $ 20,000, $ 40,000 respectively.**

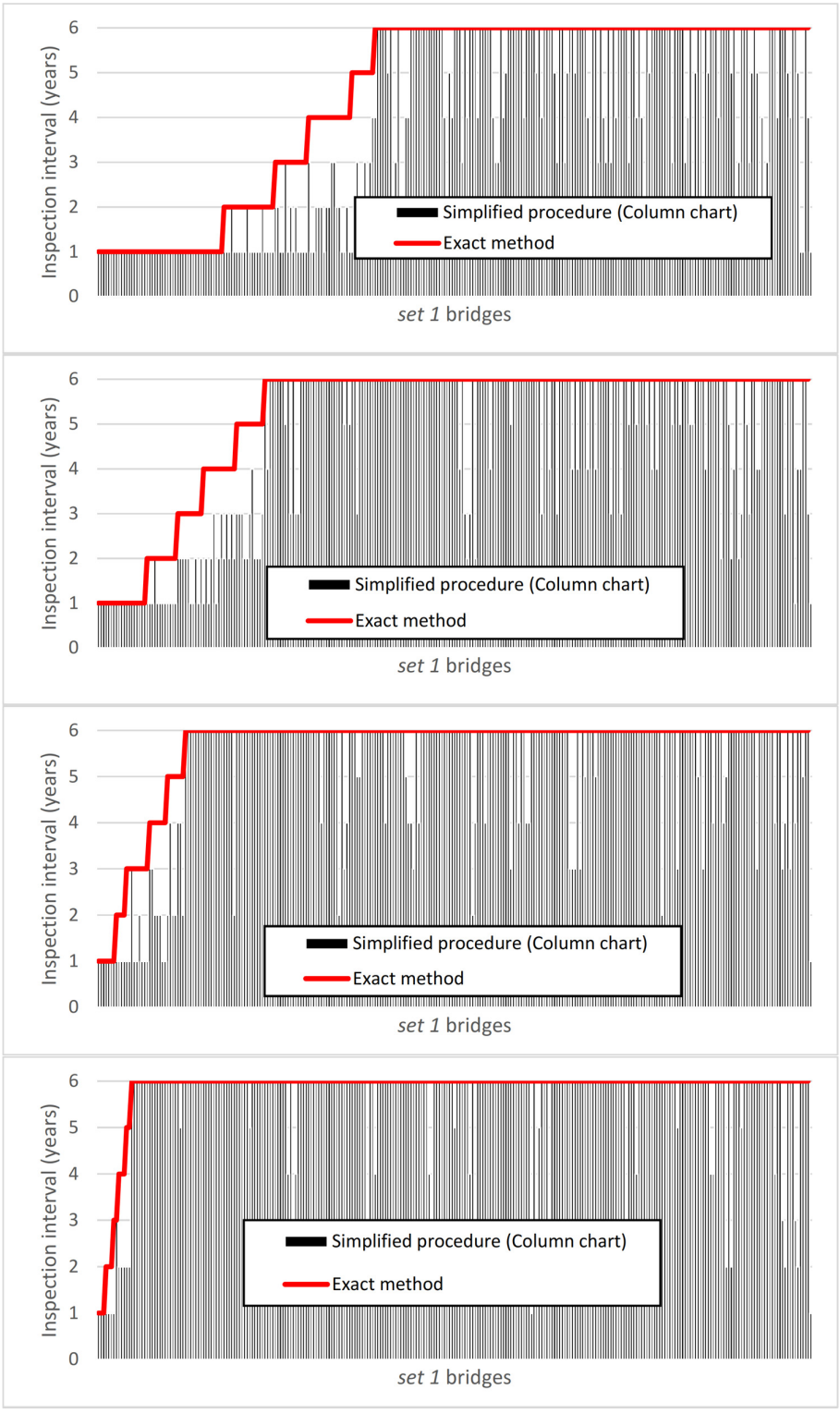


**Figure 8-21. Inspection interval calculated with the simplified procedure (column chart) and full-fledged method (red line for the medium deterioration rate. Plot a), b), c) and d) (from top to bottom) represent an inspection cost of $ 4,000, $ 10,000, $ 20,000, $ 40,000 respectively.**

The column charts plotted in Figure 8-20 and 8-21 show the bridges of *set 1* increasingly sorted according to the full-fledged method inspection interval (red line) and its corresponding inspection interval calculated with the simplified procedure (black columns). As can be seen the black columns do not perfectly fit the red line, but always provide a smaller and therefore conservative inspection interval. In this sense, in order to obtain a better fit, a small number of unconservative results (inspection interval calculated with the simplified procedure longer than the one calculated with the full-fledged method) should be accepted.

### *8.4.5 Step-by step simplified procedure application*

The application of the simplified procedure calibrated in subsection 8.4.3 and finally optimized in Subsection 8.4.4 is presented in this subsection through the flowchart shown in Figure 8-22, where the column INPUT summarizes the initial data to be collected from the user to find the OUTPUT required by the procedure and summarized in the corresponding right column.

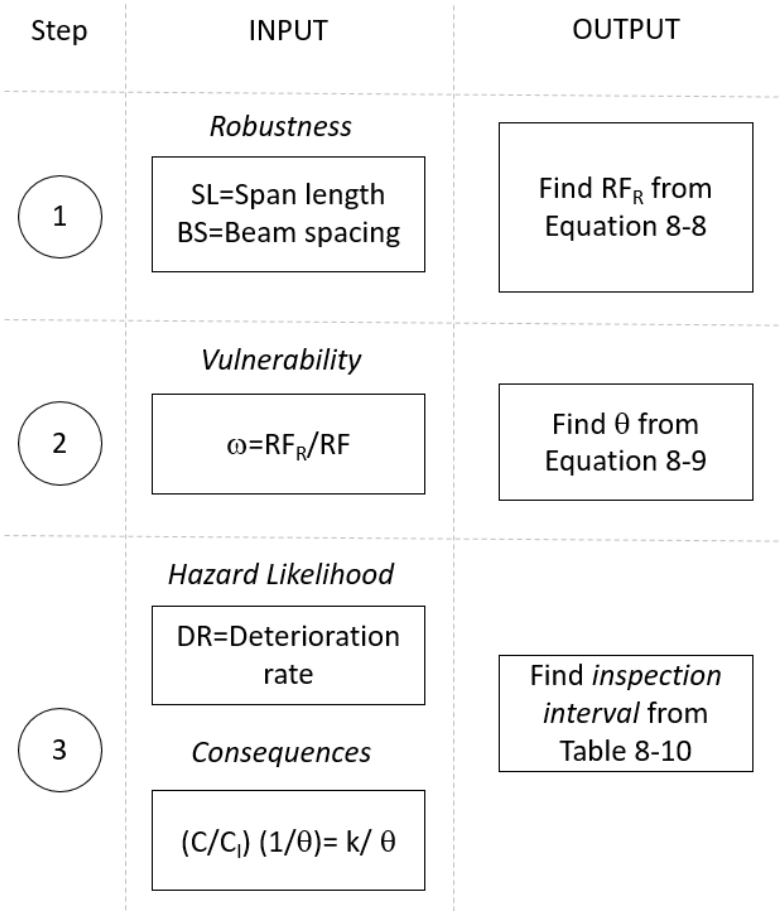


**Figure 8-22. Inspection interval calculation with step-by-step simplified procedure.**

In the first step the bridge is identified by its span length (SL) and beam spacing (BS). These two parameters are used as input to calculate the reference load rating ($RF_R$) with Equation 8-8.

$$RF_R = 0.88\, e^{SL/BS \times 0.06} \tag{8-8}$$

In the second step the ratio $\omega$ between the load rating ($RF$) obtained from the NBI file and the reference load rating ($RF_R$).calculated in the first step is calculated with Equation 8-9:

$$\omega = \frac{RF}{RF_R} \tag{8-9}$$

The $\omega$ parameter is inputed into Equation 8-10 to find the correction $\theta$ to be applied to Table 8-9.

$$\theta = \omega^{-2.1} \tag{8-10}$$

In the third step the ratio $k$ failure cost $C$ over inspection cost $C_I$ is calculated and divided by the correction coefficient $\theta$ to find the parameter $k_R$. Below the formulation is reported in Equation 8-11:

$$k_R = \frac{C}{C_I}\frac{1}{\theta} = \frac{k}{\theta} \tag{8-11}$$

Therefore, the parameter $k_R$ and the deterioration rate are used to withdraw the inspection interval as shown in Figure 8-23 (linear interpolation can be used for intermediate cases) and Table 8-10.

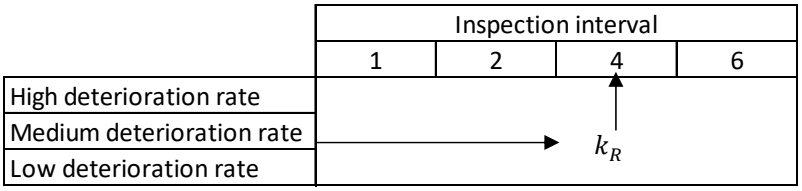


**Figure 8-23. Calculation of the inspection interval. Conceptual application.**

**Table 8-10. Calculation of the inspection interval. Numerical values.**

| | Inspection interval | | | |
|---|---|---|---|---|
| | 1 | 2 | 4 | 6 |
| High deterioration rate | 1.8.E+03 | 2.4.E+02 | 8.7.E+01 | 5.3.E+01 |
| Medium deterioration rate | 1.2.E+04 | 3.6.E+03 | 1.6.E+03 | 9.1.E+02 |
| Low deterioration rate | 1.6.E+05 | 1.4.E+05 | 1.3.E+05 | 1.1.E+05 |

For high deterioration rates the inspection interval must be finally limited to 2 years if the load rating is smaller than 1.8. Similarly, for medium deterioration rates the inspection interval must be limited to 3 years if the load rating is smaller than 1.3. The result of this calculation must be rounded down to the nearest integer. An example of this step-by-step procedure is presented in the next subsection.

### *8.4.6 Illustrative Example of the Simplified Procedure*

In this subsection the simplified procedure is applied to an example bridge spanning 34.7 m with a superstructure made of 4 beams spaced 2.45 m. The reference load rating is found to be $RF_R = 0.88\, e^{(34.7/2.45 \times 0.06)} = 2.06$ according to Equation 8-8.

Since the load rating found in the NBI database is 2.62 the parameter $\omega$ is found to be $2.62/2.06 = 1.27$ and, consequently, the parameter $\theta$ is $1.27^{-2.1} = 0.60$ according to Equation 8-9 and 8-10 respectively.

The failure cost is calculated according to the procedure presented in Chapter 7 and is found to be $ 1,813,000. It is assumed that the cost of inspection is $ 40,000 leading to a parameter $k = 75.541$ according to Equation 8-11.

Since the bridge is observed to lose member capacity at a 3% annual rate, the deterioration rate is classified as high and, together with the parameter $k$ found earlier, the inspection interval can be calculated by linear interpolation of the values found in Table 8-10 as $4 + (6-4)\,(75-87)/(53-87) = 4.7\ years$, rounded down to 4 years.

## 8.5 Chapter Conclusion

This chapter describes a procedure to decide on optimum inspection intervals based on the risk of bridge failure. The inspection time considered in this chapter refers to the so called "routine inspection" that is typically performed every two years for all bridges in the US and in similar intervals in other countries. The aim of this method is to overcome the limitations of a fixed 2-year inspection interval applied to all bridges.

This Thesis is focused on optimizing the inspection for single structures instead of full infrastructure networks. The method requires as input bridge specific parameters typically available to engineers such as structural configuration and dimensions, material properties and other information available from the NBI database. Therefore, the method is entirely based on objective measures.

The results obtained in this chapter are calculated for the entire *set 1* of bridges, generated in Chapter 3 as a representative population of structures of all the possible configurations of steel concrete composite bridges in New York State. For this reason, these results can, as a first research attempt, be considered to represent the actual infrastructure network of New York State. In this sense additional studies on different structural types and in different states are recommended to strengthen the validity of the method proposed herein.

The analysis of the results obtained for *set 1* shows that it is possible to optimize the inspection interval and adapt it to each bridge to take into account both the cost-effectiveness of the inspection expenditure and the safety of the assessed structures. Specifically, if the engineer in charge of the assessment is able to confirm that the deterioration rate is relatively low, meaning that the loss of member capacity per year is smaller than 0.5%,and the load rating is sufficiently far from RF=1.0, he/she can recommend extending the inspection interval from the typical 2-year cycle. The number of years that the inspection interval can be increased can be calculated following the numerical method described in Section 8.2 or the simplified procedure described in Section 8.4.

It is noted that the risk limit set at a load rating RF=1.0 can be increased by the appropriate authority to increase the global level of safety assuming that the additional cost can be borne by the available budget. However, it is observed that the current load rating obtained from the NBI database for the bridges forming *set 1*, are relatively high and therefore the inspection interval of only a small percentage of bridges is governed by this limitation (7% of the total in the worst possible deterioration rate and inspection cost scenario).

The typical 2-year inspection interval, currently used for all bridges, is also analyzed statistically from the cost-effectiveness point of view. The results show that, some bridges should be inspected with an interval smaller than two years while many others would require an inspection interval greater than two years. Overall, it seems that on average, a two-year inspection interval is reasonable, but is not necessarily optimum for some bridges. While, depending on the cost of inspection, the two-year interval may be unnecessarily

increasing the risk. This means that the method presented in this work can be employed to redistribute the bridge inspection cost more efficiently by reorganizing the inspection schedule of the bridges in a given jurisdiction without increasing the total costs.

# 9 Conclusions and future research

## 9.1 Thesis conclusion

The research carried out in this Thesis is aimed at developing a methodology to rationally calculate the time interval between two bridge inspections, with the objective of improving the less efficient standard routine inspection typically performed every two years for all bridges. The methodology is demonstrated in the case of composite I-beam bridges located in New York State. However, since a similar 2-year inspection interval policy can be observed in most countries, the concepts here developed can be seen in a broader perspective than just the case of USA.

One of the specific features of the method proposed in this Thesis is that it determines the inspection interval on a bridge-by-bridge basis, overcoming the difficulties of a network-based analysis. In fact, by combining all the structures of a network one loses focus on individual bridges and may "sacrifice" individual bridges for the global benefit and ignoring the importance of each bridge to the particular community it serves. Furthermore, from a practical point of view, obtaining the necessary information for a risk-based determination of an optimum inspection interval of a single bridge is easier than gathering information of an entire infrastructure network. In fact, even if the data was available, the analysis of a large set of bridges linked to an entire infrastructure network may not be the goal of a structural analyst or administration, while a relatively quick response may be needed for a specific bridge under study. For application in engineering practice of the method proposed in this Thesis, the evaluating engineer requires all usual information related to the bridge characteristics (geometry and materials and other information available from the NBI database).

Several other contributions and conclusions are assessed in this work that is worth highlighting, besides the aforementioned main goal.

The first contribution is the definition of deterioration rates from the available NBI load rating data provided by the FHWA through the NBI database. In this sense, three levels of deterioration rates are defined around the values of 3.4 % for high deterioration rate, 0.5% for medium deterioration rate and 0.07% for low deterioration rate. This contribution can be found in Chapter 3 along with a discussion on the inspection uncertainties and a method to include them in the reliability calculation adapting the statistics found in the literature about visual inspection uncertainties (Moore et al., 2001; Phares et al., 2001).

The second contribution is the development of a live load model specifically calibrated for NYS bridges to be used in structural analysis in Chapter 4. The model outlined, is particularly suit for reliability analysis where the statistical characteristics representing the uncertainties of the traffic parameters are needed to calculate the safety margin in probabilistic models. The procedure developed can also be used to calibrate a different live load model for other regions after providing site-specific WIM data. It must be emphasized these results are valid for the state of New York, and may reasonably be extended to other states of the US, but should be validated or adapted to be also used outside this state or outside the US. In this sense, the

collaboration with the authority may involve investments to carry out these kinds of necessary campaigns, including data recording, filtering and post-processing.

The third contribution is the development of a convenient procedure to calculate the reliability of bridges with a very limited number of samples using the efficient Latin Hypercube simulation combined with the First Order Reliability Method (FORM) to compute the reliability index as explained in Chapter 6. Furthermore, this procedure allows the calculation to include system non-linear behavior and post-elastic redistribution of efforts among bridge members. For this reason, this method implicitly includes the intrinsic redundancy of multi-beam bridges that cannot be directly considered with standard linear elastic models and that have been extensively studied by Ghosn & Moses (1998) and Ghosn and Yang (2014).

The fourth contribution of this work is the collection of the state of the art about the consequences of bridge failure in terms of monetary cost as outlined in Chapter 7. As a result of this research, a step-by step procedure to calculate the cost of failure is presented to be used in combination with the probability of failure obtained in Chapter 6 to address the failure risk of bridges. In particular, while some costs present an extensive literature data and are relatively easy to define (demolition and reconstruction costs) most of them represented a challenge of data interpretation because of the differences found in the source of information and the different disciplines involved (indirect, environmental, fatalities and injuries due to the collapse and accidents due to detour). Although in some cases additional data would be desirable to refine the estimations, the model finally defined in Chapter 7 is the best approximation possible to the knowledge of the author of this Thesis.

While these four contributions may alone be of interest for research purpose, they are combined in the workflow of this Thesis to assess the inspection interval of bridges based on risk, which is the ultimate objective of this work. In fact, the original motivation of this Thesis was providing engineers with rational arguments to justify the possibility of an extended inspection interval to the public administration in those cases where favorable conditions of bridges are observed and the standard two year inspection interval for routine inspections appears overly conservative. The fact that a risk-based method is used is the consequence of an extensive research trend that is being developed by different researchers (Nasrollahi & Washer, 2015; Washer et al., 2014) and is also recognized in the US as the official research path to improve the infrastructure budget allocation and to guarantee safety (MAP-21 2012) . The method proposed in this work is based in the comparison between the inspection cost and the increased risk due to the uncertainty in terms of deterioration propagation over time. As already mentioned earlier, the probability of failure upon which the risk is calculated is based on the capacity of bridges including system behavior and its post yielding internal forces redistribution, and therefore includes the intrinsic structural redundancy and robustness of multi-beam bridges. Therefore, redundant bridges will be automatically assigned with larger inspection intervals than non-redundant bridges.

The analysis of the results obtained for *set 1* shows that it is possible to optimize the inspection interval and adapt it to each bridge to take into account both the cost-effectiveness of the inspection expenditure and the safety of the assessed structures. Specifically, if the engineer in charge of the assessment is able to defend that the deterioration rate is not high, meaning that the loss of member capacity per year is smaller than 0.5%,and the load rating is sufficiently far from RF=1.0, he can recommend to extend the inspection interval from the typical 2-year. The number of years that the inspection interval can be increased from the standard 2-year interval could be calculated following the numerical procedure described in Section 8.2 which would provide a calculation of the inspection interval from a rigorous risk-approach point of view. However, for standard practice the more suitable simplified procedure presented in Subsection 8.4.5 can be adopted. Besides providing simple tools to calculate the inspection interval for bridges, one of the main conclusions of this Thesis, obtained by applying the risk-based procedure to a full representative set of bridges, is that the standard 2-year inspection interval may lead to inefficient budget allocation of bridge maintenance programs.

It should be noted that the calculation performed is considered valid under the assumption of short term projections which is limited in this Thesis to six years. For example, the deterioration rate obtained in Chapter 3 can be described by a linear trend in the short period, but different trend shapes can be observed for longer exposition intervals. Also, the cost estimation and projection outlined in Chapter 7 is acceptable for a the aforementioned six-year time window but may not be valid for larger intervals. Lastly, although it is not possible to quantify the additional anxiety of the citizen in proposing a delay in the inspection interval overly large inspection intervals are not proposed even for very favorable conditions and even in those cases where the calculation allow them.

It is worth mentioning that the method proposed in this Thesis can be seen as a simplified cost benefit model applied to a limited time window within the entire lifespan of each bridge. This peculiarity is an advantage and a limitation at the same time. In fact, typical life-cycle calculations presented by other researchers (Demos, 2006; Frangopol et al., 2017; Hawk, 2003; Orcesi & Frangopol, 2011; P. C. Ryan & Stewart, 2020; Thompson, 2017), are much more complex and present a larger number of variables than the present study. However, a simple cost-benefit model as the one presented in this work is easier to apply at a more general scale, allows the definition of the inspection interval with relatively few and typically available input data. It can be stated that the complexity of the model used is inversely related to the applicability and adaptation of such model to a larger bridge population. Therefore, the simplicity of this cost-benefit model is justified by the objective of a broad application, that is linked with the improvement of the budget allocation of the public administration, instead of the optimization of one or a limited number of structures.

Finally, it must be emphasized that although guidance is provided by the FHWA to establish qualitatively if a bridge is eligible to an inspection interval larger than two years, a rational procedure is defined in this work as a support to the already existing rules. For this reason, the method proposed in this work must be seen as a partial method able to support decision based on a broader point of view about the

bridge condition. In this sense, it is recommended that sufficient experience is developed by the engineering community before the method proposed in this Thesis is adopted as a standard procedure.

## 9.2 Future Research

From the point of view of the practical application of the method developed in this work, among the different few steps that must be carried out to calculate the inspection interval, the engineer must establish the deterioration rate for each bridge. It has been shown in Chapter 3 and Appendix B that the calculation of this parameter is fairly simple, and can be performed by any engineer by looking at the load rating value contained in the NBI database for the same bridge at different ages. Even though this method can be implemented into a spreadsheet and be very straightforward, it would be desirable to simplify it even more, for example linking the deterioration rate to a specific territory, or to the bridge exposure to deicing salts, industrial or marine environment, or weather exposure like snow precipitation, or traffic intensity. All these variables may simplify the calculation and be used as an input to typify deterioration rates for example through isoline maps. Also, the deterioration rates can be linked to the real cause of the deterioration to get a better insight of the loss of performance of the bridge and confirm or improve the deterioration rate calculation proposed in Chapter 3.

Future applications of the proposed methodology necessarily imply analyzing a broader set of bridges including and specializing the results of different standard bridge types (precast concrete beams, truss bridges etc.) and in a more advanced research stage, for non standard bridges (cable-stayed or arch bridges). Furthermore, the real application of this method should be performed with full collaboration of the bridge authority, providing complete documentation for the calibration process. For example, a complete definition of the geometry of the bridges by design or as-built drawings are needed to remove the design assumptions that are necessarily needed in this work to come up with the steel section according to the code and carry out the structural analysis. The same applies for material properties. Also, the deterioration is calculated in this work as a loss of performance from historical data. This approach is practical and pragmatic, avoiding to take care of complex corrosion mechanisms and deterioration models, with high uncertainties that certainly deserve a separate study. However, full access to inspection report and material deterioration detail may validate the method proposed in this work or adjust it properly for a more rational use.

Another aspect that should be treated in future research is the application of the method by practitioner engineers. At present, a single engineer can conveniently apply the full-fledged methodology as well as the simplified procedure to calculate the inspection intervals. While the inaccuracy of the simplified procedure is shown to be acceptable, the administration could prefer the more precise full-fledge methodology to optimize even more the budget allocation dedicated to bridge maintenance. In order to fulfil this purpose an automatization of the calculation should be implemented by using predefined digital forms to be filled by engineers before providing the correct inspection interval as output in order to speed up and standardize the process. This can be achieved by a computer program or by an interactive webpage in a similar way as the AASHTOware package of softwares has been doing in the recent years. With such a tool, the practicing

engineer would apply the full-fledge methodology, but the inputs would still be simple enough or even automatic, with only minimum check performed by the analyst.

## Bibliography

AASHTO. (2003). AASHTO Manual for Condition Evaluation and Load and Resistance Factor Rating (LRFR) of Higway Bridges. Washington, DC: American Association of State Highway and Transportation Officials.

AASHTO. (2017). AASHTO LRFD Bridge Design Specifications. Washington DC: American Association of State Highway and Transportation Officials.

AASHTO. (2018). AASHTO MBE. The Manual for bridge evaluation. Washington DC: American Association of State Highway and Transportation Officials.

Ahn, C., Peña-Mora, F., Lee, S., & Arboleda, C. A. (2013). Consideration of the Environmental Cost in Construction Contracting for Public Works: A+C and A+B+C Bidding Methods. *Journal of Management in Engineering*, *29*(1), 86–94. https://doi.org/10.1061/(ASCE)ME.1943-5479.0000124

Ang, A. H.-S., & Tang, W. H. (2004). *Probability concepts in engineering*. *Planning*. New York: Wiley.

Ang, A. H.-S., & Tang, W. H. (2007). *Probability concepts in engineering : emphasis on applications in civil & environmental engineering*. New York: Wiley.

Anitori, G., Casas, J. R., & Ghosn, M. (2013). Redundancy and Robustness in the Design and Evaluation of Bridges: European and North American Perspectives. *Journal of Bridge Engineering*, *18*(12), 1241–1251. https://doi.org/10.1061/(ASCE)BE.1943-5592.0000545

Anitori, G., Casas, J. R., & Ghosn, M. (2016). Live load model for refined analysis of short and medium-span bridge systems. In *Maintenance, Monitoring, Safety, Risk and Resilience of Bridges and Bridge Networks - Proceedings of the 8th International Conference on Bridge Maintenance, Safety and Management, IABMAS 2016*.

Anitori, G., Casas, J. R., & Ghosn, M. (2017). WIM-Based Live-Load Model for Advanced Analysis of Simply Supported Short- and Medium-Span Highway Bridges. *Journal of Bridge Engineering*, *22*(10), 04017062. https://doi.org/10.1061/(ASCE)BE.1943-5592.0001081

ASCE. (2017). *ASCE 7-16 Minimum design loads and associated criteria for buildings and other structures*. American Society of Civil Engineering. https://doi.org/10.1061/9780784414248

Bell, R., Danscheid, M., & Glade, T. (2006). Challenges in defining acceptable risk levels. In *RISK21 - Coping with Risks due to Natural Hazards in the 21st Century* (pp. 77–87). Taylor & Francis. https://doi.org/10.1201/9780203963562.ch8

Bhattacharya, B., Lu, Q., & Zhong, J. (2009). Reliability of redundant ductile structures with uncertain system failure criteria. *Sadhana Sadhana : Academy Proceedings in Engineering Sciences*, *34*(6), 903–921.

Blincoe, L. J., Miller, T. R., Zaloshnja, E., & Lawrence, B. A. (2015). *The Economic and Societal Impact of Motor Vehicle Crashes, 2010.* Washington DC: National Highway Traffic Safety Administration.

Brady, K. C., O'Reilly, M., Bevc, L., Znidaric, A., O'Brien, E. J., & Jordan, R. (2004). *COST 345, Procedures Required for the Assessment of Highway Structures*. European Commission Directorate General Transport and Energy.

Branson, D. E. (1977). *Deformation of concrete structures*. New York: McGraw-Hill.

Campbell, L. E., Connor, R. J., Whitehead, J. M., & Washer, G. A. (2020). Human factors affecting visual inspection of fatigue cracking in steel bridges. *Structure and Infrastructure Engineering*, 1–12. https://doi.org/10.1080/15732479.2020.1813783

Campbell, L. E., Snyder, L. R., Whitehead, J. M., & Connor, R. J. (2019). *Probability of Detection Study for Visual Inspection of Steel Bridges: Volume 2—Full Project Report*. West Lafayette, IN. https://doi.org/10.5703/1288284317104

Caspeele., R., Steenbergen, R. D. J. M., & Sykora., M. (2016). Partial factor methods for existing concrete structures (pp. 26–72). Lausanne: fib. https://doi.org/10.35789/fib.BULL.0080.Ch04

Cavaco, E., Casas, J. R., & Neves, L. (2013). Quantifying Redundancy and Robustness of Structures. *IABSE Symposium Report*, *100*(1), 78–99. https://doi.org/10.2749/222137813807018971

CEN. (2002). *EN 1990: Eurocode 0: Basis of Structural Design*. Brussels, Belgium: European Committee for Normalization.

CEN. (2003). *EN 1991-2: Eurocode 1: Actions on structures. Part 2: Traffic loads on bridges*. Brussels, Belgium: European Committee for Normalization.

CEN. (2004). *EN 1998-1: Eurocode 8: Design of structures for earthquake resistance—Part 1: General rules, seismic actions and rules for buildings*. Brussels, Belgium: European Committee for Normalization.

Central European Bank. (2020). Definition of price stability. Retrieved from www.ecb.europa.eu/mopo/strategy/pricestab/html/index.en.html

Delucchi, M. A. (1997). The Annualized Social Cost of Motor Vehicle Use in the U.S.-Based on 1990–1991 Data: Summary of Theory, Data, Methods, and Results. In *Social Costs and Sustainability* (pp. 380–417). Berlin, Heidelberg: Springer Berlin Heidelberg. https://doi.org/10.1007/978-3-642-60365-5_23

Demos, G. P. (2006). *Life cycle cost analysis and discount rate on pavements for the Colorado Department of Transportation*. Denver CO: Colorado Dept. of Transportation, Research Branch.

Deng, Linzhong, Ghosn, M., Znidaric, A., & Casas, J. R. (2001). Nonlinear Flexural Behavior of Prestressed Concrete Girder Bridges. *Journal of Bridge Engineering*, *6*(4), 276–284.

https://doi.org/10.1061/(ASCE)1084-0702(2001)6:4(276)

Deng, Lu, Cai, C. S., & Barbato, M. (2011). Reliability-Based Dynamic Load Allowance for Capacity Rating of Prestressed Concrete Girder Bridges. *Journal of Bridge Engineering*, *16*(6), 872–880. https://doi.org/10.1061/(ASCE)BE.1943-5592.0000178

Deutschland Bundesministerium für Verkehr. (1999). *Engineering structures in connection with roads - inspection and test - DIN 1076:1999-11*. Dortmund. https://doi.org/https://dx.doi.org/10.31030/8499929

Dirección General de Carretera. (2009). *Guía de inspecciones básicas de obras de paso : Red de carreteras del Estado*. Madrid: Centro de Publicaciones, Secretaría General Técnica, Ministerio de Fomento.

Ditlevsen, O. (1981). Principle of Normal Tail Approximation. *Journal of the Engineering Mechanics Division*, *107*(6), 1191–1208.

Ellingwood, B., Galambos, T. V., McGregor, J. G., & Cornell, C. A. (1980). Development of a Probability Based Load Criterion for American National Standard A58. *U.S. Department of Commerce, National Bureau of Standards*.

EPA. (2011). The benefits and costs of the clean air act from 1990-2020. In *Better Air: Benefits and Costs of the Clean Air Act*. Environmental Protection Agency.

Faber, M. H., & Sorensen, J. D. (2002). Indicators for inspection and maintenance planning of concrete structures. *Structural Safety*, *24*(2–4), 377–396. https://doi.org/10.1016/S0167-4730(02)00033-4

FEMA. (2010). *Federal Emergency Agency Cost Code List*. Washington DC.

FHWA. Technical Advisory 5140.21 (1988). Retrieved from https://www.fhwa.dot.gov/bridge/nbis/t514021.cfm

FHWA. (1995). Recording and Coding Guide for the Structure Inventory and Appraisal of the Nation's Bridges. *Highway Administration Report FHWA-PD-96-001*, (FHWA-PD-96-001), 124. https://doi.org/FHWA-PD-96-001

FHWA. (2012). *Addendum to the 1997 federal highway cost allocation study final report.* Federal Highway Administration, U.S. Department of Transportation.

FHWA. (2019a). FHWA FY 2019 BUDGET. Washington DC. Retrieved from https://www.transportation.gov/sites/dot.gov/files/docs/mission/budget/304501/fhwa-fy-2019-cj-final.pdf

FHWA. (2019b). NBI ASCII Files, New York. Retrieved from https://www.fhwa.dot.gov/bridge/nbi/

Fiorillo, G. (2015). *Reliability and Risk Analysis of Bridge Networks Under the Effect of Highway Traffic Load. ProQuest Dissertations and Theses*. City University of New York.

Fiorillo, G., & Ghosn, M. (2014). Procedure for Statistical Categorization of Overweight Vehicles in a WIM Database. *Journal of Transportation Engineering*, *140*(5), 04014011. https://doi.org/10.1061/(ASCE)TE.1943-5436.0000655

Frangopol, D. M., Dong, Y., & Sabatino, S. (2017). Bridge life-cycle performance and cost: analysis, prediction, optimisation and decision-making. *Structure and Infrastructure Engineering*, *13*(10), 1239–1257. https://doi.org/10.1080/15732479.2016.1267772

Fu, G., Liu, L., & Bowman, M. D. (2013). Multiple Presence Factor for Truck Load on Highway Bridges. *Journal of Bridge Engineering*, *18*(3), 240–249. https://doi.org/10.1061/(ASCE)BE.1943-5592.0000330

Garg, R. K., Chandra, S., & Kumar, A. (2020). Analysis of bridge failures in India from 1977 to 2017. *Structure and Infrastructure Engineering*, 1–18. https://doi.org/10.1080/15732479.2020.1832539

Gennarelli, T. A., & Wodzin, E. (2008). *Abbreviated injury scale 2005 : update 2008*. Barrington IL: Association for the Advancement of Automative Medicine.

Ghasemi, S. H., Nowak, A. S., & Parastesh, H. (2016). Statistical Parameters of In-A-Lane Multiple Truck Presence and a New Procedure to Analyze the Lifetime of Bridges. *Structural Engineering International*, *26*(2), 150–159. https://doi.org/10.2749/101686616X14555428758849

Gheitasi, A., & Harris, D. K. (2015). Failure Characteristics and Ultimate Load-Carrying Capacity of Redundant Composite Steel Girder Bridges: Case Study. *Journal of Bridge Engineering*, *20*(3), 05014012. https://doi.org/10.1061/(ASCE)BE.1943-5592.0000667

Ghosn, M., & Casas, J. R. (1996). *Evaluation of existing highway bridge systems*. Barcelona: CIMNE (Centre Internacional de Mètodes Numèrics en Enginyeria).

Ghosn, M., Casas, J. R., & Xu, J. M. (1996). Development of an efficient program for the nonlinear analysis of bridges. *Computers & Structures*, *61*(3), 459–470. https://doi.org/10.1016/0045-7949(96)00098-3

Ghosn, M., Fiorillo, G., Gayovyy, V., Getso, T., Ahmed, S., & Parker, N. (2015). *Effects of Overweight Vehicles on New York State DOT Infrastructure, Final Report, Research Study No. C-08-13*. Albany, NY, USA.

Ghosn, M., & Moses, F. (1985). Markov Renewal Model for Maximum Bridge Loading. *Journal of Engineering Mechanics*, *111*(9), 1093–1104. https://doi.org/10.1061/(ASCE)0733-9399(1985)111:9(1093)

Ghosn, M., & Moses, F. (1986). Reliability Calibration of Bridge Design Code. *Journal of Structural Engineering*, *112*(4), 745–763. https://doi.org/10.1061/(ASCE)0733-9445(1986)112:4(745)

Ghosn, M., & Moses, F. (1998). *Redundancy In Highway Bridge Superstructures*. *NCHRP Report 406*.

Washington DC: Transportation Research Board, National Research Council.

Ghosn, M., Moses, F., & Gobieski, J. (1986). *Evaluation of steel bridges using in-service testing*. Transportation Research Board - National Research Council.

Ghosn, M., Sivakumar, B., & Miao, F. (2011). *Load and Resistance Factor Rating (LRFR) in NYS*. New York NY: The City University of New York.

Ghosn, M., Sivakumar, B., & Miao, F. (2013). Development of State-Specific Load and Resistance Factor Rating Method. *Journal of Bridge Engineering*, *18*(5), 351–361. https://doi.org/10.1061/(ASCE)BE.1943-5592.0000382

Ghosn, M., & Yang, J. (2014). *Bridge System Safety and Redundancy*. *NCHRP Report 776*. Washington DC: Transportation Research Board, National Research Council.

González, A. (2010). Experimental Determination of Dynamic Allowance for Traffic Loading in Bridges. *Transportation Research Board 89th Annual Meeting*, (1), 1–18.

Hambly, E. C. (1991). *Bridge Deck Behaviour* (2nd ed.). London: CRC Press. https://doi.org/10.1201/9781482267167

Haukaas, T., & Der Kiureghian, A. (2004). *Finite Element Reliability and Sensitivity Methods for Performance-Based Earthquake Engineering*. *PEER Report 2003/14*. Berkeley CA.

Hawk, H. (2003). *Bridge life-cycle cost analysis*. *NCHRP report 483*. Washington DC: Transportation Research Board, National Research Council.

Hearn, G. (2007). *NCHRP Synthesis 375, Bridge Inspection Practices*. Washington DC: Transportation Research Board, National Research Council. Retrieved from http://scholar.google.com/scholar?hl=en&btnG=Search&q=intitle:NCHRP+Synthesis+375,+Bridge+Inspection+Practices#0

HEI. (2010). *Traffic-related air pollution: A critical review of the literature on emissions, exposure, and health effects*. Boston MA: Health Effects Institute (HEI). Retrieved from https://www.healtheffects.org/system/files/SR17Traffic Review.pdf

Highways England. (2020). *Inspection of highway structures (CS 450)*. Highways England.

Hirschman, I., Da Silva, E. S., Strauss-Wieder, A., & Tompkins, B. (2016). *Methodology for Estimating the Value of Travel Time Reliability for Truck Freight System Users*. *NCHRP Report 824*. Washington DC: Transportation Research Board, National Research Council. https://doi.org/10.17226/23547

Illinois DOT. (2016). *Illinois highway information system : structure information and procedure manual.* Springfield, Ill.: Illinois Dept. of Transportation prepared in cooperation with the U.S. Dept. of Transportation, Federal Highway Administration.

Imam, B. M., & Chryssanthopoulos, M. K. (2012). Causes and Consequences of Metallic Bridge Failures. *Structural Engineering International*, *22*(1), 93–98. https://doi.org/10.2749/101686612X13216060213437

Iman, R. L., & Conover, W. J. (1982). A distribution-free approach to inducing rank correlation among input variables. *Communications in Statistics - Simulation and Computation*, *11*(3), 311–334. https://doi.org/10.1080/03610918208812265

Janssens, V., O'Dwyer, D. W., & Chryssanthopoulos, M. K. (2012). Assessing the consequences of building failures. *Structural Engineering International: Journal of the International Association for Bridge and Structural Engineering (IABSE)*, *22*(1), 99–104. https://doi.org/10.2749/101686612X13216060213473

Jiang, Y., & Wu, H. (2004). *Determination of INDOT Highway Construction Production Rates and Estimation of Contract Times*. Purdue University.

Jo, S.-I., Onoufriou, T., & Crocombe, A. D. (2005). System reliability-based bridge assessment using the response surface method. In *Proceedings of the 5th International Conference on Bridge Management* (pp. 571–577). https://doi.org/10.1680/bmf.33542.0072

Kathol, S., Azizinamini, A., & Luedke, J. (1995). *Strength capacity of steel girder bridges*. Lincoln NE: Dept. of Civil Engineering, College of Engineering and Technology.

Khan, M. A. (2015). *Accelerated bridge construction : best practices and techniques*. Amsterdam: Elsevier.

Khorasani, N. E. (2010). *System-Level Structural Reliability of Bridges*. University of Toronto.

Kwon, K., & Frangopol, D. M. (2011). Bridge fatigue assessment and management using reliability-based crack growth and probability of detection models. *Probabilistic Engineering Mechanics*, *26*(3), 471–480. https://doi.org/10.1016/j.probengmech.2011.02.001

Lee, D. B. (1995). *Full cost pricing of highways*. Cambridge MA: John A. Volpe National Transportation Systems Center.

Lee, G. C., Mohan, S. B., Huang, C., & Fard, B. N. (2013). A study of U.S. bridge failures (1980–2012). *Technical Report MCEER -13-0008*.

Litman, T. (2009). *Transportation cost and benefit analysis*. Victoria CA: Victoria Transport Policy Institute.

Liu, W. D., Ghosn, M., Moses, F., & Neu-enhoffer, A. (2000). *Redundancy in highway bridge substructures*. *NCHRP Report 458*. Washington DC: Transportation Research Board, National Research Council.

Lui, W. F., & Chen, E. M. (2005). *Handbook of Structural Engineering*. *Engineering*. Ann Arbor MI: CRC Press. https://doi.org/10.1201/9781420039931

Maibach, M., Schreyer, C., Sutter, D., van Essen, H. P., Boon, B. H., Smokers, R., … Bak, M. (2008). *Handbook on estimation of external costs in the transport sector Produced within the study*.

*Internalisation Measures and Policies for All external Cost of Transport (IMPACT)*.

McKenna, F. (2011). OpenSees: A Framework for Earthquake Engineering Simulation. *Computing in Science & Engineering*, *13*(4), 58–66. https://doi.org/10.1109/MCSE.2011.66

Melchers, R. E., & Beck, A. T. (2018). *Structural reliability analysis and prediction*. Hoboken NJ: Wiley.

Ministero delle Infrastrutture e dei Trasporti. (2020). *Linee guida per la classificazione e gestione del rischio, la valutazione della sicurezza ed il monitoraggio dei ponti esistenti*. Ministero delle Infrastrutture e dei Trasporti. Consiglio Superiore dei Lavori Pubblici.

Mlynarski, M., Wassef, W. G., & Nowak, A. S. (2011). *A Comparison of AASHTO Bridge Load Rating Methods*. Washington, D.C.: Transportation Research Board. https://doi.org/10.17226/22874

Moore, M., Phares, P. M., Raybeal, B. A., Rolander, D. D., & Washer, G. A. (2001). *Reliability of Visual Inspection for Highway Bridges* (Report). (FHWA, Ed.). VA: Federal Highway Administration, U.S. Department of Transportation.

Nasrollahi, M., & Washer, G. (2015). Estimating Inspection Intervals for Bridges Based on Statistical Analysis of National Bridge Inventory Data. *Journal of Bridge Engineering*, *20*(9), 04014104. https://doi.org/10.1061/(ASCE)BE.1943-5592.0000710

Nataf, A. (1962). Détermination des distributions de probabilités dont les marges sont données. *Comptes Rendus de l'Académie Des Sciences*, (225), 42–43.

Neuenhofer, A., & Filippou, F. C. (1998). Geometrically Nonlinear Flexibility-Based Frame Finite Element. *Journal of Structural Engineering*, *124*(6), 704–711. https://doi.org/10.1061/(ASCE)0733-9445(1998)124:6(704)

Neves, L. C., & Frangopol, D. M. (2005). Condition, safety and cost profiles for deteriorating structures with emphasis on bridges. *Reliability Engineering & System Safety*, *89*(2), 185–198. https://doi.org/10.1016/j.ress.2004.08.018

NHTSA. (2016). *2015 Fatal Motor Vehicle Crashes: Overview*. *Traffic Safety Facts: Research Note (DOT HS 812318)*.

NHTSA. (2018). *2017 Fatal Motor Vehicle Crashes: Overview*. *Traffic Safety Facts: Research Note (DOT HS 812603)*.

NHTSA. (2019). *2018 Fatal Motor Vehicle Crashes: Overview*. *Traffic Safety Facts: Research Note (DOT HS 812826)*.

Nilson, A. H., Darwin, D., & Dolan, C. W. (2011). Design of concrete structures. New York: McGraw-Hill.

Nowak, A. S. (1999). *Calibration of LRFD Bridge Design Code. NCHRP Report 368:* Washington DC: Transportation Research Board, National Research Council ; National Academy Press.

Nowak, A. S., & Collins, K. (2013). *Reliability of structures*. Boca Raton FL: CRC Press.

Nowak, A. S., & Lind, N. C. (1987). System Reliability Models for Bridge Structures. In *Bulletin of the Polish Academy of Sciences: Technical Sciences* (pp. 329–338). https://doi.org/10.1007/978-3-642-83279-6_23

Nowak, A. S., & Szersezen, M. M. (2001). *Reliability-Based Calibration for Structural Concrete*. *Report UMCEE 01-04*. University of Michigan.

NTSB. (2007). *Collapse of I-35W Highway Bridge Minneapolis, Minnesota August 1, 2007*. *Highway Accident Report NTSB/HAR-08/03*. Retrieved from http://www.ntsb.gov/news/events/2008/minneapolis_mn/

O'Brien, E. J., & Enright, B. (2011). Modeling same-direction two-lane traffic for bridge loading. *Structural Safety*, *33*(4–5), 296–304. https://doi.org/10.1016/j.strusafe.2011.04.004

O'Brien, E. J., González, A., & Žnidarič, A. (2012). Recommendations for dynamic allowance in bridge assessment. In *Proceedings of the fifth International Conference on Bridge Maintenance, Saftey, Management and Life-Cycle Optimization (IABMAS'10)* (pp. 3434–3441). Stresa, Lake Maggiore, Italy.

O'Brien, E. J., & Keogh, D. L. (1999). *Bridge Deck Analysis*. Taylor and Francis.

Ontario Ministry of Transportation. (2008). Ontario structure inspection manual : OSIM. St. Catharines, ON: Ontario Ministry of Transportation, Bridge Office.

Orcesi, A. D., & Frangopol, D. M. (2011). Use of Lifetime Functions in the Optimization of Nondestructive Inspection Strategies for Bridges. *Journal of Structural Engineering*, *137*(4), 531–539. https://doi.org/10.1061/(ASCE)ST.1943-541X.0000304

Paloheimo, E., & Hannus, M. (1974). Structural design based on weighted fractiles. *Journal of Structural Division*, *100*(7), 1367–1378.

Phares, B. M., Graybeal, B. A., Rolander, D. D., Moore, M. E., & Washer, G. A. (2001). Reliability and Accuracy of Routine Inspection of Highway Bridges. *Transportation Research Record: Journal of the Transportation Research Board*, *1749*(1), 82–92. https://doi.org/10.3141/1749-13

Popovics, S. (1973). A numerical approach to the complete stress-strain curve of concrete. *Cement and Concrete Research*, *3*(5), 583–599. https://doi.org/10.1016/0008-8846(73)90096-3

Proske, D. (2020). Fatalities due to bridge collapse. *Proceedings of the Institution of Civil Engineers - Bridge Engineering*, 1–24. https://doi.org/10.1680/jbren.20.00001

Read, C. (1994). *How vehicle pollution affects our health : a summary of papers presented at a symposium in London on Wednesday 20th May 1994*. Red Lion Court, London UK: Ashden Trust.

Rosenblatt, M. (1952). Remarks on a Multivariate Transformation. *The Annals of Mathematical Statistics*, *23*(3), 470–472. https://doi.org/10.1214/aoms/1177729394

RSMeans. (2009). *Heavy Construction Cost Data*.

Ryan, P. C., & Stewart, M. G. (2020). Regional variability of climate change adaptation feasibility for timber power poles. *Structure and Infrastructure Engineering*, 1–11. https://doi.org/10.1080/15732479.2020.1843505

Ryan, T. W., EricMann, J., Chill, Z. M., & Ott, B. T. (2012). *Bridge Inspector's Reference Manual* (Vol. BIRM 1). FHWA. https://doi.org/FHWA NHI 12-049

SAMARIS. (2006). *State of the art report on assessment of structures in selected EEA and CE countries*. Deliverable D19. Document number SAM-GE-DE19-2.

Santamaria Ariza, M., Zambon, I., S. Sousa, H., Campos e Matos, J. A., & Strauss, A. (2020). Comparison of forecasting models to predict concrete bridge decks performance. *Structural Concrete*, *21*(4), 1240–1253. https://doi.org/10.1002/suco.201900434

Saydam, D. (2013). *Reliability and risk of structural systems under progressive and sudden damage*. *ProQuest Dissertations and Theses*. Lehigh University.

Scheer, J. (2010). *Failed Bridges*. *Failed Bridges: Case Studies, Causes and Consequences*. Weinheim, Germany: Wiley-VCH Verlag GmbH & Co. KGaA. https://doi.org/10.1002/9783433600634

Sivakumar, B., & Ghosn, M. (2011). *Recalibration of LRFR Live Load Factors in the AASHTO Manual for Bridge Evaluation*. *NCHRP 20-07*. Washington DC: Transportation Research Board, National Research Council.

Sivakumar, B., Ghosn, M., & Moses, F. (2011). *Protocols for Collecting and Using Traffic Data in Bridge Design*. *NCHRP report 683*. Washington DC: Transportation Research Board, National Research Council.

Sjodin, A., Persson, K., Andreasson, K., Arlander, B., & Galle, B. (1998). On-road emission factors derived from measurements in a traffic tunnel. *International Journal of Vehicle Design*, *20*(1/2/3/4), 147. https://doi.org/10.1504/IJVD.1998.001842

Smith, D. W. (1976). Bridge Failures. *Proceedings of the Institution of Civil Engineers*, *60*(3), 367–382. https://doi.org/10.1680/iicep.1976.3389

Soriano, M., Casas, J. R., & Ghosn, M. (2017). Simplified probabilistic model for maximum traffic load from weigh-in-motion data. *Structure and Infrastructure Engineering*, *13*(4), 454–467. https://doi.org/10.1080/15732479.2016.1164728

Spector, A., & Gifford, D. (1986). A computer science perspective of bridge design. *Communications of the*

*ACM*, *29*(4), 267–283. https://doi.org/10.1145/5684.6327

Steenbergen, R. D. J. M., Sýkora, M., Diamantidis, D., Holický, M., & Vrouwenvelder, T. (2015). Economic and human safety reliability levels for existing structures. *Structural Concrete*, *16*(3), 323–332. https://doi.org/10.1002/suco.201500022

Stein, S. (2007). *Risk-Based Management Guidelines for Scour at Bridges with Unknown Foundations. Project 42-25. NCHRP 107*. Washington DC: Transportation Research Board. https://doi.org/10.17226/23243

Tanner, P., & Hingorani, R. (2015). Acceptable risks to persons associated with building structures. *Structural Concrete*, *16*(3), 314–322. https://doi.org/10.1002/suco.201500012

Taylor, C., Hinton, E., Owen, D. R. J., & Oñate, E. (1984). Numerical methods for nonlinear problems II. Swansea UK: Pineridge Press.

Tenžera, D., Puž, G., & Radiæ, J. (2012). Visual inspection in evaluation of bridge condition. *Journal of the Croatian Association of Civil Engineers*, *64*(9), 717–726. https://doi.org/10.14256/JCE.718.2012

The Federal Reserve. (2019a). Federal Reserve issues FOMC statement (Press release). Retrieved from https://www.federalreserve.gov/newsevents/pressreleases/monetary20190918a.htm

The Federal Reserve. (2019b). The Fed - What are the Federal Reserve's objectives in conducting monetary policy? Retrieved from www.federalreserve.gov/faqs/money_12848.htm

The Federal Reserve. (2020). Effective Federal Funds Rate. Retrieved from https://fred.stlouisfed.org/series/FEDFUNDS

thebalance.com. (2020). US Inflation Rate by Year from 1929 to 2022. Retrieved from https://www.thebalance.com/u-s-inflation-rate-history-by-year-and-forecast-3306093

Thompson, P. D. (2017). Risk Assessment for Bridge Management Systems. In *Eleventh International Bridge and Structures Management Conference, Transportation Research Circular E-C224*. Washington DC: Transportation Research Board, National Research Council.

Thompson, P. D., Ford, K. M., Arman, M. H. R., Labi, S., Sinha, K. C., & Shirole, A. M. (2012). *Estimating Life Expectancies of Highway Assets, Volume 1: Guidebook*. *NCHRP Report 713*. Washington DC: Transportation Research Board, National Research Council. https://doi.org/10.17226/22782

TRB. (1995). *Expanding Metropolitan Highways*. Washington DC: Transportation Research Board. https://doi.org/10.17226/9676

TRB. (2006). 50 Years of Interstate Structures. *Transportation Research Circular E-C104*. Washington DC: Transportation Research Board.

Turkstra, C. J., & Madsen, H. O. (1980). Lead combinations in codified structural design. *Journal of*

*Structural Division*, *106*(12), 2527–2543. Retrieved from https://cedb.asce.org/CEDBsearch/record.jsp?dockey=0009946

USEPA. (1996). *Indicators of the environmental impacts of transportation : highway, rail, aviation, and maritime transport.* Washington DC: U.S. Environmental Protection Agency, Policy, Planning, and Evaluation.

USEPA. (2003). *User's guide to MOBILE6. 1 and MOBILE6. 2 Mobile Source Emission Factor Model*. Ann Arbor MI: U.S. Environmental Protection Agency, Policy, Planning, and Evaluation, National Vehicle and Fuel Emissions Laboratory.

USEPA. (2015). *MOVES2014a user guide*. Washington DC: U.S. Environmental Protection Agency, Policy, Planning, and Evaluation.

Valenzuela, S., de Solminihac, H., & Echaveguren, T. (2010). Proposal of an Integrated Index for Prioritization of Bridge Maintenance. *Journal of Bridge Engineering*, *15*(3), 337–343. https://doi.org/10.1061/(ASCE)BE.1943-5592.0000068

Wardhana, K., & Hadipriono, F. C. (2003). Analysis of Recent Bridge Failures in the United States. *Journal of Performance of Constructed Facilities*, *17*(3), 144–150. https://doi.org/10.1061/(ASCE)0887-3828(2003)17:3(144)

Washer, G., Connor, R., Ciolko, A., Kogler, R., Fish, P., & Forsyth, D. (2014). *Proposed Guideline for Reliability-Based Bridge Inspection Practices*. *NCHRP Report 782*. Washington DC: Transportation Research Board, National Research Council.

Washer, G., Connor, R., Nasrollahi, M., & Provines, J. (2016). New Framework for Risk-Based Inspection of Highway Bridges. *Journal of Bridge Engineering*, *21*(4), 04015077. https://doi.org/10.1061/(ASCE)BE.1943-5592.0000818

Washer, G., Connor, R., Nasrollahi, M., & Reising, R. (2016). Verification of the Framework for Risk-Based Bridge Inspection. *Journal of Bridge Engineering*, *21*(4), 04015078. https://doi.org/10.1061/(ASCE)BE.1943-5592.0000787

Wassef, W. G., Kulicki, J. M., Nassif, H., Mertz, D., & Nowak, A. S. (2014). *Calibration of AASHTO LRFD Concrete Bridge Design Specifications for Serviceability*. Washington DC: Transportation Research Board. https://doi.org/10.17226/22407

Wyss, M., & Trendafiloski, G. (2011). Trends in the Casualty Ratio of Injured to Fatalities in Earthquakes. In *Human Casualties in Earthquakes* (pp. 267–274). Dordrecht NL: Springer Netherlands. https://doi.org/10.1007/978-90-481-9455-1_18

Zhang, K., & Batterman, S. (2013). Air pollution and health risks due to vehicle traffic. *Science of The Total Environment*, *450–451*, 307–316. https://doi.org/10.1016/j.scitotenv.2013.01.074

Zhang, K., Batterman, S., & Dion, F. (2011). Vehicle emissions in congestion: Comparison of work zone, rush hour and free-flow conditions. *Atmospheric Environment*, *45*(11), 1929–1939. https://doi.org/10.1016/j.atmosenv.2011.01.030

Zokaie, T., Mish, K. D., & Imbsen, R. A. (1995). *Distribution of wheel loads on highway bridges, phase 3*. Washington DC: Transportation Research Board, National Research Council.

Zulfiqar, A., Cabieses, M., Mikhail, A., & Khan, N. (2014). *Design of a Bridge Inspection System (BIS) to Reduce Time and Cost*. Mason University.

## Legal Bibliography

National Bridge Inspection Standards, 69 Fed. Reg. § 74419 (final rule Dec. 14, 2004) (to be codified at 23 C.F.R. pt. 650)

National Bridge Inspection Standards, 74 Fed. Reg. § 68377 (final rule Dec. 24, 2009) (to be codified at 23 C.F.R. pt. 650)

National Bridge Inspection Standards, 84 Fed. Reg. § 61494 (final rule Nov. 12, 2019) (to be codified at 23 C.F.R. pt. 650)

Moving Ahead for Progress in the 21st Century Act. 112 P. L. 141 126 Stat. 405, 2002 Enacted H. R. 4348. (2012).

# Appendix A: Bridge Picture Extraction from Online Resources

The first step to obtain the pictures of NBI bridges and to count the number of beams is to find the bridge coordinates from latitude and longitude information provided in the NBI database, items 16 and 17 respectively. Bridge ID 000000001066120 is used for the example. After that, different views are selected to count "by eye" 11 beams.

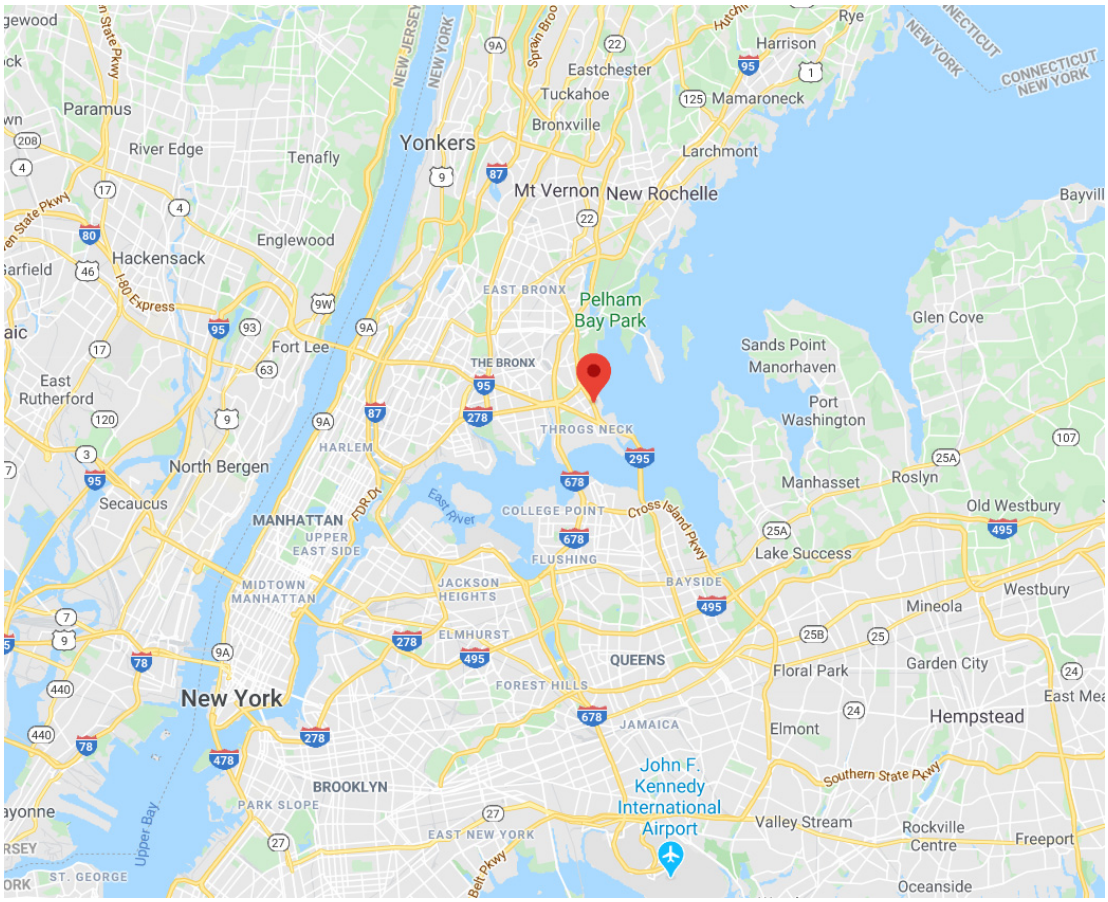


**Figure A-1. NYC area plan view.**

https://www.google.com/maps/place/40%C2%B049'40.9%22N+73%C2%B049'04.5%22W/@40.8044283,-73.956545,11z/data=!4m5!3m4!1s0x0:0x0!8m2!3d40.8280278!4d-73.8179056?hl=en


**Figure A-2. Bridge location plan view.**

https://www.google.com/maps/place/40%C2%B049'40.9%22N+73%C2%B049'04.5%22W/@40.8281673,-73.8195799,16.75z/data=!4m5!3m4!1s0x0:0x0!8m2!3d40.8280278!4d-73.8179056

**Figure A-3. 3-D view of the bridge.**


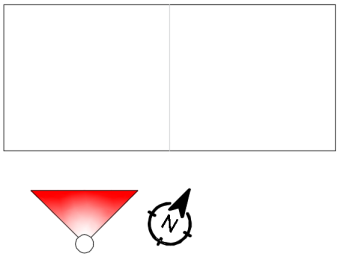

**Figure A-4.**

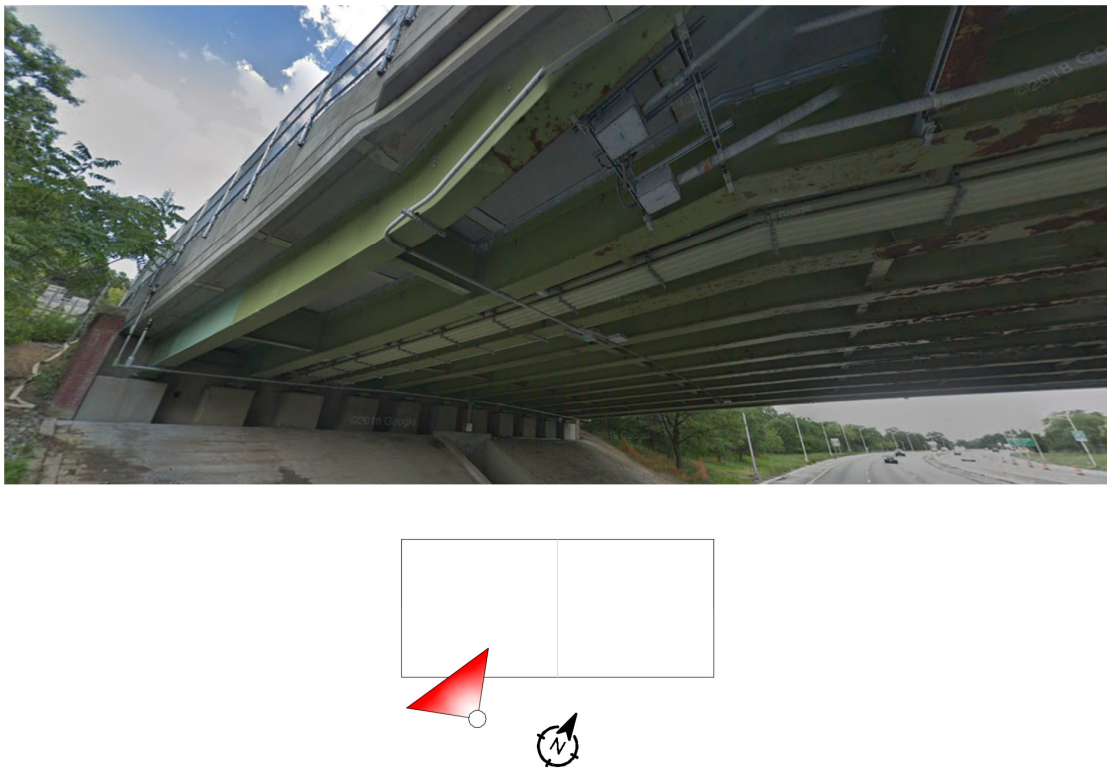

**Figure A-5.**

**Figure A-6.**

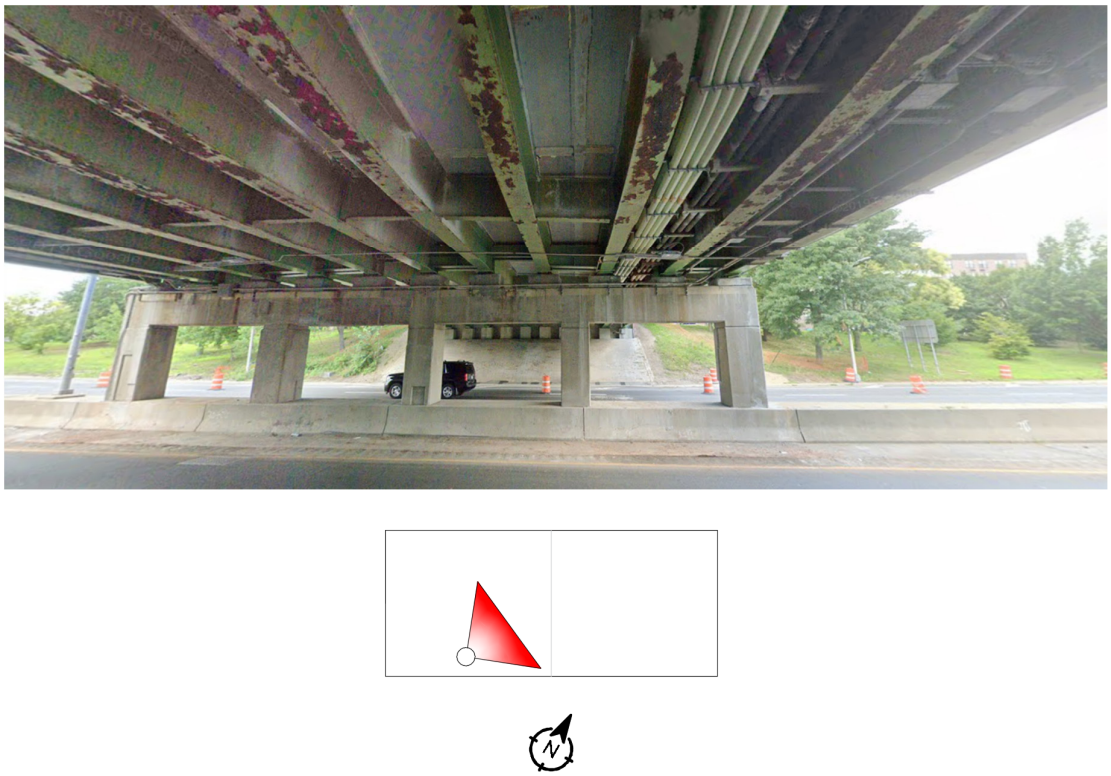

**Figure A-7.**

**Figure A-8.**



**Figure A-9.**

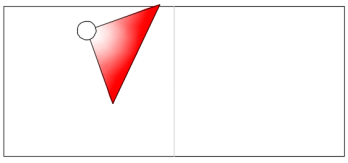

**Figure A-10.**

**Figure A-11.**

**Figure A-12.**

**Figure A-13.**

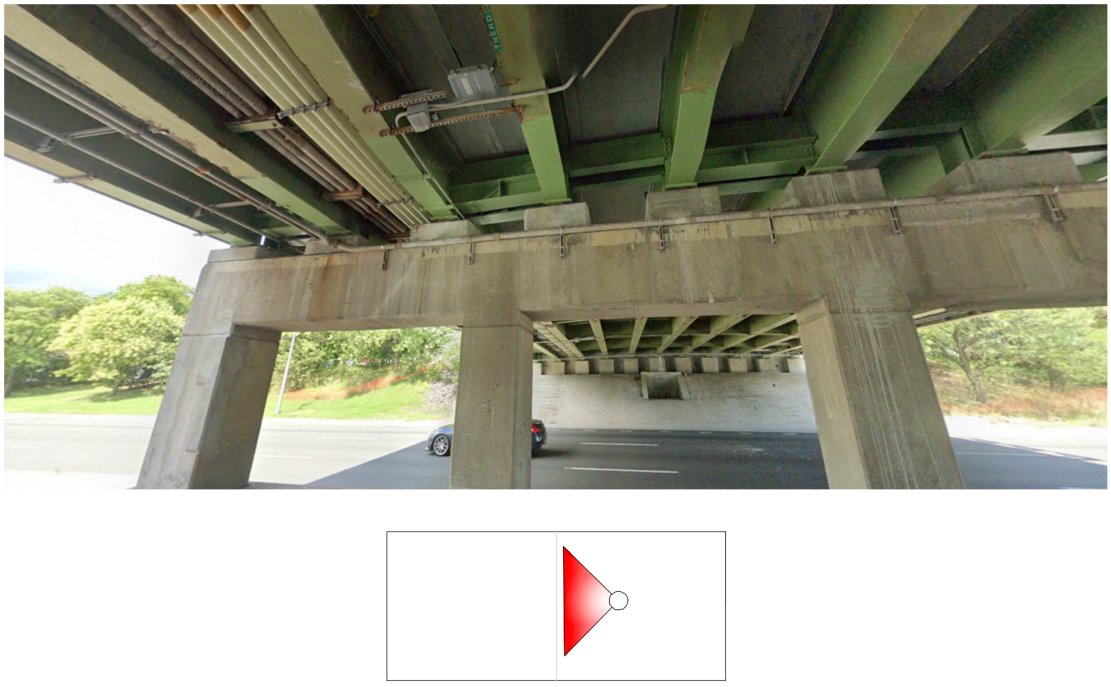

**Figure A-14.**

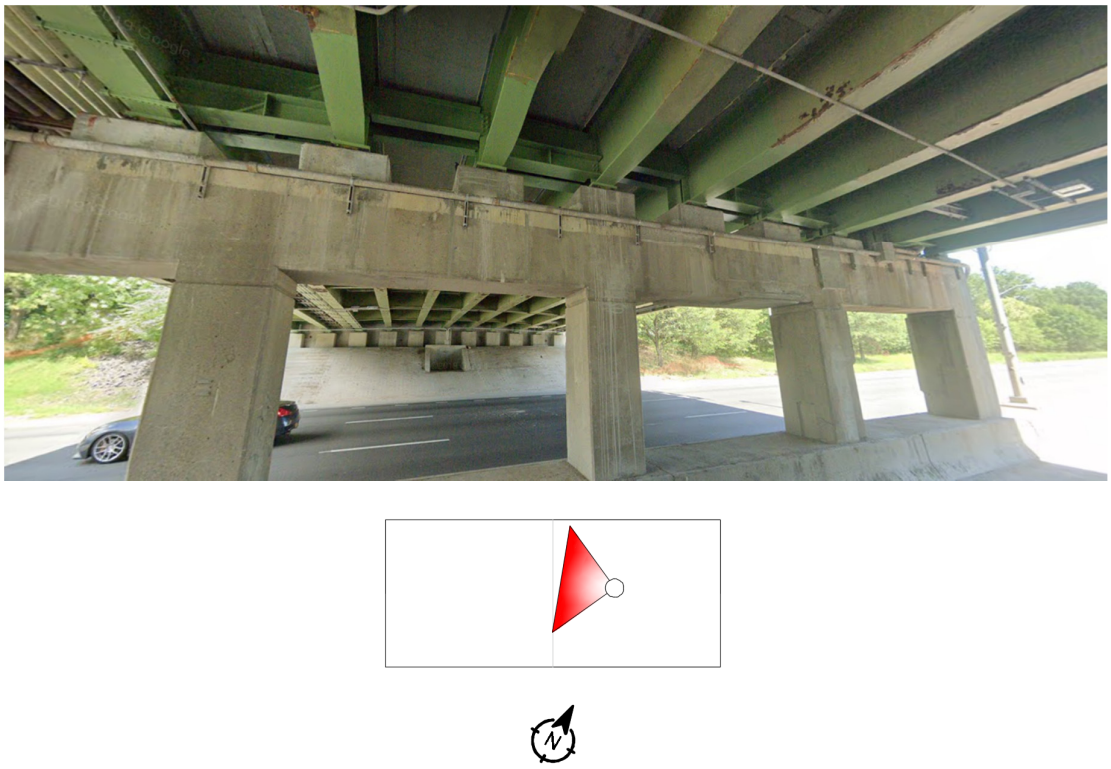

**Figure A-15.**

**Figure A-16.**

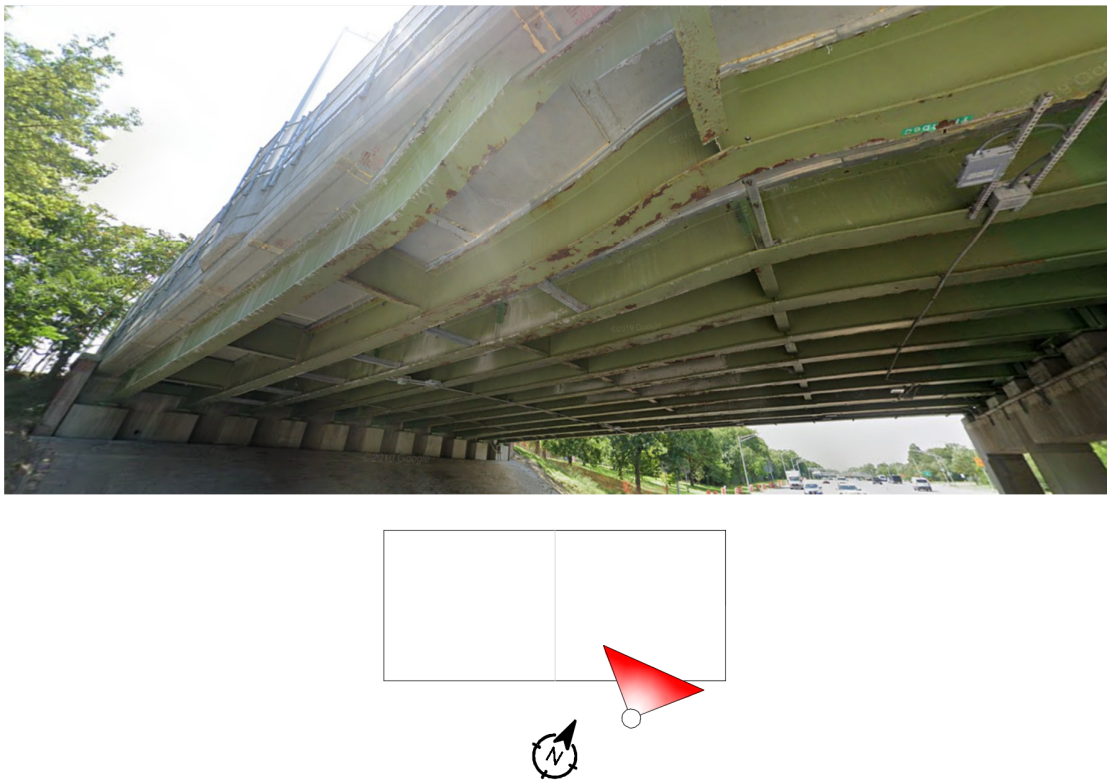

**Figure A-17.**

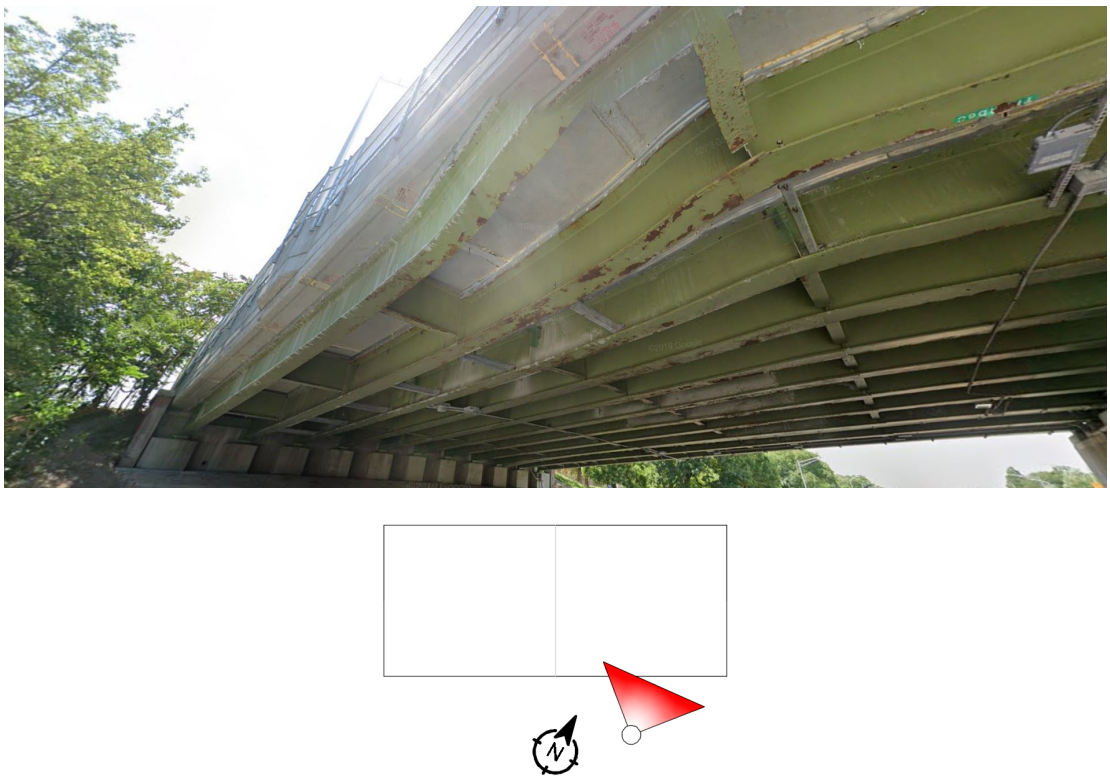

**Figure A-18.**

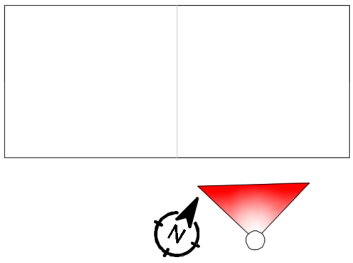

**Figure A-19.**

# Appendix B: Fit example of the deterioration ratio

Bridge 1011240 of the NBI database shows a valid set of load rating for the calculation of the deterioration ratio and therefore the linear fit is performed over the valid points of the plot shown Figure B-1.

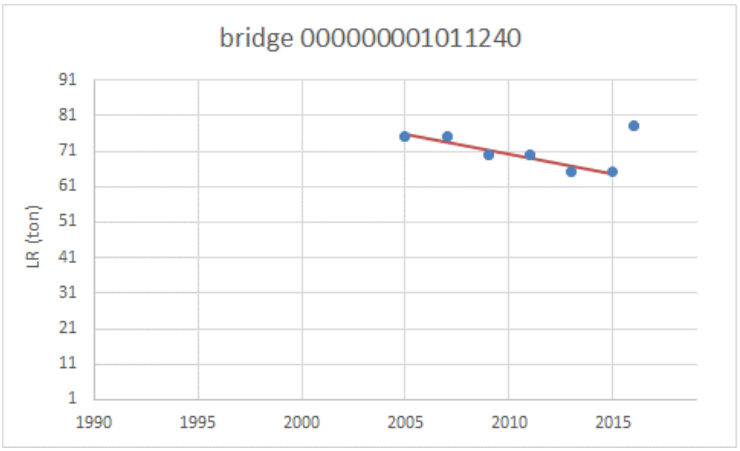


**Figure B-1. Valid load rating deterioration data series.**

A simplified calculation of the capacity is performed.

The dead load is calculated extending the results obtained for *set 1* to the rest of bridges where the curve relating span length and dead load moment for simple span bridges up to 75-m in length is plotted in (Figure B-2) and fitted through a second order polynomial.

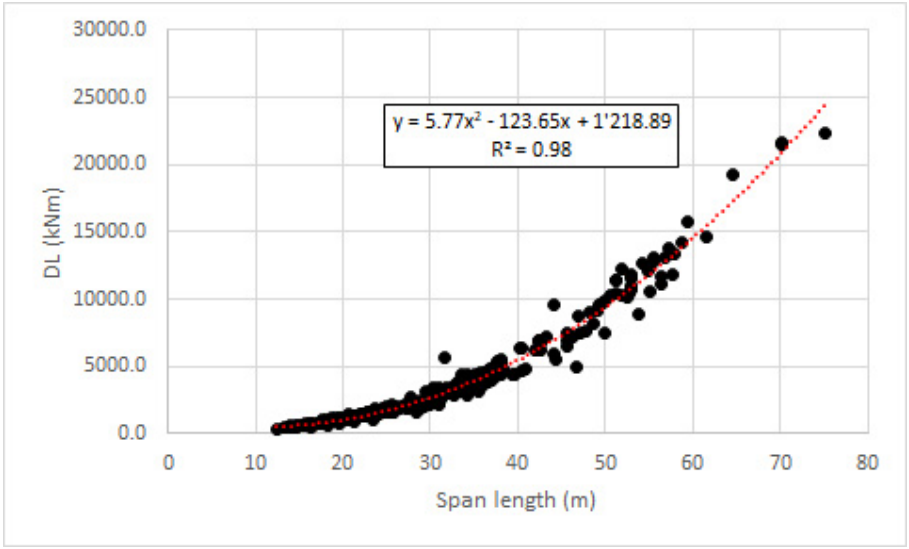


**Figure B-2. Factored dead load effect (bending moment) versus span length.**

Specifically, being this bridge 24.6 m span length

$5.77 \times 24.6^2 - 123.65 \times 24.6 + 1218.89 = 1668.9$ kNm

The impact factor is $I = 1 + 50/(24.5 / 0.304 + 125) = 1.24$

A beam spacing of 8ft (2.4 m) is considered because it is not possible to obtain the exact beam spacing for all the bridges under consideration. Therefore the lateral load distribution is 0.7 since $8/11 \approx 0.7$.

The maximum moment due to HS-20 truck is calculated interpolating values in the plot shown in Figure 3-5 and multiplying by 1/4 x SL x P, where SL is the span length and P is the truck weight.

For this case 1/4 x 24.5 x 325 =1990.6 kNm, the influence line effect from the plot shown in Figure 3-5 is 0.790, leading to a maximum live load of 1572.6 kNm.

Finally $0.7 \times LL \times I \times \gamma_{LL} = 0.7 \times 1572.6 \times 1.24 \times 1.3 = 1774.5$ kNm

The capacity $C$ can therefore be obtained for each year as $C = RF\ \gamma_{LL}\ LL\ IM\ DF + \gamma_{DL} DL$ obtaining the plot shown in Figure B-3 for the valid time interval 2006-2016.

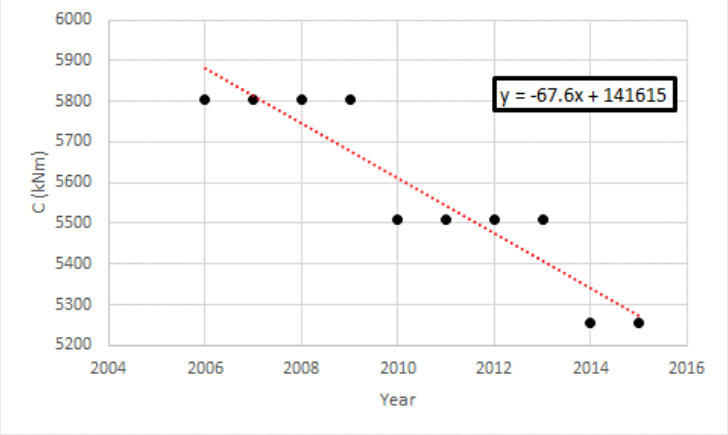


**Figure B-3. Linear fit of capacity over the valid time interval.**

The capacity at time 0 (2005, the first of the valid series) is 141615-67.6x2005=6077.0 kNm,

The capacity after 1 year is 141615-67.6 x (2005+1)=6009.4 kNm

Therefore the capacity deterioration ratio is 1-6009.4 /6077.0 =**0.01112**.

# Appendix C: Main Girder Design

In the next pages the design of the main girder of bridge 1002840 is presented.

## Bridge Properties

| | | | |
|---|---|---|---|
| Beam spacing | BS | ft | 6.99 |
| Slab thickness | ST | in | 8.00 |

## Beam geometry

| | | | |
|---|---|---|---|
| Top flange thickness | | in | 0.63 |
| Top flange width | | in | 15.35 |
| Top flange exentricity | | in | 0.00 |
| Bottom flange thickness | | in | 1.19 |
| Bottom flange width | | in | 15.35 |
| Web thickness | | in | 0.47 |
| Web inclination | | deg | 0.00 |
| Beam depth | | in | 30.31 |

## Properties

| | | | |
|---|---|---|---|
| Area non composite | | $in^2$ | 41 |
| Inertia non composite | | $in^4$ | 6578 |

## Beam geometry

| | | | |
|---|---|---|---|
| Top flange thickness | | in | 0.63 |
| Top flange width | | in | 15.35 |
| Top flange exentricity | | in | 0.00 |
| Bottom flange thickness | | in | 1.19 |
| Bottom flange width | | in | 15.35 |
| Web thickness | | in | 0.47 |
| Web inclination | | degree | 0.00 |
| Beam depth | | in | 30.31 |

## Concrete

| | | | |
|---|---|---|---|
| Concrete weight | | $kip/ft^3$ | 0.15 |

| | | | |
|---|---|---|---|
| Slab concrete strength | f'c,b | ksi | 3.5 |
| Concrete Young's modulus | Ec,b | ksi | 3587 |

## Steel

| | | | |
|---|---|---|---|
| Steel weight | | $kip/ft^3$ | 0.49 |

| | | | |
|---|---|---|---|
| Steel yielding strenght | Fy | ksi | 50 |
| Steel Young's modulus | $E_s$ | ksi | 29000 |

## Beam property

| | | | |
|---|---|---|---|
| Area | $A_g$ | $in^2$ | 41 |

## Strong axis y

| | | | |
|---|---|---|---|
| Top flange area | | $in^2$ | 9.7 |
| Top flange centroid (from the bottom) y | | in | 30 |
| Top flange static moment (from the bottom) y | | $in^3$ | 290 |
| Top flange local moment of inertia yloc (weak axis) | | $in^3$ | 0.32 |
| Top flange local moment of inertia xloc (strong axis) | | $in^3$ | 190 |

| | | | |
|---|---|---|---|
| Web area | | in | 13.5 |
| Web centroid (from the bottom) y | | in | 15 |
| Web static moment (from the bottom) y | | $in^3$ | 208 |

Moments of Inertia and the Polar Moment of Inertia with Respect to Centroidal Axial Axis Parallelogram

$$I_{\bar{y}} = \frac{1}{12}bd^3$$
$$I_{\bar{z}} = \frac{1}{12}bd(b^2 + a^2)$$
$$I_{\bar{y}\bar{z}} = -\frac{1}{12}abd^2$$

| | | | |
|---|---|---|---|
| See figure | a | in | 0.00 |
| See figure | b | in | 28.50 |
| Web flange local moment of inertia yloc (weak axis) | | $in^4$ | 0 |
| Web flange local moment of inertia xloc (strong axis) | | $in^4$ | 911 |
| Web flange local xy moment of inertia xloc,yloc | | $in^4$ | 0 |

$$I_u = \frac{I_x + I_y}{2} + \frac{I_x - I_y}{2}\cos 2\varphi - I_{xy}\sin 2\varphi$$
$$I_v = \frac{I_x + I_y}{2} - \frac{I_x - I_y}{2}\cos 2\varphi + I_{xy}\sin 2\varphi$$
$$I_{uv} = \frac{I_x - I_y}{2}\sin 2\varphi + I_{xy}\cos 2\varphi$$

| | | | |
|---|---|---|---|
| Web flange local moment of inertia yloc (strong axis) rotated in load direction | | $in^4$ | 911 |
| Web flange local moment of inertia xloc (weak axis) rotated in load direction | | $in^4$ | 0 |

| | | | |
|---|---|---|---|
| Bottom flange area | | $in^2$ | 18.3 |
| Bottom flange centroid (from the bottom) y | | in | 1 |
| Bottom flange static moment (from the bottom) y | | $in^3$ | 11 |
| Bottom flange local moment of inertia yloc (weak axis) | | $in^4$ | 2.15 |
| Bottom flange local moment of inertia xloc (strong axis) | | $in^4$ | 359 |

| | | | |
|---|---|---|---|
| Section centroid (from the bottom) y | | in | **12** |

| | | | |
|---|---|---|---|
| Top flange inertia y | | $in^4$ | 3033 |
| Web Inertia y | | $in^4$ | 1044 |
| Bottom flange inertia y | | $in^4$ | 2501 |

| | | | |
|---|---|---|---|
| Moment of Inertia y | | $in^4$ | **6578** |

| | | | |
|---|---|---|---|
| Top flange section modulus y | $S_{top,y}$ | $in^3$ | **365** |
| Bottom flange section modulus y | $S_{bot,y}$ | $in^3$ | **535** |

## Materials

### Steel

| | | | |
|---|---|---|---|
| Steel yielding strenght | Fy | ksi | 50 |
| Steel Young's modulus | $E_s$ | ksi | 29000 |

### Concrete

| | | | |
|---|---|---|---|
| Slab concrete strength | f'c,b | ksi | 3.5 |
| Concrete Young's modulus | Ec,b | ksi | 3587 |

| | | |
|---|---|---|
| n | - | 8.5 |
| 3n | - | 25.6 |

## Composite section geometry

| | | | |
|---|---|---|---|
| Slab thickness | | in | 8.0 |
| Slab width riight (towards outside) | | in | 42 |
| Slab width left (towards traffic) | | in | 42 |

### Section dimensions

| | | | |
|---|---|---|---|
| Top flange thickness | | in | 0.630 |
| Top flange width | | in | 15.4 |
| Top flange exentricity | | in | 0.0 |

| | | | |
|---|---|---|---|
| Bottom flange thickness | | in | 1.189 |
| Bottom flange width | | in | 15.4 |

| | | | |
|---|---|---|---|
| Web thickness | | in | 0.472 |
| Web inclination | | degrees | 0.0 |

| | | | |
|---|---|---|---|
| Beam depth | | in | 30.3 |

## Beam property

| | | | |
|---|---|---|---|
| Slab area | $A_s$ | $in^2$ | 671 |
| Slab area (effective) | $A_{c,eff}$ | $in^2$ | 671 |
| Slab local centroid (from the bottom) | | in | 34 |

| | | | |
|---|---|---|---|
| Top steel area (within the effective width, from the bottom) | | $in^2$ | 0 |
| Top steel centroid (within the effective width, from the bottom) | | in | 38 |

| | | | |
|---|---|---|---|
| Bottom steel area (within the effective width, from the bottom) | | $in^2$ | 0 |
| Bottom steel centroid (within the effective width, from the bottom) | | in | 30 |

### Section properties for n

| | | | |
|---|---|---|---|
| Slab area (effective, with n) | $A_{c,eff,n}$ | $in^2$ | 78.7 |
| Composite section centroid | | in | 26.7 |
| Slab local moment of inertia (effective, with n) | $I_{x,loc}$ | $in^4$ | 420 |

| | | | |
|---|---|---|---|
| Composite area n | A | $in^4$ | 120 |
| Moment of inertia of the composite section with n | | $in^4$ | 20149 |
| Section modulus bottom flange with n | | $in^3$ | 754 |
| Section modulus top flange with n | | $in^3$ | 5610 |
| Section modulus top concrete with n | | $in^3$ | 1738 |

## Section properties for 3n

| | | | |
|---|---|---|---|
| Slab area (effective, with 3n) | $A_{c,eff,n}$ | $in^2$ | 26.2 |
| Composite section centroid | | in | 20.8 |
| Slab local moment of inertia (effective, with 3n) | $I_{x,loc}$ | $in^4$ | 139.9 |

| | | | |
|---|---|---|---|
| Moment of inertia of the composite section with 3n | | $in^4$ | 14502 |
| Section modulus bottom flange with 3n | | $in^3$ | 696 |
| Section modulus top flange with 3n | | $in^3$ | 1530 |
| Section modulus top concrete with 3n | | $in^3$ | 830 |

## Positive plastic flexure

| | | | |
|---|---|---|---|
| | bs | in | **83.9** |
| | ts | in | **8.0** |
| | haunch | in | **0.0** |
| | bc | in | 15.4 |
| | tc | in | 0.63 |
| | D | in | 28.5 |
| | tw | in | 0.47 |
| | bt | in | 15.4 |
| | tt | in | 1.19 |
| | Fy | ksi | 50 |
| | Fc | ksi | 3.5 |

| | | | |
|---|---|---|---|
| Plastic moment | | | 45280 |
| Neutral Axis (Y in the AASHTO formula, carefull) | | | 0.05 |
| Case of analysis | | | 2 |
| Web in compression | dw | | 0.0 |
| | | | 0.21 |

| | | | |
|---|---|---|---|
| Plastic moment | Mp | kip-ft | 3773 |
| Yielding moment | My | kip-ft | 2880 |

## Compactness condition

| | | | |
|---|---|---|---|
| Slenderness of the compressed web | $\lambda$=2Dcp/wt | | 0.0 |
| Slenderness limit for compressed web | 3.76*(Es/Fy)^0.5 | | 90.6 |

use Mp

| | | | |
|---|---|---|---|
| Plastic moment (considering web slenderness) | Mp | kip-ft | 3773 |

| | | | |
|---|---|---|---|
| Ultimate moment | Mu | kip-ft | **3773** |

| | | | |
|---|---|---|---|
| Ultimate moment | Mu | kNm | **5116** |

## Ultimate

| | | | |
|---|---|---|---|
| Bending SF | | - | 1.00 |

| | | | |
|---|---|---|---|
| Structure DL | | - | 1.30 |
| Superimposed DL | | - | 1.30 |
| Live Load | | - | 1.30 |

| | | | |
|---|---|---|---|
| Steel yielding strenght | Fy | ksi | 50 |

| | | | |
|---|---|---|---|
| Unfactored moment structural DL | | kip-ft | 592.32 |
| Unfactored moment superimposed DL | | kip-ft | 273.50 |

| | | | |
|---|---|---|---|
| Factored moment structural DL | | kip-ft | 568 |
| Factored moment superimposed DL | | kip-ft | 356 |

| | | | |
|---|---|---|---|
| Section modulus non composite section | | $in^3$ | 535 |
| Section modulus composite section n | | $in^3$ | 754 |
| Section modulus composite section 3n | | $in^3$ | 696 |

| | | | |
|---|---|---|---|
| Yielding moment | My | kip-ft | 2880 |

| | | | |
|---|---|---|---|
| Yielding moment (based on unfactored) | My | kip-ft | 2877 |

# Appendix D: Concrete Deck Design

In the next pages the design of the concrete deck of bridge 1002840 is presented.

## Bridge Properties

| | | | |
|---|---|---|---|
| Beam spacing | BS | ft | 9.27 |
| Slab thickness | ST | in | 8.00 |
| Span length | SL | ft | 112.17 |
| Clear cover | CC | in | 1.00 |
| Top flange width (approximated) | | in | 14.81 |

## Concrete

| | | | |
|---|---|---|---|
| Slab concrete strength | f'c,b | ksi | 3.50 |
| Concrete Young's modulus | Ec,b | ksi | 3587 |
| Modulus of rupture | fr | ksi | 0.41 |

## Steel

| | | | |
|---|---|---|---|
| Steel yielding strenght | Fy | ksi | 50.00 |
| Steel Young's modulus | $E_s$ | ksi | 29000.00 |

## Composite section properties

| | | | |
|---|---|---|---|
| Material stiffness relationship | n | - | **8.09** |

## Wearing surface

| | | | |
|---|---|---|---|
| Asphalt load | AL | $kip/ft^3$ | 0.14 |
| Asphalt load (3 inches thickness) | AL | $kip/ft^2$ | 0.04 |

| | | | |
|---|---|---|---|
| Unfactored moment WS (positive) | MwsPos | kip-ft | 0.15 |
| Unfactored moment WS (negative) | MwsNeg | kip-ft | 0.25 |

## Parapet

| | | | |
|---|---|---|---|
| Asphalt load | PLNom | kip/ft | 0.41 |

| | | | |
|---|---|---|---|
| COG parapet | pbs | ft | 0.70 |
| Unfactored moment WS (negative) | MppNeg | kip-ft | 1.62 |

## Concrete Self Weight

| | | | |
|---|---|---|---|
| Concrete weight | | kip/ft$^3$ | 0.15 |

| | | | |
|---|---|---|---|
| Unfactored moment SW (positive) | MswPos | kip-ft | 0.43 |
| Unfactored moment SW (negative) | MswNeg | kip-ft | 0.72 |

## Live Load

| | | | |
|---|---|---|---|
| Unfactored moment SW (positive) | MLLPos | kip-ft | 6.45 |
| Unfactored moment SW (negative) | MLLNeg | kip-ft | 4.82 |

## Ultimate

| | | | |
|---|---|---|---|
| Structure DL | | - | 1.25 |
| Superimposed DL | | - | 1.50 |
| Superimposed DL (unfavourable) | | - | 0.90 |
| Live Load | | - | 2.20 |

| | | | |
|---|---|---|---|
| Factored positive moment | MposULS | kip-ft | 12.5 |
| Factored negative moment | MnegULS | kip-ft | 14.3 |

## Ultimate section resistance

| | | | |
|---|---|---|---|
| Bending SF | | - | 0.90 |

| | | | |
|---|---|---|---|
| Effective depth (assuming rebar #5) | deff | in | 6.69 |
| Slab concrete strength | f'c | ksi | 3.50 |
| Steel yielding strenght | Fy | ksi | 50.00 |

| | | | |
|---|---|---|---|
| Bottom rebar area | As,bot | in$^2$/ft | **0.53** |
| Spacing (assuming rebar #5) | s | in | 7.04 |

| | | | |
|---|---|---|---|
| Stress block depth | a,pos | in | 0.74 |
| Unfactored ultimate moment | Mu,pos | kip-ft | 13.92 |

| | | | |
|---|---|---|---|
| Top rebar area | As,top | in$^2$/ft | **0.61** |
| Spacing (assuming rebar #5) | s | in | 6.11 |

| | | | |
|---|---|---|---|
| Stress block depth | a,nog | in | 0.85 |
| Unfactored ultimate moment | Mu,neg | kip-ft | 15.89 |

# Appendix E: Cross Bracing Design

In the next pages the design of the cross-bracing of bridge 1002840 is presented.

## Bridge Properties

| | | | |
|---|---|---|---|
| Beam spacing | BS | ft | 9.27 |
| Slab thickness | ST | in | 8.00 |
| Span length | SL | ft | 112.17 |
| Number of beams | NB | - | 6.00 |
| Beam depth | d | in | 44.42 |

| | | | |
|---|---|---|---|
| Bracing spacing | Lb | ft | 28.04 |

| | | | |
|---|---|---|---|
| Connection plate thickness | tp | in | 0.50 |

## Section Properties

Bottom chord

| | | | |
|---|---|---|---|
| Depth | d | in | 4.0000 |
| Thickness | t | in | 0.3125 |

Diagonals

| | | | |
|---|---|---|---|
| Depth | d | in | 4.0000 |
| Thickness | t | in | 0.3125 |

## Concrete

| | | | |
|---|---|---|---|
| Slab concrete strength | f'c,b | ksi | 3.50 |
| Concrete Young's modulus | Ec,b | ksi | 3587 |
| Modulus of rupture | fr | ksi | 0.41 |

## Steel

| | | | |
|---|---|---|---|
| Steel yielding strenght | Fy | ksi | 50.00 |
| Steel Young's modulus | $E_s$ | ksi | 29000.00 |

## Composite section properties

| | | | |
|---|---|---|---|
| Material stiffness relationship | n | - | **8.09** |

## Wind load

| | | | |
|---|---|---|---|
| Wind load | p | ksf | 0.05 |
| Asphalt load (3 inches thickness) | d | in | 44.42 |

| | | | |
|---|---|---|---|
| Wind load per unit length | w | k/ft | 0.093 |

## Bottom chord

| | | | |
|---|---|---|---|
| Force on bottom chord | Pw | kips | 2.60 |

## Diagonals

| | | | |
|---|---|---|---|
| Force on diagonals | Pw | kips | 0.23 |

## Section Properties

| | | | |
|---|---|---|---|
| Depth | d | in | 4.0000 |
| Thickness | t | in | 0.3125 |

| | | | |
|---|---|---|---|
| Area | A | $in^2$ | 2.40 |

| | | | |
|---|---|---|---|
| cog y (from bottom) | cog,y | in | 1.12 |
| cog x (from left) | cog,x | in | 1.12 |

| | | | |
|---|---|---|---|
| Inertia y | I,y | $in^4$ | 3.71 |
| Inertia x | I,x | $in^4$ | 3.71 |
| Inertia xy | I,xy | $in^4$ | -2.21 |
| Inertia z | I,z | $in^4$ | 7.43 |

## Principal axes

The principal moments of inertia $I_I, I_{II}$ about principal axes I and II, and the rotation angle $\theta$ of the principal axes from centroidal x, y ones can be found, using the formulas:

$$I_{I,II} = \frac{I_x + I_y}{2} \pm \sqrt{\left(\frac{I_x - I_y}{2}\right)^2 + I_{xy}^2}$$

$$\tan 2\theta = -\frac{2I_{xy}}{I_x - I_y}$$

By definition, $I_I$ is considered the major principal moment (maximum one) and $I_{II}$ the minor principal moment (minimum one).

| | | | |
|---|---|---|---|
| Principal moi I | $I_I$ | $in^4$ | 5.93 |
| Principal moi II | $I_{II}$ | $in^4$ | 1.50 |

| | | | |
|---|---|---|---|
| Angle of principal axis I | θI | º | 45.00 |
| Angle of principal axis II | θII | º | 135.00 |

| | | | |
|---|---|---|---|
| radius of inertia I | rI | in | 1.57 |
| radius of inertia II | rII | in | 0.79 |
| radius of inertia x | rx | in | 1.24 |
| radius of inertia y | ry | in | 1.24 |

## Connection properties

The force on the angle is introduced with a plate welded on the exterior of one leg

| | | | |
|---|---|---|---|
| x of the force applied | x1 | in | -0.31 |
| y of the force applied | y1 | in | 2.00 |

| | | | |
|---|---|---|---|
| x of the force applied (respect cog) | x2 | in | -1.43 |
| y of the force applied (respect cog) | y2 | in | 0.88 |

| | | | |
|---|---|---|---|
| Distance from the cog to the point | r | in | 1.68 |
| Angle from the cog x axis to the point | θ | º | 148.19 |

| | | | |
|---|---|---|---|
| New angle | θ | º | 103.19 |

| | | | |
|---|---|---|---|
| x of the force applied (respect cog, in principal axis) | x3 | in | -0.38 |
| y of the force applied (respect cog, in principal axis) | y3 | in | 1.63 |

# Edges

## top

| | | | |
|---|---|---|---|
| x edge | x1 | in | 0.00 |
| y edge | y1 | in | 4.00 |

| | | | |
|---|---|---|---|
| x of the edge (respect cog) | x2 | in | -1.12 |
| y of the edge (respect cog) | y2 | in | 2.88 |

| | | | |
|---|---|---|---|
| Distance from the cog to the point | r | in | 3.09 |
| Angle from the cog x axis to the point | θ | º | 111.14 |

| | | | |
|---|---|---|---|
| New angle | θ | º | -45.00 |

| | | | |
|---|---|---|---|
| x of the force applied (respect cog, in principal axis) | x3 | in | 0.00 |
| y of the force applied (respect cog, in principal axis) | y3 | in | 0.00 |

## right

| | | | |
|---|---|---|---|
| x edge | x1 | in | 4.00 |
| y edge | y1 | in | 0.00 |

| | | | |
|---|---|---|---|
| x of the edge (respect cog) | x2 | in | 2.88 |
| y of the edge (respect cog) | y2 | in | -1.12 |

| | | | |
|---|---|---|---|
| Distance from the cog to the point | r | in | 3.09 |
| Angle from the cog x axis to the point | θ | º | -21.14 |

| | | | |
|---|---|---|---|
| New angle | θ | º | -66.14 |

| | | | |
|---|---|---|---|
| x of the force applied (respect cog, in principal axis) | x3 | in | 1.25 |
| y of the force applied (respect cog, in principal axis) | y3 | in | -2.83 |

## corner edge

| | | | |
|---|---|---|---|
| x edge | x1 | in | 0.00 |
| y edge | y1 | in | 0.00 |

| | | | |
|---|---|---|---|
| x of the edge (respect cog) | x2 | in | -1.12 |
| y of the edge (respect cog) | y2 | in | -1.12 |

| | | | |
|---|---|---|---|
| Distance from the cog to the point | r | in | 1.58 |
| Angle from the cog x axis to the point | θ | º | -135.00 |

| | | | |
|---|---|---|---|
| New angle | θ | º | -180.00 |

| | | | |
|---|---|---|---|
| x of the force applied (respect cog, in principal axis) | x3 | in | -1.58 |
| y of the force applied (respect cog, in principal axis) | y3 | in | 0.00 |

Design of bottom chord

## Force

| | | | |
|---|---|---|---|
| Force on element | Pw | kips | 2.60 |

| | | | |
|---|---|---|---|
| Safety factor (Strength III) | $\gamma_w$ | - | 1.40 |

| | | | |
|---|---|---|---|
| Force on bottom chord (Factored) | Pu | kips | 2.60 |

| | | | |
|---|---|---|---|
| Force on bottom chord about the major axis (Factored) (Pu x e) | Mw | kips-in | 4.24 |

| | | | |
|---|---|---|---|
| Force on bottom chord about the major axis (Factored) (Pu x ez) | Mz | kips-in | 0.99 |

## L-shaped section

| | | | |
|---|---|---|---|
| Unbraced length (minor axis) | Lb,min | in | 55.6 |
| Unbraced length (major axis) | Lb,max | in | 111.2 |

| | | | |
|---|---|---|---|
| K factor (effective length) (4.6.2.5) | K | - | 0.75 |
| Limit slenderness | | - | 140 |

| | | | |
|---|---|---|---|
| | rz,min | in | 0.30 |
| | ry,max | in | 0.60 |

Design according to AISC LRFD

## Axial compression

### Buckling critical stress based on the minor principal axis

| | | | |
|---|---|---|---|
| Slenderness | $\lambda_c$ | - | 0.7 |

Selection of the equation based on the b/t ratio

| | | | |
|---|---|---|---|
| | b/t | - | 12.8 |
| | b/t,lim1 | - | 10.7 |
| | | | FALSE |

| | | | |
|---|---|---|---|
| Reduction factor | Q1 | - | 1.00 |
| | b/t,lim2 | - | 21.9 |
| | | | TRUE |
| Reduction factor | Q2 | - | 0.94 |

a. For $\lambda_c \sqrt{Q} \leq 1.5$

$$F_{cr} = Q(0.658^{Q\lambda_c^2})F_y$$

b. For $\lambda_c \sqrt{Q} > 1.5$

$$F_{cr} = \left[\frac{0.877}{\lambda_c^2}\right]F_y$$

| | | | |
|---|---|---|---|
| Verification of reduction factor | | - | TRUE |

| | | | |
|---|---|---|---|
| Critical buckling stress 1 | $F_{cr1}$ | ksi | 38.7 |
| Critical buckling stress 2 | $F_{cr2}$ | ksi | 90.4 |

| | | | |
|---|---|---|---|
| Critical buckling stress | $F_{cr}$ | ksi | 38.7 |

## Buckling critical stress based on the y-axis

| | | | |
|---|---|---|---|
| Slenderness | $\lambda_c$ | - | 0.9 |
| Verification of reduction factor | | - | TRUE |
| Critical buckling stress 1 | $F_{cr1}$ | ksi | 34.4 |
| Critical buckling stress 2 | $F_{cr2}$ | ksi | 55.8 |
| Critical buckling stress | $F_{cr}$ | ksi | 34.4 |

## Lower chord critical stress

| | | | |
|---|---|---|---|
| Resistant Factor | | - | 0.90 |
| Critical stress nominal | Pn | ksi | 82.6 |
| Critical stress resistant | Pr | ksi | 74.4 |
| Force on bottom chord (Factored) | Pu | kips | 2.60 |
| Verification | | - | TRUE |

## Flexure

Verification when the tip of the angle is in compression

| | | | |
|---|---|---|---|
| | b/t | - | 12.8 |
| | b/t,lim1 | - | 13.0 |
| | | | TRUE |
| Moment resistance1 | Mnw1 | kips-in | 444.40 |
| | b/t,lim2 | - | 21.9 |
| | | | TRUE |
| Moment resistance2 | Mnw2 | kips-in | 448.74 |
| Reduction factor | Q3 | - | 1.89 |
| Moment resistance3 | Mnw3 | kips-in | 750.5 |
| Moment resistance3 | Mnw | kips-in | 444.4 |

| | | | |
|---|---|---|---|
| Factor accounting for the moment gradient. 1.0 for equal end moments | Cm | - | 1.0 |

| | | | |
|---|---|---|---|
| Slenderness | $\lambda_{cw}$ | - | 0.35 |

| | | | |
|---|---|---|---|
| $P_{e_{1w}} = \frac{A_g F_y}{\lambda_{cw}^{\ 2}}$ | Pe1w | kips | 975.57 |

| | | | |
|---|---|---|---|
| $B_{1w} = \frac{C_m}{1 - P_u / P_{e1w}} \geq 1.0$ | B1w | kips | 1.00 |

| | | | |
|---|---|---|---|
| Ultimat moment | Muw | kips-in | 4.25 |
| Verification (Mr>Muw) | | - | TRUE |

Verification when the corner of the angle is in compression

| | | | |
|---|---|---|---|
| Flexural capacity about the minor axis | Mnz | kips-in | 71.79 |

| | | | |
|---|---|---|---|
| Slenderness | $\lambda_{cz}$ | - | 0.70 |

| | | | |
|---|---|---|---|
| $P_{e_{1w}} = \frac{A_g F_y}{\lambda_{cw}^{\ 2}}$ | Pe1z | kips | 247.51 |

| | | | |
|---|---|---|---|
| $B_{1z} = \frac{C_m}{1 - P_u / P_{e1z}} \geq 1.0$ | B1z | kips | 1.01 |

| | | | |
|---|---|---|---|
| Ultimat moment | Muz | kips-in | 1.00 |
| Verification (Mr>Muz) | | - | TRUE |

## Lateral-torsional buckling

| | | | |
|---|---|---|---|
| Elastic lateral-torsional buckling capacity | Mob | kips-in | 187.47 |
| Yield moment | My | kips-in | 104.75 |
| Verification (Mob>My) | | | TRUE |
| Lateral torsional buckling capacity | Mnw | kips-in | 109.51 |
| Verification (Mnw<1.5My) | | | TRUE |
| Verification (Mnw>Muw) | | | TRUE |

## Flexural-Axial compression

| | | | |
|---|---|---|---|
| | Pu | kips | 2.60 |
| | Pr | kips | 82.61 |
| | Muw | k-in | 4.25 |
| | Mrw | k-in | 109.51 |
| | Muz | k-in | 1.00 |
| | Mrz | k-in | 71.79 |
| $\left\lvert \frac{P_u}{2\phi P_n} + \left( \frac{M_{uw}}{\phi_b M_{nw}} + \frac{M_{uz}}{\phi_b M_{nz}} \right) \right\rvert \leq 1.0$ | | | 0.07 < 1 |
| | | | TRUE |

The procedure presented in this appendix are also applied for the design of the diagonals of the cross-frame.

# Appendix F: Comparison of the Grillage Model with and without Cross-Bracings

In this appendix the effects of the cross-bracings on the global bridge behavior is evaluated. These elements are originally designed for the temporary construction phases as explained in Appendix E. Furthermore, the effect on the flexibility and internal forces of the cross-frames has already been shown by Hambly (1991) to be of little relevance for discontinuous cross-frames (Figure F-1).

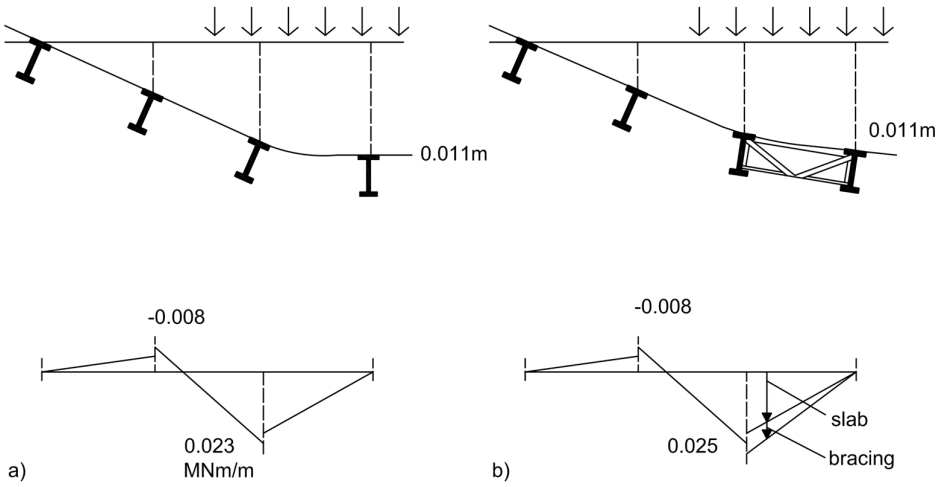


**Figure F-1. Frame model carried out by Hambly (1991) comparing no cross-frame (a) and discontinuous cross-frame (b) in terms of displacements (above) and bending moments (below).**

The calculation reported below are meant to check and confirm that the transverse behavior of the bridge is sufficiently described by using only slab elements. Instead of a plane element of the cross-frame only a full modified grillage is compared to a standard grillage without cross-frames as shown in Figure F-2.

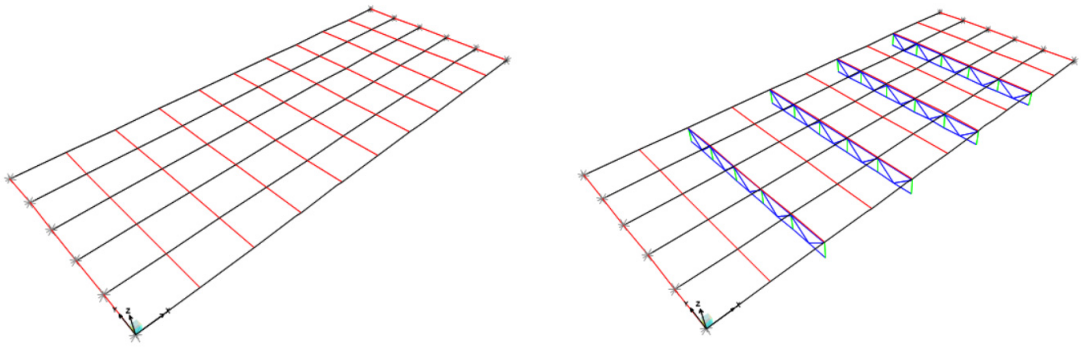

**Figure F-2. Grillage with no cross-frame (left) and modified with cross-frame (right).**

The input of the two models are the same except for the cross-frame elements added representing steel L-shape profiles organized in a k-configuration and shown in Figure F-3.

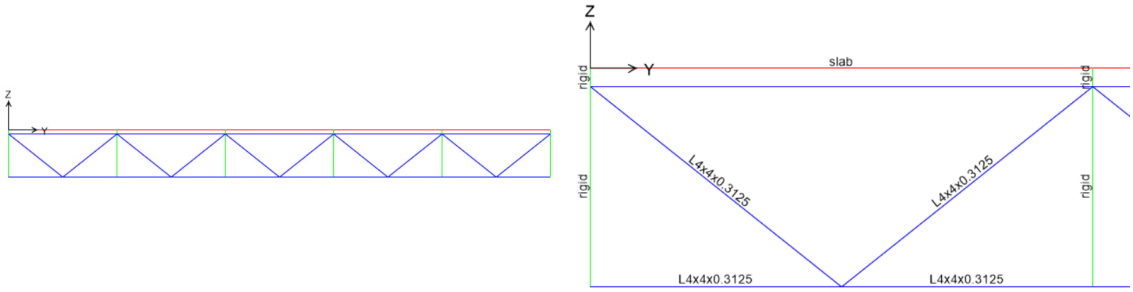


**Figure F-3. Cross-frame geometry for the full superstructure (left) and cross frame detail and section employed for the frames (right).**

Finally, longitudinal elements represent composite slab-girder behavior and transverse elements represent the slab behavior between girders.

The results show that the two models provide similar results in terms of deflections Figure F-4 and moment Figure F-5 in the main longitudinal element, even in a simple linear elastic model.

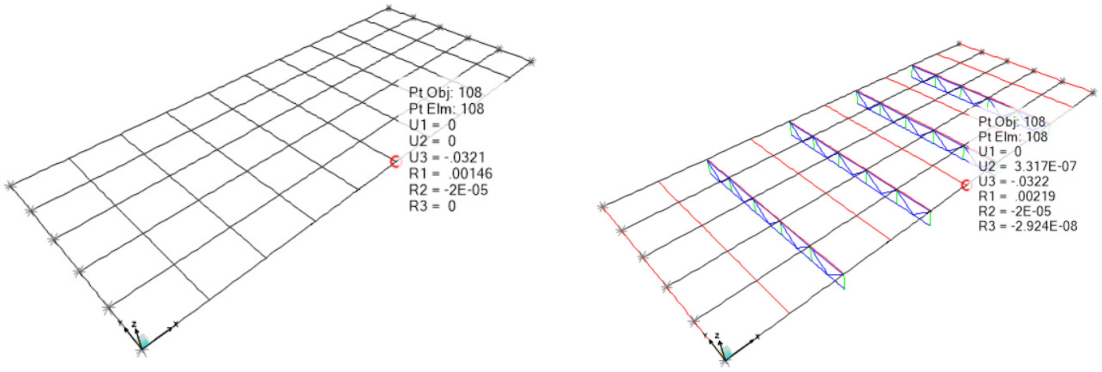


**Figure F-4. Maximum deflection of the grillage without cross-frames (left) and with cross frames (right).**

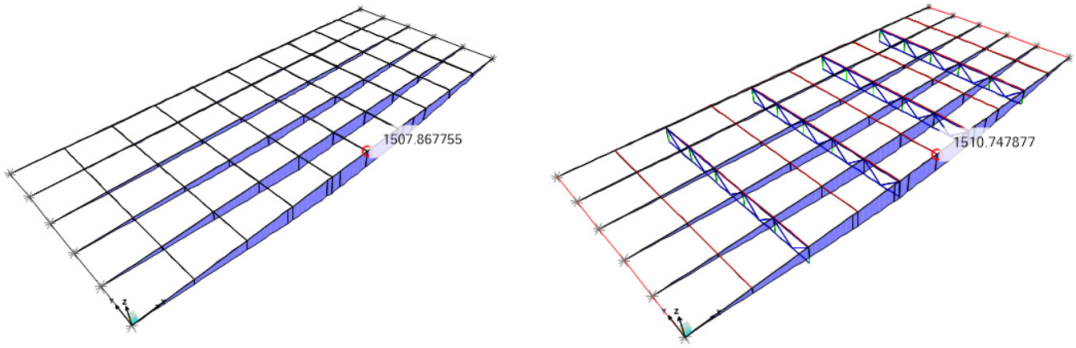


**Figure F-5. Maximum moment of the grillage without cross-frames (left) and with cross frames (right).**

Both the maximum deflection and maximum moment are practically the same value, allowing to conclude that it is possible to ignore the cross-frame system in the modelling of composite slab-girder superstructure.

# Appendix G: Cost estimation calculation detail

The cost estimation calculations are outlined below for the example bridge NBI 000000001003209, ID 21 of *set 1*.

## G.1. Cost of demolition and reconstruction

The dimensions of the example bridge are descripted in Figure G 1.

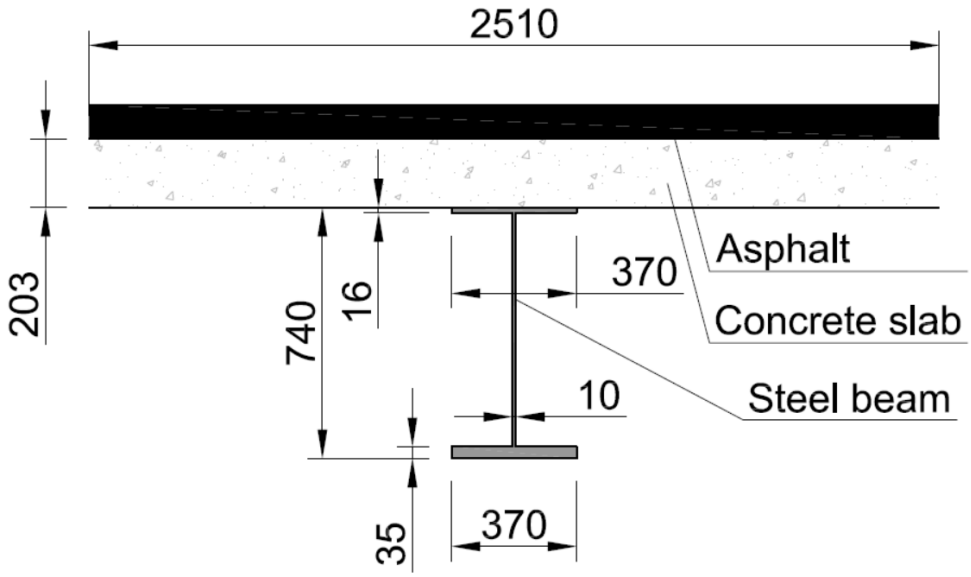


**Figure G 1. Example bridge cross section.**

The cost of reconstruction is related to the surface of the bridge calculated as its width (42.6 m) by its length (22.0 m) resulting in $S = 22.2 \times 42.6 = 945.72 m^2$.

The equation outlined in subsection 7.3.1 is used resulting in $1859.58\,\$/m^2 \times 945.72 m^2 = \$\,1{,}758{,}651$.

The cost of demolition is related to the volume of the bridge calculated in Table G 1.

**Table G 1. Bridge volume calculation.**

| Slab volume (per beam) | Steel volume (per beam) | Asphalt volume (per beam) |
|---|---|---|
| $m^3/m$ | $m^3/m$ | $m^3/m$ |
| 0.510 | 0.02583x1.1 | 0.251 |

The total is calculated as the volume per beam by the number of beams by the bridge length $0.7894 \times 22.2 \times 17 = 297.92\ m^3$. The steel volume is multiplied by a factor of 1.1 to account for diaphragms and joints.

The equation outlined in subsection 7.3.1 is used resulting in $35.2\ \$/m^3 \times\ 297.28 m^2 = \$\ 10{,}464$.

The cost of demolition and reconstruction is $\$\ 1{,}769{,}115$.

## G.2. Disruption Time

The disruption time is calculated with Equation 7-4 for Interstate bridge replacement $T = \alpha\ \ln[C_C] - \gamma = 41.26\ \ln[1{,}758{,}651] - 445 = 148.32\ days$

## G.3. Indirect Cost

The cost of operating vehicle is the sum of the cost of delay and the cost of time loss according to Equation 7-5.

The unit cost of automobile delay is $35.2\ \$/h$ the detour length is $8\ km$, the $ADT$ is $63{,}722\ vehicles$, and the disruption time $148.32\ days$, the percentage of heavy trucks is 4%, the average vehicle occupancy 1.35 $persons$,

$$C_{I1} =$$

$$= C_3\ D\ ADT\ T + \left[C_4\ O\ \left(1 - \frac{\rho}{100}\right) + C_5\ \frac{\rho}{100}\right]\frac{D\ ADT\ T}{S} =$$

$$= 0.36622 \times 8 \times 63{,}722 \times 148.32\ + \left[13.46 \times\ 1.35\ \left(1 - \frac{4}{100}\right) + 26.93\ \frac{4}{100}\right]\frac{8 \times 63{,}722 \times 148.32}{20.92}$$

$$= \$\ 27'689'886\ + \$\ 66'940'707 = \$\ 94'630'592$$

The indirect cost is $\$\ 94'630'593$.

## G.4. Accidents due to detour

The number of fatalities, injured and property damage due to detour during the disruption time is calculated with Equation 7-6, 7-7 and 7-8.

$$n_{fatalities} = \frac{1.13}{10^8}\, ADT\ \ T\ D\ \ \frac{1}{1.609} = \frac{1.13}{10^8} 63{,}722 \times 148.32 \times 8\ \ \frac{1}{1.609} = 0.53\ persons$$

$$n_{fatalities} = \frac{77.00}{10^8}\, ADT\ \ T\ D\ \ \frac{1}{1.609} = \frac{77.00}{10^8} 63{,}722 \times 148.32 \times 8\ \ \frac{1}{1.609} = 36.18\ persons$$

$$n_{vehicle} = \frac{n_{fatalities} + n_{injured}}{O} = \frac{0.53 + 36.18}{1.35} = 27.19\ vehicles$$

These values are multiplied by the nominal corresponding cost.

$C_{I2,1} = 0.53 \times 1{,}678{,}357 = \$\ 889{,}529$

$C_{I2,2} = 36.18 \times 16{,}493 = \$\ 596{,}717$

$C_{I2,3} = 27.19 \times 3{,}355. = \$\ 91{,}222$

The cost of accidents due to detour is $\$\ 1'577'468$.

## G.5. Environmental Cost

The environmental cost is calculated according to Equation 7-9 considering rural environment.

The $ADT$ is $63{,}722\ vehicles$, the $ADTT$ is $2{,}549\ vehicles$,

$C_{I3} =$

$= \left((ADT - ADTT)\ C_{pc} + 0.87\ ADTT\ C_{pht} + 0.13\ ADTT\ C_{plt}\right)\ T =$

$= \left((63{,}722 - 2{,}549)\ 0.0304 + 0.87 \times 2{,}549 \times 0.0449 + 0.13 \times 2{,}549 \times 0.1714\right) 8 \times 148.32 =$

$= \$\ 2{,}392{,}138$

The environmental cost is $\$\ 2{,}392{,}138$.

## G.6. Fatalities and injuries

The number of fatalities due to bridge failure is calculated with the equation 0.0762 SL and with a probability of mortality of 0.055. The number of injured is calculated as twice the number of fatalities.

$$n_{fatalities} = 0.0762 \times SL \times 0.055 = 0.0762 \times 22.2 \times 0.055 = 0.093\ persons$$

$$n_{fatalities} = 2.0\ n_{fatalities} = 2.0 \times 0.093 = 0.0186\ persons$$

$$n_{vehicle} = \frac{n_{fatalities} + n_{injured}}{O} = \frac{0.0903 + 0.0186}{1.35} = 0.207\ vehicles$$

These values are multiplied by the nominal corresponding cost.

$$C_{I4,1} = 0.093 \times 1{,}678{,}357 = \$\ 156{,}087$$

$$C_{I4,2} = 0.093 \times 1{,}594{,}439 = \$\ 296'566$$

$$C_{I4,3} = 0.207 \times 3{,}355 = \$\ 694$$

The cost of fatalities and injured due to failure is $\$\ 453'347$.

## G.7. Total cost

The total cost and the summary of the different cost contributions are summarized in Table G 2.

**Table G 2. Cost summary and total cost of bridge failure.**

| | Cost | Percentage |
|---|---|---|
| System reconstruction cost | $ 1,769,115 | 1.8% |
| Environmental cost | $ 2,392,138 | 2.4% |
| Indirect cost | $ 94,630,593 | 93.9% |
| Accidents due to detour | $ 1,577,468 | 1.6% |
| Fatalities and injuried | $ 453,347 | 0.4% |

| | | |
|---|---|---|
| Total | $ | 100,822,662 |

# Appendix H: Results of Inspection Interval

In the next pages the inspection interval results are presented.

The following abbreviations have been used in the tables:

NB = Number of beams

SL = Span length

BS = Beam spacing

RF = Load rating factor

| bridgeID | Bridge Label (NBI) | NB | SL | BS | RF | Section capacity |
|---|---|---|---|---|---|---|
| - | - | - | m | m | - | kNm |
| 1 | 000000001000090 | 8 | 73.8 | 7.5 | 2.3 | 5123 |
| 2 | 000000001000500 | 7 | 80.7 | 8.1 | 1.6 | 4830 |
| 3 | 000000001000871 | 6 | 101.4 | 8.8 | 2.5 | 10133 |
| 4 | 000000001000872 | 5 | 101.4 | 8.3 | 2.6 | 9781 |
| 5 | 000000001001429 | 14 | 77.8 | 7.4 | 1.7 | 4322 |
| 6 | 000000001001439 | 14 | 78.7 | 7.4 | 1.9 | 4789 |
| 7 | 000000001001639 | 17 | 110.9 | 7.2 | 1.8 | 7591 |
| 8 | 000000001002131 | 8 | 84.0 | 7.2 | 2.2 | 5770 |
| 9 | 000000001002132 | 6 | 84.0 | 7.2 | 2.2 | 5758 |
| 10 | 000000001002219 | 12 | 64.0 | 7.3 | 1.7 | 3198 |
| 11 | 000000001002249 | 14 | 68.9 | 6.3 | 1.9 | 3308 |
| 12 | 000000001002259 | 14 | 64.0 | 6.3 | 2.0 | 3083 |
| 13 | 000000001002610 | 10 | 68.9 | 7.7 | 2.4 | 4803 |
| 14 | 000000001002621 | 12 | 129.9 | 6.5 | 2.8 | 11388 |
| 15 | 000000001002622 | 12 | 129.9 | 6.5 | 2.8 | 11360 |
| 16 | 000000001002840 | 4 | 75.8 | 7.0 | 2.1 | 4702 |
| 17 | 000000001002950 | 6 | 71.9 | 7.7 | 2.4 | 5135 |
| 18 | 000000001002960 | 5 | 79.7 | 7.5 | 2.8 | 6611 |
| 19 | 000000001003081 | 6 | 57.7 | 6.9 | 2.3 | 3229 |
| 20 | 000000001003082 | 6 | 53.8 | 6.9 | 2.3 | 2926 |
| 21 | 000000001003209 | 17 | 72.8 | 8.2 | 2.2 | 5156 |
| 22 | 000000001003229 | 16 | 65.0 | 7.4 | 2.4 | 4277 |
| 23 | 000000001003270 | 4 | 57.7 | 8.3 | 2.4 | 4115 |
| 24 | 000000001003300 | 5 | 61.7 | 8.6 | 2.3 | 4550 |
| 25 | 000000001003340 | 10 | 66.9 | 6.9 | 3.1 | 5031 |
| 26 | 000000001003670 | 8 | 44.0 | 7.9 | 2.7 | 2712 |
| 27 | 000000001003711 | 6 | 58.7 | 7.0 | 2.3 | 3458 |
| 28 | 000000001003712 | 6 | 60.7 | 8.7 | 2.2 | 4172 |

| | Inspection time (years) | | | | | | | | | | | |
|---|---|---|---|---|---|---|---|---|---|---|---|---|
| | High deterioration rate (3.4%) | | | | Medium deterioration rate (0.5%) | | | | Low deterioration rate (0.07%) | | | |
| Inspection cost ($) | 4k | 10k | 20k | 40k | 4k | 10k | 20k | 40k | 4k | 10k | 20k | 40k |
| 1 | 1 | 2 | 4 | 6 | 6 | 6 | 6 | 6 | 6 | 6 | 6 | 6 |
| 1 | 1 | 1 | 2 | 3 | 6 | 6 | 6 | 6 | 6 | 6 | 6 | 6 |
| 1 | 2 | 4 | 6 | 6 | 6 | 6 | 6 | 6 | 6 | 6 | 6 | 6 |
| 1 | 2 | 4 | 6 | 6 | 6 | 6 | 6 | 6 | 6 | 6 | 6 | 6 |
| 1 | 3 | 3 | 3 | 6 | 6 | 6 | 6 | 6 | 6 | 6 | 6 | 6 |
| 2 | 4 | 4 | 4 | 6 | 6 | 6 | 6 | 6 | 6 | 6 | 6 | 6 |
| 1 | 1 | 1 | 1 | 1 | 1 | 2 | 4 | 6 | 6 | 6 | 6 | 6 |
| 1 | 2 | 3 | 6 | 6 | 6 | 6 | 6 | 6 | 6 | 6 | 6 | 6 |
| 1 | 2 | 3 | 6 | 6 | 6 | 6 | 6 | 6 | 6 | 6 | 6 | 6 |
| 1 | 1 | 2 | 3 | 6 | 6 | 6 | 6 | 6 | 6 | 6 | 6 | 6 |
| 1 | 1 | 2 | 4 | 6 | 6 | 6 | 6 | 6 | 6 | 6 | 6 | 6 |
| 1 | 1 | 1 | 2 | 5 | 6 | 6 | 6 | 6 | 6 | 6 | 6 | 6 |
| 4 | 4 | 4 | 4 | 6 | 6 | 6 | 6 | 6 | 6 | 6 | 6 | 6 |
| 1 | 1 | 1 | 2 | 6 | 6 | 6 | 6 | 6 | 6 | 6 | 6 | 6 |
| 1 | 1 | 1 | 2 | 6 | 6 | 6 | 6 | 6 | 6 | 6 | 6 | 6 |
| 1 | 1 | 1 | 2 | 4 | 6 | 6 | 6 | 6 | 6 | 6 | 6 | 6 |
| 1 | 2 | 3 | 6 | 6 | 6 | 6 | 6 | 6 | 6 | 6 | 6 | 6 |
| 1 | 1 | 3 | 4 | 6 | 6 | 6 | 6 | 6 | 6 | 6 | 6 | 6 |
| 4 | 6 | 6 | 6 | 6 | 6 | 6 | 6 | 6 | 6 | 6 | 6 | 6 |
| 4 | 6 | 6 | 6 | 6 | 6 | 6 | 6 | 6 | 6 | 6 | 6 | 6 |
| 1 | 1 | 1 | 1 | 1 | 4 | 6 | 6 | 6 | 6 | 6 | 6 | 6 |
| 2 | 4 | 6 | 6 | 6 | 6 | 6 | 6 | 6 | 6 | 6 | 6 | 6 |
| 6 | 6 | 6 | 6 | 6 | 6 | 6 | 6 | 6 | 6 | 6 | 6 | 6 |
| 6 | 6 | 6 | 6 | 6 | 6 | 6 | 6 | 6 | 6 | 6 | 6 | 6 |
| 3 | 3 | 3 | 3 | 6 | 6 | 6 | 6 | 6 | 6 | 6 | 6 | 6 |
| 4 | 4 | 4 | 4 | 6 | 6 | 6 | 6 | 6 | 6 | 6 | 6 | 6 |
| 5 | 6 | 6 | 6 | 6 | 6 | 6 | 6 | 6 | 6 | 6 | 6 | 6 |
| 4 | 4 | 4 | 4 | 6 | 6 | 6 | 6 | 6 | 6 | 6 | 6 | 6 |

| bridgeID | Bridge Label (NBI) | NB | SL | BS | RF | Section capacity |
|---|---|---|---|---|---|---|
| - | - | - | m | m | - | kNm |
| 29 | 000000001004200 | 12 | 69.9 | 5.0 | 1.9 | 2737 |
| 30 | 000000001004249 | 9 | 70.9 | 6.8 | 1.8 | 3618 |
| 31 | 000000001004261 | 10 | 60.0 | 5.1 | 3.1 | 3208 |
| 32 | 000000001005051 | 5 | 78.7 | 7.0 | 2.7 | 5928 |
| 33 | 000000001005130 | 10 | 104.7 | 8.7 | 2.6 | 10498 |
| 34 | 000000001005140 | 11 | 164.0 | 8.9 | 2.9 | 22913 |
| 35 | 000000001005290 | 10 | 47.9 | 6.6 | 2.9 | 2755 |
| 36 | 000000001005679 | 16 | 89.9 | 6.5 | 1.5 | 4461 |
| 37 | 000000001005741 | 5 | 110.9 | 6.7 | 3.0 | 10060 |
| 38 | 000000001005851 | 5 | 123.7 | 8.4 | 2.1 | 11494 |
| 39 | 000000001005912 | 5 | 140.1 | 8.7 | 3.1 | 18314 |
| 40 | 000000001006762 | 7 | 73.8 | 6.7 | 2.2 | 4443 |
| 41 | 000000001006922 | 5 | 125.0 | 8.6 | 2.3 | 12592 |
| 42 | 000000001007041 | 6 | 111.9 | 9.3 | 2.5 | 12165 |
| 43 | 000000001007042 | 6 | 111.9 | 8.6 | 2.5 | 11341 |
| 44 | 000000001007270 | 5 | 52.8 | 6.6 | 1.4 | 1925 |
| 45 | 000000001008070 | 5 | 48.9 | 6.6 | 1.8 | 2021 |
| 46 | 000000001009100 | 6 | 132.9 | 9.2 | 2.9 | 17030 |
| 47 | 000000001009509 | 12 | 78.7 | 8.3 | 2.7 | 6742 |
| 48 | 000000001010590 | 5 | 67.9 | 6.9 | 1.4 | 2968 |
| 49 | 000000001011009 | 18 | 47.9 | 7.5 | 1.2 | 1577 |
| 50 | 000000001011151 | 5 | 161.1 | 8.3 | 2.7 | 20004 |
| 51 | 000000001011152 | 5 | 161.1 | 8.3 | 2.6 | 19785 |
| 52 | 000000001011240 | 5 | 80.7 | 6.6 | 2.4 | 5333 |
| 53 | 000000001013131 | 6 | 153.9 | 9.0 | 2.7 | 20327 |
| 54 | 000000001013300 | 4 | 52.8 | 5.8 | 2.4 | 2535 |
| 55 | 000000001013959 | 14 | 120.7 | 9.1 | 2.2 | 11947 |

| | Inspection time (years) | | | | | | | | | | | |
|---|---|---|---|---|---|---|---|---|---|---|---|---|
| | High deterioration rate (3.4%) | | | | Medium deterioration rate (0.5%) | | | | Low deterioration rate (0.07%) | | | |
| Inspection cost ($) | 4k | 10k | 20k | 40k | 4k | 10k | 20k | 40k | 4k | 10k | 20k | 40k |
| | 1 | 2 | 4 | 4 | 6 | 6 | 6 | 6 | 6 | 6 | 6 | 6 |
| | 3 | 3 | 3 | 3 | 6 | 6 | 6 | 6 | 6 | 6 | 6 | 6 |
| | 2 | 3 | 3 | 3 | 6 | 6 | 6 | 6 | 6 | 6 | 6 | 6 |
| | 2 | 4 | 6 | 6 | 6 | 6 | 6 | 6 | 6 | 6 | 6 | 6 |
| | 1 | 2 | 3 | 5 | 6 | 6 | 6 | 6 | 6 | 6 | 6 | 6 |
| | 1 | 1 | 2 | 3 | 6 | 6 | 6 | 6 | 6 | 6 | 6 | 6 |
| | 3 | 4 | 4 | 5 | 6 | 6 | 6 | 6 | 6 | 6 | 6 | 6 |
| | 1 | 1 | 1 | 2 | 3 | 6 | 6 | 6 | 6 | 6 | 6 | 6 |
| | 1 | 1 | 2 | 5 | 6 | 6 | 6 | 6 | 6 | 6 | 6 | 6 |
| | 1 | 2 | 4 | 4 | 6 | 6 | 6 | 6 | 6 | 6 | 6 | 6 |
| | 1 | 1 | 1 | 2 | 3 | 6 | 6 | 6 | 6 | 6 | 6 | 6 |
| | 4 | 6 | 6 | 6 | 6 | 6 | 6 | 6 | 6 | 6 | 6 | 6 |
| | 1 | 3 | 6 | 6 | 6 | 6 | 6 | 6 | 6 | 6 | 6 | 6 |
| | 1 | 1 | 1 | 2 | 6 | 6 | 6 | 6 | 6 | 6 | 6 | 6 |
| | 1 | 1 | 1 | 2 | 5 | 6 | 6 | 6 | 6 | 6 | 6 | 6 |
| | 2 | 2 | 2 | 2 | 6 | 6 | 6 | 6 | 6 | 6 | 6 | 6 |
| | 1 | 2 | 3 | 3 | 6 | 6 | 6 | 6 | 6 | 6 | 6 | 6 |
| | 2 | 4 | 6 | 6 | 6 | 6 | 6 | 6 | 6 | 6 | 6 | 6 |
| | 1 | 4 | 4 | 4 | 6 | 6 | 6 | 6 | 6 | 6 | 6 | 6 |
| | 1 | 1 | 1 | 1 | 1 | 2 | 4 | 6 | 6 | 6 | 6 | 6 |
| | 1 | 1 | 1 | 1 | 1 | 1 | 1 | 3 | 6 | 6 | 6 | 6 |
| | 1 | 1 | 1 | 1 | 1 | 1 | 1 | 2 | 6 | 6 | 6 | 6 |
| | 1 | 1 | 1 | 1 | 1 | 1 | 1 | 2 | 6 | 6 | 6 | 6 |
| | 3 | 6 | 6 | 6 | 6 | 6 | 6 | 6 | 6 | 6 | 6 | 6 |
| | 1 | 1 | 2 | 3 | 6 | 6 | 6 | 6 | 6 | 6 | 6 | 6 |
| | 4 | 6 | 6 | 6 | 6 | 6 | 6 | 6 | 6 | 6 | 6 | 6 |
| | 1 | 2 | 3 | 5 | 6 | 6 | 6 | 6 | 6 | 6 | 6 | 6 |

| bridgeID | Bridge Label (NBI) | NB | SL | BS | RF | Section capacity |
|---|---|---|---|---|---|---|
| - | - | - | m | m | - | kNm |
| 56 | 000000001014841 | 5 | 79.1 | 7.1 | 2.5 | 5700 |
| 57 | 000000001014880 | 5 | 116.8 | 6.6 | 2.6 | 9846 |
| 58 | 000000001015210 | 7 | 54.1 | 6.1 | 2.6 | 2878 |
| 59 | 000000001015620 | 7 | 113.8 | 6.7 | 2.1 | 8249 |
| 60 | 000000001015879 | 12 | 63.0 | 8.4 | 2.2 | 4378 |
| 61 | 000000001015980 | 11 | 56.8 | 6.8 | 2.0 | 2733 |
| 62 | 000000001018219 | 16 | 70.9 | 7.9 | 1.7 | 4012 |
| 63 | 000000001018290 | 11 | 74.8 | 6.5 | 1.8 | 3756 |
| 64 | 000000001019360 | 5 | 75.1 | 7.6 | 1.8 | 4551 |
| 65 | 000000001019449 | 10 | 96.8 | 9.1 | 2.8 | 10217 |
| 66 | 000000001020079 | 18 | 60.0 | 7.4 | 1.8 | 2994 |
| 67 | 000000001021640 | 9 | 81.7 | 7.6 | 2.7 | 6529 |
| 68 | 000000001021661 | 9 | 75.8 | 7.0 | 1.3 | 3279 |
| 69 | 000000001022320 | 6 | 84.0 | 7.2 | 2.3 | 5869 |
| 70 | 000000001022479 | 16 | 117.8 | 6.8 | 1.8 | 7786 |
| 71 | 000000001022570 | 8 | 74.8 | 8.3 | 2.4 | 5868 |
| 72 | 000000001022670 | 4 | 107.0 | 7.7 | 2.4 | 9484 |
| 73 | 000000001022710 | 5 | 86.0 | 7.2 | 2.9 | 7234 |
| 74 | 000000001025951 | 9 | 109.9 | 7.0 | 1.6 | 6929 |
| 75 | 000000001026240 | 6 | 161.4 | 9.1 | 1.8 | 17799 |
| 76 | 000000001027840 | 5 | 117.1 | 8.6 | 2.4 | 11927 |
| 77 | 000000001029480 | 4 | 113.8 | 8.1 | 2.6 | 11389 |
| 78 | 000000001029490 | 4 | 116.8 | 8.1 | 1.9 | 9595 |
| 79 | 000000001030290 | 10 | 111.9 | 7.6 | 2.5 | 10071 |
| 80 | 000000001031060 | 5 | 75.1 | 6.6 | 1.7 | 3823 |
| 81 | 000000001031201 | 5 | 40.7 | 6.6 | 3.1 | 2300 |
| 82 | 000000001031211 | 5 | 49.9 | 6.6 | 2.4 | 2624 |

| | Inspection time (years) | | | | | | | | | | | |
|---|---|---|---|---|---|---|---|---|---|---|---|---|
| | High deterioration rate (3.4%) | | | | Medium deterioration rate (0.5%) | | | | Low deterioration rate (0.07%) | | | |
| Inspection cost ($) | 4k | 10k | 20k | 40k | 4k | 10k | 20k | 40k | 4k | 10k | 20k | 40k |
| | 3 | 6 | 6 | 6 | 6 | 6 | 6 | 6 | 6 | 6 | 6 | 6 |
| | 2 | 3 | 6 | 6 | 6 | 6 | 6 | 6 | 6 | 6 | 6 | 6 |
| | 2 | 4 | 4 | 5 | 6 | 6 | 6 | 6 | 6 | 6 | 6 | 6 |
| | 1 | 1 | 1 | 1 | 1 | 4 | 6 | 6 | 6 | 6 | 6 | 6 |
| | 1 | 4 | 5 | 6 | 6 | 6 | 6 | 6 | 6 | 6 | 6 | 6 |
| | 1 | 1 | 2 | 4 | 6 | 6 | 6 | 6 | 6 | 6 | 6 | 6 |
| | 1 | 1 | 2 | 3 | 6 | 6 | 6 | 6 | 6 | 6 | 6 | 6 |
| | 1 | 2 | 3 | 3 | 6 | 6 | 6 | 6 | 6 | 6 | 6 | 6 |
| | 1 | 1 | 2 | 3 | 6 | 6 | 6 | 6 | 6 | 6 | 6 | 6 |
| | 1 | 2 | 3 | 6 | 6 | 6 | 6 | 6 | 6 | 6 | 6 | 6 |
| | 1 | 1 | 1 | 1 | 1 | 4 | 6 | 6 | 6 | 6 | 6 | 6 |
| | 2 | 6 | 6 | 6 | 6 | 6 | 6 | 6 | 6 | 6 | 6 | 6 |
| | 1 | 1 | 1 | 1 | 2 | 5 | 6 | 6 | 6 | 6 | 6 | 6 |
| | 1 | 1 | 1 | 1 | 1 | 2 | 5 | 6 | 6 | 6 | 6 | 6 |
| | 1 | 1 | 1 | 1 | 1 | 4 | 6 | 6 | 6 | 6 | 6 | 6 |
| | 2 | 5 | 6 | 6 | 6 | 6 | 6 | 6 | 6 | 6 | 6 | 6 |
| | 1 | 1 | 2 | 4 | 6 | 6 | 6 | 6 | 6 | 6 | 6 | 6 |
| | 4 | 6 | 6 | 6 | 6 | 6 | 6 | 6 | 6 | 6 | 6 | 6 |
| | 1 | 1 | 1 | 1 | 2 | 5 | 6 | 6 | 6 | 6 | 6 | 6 |
| | 1 | 1 | 1 | 1 | 1 | 3 | 5 | 6 | 6 | 6 | 6 | 6 |
| | 1 | 1 | 1 | 1 | 2 | 5 | 6 | 6 | 6 | 6 | 6 | 6 |
| | 2 | 3 | 6 | 6 | 6 | 6 | 6 | 6 | 6 | 6 | 6 | 6 |
| | 1 | 3 | 3 | 3 | 6 | 6 | 6 | 6 | 6 | 6 | 6 | 6 |
| | 1 | 1 | 3 | 5 | 6 | 6 | 6 | 6 | 6 | 6 | 6 | 6 |
| | 1 | 1 | 2 | 3 | 6 | 6 | 6 | 6 | 6 | 6 | 6 | 6 |
| | 6 | 6 | 6 | 6 | 6 | 6 | 6 | 6 | 6 | 6 | 6 | 6 |
| | 6 | 6 | 6 | 6 | 6 | 6 | 6 | 6 | 6 | 6 | 6 | 6 |

| bridgeID | Bridge Label (NBI) | NB | SL | BS | RF | Section capacity |
|---|---|---|---|---|---|---|
| - | - | - | m | m | - | kNm |
| 83 | 000000001031230 | 5 | 54.8 | 6.6 | 1.7 | 2345 |
| 84 | 000000001031529 | 14 | 65.0 | 7.1 | 2.7 | 4422 |
| 85 | 000000001031549 | 16 | 60.7 | 6.9 | 2.7 | 3893 |
| 86 | 000000001031569 | 10 | 119.8 | 9.0 | 1.8 | 10520 |
| 87 | 000000001031690 | 11 | 102.0 | 6.9 | 2.1 | 6946 |
| 88 | 000000001032020 | 5 | 52.8 | 7.0 | 1.5 | 2144 |
| 89 | 000000001032252 | 5 | 45.9 | 7.0 | 2.4 | 2422 |
| 90 | 000000001032612 | 5 | 68.9 | 6.6 | 2.8 | 4717 |
| 91 | 000000001033670 | 4 | 112.9 | 7.2 | 2.4 | 9521 |
| 92 | 000000001033730 | 4 | 125.0 | 7.2 | 2.3 | 10916 |
| 93 | 000000001034161 | 6 | 62.0 | 7.6 | 2.0 | 3521 |
| 94 | 000000001034491 | 6 | 126.0 | 7.6 | 2.7 | 12645 |
| 95 | 000000001034492 | 6 | 113.8 | 7.2 | 2.1 | 8703 |
| 96 | 000000001036069 | 12 | 107.0 | 8.2 | 2.4 | 9668 |
| 97 | 000000001036900 | 5 | 99.7 | 8.8 | 1.3 | 6533 |
| 98 | 000000001037859 | 14 | 80.7 | 6.8 | 2.2 | 5094 |
| 99 | 000000001037909 | 14 | 56.8 | 7.5 | 2.5 | 3647 |
| 100 | 000000001037949 | 20 | 95.8 | 6.2 | 2.2 | 5886 |
| 101 | 00000000103989B | 5 | 64.0 | 5.1 | 2.2 | 2773 |
| 102 | 00000000103989C | 5 | 101.7 | 5.1 | 1.6 | 4654 |
| 103 | 000000001040129 | 13 | 132.2 | 9.4 | 3.1 | 17882 |
| 104 | 000000001040292 | 5 | 99.7 | 8.6 | 2.3 | 8931 |
| 105 | 000000001043270 | 5 | 67.9 | 7.0 | 1.8 | 3504 |
| 106 | 000000001043751 | 10 | 89.9 | 6.5 | 1.7 | 4835 |
| 107 | 000000001049229 | 25 | 107.0 | 6.8 | 2.5 | 8216 |
| 108 | 000000001049371 | 6 | 77.8 | 9.1 | 1.8 | 5630 |
| 109 | 000000001050002 | 6 | 88.9 | 7.7 | 2.0 | 6111 |

| | Inspection time (years) | | | | | | | | | | | |
|---|---|---|---|---|---|---|---|---|---|---|---|---|
| | High deterioration rate (3.4%) | | | | Medium deterioration rate (0.5%) | | | | Low deterioration rate (0.07%) | | | |
| Inspection cost ($) | 4k | 10k | 20k | 40k | 4k | 10k | 20k | 40k | 4k | 10k | 20k | 40k |
| | 3 | 5 | 5 | 5 | 6 | 6 | 6 | 6 | 6 | 6 | 6 | 6 |
| | 1 | 3 | 4 | 4 | 6 | 6 | 6 | 6 | 6 | 6 | 6 | 6 |
| | 2 | 5 | 6 | 6 | 6 | 6 | 6 | 6 | 6 | 6 | 6 | 6 |
| | 1 | 1 | 1 | 1 | 1 | 3 | 6 | 6 | 6 | 6 | 6 | 6 |
| | 1 | 1 | 2 | 4 | 6 | 6 | 6 | 6 | 6 | 6 | 6 | 6 |
| | 2 | 3 | 3 | 3 | 6 | 6 | 6 | 6 | 6 | 6 | 6 | 6 |
| | 3 | 4 | 4 | 4 | 6 | 6 | 6 | 6 | 6 | 6 | 6 | 6 |
| | 2 | 4 | 6 | 6 | 6 | 6 | 6 | 6 | 6 | 6 | 6 | 6 |
| | 1 | 2 | 5 | 6 | 6 | 6 | 6 | 6 | 6 | 6 | 6 | 6 |
| | 1 | 1 | 1 | 1 | 2 | 6 | 6 | 6 | 6 | 6 | 6 | 6 |
| | 1 | 2 | 3 | 3 | 6 | 6 | 6 | 6 | 6 | 6 | 6 | 6 |
| | 1 | 1 | 1 | 2 | 3 | 6 | 6 | 6 | 6 | 6 | 6 | 6 |
| | 1 | 1 | 1 | 1 | 1 | 3 | 6 | 6 | 6 | 6 | 6 | 6 |
| | 1 | 1 | 1 | 1 | 2 | 6 | 6 | 6 | 6 | 6 | 6 | 6 |
| | 1 | 1 | 1 | 1 | 6 | 6 | 6 | 6 | 6 | 6 | 6 | 6 |
| | 2 | 6 | 6 | 6 | 6 | 6 | 6 | 6 | 6 | 6 | 6 | 6 |
| | 1 | 1 | 1 | 2 | 4 | 6 | 6 | 6 | 6 | 6 | 6 | 6 |
| | 1 | 1 | 1 | 1 | 1 | 2 | 5 | 6 | 6 | 6 | 6 | 6 |
| | 2 | 4 | 6 | 6 | 6 | 6 | 6 | 6 | 6 | 6 | 6 | 6 |
| | 1 | 1 | 1 | 2 | 3 | 6 | 6 | 6 | 6 | 6 | 6 | 6 |
| | 1 | 1 | 2 | 4 | 6 | 6 | 6 | 6 | 6 | 6 | 6 | 6 |
| | 1 | 1 | 2 | 4 | 6 | 6 | 6 | 6 | 6 | 6 | 6 | 6 |
| | 3 | 3 | 3 | 3 | 6 | 6 | 6 | 6 | 6 | 6 | 6 | 6 |
| | 1 | 1 | 1 | 2 | 2 | 6 | 6 | 6 | 6 | 6 | 6 | 6 |
| | 1 | 1 | 1 | 1 | 1 | 1 | 3 | 5 | 6 | 6 | 6 | 6 |
| | 1 | 3 | 3 | 3 | 6 | 6 | 6 | 6 | 6 | 6 | 6 | 6 |
| | 1 | 1 | 3 | 4 | 6 | 6 | 6 | 6 | 6 | 6 | 6 | 6 |

| bridgeID | Bridge Label (NBI) | NB | SL | BS | RF | Section capacity |
|---|---|---|---|---|---|---|
| - | - | - | m | m | - | kNm |
| 110 | 000000001050390 | 5 | 71.9 | 7.2 | 1.9 | 4195 |
| 111 | 000000001050610 | 4 | 59.1 | 8.3 | 2.3 | 4046 |
| 112 | 000000001050780 | 5 | 90.9 | 7.4 | 3.0 | 8320 |
| 113 | 000000001050921 | 4 | 69.9 | 7.0 | 3.0 | 5452 |
| 114 | 000000001051050 | 11 | 69.9 | 7.1 | 2.8 | 5091 |
| 115 | 000000001051119 | 14 | 87.9 | 7.3 | 2.9 | 7504 |
| 116 | 000000001051139 | 6 | 103.7 | 15.0 | 1.8 | 13768 |
| 117 | 000000001051441 | 6 | 105.0 | 7.1 | 2.0 | 7416 |
| 118 | 000000001051511 | 4 | 84.0 | 8.2 | 2.3 | 6749 |
| 119 | 000000001052080 | 4 | 162.7 | 8.6 | 2.4 | 20022 |
| 120 | 000000001052129 | 9 | 119.8 | 8.5 | 2.4 | 11899 |
| 121 | 000000001052242 | 6 | 121.7 | 7.2 | 2.2 | 10042 |
| 122 | 000000001052319 | 12 | 159.8 | 7.7 | 3.0 | 19144 |
| 123 | 000000001052329 | 12 | 109.9 | 7.6 | 1.9 | 8161 |
| 124 | 000000001052351 | 5 | 118.8 | 8.4 | 2.3 | 11487 |
| 125 | 000000001052422 | 6 | 102.7 | 7.1 | 2.0 | 7155 |
| 126 | 000000001052480 | 6 | 139.8 | 7.8 | 2.8 | 15499 |
| 127 | 000000001052651 | 6 | 125.0 | 7.1 | 2.7 | 11575 |
| 128 | 000000001052850 | 6 | 94.8 | 7.5 | 1.9 | 6487 |
| 129 | 000000001053281 | 6 | 149.9 | 8.1 | 2.3 | 16121 |
| 130 | 000000001053711 | 4 | 138.8 | 8.8 | 2.8 | 17514 |
| 131 | 00000000105384A | 5 | 125.0 | 7.2 | 2.0 | 9837 |
| 132 | 000000001053860 | 5 | 111.9 | 6.8 | 1.7 | 7118 |
| 133 | 000000001053882 | 6 | 111.9 | 5.6 | 2.0 | 6703 |
| 134 | 000000001054020 | 7 | 65.0 | 6.9 | 3.0 | 4770 |
| 135 | 000000001054180 | 4 | 85.0 | 7.2 | 2.0 | 5626 |
| 136 | 000000001054190 | 4 | 125.0 | 7.2 | 2.4 | 11228 |

| | Inspection time (years) | | | | | | | | | | | |
|---|---|---|---|---|---|---|---|---|---|---|---|---|
| | High deterioration rate (3.4%) | | | | Medium deterioration rate (0.5%) | | | | Low deterioration rate (0.07%) | | | |
| Inspection cost ($) | 4k | 10k | 20k | 40k | 4k | 10k | 20k | 40k | 4k | 10k | 20k | 40k |
| | 2 | 3 | 4 | 4 | 6 | 6 | 6 | 6 | 6 | 6 | 6 | 6 |
| | 6 | 6 | 6 | 6 | 6 | 6 | 6 | 6 | 6 | 6 | 6 | 6 |
| | 2 | 5 | 6 | 6 | 6 | 6 | 6 | 6 | 6 | 6 | 6 | 6 |
| | 4 | 6 | 6 | 6 | 6 | 6 | 6 | 6 | 6 | 6 | 6 | 6 |
| | 1 | 2 | 4 | 6 | 6 | 6 | 6 | 6 | 6 | 6 | 6 | 6 |
| | 1 | 1 | 2 | 3 | 6 | 6 | 6 | 6 | 6 | 6 | 6 | 6 |
| | 1 | 1 | 1 | 1 | 2 | 4 | 6 | 6 | 6 | 6 | 6 | 6 |
| | 1 | 2 | 3 | 5 | 6 | 6 | 6 | 6 | 6 | 6 | 6 | 6 |
| | 3 | 6 | 6 | 6 | 6 | 6 | 6 | 6 | 6 | 6 | 6 | 6 |
| | 1 | 1 | 1 | 2 | 5 | 6 | 6 | 6 | 6 | 6 | 6 | 6 |
| | 1 | 1 | 2 | 3 | 6 | 6 | 6 | 6 | 6 | 6 | 6 | 6 |
| | 1 | 2 | 3 | 6 | 6 | 6 | 6 | 6 | 6 | 6 | 6 | 6 |
| | 1 | 1 | 1 | 1 | 1 | 4 | 6 | 6 | 6 | 6 | 6 | 6 |
| | 1 | 1 | 1 | 1 | 1 | 1 | 3 | 6 | 6 | 6 | 6 | 6 |
| | 1 | 1 | 1 | 1 | 1 | 3 | 6 | 6 | 6 | 6 | 6 | 6 |
| | 1 | 1 | 2 | 3 | 6 | 6 | 6 | 6 | 6 | 6 | 6 | 6 |
| | 1 | 1 | 2 | 3 | 6 | 6 | 6 | 6 | 6 | 6 | 6 | 6 |
| | 2 | 4 | 6 | 6 | 6 | 6 | 6 | 6 | 6 | 6 | 6 | 6 |
| | 1 | 1 | 1 | 1 | 1 | 3 | 6 | 6 | 6 | 6 | 6 | 6 |
| | 1 | 1 | 2 | 3 | 6 | 6 | 6 | 6 | 6 | 6 | 6 | 6 |
| | 1 | 2 | 4 | 6 | 6 | 6 | 6 | 6 | 6 | 6 | 6 | 6 |
| | 1 | 1 | 2 | 3 | 6 | 6 | 6 | 6 | 6 | 6 | 6 | 6 |
| | 1 | 1 | 1 | 1 | 1 | 1 | 3 | 6 | 6 | 6 | 6 | 6 |
| | 1 | 1 | 1 | 2 | 3 | 6 | 6 | 6 | 6 | 6 | 6 | 6 |
| | 2 | 2 | 3 | 3 | 6 | 6 | 6 | 6 | 6 | 6 | 6 | 6 |
| | 1 | 2 | 3 | 6 | 6 | 6 | 6 | 6 | 6 | 6 | 6 | 6 |
| | 1 | 1 | 1 | 2 | 3 | 6 | 6 | 6 | 6 | 6 | 6 | 6 |

| bridgeID | Bridge Label (NBI) | NB | SL | BS | RF | Section capacity |
|---|---|---|---|---|---|---|
| - | - | - | m | m | - | kNm |
| 137 | 000000001054270 | 4 | 65.0 | 6.7 | 2.4 | 3960 |
| 138 | 000000001054629 | 12 | 149.9 | 7.8 | 2.2 | 14819 |
| 139 | 000000001054641 | 6 | 109.9 | 7.2 | 2.3 | 8763 |
| 140 | 000000001055209 | 14 | 65.9 | 7.4 | 1.3 | 2755 |
| 141 | 000000001055210 | 5 | 53.8 | 7.2 | 2.2 | 2939 |
| 142 | 000000001055250 | 4 | 81.7 | 7.7 | 2.7 | 6796 |
| 143 | 000000001055559 | 12 | 110.9 | 8.4 | 2.2 | 9942 |
| 144 | 000000001056079 | 16 | 65.9 | 7.2 | 2.1 | 3805 |
| 145 | 000000001056130 | 10 | 67.9 | 8.9 | 2.5 | 5659 |
| 146 | 000000001056220 | 7 | 190.0 | 8.6 | 1.9 | 22979 |
| 147 | 000000001056369 | 12 | 137.8 | 8.6 | 2.1 | 13841 |
| 148 | 000000001058780 | 9 | 46.9 | 6.4 | 1.9 | 1875 |
| 149 | 000000001059949 | 14 | 51.8 | 9.3 | 1.8 | 3086 |
| 150 | 000000001060070 | 10 | 114.8 | 7.6 | 2.3 | 9771 |
| 151 | 000000001060160 | 6 | 109.9 | 7.7 | 2.8 | 10564 |
| 152 | 000000001060390 | 5 | 66.9 | 7.0 | 2.1 | 3838 |
| 153 | 000000001061290 | 5 | 119.8 | 6.8 | 3.1 | 11601 |
| 154 | 000000001061611 | 6 | 103.7 | 7.1 | 3.0 | 9562 |
| 155 | 000000001061660 | 8 | 119.8 | 8.3 | 2.7 | 12510 |
| 156 | 000000001061701 | 5 | 123.7 | 8.8 | 3.0 | 15149 |
| 157 | 000000001061790 | 4 | 99.7 | 7.2 | 2.5 | 8297 |
| 158 | 000000001061880 | 8 | 116.8 | 7.8 | 2.7 | 11283 |
| 159 | 000000001061901 | 5 | 169.9 | 8.4 | 1.8 | 18004 |
| 160 | 000000001062042 | 6 | 122.7 | 7.0 | 2.6 | 10944 |
| 161 | 000000001062230 | 5 | 151.9 | 7.2 | 3.1 | 17503 |
| 162 | 000000001062359 | 18 | 128.9 | 6.7 | 2.9 | 11893 |
| 163 | 000000001063100 | 5 | 100.7 | 7.0 | 2.4 | 7889 |

| | Inspection time (years) | | | | | | | | | | | |
|---|---|---|---|---|---|---|---|---|---|---|---|---|
| | High deterioration rate (3.4%) | | | | Medium deterioration rate (0.5%) | | | | Low deterioration rate (0.07%) | | | |
| Inspection cost ($) | 4k | 10k | 20k | 40k | 4k | 10k | 20k | 40k | 4k | 10k | 20k | 40k |
| | 3 | 4 | 5 | 5 | 6 | 6 | 6 | 6 | 6 | 6 | 6 | 6 |
| | 1 | 1 | 1 | 1 | 1 | 3 | 5 | 6 | 6 | 6 | 6 | 6 |
| | 1 | 2 | 3 | 6 | 6 | 6 | 6 | 6 | 6 | 6 | 6 | 6 |
| | 1 | 1 | 1 | 1 | 6 | 6 | 6 | 6 | 6 | 6 | 6 | 6 |
| | 4 | 6 | 6 | 6 | 6 | 6 | 6 | 6 | 6 | 6 | 6 | 6 |
| | 2 | 6 | 6 | 6 | 6 | 6 | 6 | 6 | 6 | 6 | 6 | 6 |
| | 1 | 1 | 1 | 1 | 2 | 5 | 6 | 6 | 6 | 6 | 6 | 6 |
| | 1 | 2 | 3 | 5 | 6 | 6 | 6 | 6 | 6 | 6 | 6 | 6 |
| | 4 | 5 | 6 | 6 | 6 | 6 | 6 | 6 | 6 | 6 | 6 | 6 |
| | 1 | 1 | 1 | 1 | 1 | 4 | 6 | 6 | 6 | 6 | 6 | 6 |
| | 1 | 1 | 1 | 1 | 2 | 5 | 6 | 6 | 6 | 6 | 6 | 6 |
| | 2 | 4 | 4 | 4 | 6 | 6 | 6 | 6 | 6 | 6 | 6 | 6 |
| | 1 | 1 | 2 | 4 | 6 | 6 | 6 | 6 | 6 | 6 | 6 | 6 |
| | 1 | 3 | 6 | 6 | 6 | 6 | 6 | 6 | 6 | 6 | 6 | 6 |
| | 1 | 1 | 1 | 2 | 4 | 6 | 6 | 6 | 6 | 6 | 6 | 6 |
| | 1 | 2 | 3 | 6 | 6 | 6 | 6 | 6 | 6 | 6 | 6 | 6 |
| | 1 | 2 | 3 | 6 | 6 | 6 | 6 | 6 | 6 | 6 | 6 | 6 |
| | 2 | 4 | 6 | 6 | 6 | 6 | 6 | 6 | 6 | 6 | 6 | 6 |
| | 1 | 1 | 1 | 2 | 5 | 6 | 6 | 6 | 6 | 6 | 6 | 6 |
| | 1 | 2 | 4 | 6 | 6 | 6 | 6 | 6 | 6 | 6 | 6 | 6 |
| | 2 | 4 | 6 | 6 | 6 | 6 | 6 | 6 | 6 | 6 | 6 | 6 |
| | 1 | 1 | 1 | 2 | 4 | 6 | 6 | 6 | 6 | 6 | 6 | 6 |
| | 1 | 1 | 1 | 3 | 4 | 6 | 6 | 6 | 6 | 6 | 6 | 6 |
| | 1 | 2 | 3 | 6 | 6 | 6 | 6 | 6 | 6 | 6 | 6 | 6 |
| | 1 | 2 | 3 | 6 | 6 | 6 | 6 | 6 | 6 | 6 | 6 | 6 |
| | 1 | 1 | 1 | 1 | 1 | 1 | 3 | 6 | 6 | 6 | 6 | 6 |
| | 1 | 2 | 3 | 6 | 6 | 6 | 6 | 6 | 6 | 6 | 6 | 6 |

| bridgeID | Bridge Label (NBI) | NB | SL | BS | RF | Section capacity |
|---|---|---|---|---|---|---|
| - | - | - | m | m | - | kNm |
| 164 | 000000001063110 | 4 | 139.8 | 8.8 | 1.3 | 11461 |
| 165 | 000000001063189 | 12 | 107.0 | 8.3 | 2.4 | 9785 |
| 166 | 000000001063239 | 12 | 122.7 | 8.4 | 2.7 | 12924 |
| 167 | 000000001064049 | 14 | 76.8 | 8.2 | 1.7 | 4710 |
| 168 | 000000001064139 | 10 | 109.9 | 7.6 | 1.5 | 7142 |
| 169 | 000000001064780 | 5 | 46.9 | 7.0 | 1.3 | 1552 |
| 170 | 000000001065210 | 7 | 76.8 | 4.4 | 2.1 | 2993 |
| 171 | 00000000106531P | 7 | 246.4 | 7.1 | 1.7 | 31401 |
| 172 | 000000001065399 | 10 | 90.9 | 9.7 | 1.8 | 7441 |
| 173 | 000000001065449 | 16 | 97.8 | 6.4 | 2.1 | 6151 |
| 174 | 000000001065589 | 10 | 99.7 | 8.9 | 1.6 | 7279 |
| 175 | 000000001066120 | 11 | 82.7 | 6.5 | 1.7 | 4314 |
| 176 | 000000001066220 | 18 | 123.7 | 8.8 | 1.6 | 10059 |
| 177 | 000000001066349 | 12 | 201.8 | 8.2 | 2.0 | 24395 |
| 178 | 000000001066419 | 12 | 133.9 | 7.1 | 1.7 | 9833 |
| 179 | 000000001067530 | 10 | 89.9 | 7.3 | 3.0 | 7951 |
| 180 | 000000001067681 | 6 | 72.8 | 7.7 | 1.9 | 4470 |
| 181 | 000000001067712 | 9 | 100.7 | 7.6 | 2.4 | 8335 |
| 182 | 000000001068490 | 6 | 117.8 | 7.7 | 2.2 | 10099 |
| 183 | 000000001068502 | 7 | 116.8 | 8.1 | 2.1 | 10010 |
| 184 | 000000001069110 | 11 | 188.0 | 9.1 | 3.1 | 29615 |
| 185 | 000000001069120 | 10 | 179.8 | 8.8 | 3.1 | 26863 |
| 186 | 000000001070699 | 11 | 100.1 | 9.1 | 3.1 | 11667 |
| 187 | 000000001070790 | 8 | 116.8 | 8.3 | 3.0 | 13013 |
| 188 | 000000001070900 | 10 | 186.7 | 8.7 | 3.1 | 28258 |
| 189 | 000000001071001 | 5 | 173.9 | 8.8 | 2.8 | 24456 |
| 190 | 000000001071851 | 6 | 177.8 | 9.4 | 2.9 | 27480 |

| | Inspection time (years) | | | | | | | | | | | |
|---|---|---|---|---|---|---|---|---|---|---|---|---|
| | High deterioration rate (3.4%) | | | | Medium deterioration rate (0.5%) | | | | Low deterioration rate (0.07%) | | | |
| Inspection cost ($) | 4k | 10k | 20k | 40k | 4k | 10k | 20k | 40k | 4k | 10k | 20k | 40k |
| | 1 | 1 | 1 | 1 | 2 | 4 | 6 | 6 | 6 | 6 | 6 | 6 |
| | 1 | 1 | 1 | 1 | 1 | 3 | 6 | 6 | 6 | 6 | 6 | 6 |
| | 1 | 1 | 1 | 1 | 2 | 4 | 6 | 6 | 6 | 6 | 6 | 6 |
| | 2 | 2 | 2 | 2 | 6 | 6 | 6 | 6 | 6 | 6 | 6 | 6 |
| | 1 | 1 | 1 | 1 | 1 | 3 | 5 | 6 | 6 | 6 | 6 | 6 |
| | 2 | 2 | 2 | 2 | 6 | 6 | 6 | 6 | 6 | 6 | 6 | 6 |
| | 2 | 5 | 6 | 6 | 6 | 6 | 6 | 6 | 6 | 6 | 6 | 6 |
| | 1 | 1 | 1 | 1 | 1 | 1 | 1 | 1 | 1 | 6 | 6 | 6 |
| | 1 | 1 | 1 | 1 | 2 | 5 | 6 | 6 | 6 | 6 | 6 | 6 |
| | 1 | 2 | 5 | 6 | 6 | 6 | 6 | 6 | 6 | 6 | 6 | 6 |
| | 1 | 1 | 1 | 1 | 1 | 2 | 5 | 6 | 6 | 6 | 6 | 6 |
| | 1 | 2 | 3 | 3 | 6 | 6 | 6 | 6 | 6 | 6 | 6 | 6 |
| | 1 | 1 | 1 | 1 | 2 | 4 | 6 | 6 | 6 | 6 | 6 | 6 |
| | 1 | 1 | 1 | 2 | 3 | 6 | 6 | 6 | 6 | 6 | 6 | 6 |
| | 1 | 1 | 1 | 1 | 1 | 1 | 2 | 5 | 6 | 6 | 6 | 6 |
| | 3 | 6 | 6 | 6 | 6 | 6 | 6 | 6 | 6 | 6 | 6 | 6 |
| | 1 | 1 | 2 | 3 | 6 | 6 | 6 | 6 | 6 | 6 | 6 | 6 |
| | 1 | 1 | 1 | 2 | 5 | 6 | 6 | 6 | 6 | 6 | 6 | 6 |
| | 1 | 1 | 2 | 3 | 6 | 6 | 6 | 6 | 6 | 6 | 6 | 6 |
| | 1 | 2 | 4 | 4 | 6 | 6 | 6 | 6 | 6 | 6 | 6 | 6 |
| | 1 | 1 | 2 | 3 | 6 | 6 | 6 | 6 | 6 | 6 | 6 | 6 |
| | 1 | 2 | 3 | 6 | 6 | 6 | 6 | 6 | 6 | 6 | 6 | 6 |
| | 2 | 5 | 6 | 6 | 6 | 6 | 6 | 6 | 6 | 6 | 6 | 6 |
| | 1 | 3 | 6 | 6 | 6 | 6 | 6 | 6 | 6 | 6 | 6 | 6 |
| | 1 | 1 | 2 | 2 | 6 | 6 | 6 | 6 | 6 | 6 | 6 | 6 |
| | 1 | 2 | 3 | 5 | 6 | 6 | 6 | 6 | 6 | 6 | 6 | 6 |
| | 1 | 1 | 1 | 2 | 4 | 6 | 6 | 6 | 6 | 6 | 6 | 6 |

| bridgeID | Bridge Label (NBI) | NB | SL | BS | RF | Section capacity |
|---|---|---|---|---|---|---|
| - | - | - | m | m | - | kNm |
| 191 | 000000001072409 | 10 | 110.9 | 9.1 | 3.0 | 13257 |
| 192 | 000000001072631 | 10 | 184.7 | 8.1 | 1.8 | 19765 |
| 193 | 000000001072661 | 6 | 168.0 | 9.8 | 2.6 | 24409 |
| 194 | 000000001072662 | 6 | 168.0 | 9.8 | 2.6 | 24409 |
| 195 | 000000001072689 | 12 | 138.8 | 9.3 | 2.8 | 17910 |
| 196 | 000000001073580 | 5 | 158.1 | 8.6 | 2.6 | 19611 |
| 197 | 000000001073630 | 5 | 194.9 | 9.3 | 2.8 | 31531 |
| 198 | 000000001073830 | 4 | 144.7 | 6.3 | 3.1 | 14491 |
| 199 | 000000001074090 | 4 | 189.0 | 6.9 | 2.5 | 21804 |
| 200 | 000000001074561 | 5 | 139.8 | 8.6 | 2.3 | 15256 |
| 201 | 000000001075559 | 13 | 81.7 | 8.0 | 2.4 | 6374 |
| 202 | 000000001075930 | 7 | 176.8 | 6.4 | 1.8 | 15251 |
| 203 | 000000001075970 | 7 | 152.9 | 4.7 | 1.6 | 8756 |
| 204 | 000000001075990 | 5 | 71.9 | 6.6 | 1.7 | 3498 |
| 205 | 000000001077530 | 4 | 173.9 | 9.0 | 2.7 | 24696 |
| 206 | 000000001078052 | 5 | 192.6 | 8.6 | 2.7 | 27403 |
| 207 | 000000001078410 | 8 | 164.0 | 6.5 | 2.3 | 15214 |
| 208 | 000000001078730 | 5 | 84.0 | 5.6 | 2.6 | 5122 |
| 209 | 000000001079250 | 5 | 111.5 | 7.7 | 2.4 | 9975 |
| 210 | 000000001091110 | 7 | 114.8 | 8.7 | 3.1 | 13613 |
| 211 | 000000001091171 | 5 | 65.9 | 6.6 | 3.1 | 4749 |
| 212 | 000000001091250 | 4 | 173.9 | 8.1 | 2.7 | 22371 |
| 213 | 000000001091310 | 5 | 149.9 | 6.6 | 2.3 | 13473 |
| 214 | 000000001091790 | 5 | 125.0 | 9.2 | 1.9 | 12194 |
| 215 | 000000001092099 | 7 | 99.7 | 9.2 | 2.9 | 11166 |
| 216 | 000000001092389 | 7 | 172.9 | 8.3 | 2.1 | 19576 |
| 217 | 000000001092409 | 12 | 154.9 | 7.6 | 2.8 | 17503 |

| | Inspection time (years) | | | | | | | | | | | |
|---|---|---|---|---|---|---|---|---|---|---|---|---|
| | High deterioration rate (3.4%) | | | | Medium deterioration rate (0.5%) | | | | Low deterioration rate (0.07%) | | | |
| Inspection cost ($) | 4k | 10k | 20k | 40k | 4k | 10k | 20k | 40k | 4k | 10k | 20k | 40k |
| | 1 | 2 | 3 | 6 | 6 | 6 | 6 | 6 | 6 | 6 | 6 | 6 |
| | 1 | 1 | 1 | 2 | 4 | 6 | 6 | 6 | 6 | 6 | 6 | 6 |
| | 1 | 2 | 3 | 3 | 6 | 6 | 6 | 6 | 6 | 6 | 6 | 6 |
| | 1 | 2 | 3 | 3 | 6 | 6 | 6 | 6 | 6 | 6 | 6 | 6 |
| | 1 | 3 | 6 | 6 | 6 | 6 | 6 | 6 | 6 | 6 | 6 | 6 |
| | 1 | 1 | 1 | 1 | 1 | 1 | 1 | 1 | 6 | 6 | 6 | 6 |
| | 1 | 1 | 4 | 5 | 6 | 6 | 6 | 6 | 6 | 6 | 6 | 6 |
| | 1 | 2 | 5 | 6 | 6 | 6 | 6 | 6 | 6 | 6 | 6 | 6 |
| | 1 | 1 | 1 | 4 | 4 | 6 | 6 | 6 | 6 | 6 | 6 | 6 |
| | 1 | 2 | 3 | 6 | 6 | 6 | 6 | 6 | 6 | 6 | 6 | 6 |
| | 2 | 4 | 6 | 6 | 6 | 6 | 6 | 6 | 6 | 6 | 6 | 6 |
| | 1 | 1 | 1 | 1 | 1 | 1 | 3 | 6 | 6 | 6 | 6 | 6 |
| | 1 | 1 | 1 | 1 | 1 | 1 | 1 | 2 | 6 | 6 | 6 | 6 |
| | 1 | 1 | 1 | 2 | 3 | 6 | 6 | 6 | 6 | 6 | 6 | 6 |
| | 1 | 2 | 3 | 4 | 6 | 6 | 6 | 6 | 6 | 6 | 6 | 6 |
| | 1 | 1 | 4 | 4 | 6 | 6 | 6 | 6 | 6 | 6 | 6 | 6 |
| | 1 | 1 | 1 | 1 | 1 | 3 | 6 | 6 | 6 | 6 | 6 | 6 |
| | 3 | 6 | 6 | 6 | 6 | 6 | 6 | 6 | 6 | 6 | 6 | 6 |
| | 1 | 1 | 1 | 2 | 4 | 6 | 6 | 6 | 6 | 6 | 6 | 6 |
| | 1 | 1 | 2 | 3 | 6 | 6 | 6 | 6 | 6 | 6 | 6 | 6 |
| | 1 | 2 | 2 | 2 | 6 | 6 | 6 | 6 | 6 | 6 | 6 | 6 |
| | 1 | 1 | 2 | 4 | 6 | 6 | 6 | 6 | 6 | 6 | 6 | 6 |
| | 1 | 1 | 1 | 1 | 1 | 4 | 6 | 6 | 6 | 6 | 6 | 6 |
| | 1 | 2 | 3 | 3 | 6 | 6 | 6 | 6 | 6 | 6 | 6 | 6 |
| | 4 | 6 | 6 | 6 | 6 | 6 | 6 | 6 | 6 | 6 | 6 | 6 |
| | 1 | 1 | 1 | 4 | 3 | 6 | 6 | 6 | 6 | 6 | 6 | 6 |
| | 1 | 1 | 2 | 4 | 6 | 6 | 6 | 6 | 6 | 6 | 6 | 6 |

| bridgeID | Bridge Label (NBI) | NB | SL | BS | RF | Section capacity |
|---|---|---|---|---|---|---|
| - | - | - | m | m | - | kNm |
| 218 | 000000001092480 | 8 | 108.9 | 8.8 | 1.9 | 9198 |
| 219 | 000000001092492 | 4 | 156.8 | 7.0 | 2.8 | 16767 |
| 220 | 000000001093121 | 7 | 107.0 | 7.3 | 2.0 | 7689 |
| 221 | 000000001093280 | 4 | 173.9 | 8.1 | 2.3 | 20683 |
| 222 | 000000001093290 | 4 | 141.7 | 8.8 | 2.5 | 16777 |
| 223 | 000000001093310 | 5 | 168.0 | 8.8 | 2.1 | 20142 |
| 224 | 000000001093349 | 20 | 85.0 | 6.1 | 2.8 | 5751 |
| 225 | 000000001093430 | 5 | 169.9 | 10.1 | 2.8 | 26552 |
| 226 | 000000001093460 | 6 | 165.7 | 9.0 | 2.3 | 20838 |
| 227 | 000000001093479 | 12 | 109.9 | 10.2 | 2.6 | 13073 |
| 228 | 000000001093510 | 5 | 122.7 | 8.4 | 3.1 | 14601 |
| 229 | 000000001093992 | 6 | 180.8 | 7.3 | 2.0 | 18736 |
| 230 | 000000001094190 | 4 | 45.9 | 7.5 | 2.1 | 2281 |
| 231 | 000000002065973 | 4 | 108.9 | 7.1 | 2.3 | 8763 |
| 232 | 000000002231559 | 24 | 53.8 | 5.5 | 3.0 | 2869 |
| 233 | 00000000224001B | 5 | 94.8 | 5.5 | 1.0 | 3572 |
| 234 | 000000002242380 | 26 | 50.9 | 7.1 | 2.1 | 2548 |
| 235 | 000000002269600 | 9 | 124.0 | 7.4 | 2.8 | 12128 |
| 236 | 000000003358690 | 5 | 116.8 | 6.7 | 2.4 | 9332 |
| 237 | 000000004051011 | 5 | 230.0 | 8.4 | 2.1 | 33999 |
| 238 | 000000004051012 | 5 | 230.0 | 8.4 | 2.0 | 33463 |
| 239 | 000000004051180 | 5 | 184.7 | 7.3 | 1.7 | 18145 |
| 240 | 000000005000029 | 18 | 132.9 | 7.0 | 2.1 | 10656 |
| 241 | 000000005002939 | 16 | 86.9 | 7.1 | 2.5 | 6471 |
| 242 | 000000005004660 | 4 | 102.0 | 6.7 | 2.0 | 6936 |
| 243 | 000000005006132 | 8 | 86.0 | 7.1 | 2.6 | 6513 |
| 244 | 000000005007299 | 12 | 80.7 | 7.4 | 1.8 | 4672 |

| | Inspection time (years) | | | | | | | | | | | |
|---|---|---|---|---|---|---|---|---|---|---|---|---|
| | High deterioration rate (3.4%) | | | | Medium deterioration rate (0.5%) | | | | Low deterioration rate (0.07%) | | | |
| Inspection cost ($) | 4k | 10k | 20k | 40k | 4k | 10k | 20k | 40k | 4k | 10k | 20k | 40k |
| | 1 | 1 | 2 | 3 | 6 | 6 | 6 | 6 | 6 | 6 | 6 | 6 |
| | 1 | 2 | 3 | 6 | 6 | 6 | 6 | 6 | 6 | 6 | 6 | 6 |
| | 1 | 1 | 2 | 4 | 6 | 6 | 6 | 6 | 6 | 6 | 6 | 6 |
| | 1 | 1 | 1 | 1 | 2 | 4 | 6 | 6 | 6 | 6 | 6 | 6 |
| | 1 | 1 | 1 | 2 | 4 | 6 | 6 | 6 | 6 | 6 | 6 | 6 |
| | 1 | 1 | 1 | 1 | 1 | 2 | 4 | 6 | 6 | 6 | 6 | 6 |
| | 1 | 1 | 1 | 1 | 3 | 6 | 6 | 6 | 6 | 6 | 6 | 6 |
| | 1 | 1 | 1 | 2 | 4 | 6 | 6 | 6 | 6 | 6 | 6 | 6 |
| | 1 | 1 | 1 | 2 | 5 | 6 | 6 | 6 | 6 | 6 | 6 | 6 |
| | 1 | 1 | 2 | 2 | 6 | 6 | 6 | 6 | 6 | 6 | 6 | 6 |
| | 1 | 1 | 1 | 1 | 2 | 6 | 6 | 6 | 6 | 6 | 6 | 6 |
| | 1 | 1 | 1 | 4 | 4 | 6 | 6 | 6 | 6 | 6 | 6 | 6 |
| | 1 | 4 | 4 | 4 | 6 | 6 | 6 | 6 | 6 | 6 | 6 | 6 |
| | 1 | 1 | 1 | 1 | 2 | 5 | 6 | 6 | 6 | 6 | 6 | 6 |
| | 1 | 1 | 1 | 2 | 5 | 6 | 6 | 6 | 6 | 6 | 6 | 6 |
| | 1 | 1 | 1 | 1 | 1 | 1 | 3 | 3 | 6 | 6 | 6 | 6 |
| | 1 | 1 | 2 | 2 | 6 | 6 | 6 | 6 | 6 | 6 | 6 | 6 |
| | 1 | 1 | 2 | 3 | 6 | 6 | 6 | 6 | 6 | 6 | 6 | 6 |
| | 1 | 1 | 1 | 2 | 4 | 6 | 6 | 6 | 6 | 6 | 6 | 6 |
| | 1 | 1 | 1 | 1 | 1 | 2 | 4 | 6 | 6 | 6 | 6 | 6 |
| | 1 | 1 | 1 | 1 | 1 | 2 | 4 | 6 | 6 | 6 | 6 | 6 |
| | 1 | 1 | 1 | 1 | 1 | 1 | 2 | 4 | 6 | 6 | 6 | 6 |
| | 1 | 1 | 1 | 1 | 1 | 1 | 2 | 4 | 6 | 6 | 6 | 6 |
| | 1 | 1 | 1 | 2 | 4 | 6 | 6 | 6 | 6 | 6 | 6 | 6 |
| | 1 | 1 | 2 | 4 | 6 | 6 | 6 | 6 | 6 | 6 | 6 | 6 |
| | 1 | 3 | 5 | 6 | 6 | 6 | 6 | 6 | 6 | 6 | 6 | 6 |
| | 1 | 1 | 1 | 2 | 3 | 6 | 6 | 6 | 6 | 6 | 6 | 6 |

| bridgeID | Bridge Label (NBI) | NB | SL | BS | RF | Section capacity |
|---|---|---|---|---|---|---|
| - | - | - | m | m | - | kNm |
| 245 | 000000005007949 | 16 | 118.1 | 7.2 | 2.7 | 10767 |
| 246 | 000000005014082 | 8 | 124.0 | 8.3 | 2.0 | 10840 |
| 247 | 000000005038059 | 16 | 70.9 | 7.8 | 1.9 | 4254 |
| 248 | 000000005038799 | 12 | 47.9 | 9.4 | 0.8 | 1566 |
| 249 | 000000005038810 | 17 | 53.2 | 6.7 | 2.8 | 3227 |
| 250 | 000000005040851 | 8 | 74.1 | 7.0 | 2.2 | 4610 |
| 251 | 000000005040852 | 8 | 74.1 | 7.0 | 1.8 | 4019 |
| 252 | 000000005046459 | 14 | 121.1 | 7.4 | 1.6 | 8395 |
| 253 | 000000005047170 | 5 | 79.1 | 6.6 | 1.4 | 3687 |
| 254 | 000000005075309 | 16 | 101.1 | 8.0 | 1.9 | 7396 |
| 255 | 000000005075380 | 6 | 116.1 | 5.8 | 2.6 | 8452 |
| 256 | 000000005349010 | 4 | 52.8 | 7.3 | 2.5 | 3294 |
| 257 | 000000005501210 | 10 | 79.7 | 7.1 | 2.9 | 6364 |
| 258 | 000000005501650 | 7 | 64.0 | 8.1 | 2.9 | 5314 |
| 259 | 000000005510140 | 12 | 100.1 | 5.9 | 2.6 | 6821 |
| 260 | 000000005510150 | 10 | 92.8 | 5.1 | 2.1 | 4587 |
| 261 | 000000005510200 | 6 | 65.0 | 7.2 | 1.6 | 3156 |
| 262 | 000000005511200 | 7 | 65.0 | 6.2 | 1.7 | 2804 |
| 263 | 000000005511980 | 8 | 83.0 | 7.8 | 2.6 | 6836 |
| 264 | 000000005512089 | 20 | 120.1 | 7.1 | 2.5 | 10219 |
| 265 | 000000005513400 | 6 | 145.0 | 11.7 | 2.9 | 24484 |
| 266 | 000000005513749 | 18 | 53.2 | 7.0 | 2.2 | 2763 |
| 267 | 000000005513950 | 9 | 82.7 | 6.9 | 2.3 | 5587 |
| 268 | 000000005514009 | 16 | 47.9 | 7.1 | 1.1 | 1469 |
| 269 | 000000005514019 | 17 | 46.9 | 6.9 | 1.5 | 1673 |
| 270 | 000000005514181 | 8 | 182.1 | 9.3 | 2.8 | 27379 |
| 271 | 000000005514182 | 8 | 182.1 | 9.3 | 2.1 | 23703 |

| | Inspection time (years) | | | | | | | | | | | |
|---|---|---|---|---|---|---|---|---|---|---|---|---|
| | High deterioration rate (3.4%) | | | | Medium deterioration rate (0.5%) | | | | Low deterioration rate (0.07%) | | | |
| Inspection cost ($) | 4k | 10k | 20k | 40k | 4k | 10k | 20k | 40k | 4k | 10k | 20k | 40k |
| | 1 | 1 | 1 | 1 | 1 | 1 | 3 | 6 | 6 | 6 | 6 | 6 |
| | 1 | 1 | 1 | 2 | 3 | 6 | 6 | 6 | 6 | 6 | 6 | 6 |
| | 1 | 1 | 1 | 1 | 1 | 2 | 3 | 6 | 6 | 6 | 6 | 6 |
| | 1 | 1 | 1 | 1 | 1 | 1 | 1 | 1 | 1 | 1 | 1 | 1 |
| | 6 | 6 | 6 | 6 | 6 | 6 | 6 | 6 | 6 | 6 | 6 | 6 |
| | 1 | 2 | 3 | 6 | 6 | 6 | 6 | 6 | 6 | 6 | 6 | 6 |
| | 1 | 1 | 2 | 3 | 5 | 6 | 6 | 6 | 6 | 6 | 6 | 6 |
| | 1 | 1 | 1 | 1 | 1 | 2 | 5 | 6 | 6 | 6 | 6 | 6 |
| | 1 | 1 | 1 | 2 | 5 | 6 | 6 | 6 | 6 | 6 | 6 | 6 |
| | 1 | 1 | 1 | 1 | 1 | 3 | 6 | 6 | 6 | 6 | 6 | 6 |
| | 1 | 2 | 4 | 6 | 6 | 6 | 6 | 6 | 6 | 6 | 6 | 6 |
| | 1 | 2 | 4 | 6 | 6 | 6 | 6 | 6 | 6 | 6 | 6 | 6 |
| | 2 | 4 | 4 | 5 | 6 | 6 | 6 | 6 | 6 | 6 | 6 | 6 |
| | 1 | 3 | 5 | 6 | 6 | 6 | 6 | 6 | 6 | 6 | 6 | 6 |
| | 1 | 2 | 3 | 6 | 6 | 6 | 6 | 6 | 6 | 6 | 6 | 6 |
| | 1 | 1 | 1 | 2 | 4 | 6 | 6 | 6 | 6 | 6 | 6 | 6 |
| | 1 | 1 | 1 | 1 | 2 | 5 | 6 | 6 | 6 | 6 | 6 | 6 |
| | 3 | 3 | 3 | 3 | 6 | 6 | 6 | 6 | 6 | 6 | 6 | 6 |
| | 2 | 6 | 6 | 6 | 6 | 6 | 6 | 6 | 6 | 6 | 6 | 6 |
| | 1 | 1 | 1 | 1 | 2 | 5 | 6 | 6 | 6 | 6 | 6 | 6 |
| | 1 | 1 | 1 | 1 | 1 | 2 | 4 | 6 | 6 | 6 | 6 | 6 |
| | 1 | 1 | 1 | 1 | 2 | 5 | 6 | 6 | 6 | 6 | 6 | 6 |
| | 1 | 2 | 3 | 6 | 6 | 6 | 6 | 6 | 6 | 6 | 6 | 6 |
| | 1 | 1 | 1 | 1 | 6 | 6 | 6 | 6 | 6 | 6 | 6 | 6 |
| | 1 | 1 | 1 | 1 | 1 | 2 | 4 | 6 | 6 | 6 | 6 | 6 |
| | 1 | 1 | 1 | 2 | 4 | 6 | 6 | 6 | 6 | 6 | 6 | 6 |
| | 1 | 1 | 1 | 1 | 1 | 4 | 6 | 6 | 6 | 6 | 6 | 6 |

| bridgeID | Bridge Label (NBI) | NB | SL | BS | RF | Section capacity |
|---|---|---|---|---|---|---|
| - | - | - | m | m | - | kNm |
| 272 | 000000005514509 | 14 | 65.0 | 7.2 | 2.9 | 4852 |
| 273 | 000000005514799 | 16 | 145.3 | 6.6 | 1.8 | 10803 |
| 274 | 000000005514809 | 12 | 211.9 | 9.8 | 2.5 | 35059 |
| 275 | 000000005515240 | 4 | 121.1 | 8.3 | 1.9 | 10518 |
| 276 | 000000005515479 | 14 | 65.0 | 8.1 | 1.7 | 3557 |
| 277 | 000000005516130 | 5 | 67.9 | 6.6 | 2.0 | 3588 |
| 278 | 000000005523350 | 12 | 123.7 | 8.2 | 2.8 | 13479 |
| 279 | 000000005523550 | 6 | 171.9 | 7.9 | 3.0 | 22490 |

| | Inspection time (years) | | | | | | | | | | | |
|---|---|---|---|---|---|---|---|---|---|---|---|---|
| | High deterioration rate (3.4%) | | | | Medium deterioration rate (0.5%) | | | | Low deterioration rate (0.07%) | | | |
| Inspection cost ($) | 4k | 10k | 20k | 40k | 4k | 10k | 20k | 40k | 4k | 10k | 20k | 40k |
| | 1 | 1 | 2 | 3 | 6 | 6 | 6 | 6 | 6 | 6 | 6 | 6 |
| | 1 | 1 | 1 | 1 | 1 | 2 | 4 | 6 | 6 | 6 | 6 | 6 |
| | 1 | 1 | 1 | 1 | 1 | 1 | 3 | 6 | 6 | 6 | 6 | 6 |
| | 1 | 2 | 3 | 3 | 6 | 6 | 6 | 6 | 6 | 6 | 6 | 6 |
| | 1 | 1 | 1 | 1 | 1 | 1 | 1 | 1 | 1 | 6 | 6 | 6 |
| | 1 | 1 | 1 | 1 | 2 | 5 | 6 | 6 | 6 | 6 | 6 | 6 |
| | 1 | 2 | 3 | 6 | 6 | 6 | 6 | 6 | 6 | 6 | 6 | 6 |
| | 1 | 1 | 1 | 2 | 4 | 6 | 6 | 6 | 6 | 6 | 6 | 6 |